THE JOURNAL
OF
CHEMICAL PHYSICS

VOLUME 18, NUMBER 6 JUNE, 1950

Electronic Processes in Zinc Fluoride and in the Manganese-Activated Zinc Fluoride Phosphor*

JAMES H. CRAWFORD, JR.† AND FERD E. WILLIAMS‡
Chemistry Department, University of North Carolina, Chapel Hill, North Carolina
(Received February 23, 1950)

Measurements have been made of the temperature-dependence of electrical conductivity and thermal e.m.f. on ZnF_2 and ZnF_2:Mn, and of the Hall coefficient and rectifying power at 25°C on ZnF_2. Both ZnF_2 and ZnF_2:Mn are *N*-type impurity semiconductors. The presence of MnF_2 in ZnF_2 decreases the electronic conductivity by a factor of about 10^3, indicating a decrease in the concentration of electron donors by oxidation. A marked dependence of the temperature variation of conductivity on heat treatment has been observed. Contrary to the simple theory, the absolute values of the thermal e.m.f. increase with temperature. From the Hall coefficient and conductance at 25°C of heat-treated ZnF_2, a concentration of free electrons of 3×10^{16} cm^{-3} and a mean free path of 6.7×10^{-8} cm are deduced. ZnF_2 rectifies in the expected direction.

INTRODUCTION

IN the course of a fundamental research program on the luminescence of ionic solids, fused samples of both pure zinc fluoride and the manganese-activated zinc fluoride phosphor were found to exhibit high electronic conductivity. Subsequent measurements of the Hall and Seebeck effects proved these materials to be *N*-type impurity semiconductors. The impurity centers are presumably zinc atoms or Zn^+ interstitial in the rutile lattice. The centers are produced by thermal decomposition of ZnF_2 at temperatures above the melting point (872°C), either directly or via a small concentration of ZnO intermediate. Increased conductance indicates that the concentration of centers increases with the maximum temperature of heating during preparation. Although Jellinek and Rudat[1] have determined the equilibrium fluorine pressure of ZnF_2 at elevated temperatures, calculation of the degree of direct decomposition is not possible because of the entropy increase involved in the solution of the free zinc in the molten salt and because the samples are prepared in an open system where equilibrium fluorine pressures are not attained. The situation is similar to that encountered in the preparation of semiconducting ZnO except for the lack of equilibrium with the free anionic constituent and for the greater heat content of ZnF_2. Johnson and Williams[2] report a concentration of 10^{18} atoms of zinc per cm^3 in ZnF_2:Mn as determined by reducing action toward dilute acid $KMnO_4$ solution.

In order to characterize these semiconductors according to their electronic properties, the conductivity, thermal e.m.f., Hall effect, and rectifying power were measured. Complete conductivity and high temperature thermal e.m.f. data were taken on pure ZnF_2 and on phosphors containing 4 mole percent MnF_2. Also, high temperature conductivity measurements were made on a sample containing 10 mole percent MnF_2. Because of the higher resistance of the manganese activated material, Hall effect and rectification and low temperature thermal e.m.f. measurements were confined to the pure ZnF_2.

MEASUREMENTS OF CONDUCTIVITY AND THERMAL E.M.F.

In order to cover the temperature range from −180 to +325°C, two different arrangements were used. The apparatus used above room temperature is shown in Fig. 1 while that used below room temperature is shown

* Supported by the ONR through Contract N7onr-284, Task Order 1. Part of a dissertation submitted by J. H. Crawford to the University of North Carolina in partial fulfillment of the requirements for the Ph.D. degree.
† Present address: Oak Ridge National Laboratory, Oak Ridge, Tennessee.
‡ Present address: General Electric Research Laboratory, Schenectady, New York.
[1] K. Jellinek and A. Rudat, Zeits. f. anorg. allgem. Chemie **175**, 281 (1928).
[2] P. D. Johnson and F. E. Williams, J. Chem. Phys. **18**, 323 (1950).

in Fig. 2. Both were designed so that thermal e.m.f. and conductivity data could be taken concurrently.

In the high temperature range the resistance of the sample was measured with a RCA volt-ohmist. The accuracy of the instrument was about 10 percent, but since the logarithm of the conductivity was used and because of the large temperature coefficient of the conductivity in this range, the accuracy was sufficient. Temperatures at the ends of the sample were measured potentiometrically with iron-constantan thermocouples soldered into the contact electrodes using a Leeds and Northrup Type-K potentiometer. The temperature of the heating sleeve was controlled manually with a Variac, and for thermal e.m.f. measurements, a nearly constant temperature difference of about 20°C was maintained across the sample by a heating coil on one of the electrodes controlled by a second Variac. Sudden discontinuities would be obscured by this large a gradient which was necessary to minimize errors in temperature differential. When conductivity measurements were taken with a temperature gradient across the sample, the resistance was measured in both directions and the mean temperature of the sample was used. The thermal e.m.f. was measured with the same potentiometer that was used for temperature measurement.

For the low temperature range, the apparatus was placed in a Dewar flask containing liquid air. The rate of heating or cooling and the temperature differential across the sample were controlled by the two heating coils each operated by separate Variacs. Resistances were measured by a Wheatstone bridge and copper-constantan thermocouples were used.

The samples of ZnF_2 were prepared by fusing in a platinum crucible a sufficient quantity of ZnF_2, prepared from spectroscopically pure ZnO and reagent grade HF, and heating to about 1200°C over a Meker burner for 10 to 15 min. The fused material was removed from the crucible and shaped to the desired dimensions on garnet paper. The phosphor samples were prepared in the same manner after adding the MnF_2. In order to minimize the contact resistance, aluminum films were evaporated onto opposite faces of the crystal. The contacts were found to have a negligible resistance compared to the over-all resistance of the sample.

RESULTS OF CONDUCTIVITY AND THERMAL E.M.F. MEASUREMENTS

Representative curves of $\log\sigma$ *vs.* $1/T$ in the high temperature range are shown in Fig. 3 for ZnF_2 and in Fig. 4 for ZnF_2:0.04 MnF_2. One curve on ZnF_2:0.10 Mn is also shown. Except for *S*1 of Fig. 3, the curves are straight lines which change discontinuously to a greater slope at higher temperatures as is expected from the conductivity equation:

$$\sigma = A_1 \exp(-E_1/kT) + A_2 \exp(-E_2/kT) + \cdots, \quad (1)$$

where the A's are only slightly temperature-dependent and the E's represent the apparent activation energies. The properties of these and other samples are recorded in Table I.

All ZnF_2 samples, denoted by *S*, were cooled slowly from the maximum temperature of heating, about 10 min. from 1200 to 500°C, except for *S*1 which was air quenched. The differences in conductivity of the samples are due to the differences in duration of heat treatment. In general, all phosphor samples, denoted by *P*, were given a longer heat treatment at 1200°C than the ZnF_2 samples in order to increase the conductivity. Samples containing MnF_2, when given the same heat treatment as pure ZnF_2, have resistances 10^2 to 10^3 times greater. The phosphor samples, with the exception of *P*3 and *P*4, were cooled slowly.

Examination of the data shows a change in slope of the $\log\sigma$ *vs.* $1/T$ plot at 400 to 500°K. This indicates two impurity levels with the deeper level dominating the conductivity at the higher temperatures in all samples except *S*1, *P*3, and *P*4.

In the case of the quenched samples, Eq. (1) is not valid and a transition from a high apparent activation energy to one about half this value at higher temperatures takes place. Thus for *S*1*A*, the ratio of E_2 to E_1 is 2.2; for *S*1*B*, 2.0; for *P*3*A*, 1.6; and for *P*4*A*, 2.1. This phenomenon has been observed with ZnO and has been

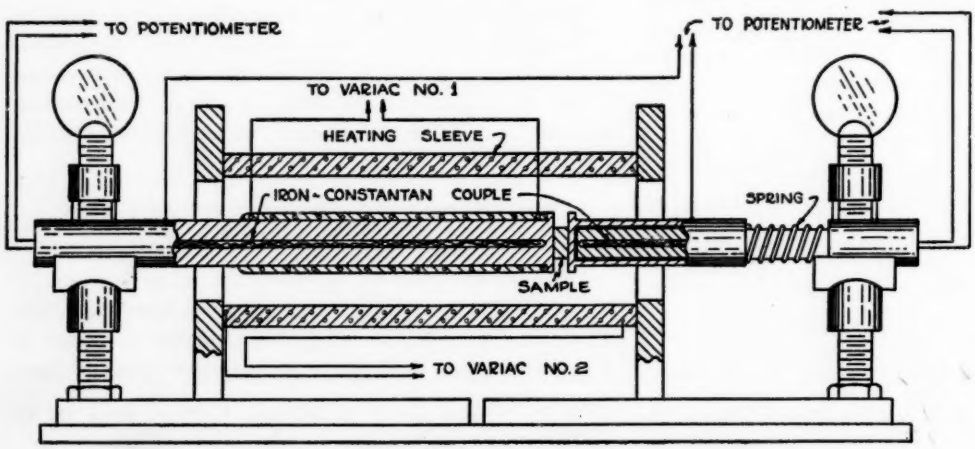

FIG. 1. Apparatus for electronic conductivity and thermal e.m.f. measurements above room temperature.

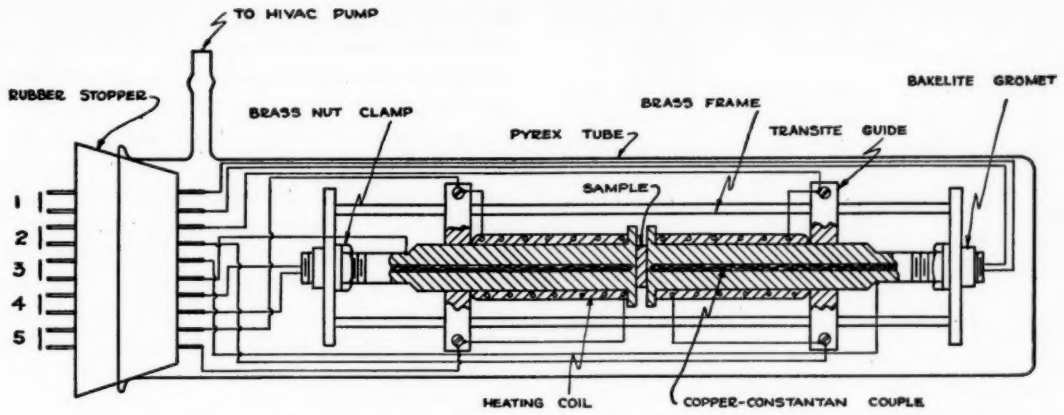

FIG. 2. Apparatus for electronic conductivity and thermal e.m.f. measurements below room temperature. 1—lower thermocouple; 2—lower heating coil; 3—thermal e.m.f. leads; 4—upper thermocouple; 5—upper heating coil.

explained by assuming that the number of impurity levels is greater than the number of electrons available and by considering the low and high temperature conditions when the number of conduction electrons is small and large, respectively, compared to the difference in numbers of impurity levels and available electrons.[3]

Representative conductivity data obtained below room temperature are shown in Fig. 5. It is surprising to note the conductance as great as 4.3×10^{-3} ohm^{-1} cm^{-1} at 113°K for ZnF_2. The distribution of apparent activation energies of the order of kT indicates the existence of a series of impurity levels close to the conduction band. Because the mean free path limited by lattice scattering increases with decreasing temperature,[4] the true activation energies dominating the conductivity at low temperatures are probably greater than the apparent activation energies obtained from Fig. 5. In the case of the ZnF_2:Mn ($P5A$), the activation energies are greater; namely, 0.07 to 0.25 ev. The variation of mean free path is not important for the phosphors because of impurity scattering.[5] For both substances, the electron traps reported by Johnson and Williams[6] from thermoluminescence data on ZnF_2:Mn are probably related to the donor levels.

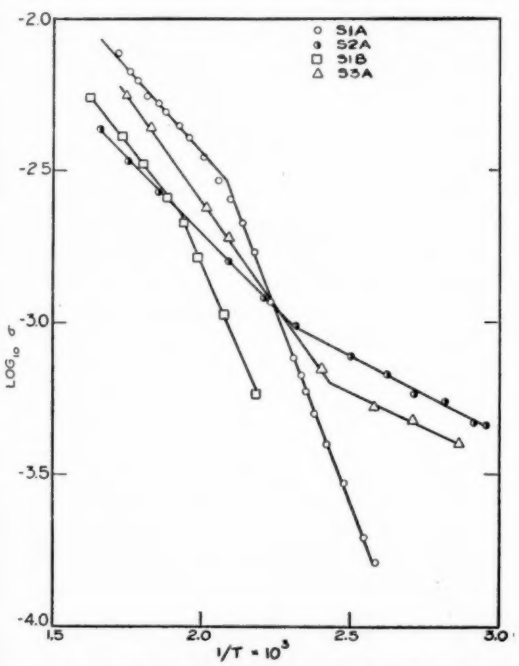

FIG. 3. Temperature dependence of conductivity above 25°C of typical ZnF_2 samples.

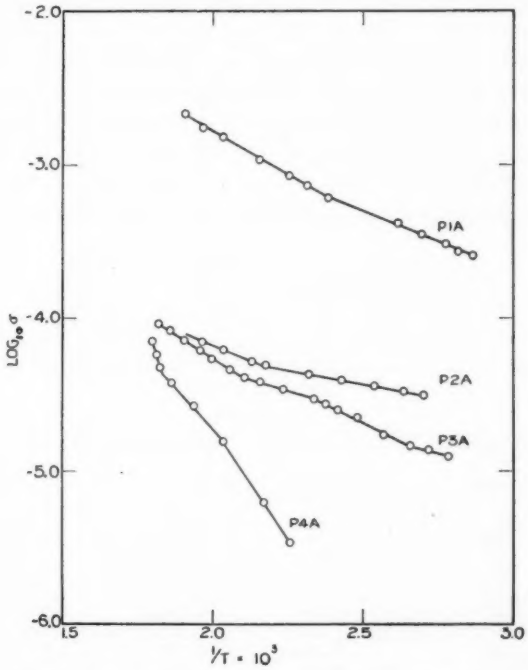

FIG. 4. Temperature dependence of conductivity above 25°C of typical ZnF_2 Mn phosphors.

[3] J. H. de Boer and W. C. van Geel, Physica **2**, 286 (1935); B. R. A. Nyboer, Proc. Phys. Soc. **51**, 575 (1939).

[4] H. Frohlich and N. F. Mott, Proc. Roy. Soc. **A171**, 496 (1939).

[5] E. Conwell and V. F. Weiskopf, Phys. Rev. **77**, 388 (1950).

[6] J. S. Johnson and F. E. Williams, J. Opt. Soc. Am. **39**, 709 (1949).

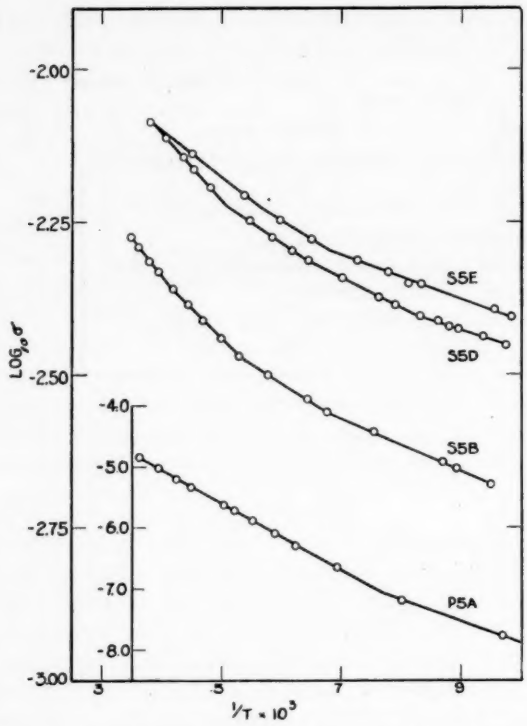

FIG. 5. Temperature dependence of conductivity below 25°C of typical ZnF_2 samples and of a typical ZnF_2:Mn phosphor. Note different $\log_{10}\sigma$-scale for phosphor data.

The results of thermal e.m.f. measurements on both ZnF_2 and ZnF_2:Mn for the high temperature range are shown in Fig. 6. Measurements from room to liquid air temperature gave curves of an analogous form. The absolute value of $d\theta/dT$ for ZnF_2 increases in a complicated manner with increasing temperature from a value of about 0.09 mv/deg. at −180° to about 0.23 mv/deg. at 350°C. This seems to be in contradiction to the simple theory of thermal e.m.f. in semiconductors:[7]

$$\frac{d\theta}{dT}=-\frac{k}{e}\left[2+\tfrac{1}{2}\ln\frac{2(2\pi m^*kT)^{\frac{3}{2}}}{n_b h^3}+\frac{\Delta E}{2kT}\right], \qquad (2)$$

when $-\Delta E/2eT$ is presumably the dominant term.

TABLE I.‖

Sample	E_1 (ev)	E_2 (ev)	$\sigma_{298°K}$ (ohm^{-1} cm^{-1})
S1A	0.22	0.50	2.1×10^{-6}
S1B	0.21	0.42	4.8×10^{-7}
S2A	0.18	0.095	3.1×10^{-4}
S3A	0.23	0.082	1.6×10^{-4}
S4A	0.139	0.091	4.3×10^{-4}
S5A	—	0.043	1×10^{-3}
P1A	0.22	0.156	1.1×10^{-4}
P1B	0.25	0.165	1.0×10^{-4}
P2A	0.152	0.078	1.8×10^{-5}
P3A	0.25	0.139	1.7×10^{-6}
P4A	0.27	0.57	10^{-8}

[7] R. H. Fowler, *Statistical Mechanics* (Cambridge University Press, London, 1936), second edition, Chapter XI.

However (2) applies only to a simple semiconductor with either donor or acceptor levels of uniform energy, whereas in the present case there exists a complicated equilibrium between a distribution of electron traps or impurity levels and the conduction band so that the activation energy effectively increases with increasing temperature.§ The discontinuities shown in Fig. 6 are probably due in some manner to transitions between processes governed by different values of ΔE, the energy gap between the impurity level and the conduction band. Except for additional discontinuities, the manganese activated materials behaved quite similarly to the pure ZnF_2, as regards their thermal e.m.f. even though their conductivities were quite different. From the negative sign of the thermal e.m.f. it is apparent that both materials are *N*-type.

THE HALL EFFECT

Considerable difficulty was encountered in attempts to measure the Hall effects of ZnF_2 because the residual or zero field e.m.f. across the Hall probes constantly fluctuated. These fluctuations, due to oscillations of potential gradient surfaces in the sample, were as large as 1 mv with most samples which is of the order of magnitude of the expected Hall e.m.f. After trying many samples prepared in a variety of ways, one sample,

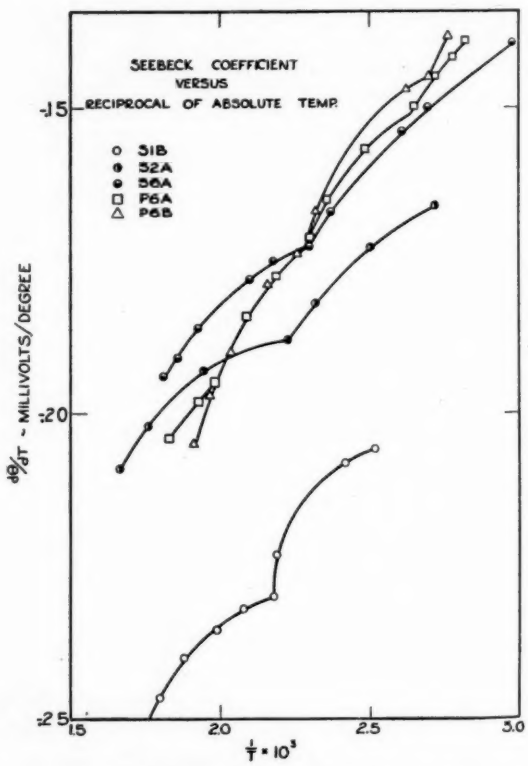

FIG. 6. Temperature dependence of thermal e.m.f. above 25°C of typical ZnF_2 and ZnF_2:Mn samples.

§ In private correspondence Professor K. Lark-Horovitz suggests the equation announced in the following: V. A. Johnson and K. Lark-Horovitz, Phys. Rev. 69, 259 (1946).

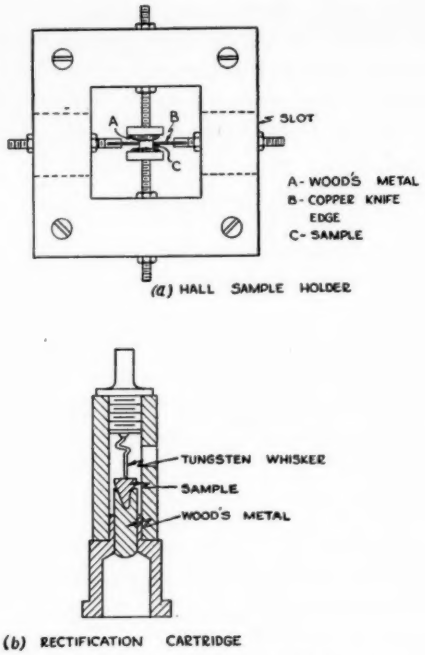

FIG. 7. Sample chambers for (a) Hall e.m.f. and (b) rectification measurements.

S5, was found in which the fluctuations were less than 0.1 mv. The following measurements were made on this sample.

A magnet capable of producing uniform fields up to 12,000 gauss with a gap between pole pieces of 1.5 cm was used. A calibration curve relating the field to the coil current was obtained with a G.E. fluxmeter. The sample was clamped in a special sample holder shown in Fig. 7(a). The ends of the sample through which the working current was passed were imbedded in Wood's metal to maintain optimum electrical contact. This method was found to be as effective as evaporated metal films. The Hall probes were copper knife edges. The working current was supplied from four $1\frac{1}{2}$-volt batteries connected in parallel for current stability. Because of the fluctuations of the residual e.m.f., the total transverse e.m.f. was measured as a function of field strength, a large number of readings being taken, and the ratio of the Hall e.m.f. to the magnetic field was obtained as the slope of the total transverse e.m.f. *vs.* magnetic field curve. In this manner the best straight line averaged out the effect of fluctuations, and also some idea of the accuracy of the method could be ascertained.

The Hall constant R_H is defined:

$$R_H = Vt/HI, \tag{3}$$

where t is the thickness of the sample, I is the current, H is the magnetic field, and V is the Hall voltage. For the sample S5, the value, accurate to within a factor of two, is -1.9×10^{-6} volt cm amp.$^{-1}$ gauss^{-1}. The negative sign of R_H demonstrates that ZnF_2 is N-type. Thus, from the relationship:[8]

$$R_H = 3\pi/8ne, \tag{4}$$

where R_H is expressed in e.m.u., the number of conduction electrons n is 3×10^{16} cm^{-3}. The mobility, given by the product of R_H and the specific conductivity σ, is approximately 10 cm^2 volt^{-1} sec.$^{-1}$ and on the assumptions that the electrons in the conduction band obey classical statistics and the mass is the same as the rest mass, the mean free path l is approximately 6.7×10^{-8} cm. All values are for 25°C.

Comparison of the above value of l with those of other ionic semiconductors at room temperature shows that the order of magnitude is correct. Engelhard[9] reports that for Cu_2O, $l=4\times10^{-7}$ cm, Fritsch[10] found for ZnO, $l=2.8\times10^{-8}$ to 2.2×10^{-7} cm, and for UO_2 Hartmann[11] has shown, $l=5.6\times10^{-8}$ cm.

RECTIFYING PROPERTIES

The theory[12] of crystal rectifiers shows that rectification does not become appreciable until the voltage across the contact is comparable with kT/e, 0.025 volt at 25°C. In practice, the high resistance contact is formed either by a thin "blocking layer" of high resistance or by a metal point contact. Both types of contacts

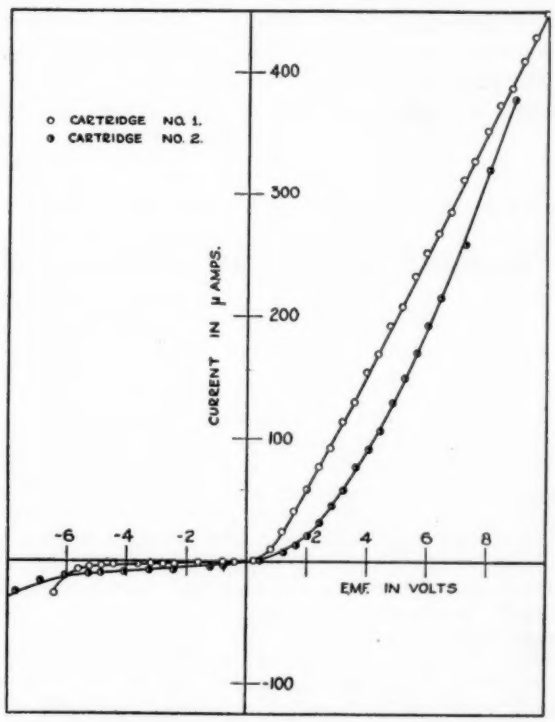

FIG. 8. Current-voltage characteristics of typical ZnF_2-tungsten point contacts.

[8] F. Seitz, *Modern Theory of Solids* (McGraw-Hill Book Company, Inc., New York, 1940), p. 68.
[9] E. Engelhard, Ann. d. Physik **17**, 501 (1933).
[10] O. Fritsch, Ann. d. Physik **22**, 375 (1935).
[11] W. Hartmann, Zeits. f. Physik **102**, 709 (1936).
[12] N. F. Mott and R. W. Gurney, *Electronic Processes in Ionic Crystals* (Oxford University Press, London, 1948), p. 176.

were used in preliminary qualitative measurements on ZnF_2. A layer of shellac about 10^{-4} cm thick on copper was used for the blocking layer contact and a steel needle was first used for the point contact method. Although rectification was readily apparent with both techniques, the forward-to-back current ratio was never greater than seven, and the measurements were complicated by current fluctuations and the contact "burned out" with moderate voltages.

Quantitative measurements were made by the point contact method. A number of 1*N*21 silicon rectifier cartridges were dismantled and the silicon wafer was replaced with a sample of ZnF_2 imbedded in Wood's metal. The surface of the sample was polished on 00 grade emery paper and contact was made with a tungsten cat whisker. This arrangement is shown in Fig. 7(b). Two representative d.c. characteristic curves are shown in Fig. 8. The resistance in the forward direction is smaller by a factor of 10 to 50 than that encountered in the other direction. In every case investigated the direction of easy electron flow was from the semiconductor to the metal, thus confirming that ZnF_2 is *N*-type.

A rather unusual effect was observed during the above experiment. When the current was in the forward direction, the initial value increased steadily for a period of a minute before a steady current was reached and the final value was about double the initial value of the current. If the polarity was suddenly reversed, the initial back current was high by at least a factor of two but fell to the expected value after about a minute. If the electric field was turned off for a short period before being applied in the reverse direction, the initial back current was constant at the expected value. This phenomenon probably results from Joule heating at the point of contact.

CONCLUSIONS

The above experiments show that ZnF_2 and its manganese activated phosphors are *N*-type impurity semiconductors. The conductivity of the fluoride is materially decreased by the addition of the manganese ion. This effect, other than that expected from the decrease of the mean free path which would not account for such a large effect, is due to a decrease in the number of electron donors, probably from oxidation by the manganese.

The thermal e.m.f. increases with increasing temperature in opposition to the behavior predicted from the simple theory. Though other disagreements have been reported,[13] an extensive theoretical analysis of the present case is necessary before any conclusion concerning agreement with theory can be made. Hall effect measurements show that the mean free path of ZnF_2 is comparable with those of other ionic semiconductors. ZnF_2 rectifies in the expected direction for an *N*-type impurity semiconductor.

[13] B. M. Hochberg and M. S. Sominskii, J. Exper. Theor. Phys. U.S.S.R. **7**, 1099 (1937); M. C. Anderson and J. S. Morton, Trans. Faraday Soc. **43**, 185 (1947).

THE JOURNAL OF CHEMICAL PHYSICS VOLUME 18, NUMBER 6 JUNE, 1950

Spectra of Rare Earths in Solutions Fluid at the Temperatures of Liquid Nitrogen*

SIMON FREED** AND C. J. HOCHANADEL
Oak Ridge National Laboratory, Oak Ridge, Tennessee
(Received February 23, 1950)

The solutions were prepared by first dissolving the salt in a solvent which is liquid at room temperature, such as *n*-propyl alcohol or di-*n*-propyl ether. Pairs of low melting hydrocarbons such as methane, propane, propylene, butene-1 and iso-pentane were then condensed into the solution after the temperature had been sufficiently reduced. A number of combinations gave solutions which were homogeneous and fluid at liquid nitrogen temperature. One of the solvents remained fluid to about five degrees below the freezing point of nitrogen.

Some hexahydrated rare earth nitrates and bromides were found to have solubilities at 77°K sufficient for obtaining spectra through light-paths of twenty-five centimeters. The spectra were comparable in sharpness with those from crystals of rare earths at low temperatures. Since the bands arising at room temperature were resolved into discrete lines at the low temperature, the possibility is open to investigate the symmetries and intensities of the electric fields about the positive ions in solution.

Corresponding groups in the spectra from the nitrates and bromides consisted of different numbers of lines of widely different spacing. In neodymium nitrate there was a marked transformation in the structure of the spectrum when the temperature of the solution was changed from 193°K to 77°K. At 77°K there was no change observed throughout nine days. The change with temperature was especially striking in the spectra of samarium bromide.

Electrical conductances of some of the solutions were measured at 193°K and 77°K. The magnitudes were very low and strongly dependent on viscosity.

IT was our aim to prepare solutions of salts and chelate compounds of the rare earths having rather low viscosity at the temperature of liquid nitrogen in the hope that the absorption bands would be resolved into lines and at the same time that there would be enough transformability among the various species that one or

* This document is based on work performed under Contract Number W-7405 eng 26 for the Atomic Energy Project at Oak Ridge National Laboratory.

** Present address: Brookhaven National Laboratory, Upton, New York.

only a few would survive at the low temperature and be measured by the spectra.

Trivalent europium ion Eu^{+++} seems to be the only one[1] whose salts in solution have spectra so sharp at room temperature that the usual bands are resolvable into lines. Since it is the number of lines within a group which is determined by the quantum character of the transition and the symmetry of the fields about the ions, a more general study of quantum transitions of ions in solutions required a search for those conditions under which solutions exhibited discrete spectra.

In the past, efforts to obtain solvents fluid at low temperatures consisted in mixing at room temperature substances having low freezing points which together had a "freezing point" lower than any of the single or pairs, etc., of the component liquids. Solvent properties had, of course, to be kept in mind. For example, G. N. Lewis and his associates[2] employed a mixture of ether, isopentane and ethanol to keep substances such as dyes and leuco-bases in solution near the temperature of liquid air. However, at that temperature the mixtures became rigid.

To synthesize our solutions,[3] the first step was to dissolve the salt near room temperature rather than at low temperatures so that the rate of solution would not be extremely slow; further dilution with solvents of low melting points proceeded quickly at much lower temperatures than did the initial solution of the salt. *N*-propyl alcohol, *n*-butyl alcohol, or *n*-propyl ether served as the initial solvent, and for the dilution, pairs of the following hydrocarbons were used in various proportions—methane, propane, propene, butene-1, and isopentane.

The apparatus, as shown in Fig. 1, consisted of a Dewar flask *D* containing a mixing vessel *M* which was connected with a 3-mm capillary optical tube *O*, provided at its ends with windows W_1 and W_2 of corex *D* glass. Clouding of the outer surfaces of these windows by condensation was prevented by the evacuated tubes terminated by windows W_3 and W_4.

The procedure for preparing a solution and measuring the spectrum can be described by a typical experiment:

TABLE I.

Spectral region	Temperature	Solution	Approx. no. of lines	Spread
5200A	193°K	$Nd(NO_3)_3 \cdot 6H_2O$	4 diffuse	60A
	77°	$Nd(NO_3)_3 \cdot 6H_2O$	10 sharp	100
	77°	$NdBr_3 \cdot 6H_2O$	10 sharp	90
5000A	193°	$Nd(NO_3)_3 \cdot 6H_2O$	structureless blur	
	77°	$Nd(NO_3)_3 \cdot 6H_2O$	4 or 5 sharp	40
	77°	$NdBr_3 \cdot 6H_2O$	7 sharp	100

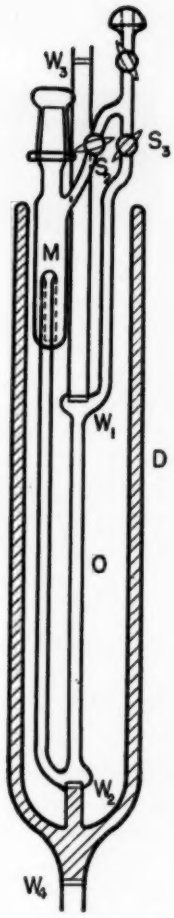

FIG. 1. Dewar assembly containing the optical absorption tube and the vessel for preparing solutions.

20 mg of pure neodymium bromide hexahydrate ($NdBr_3 \cdot 6H_2O$) was introduced into the mixing vessel and the system evacuated. After cooling tube *M* to about −20°C, using a jet of cooled nitrogen gas, 0.8 ml of previously purified *n*-propyl alcohol was distilled onto the salt through stopcock S_2. After the salt had dissolved (this could be speeded by allowing the tube to warm by bubbling helium through the solution via stopcock S_3), the tube was further cooled to about −90°C, and propane and propylene were successively bubbled through the solution (through stopcock S_3) until about 4 ml of each liquid was present in solution. The hydrocarbons used were either Phillips research grade or pure grade materials introduced into the vacuum system directly from the gas cylinders. The resulting solution, about 0.005 molar, was siphoned into the optical tube by cooling the latter to a temperature below that of mixing tube *M*. The liquid coolant was then added to the Dewar. At times, helium gas was used to transfer the solution from one tube to another while at the temperature of liquid nitrogen. However, the solubility of helium in the solution at this temperature led to complications in some measurements.

The resulting solution remained clear for nine days at the low temperature, and its spectrum continued unchanged. There is evidence that some transformations

[1] For a review of previous work, Simon Freed, Rev. Mod. Phys. 14, 105 (1942). There are indications that the salts of americium ion have spectra comparable in sharpness with those of trivalent europium. Simon Freed and Fred J. Leitz, Jr., J. Chem. Phys. 17, 540 (1949).

[2] Lewis, Magel, and Lipkin, J. Am. Chem. Soc. 62, 2973 (1940).

[3] S. Freed and C. J. Hochanadel, J. Chem. Phys. 17, 664 (1949).

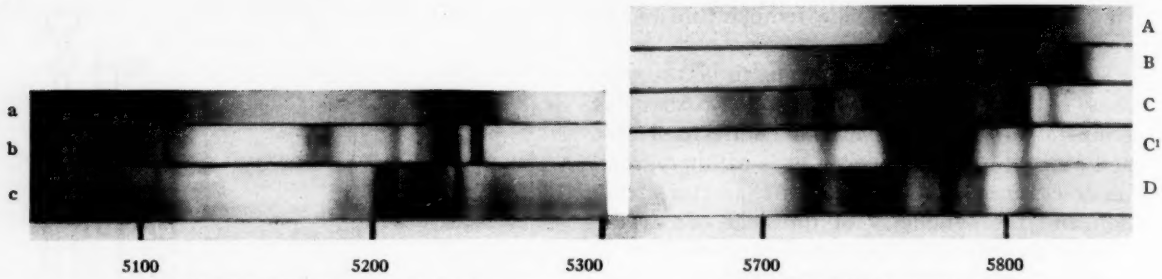

a. $Nd(NO_3)_3 \cdot 6H_2O$ in solution at 193°K
b. $Nd(NO_3)_3 \cdot 6H_2O$ in solution at 77°
c. $NdBr_3 \cdot 6H_2O$ in solution at 77°

A. $Nd(NO_3) \cdot 6H_2O$ in solution at 298°K
B. $Nd(NO_3) \cdot 6H_2O$ in solution at 193°
C. $Nd(NO_3) \cdot 6H_2O$ in solution at 77°
C¹. $Nd(NO_3) \cdot 6H_2O$ in solution at 77° (different exposure time)
D. $NdBr_3 \cdot 6H_2O$ in solution at 77°

FIG. 2. Absorption spectra of solutions of salts at low temperatures. Solvent consisted of *n*-propyl alcohol, 10 parts by volume, liquid propane, 45 parts, and liquid propene, 45 parts. Concentrations about 0.005 M.

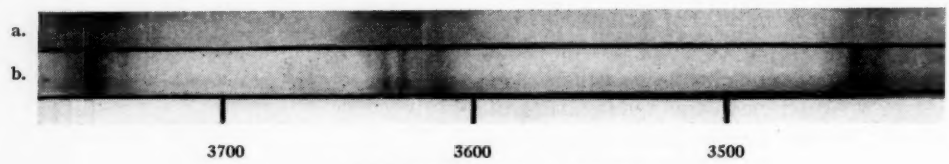

a. $SmBr_3 \cdot 6H_2O$ in solution at 193°K
b. $SmBr_3 \cdot 6H_2O$ in solution at 77°

FIG. 3. Absorption spectra of solutions of salts at low temperatures. Solvent consisted of *n*-propyl alcohol, 10 parts by volume, liquid propane, 45 parts, and liquid propene, 45 parts. Concentrations about 0.005 M.

occur at these temperatures. A solution of europium nitrate hexahydrate gave a clear solution at 193°K (temperature of "dry ice") which became turbid on being cooled to 77°K. However, on increasing the quantity of solvent by one-fourth, the solution remained clear at 77°K and gave a satisfactory spectrum through the twenty-five centimeters of light path.

A test was carried out with the solvent (10 percent propyl alcohol, 45 percent propane, 45 percent propene) to find out at what temperature it ceased to be fluid. It was found still fluid at 58°K, about five degrees below the freezing point of nitrogen.

The spectra from the solutions at low temperatures were so sharp that all spectra were taken at rather high dispersion, on a twenty-one foot Jarrel-Ash grating spectrograph in Wadsworth mounting having a dispersion of 5A/mm in the first order.

The spectra of solutions of neodymium nitrate hexahydrate and of neodymium bromide hexahydrate at 77°K consisted of groups of lines, in some instances as sharp as 1A, but for most part, they varied from 2A to 6A. At 193°K, the lines were broader, and some regions were diffuse. These were gathered up into lines at the lower temperature, and thus the general change which the lower temperature brought about was the appearance of an increased number of lines (see Fig. 2).

Neodymium bromide hexahydrate in solution had groups of lines in the same wave-length regions as the nitrate, but the structures of the groups were strikingly different. Even when the numbers of component lines within a group were the same, the intensity distribution and the spacings differed widely (see Fig. 2). Table I is an illustration of differences in the spectra of solutions of neodymium nitrate hexahydrate and of neodymium bromide hexahydrate in the solvent whose composition was previously given.

The spectrum of samarium bromide hexahydrate in the same solvent underwent great refinement when the temperature of the solution was reduced from 193°K to 77°K. See Fig. 3.

Europium bromide hexahydrate in solution possessed absorption lines of extreme sharpness at 77°K as was to be anticipated. The group at 4600A consisted of four lines, two of which in the middle were separated by about one-half angstrom. The general appearance of this group resembled the four lines in the aqueous solution of europium chloride at room temperature. (See the review cited in reference 1.) In the same way, this group in the spectrum of the nitrate hexahydrate at 77°K closely resembled the three lines arising from aqueous solution of the nitrate at room temperature. This group has been identified as a transition from $J=0$ to $J=3$ with a maximum of seven lines. The appearance of only four or three lines indicates that there is only one species of europium ion Eu^{+++} present in solution rather than a mixture of configurations.

The electrical conductances of the solutions was measured at 193°K and 77°K and were found sensitive to temperature and viscosity. The values were very low, of the order of 10^{-11} mhos for the specific conductance at 77°K.

We are much indebted to Dr. Fred J. Leitz, Jr. for his collaboration in the design of apparatus and the earlier experimental work.

Chemical Kinetics of Bromine Following Neutron Capture*

RUSSELL R. WILLIAMS, JR. AND WILLIAM H. HAMILL
University of Notre Dame,† Notre Dame, Indiana

(Received October 3, 1949)

The kinetic behavior of Br^{80} produced by neutron capture has been investigated in gaseous systems containing ethyl bromide, ethylene and hydrogen bromide. The distribution of active bromine between organic and inorganic form has been shown to be principally dependent on the ethylene pressure. A kinetic scheme, incorporating a "hot atom" reaction, is postulated and shown to be in agreement with the experimental facts. Additional experimental tests of critical points in the proposed scheme have been successful.

INTRODUCTION

THE capture of a thermal neutron by a stable nucleus is exoergic by approximately 8 Mev (1.8×10^8 kcal./mole) for most elements. This energy is evolved largely by the emission of one or more energetic quanta of gamma-radiation, although recent physical and chemical evidence[1] indicates that internal conversion occurs in some of these transitions. The great likelihood of chemical bond rupture in either case has been the subject of much discussion and experimentation[2,3] with considerable emphasis on the reactivity of the "hot" (high velocity) atom which must result from the gamma-recoil.

In 1939 Suess[4] investigated the kinetics of the bromine atoms produced by neutron capture in two gaseous systems: ethyl bromide with small proportions of acetylene and hydrogen bromide, and hydrogen bromide with a small proportion of acetylene. In these systems he assumed that the activated bromine atoms were consumed by two competing reactions: exchange with hydrogen bromide or addition to the unsaturated compound. In the former case the radioactive bromine appears in inorganic form, while in the latter case it returns to an organic form. A kinetic expression for the variation of this partition with concentration of various reagents is given below.

TABLE I. Bromine activities.

Stable isotope	Capture cross section	Half-life	Activity Decay
Br^{79}	3.05×10^{-24} cm²	4.4 hr.	Isomeric transition
Br^{79}	8.9×10^{-24} cm²	18 min.	β^-, 2.0 Mev (β^+, K-capture, minor)
Br^{81}	2.25×10^{-24} cm²	34 hr.	β^-

The present experiments represent an extension of the earlier work, except that ethylene rather than acetylene is used as the unsaturated reagent. By use of a more intense neutron source we have been able to examine the phenomena over a wider range of conditions and to test quantitatively various qualitative proposals made by Suess.

APPARATUS AND PROCEDURES

The neutron source used in these experiments consisted of 300 mg of radium intimately mixed with beryllium and contained in a cylindrical stainless steel capsule $\frac{1}{2}\times2$ in. Paraffin wax in and around the reaction vessel (see Fig. 1) served as a moderator to reduce the neutrons to thermal energies.

Three activities are produced in bromine by thermal neutron capture. Their characteristics are indicated in Table I. In the present experiments, bombardments were limited to 15 min. and activity determinations were completed approximately 10 min. after the end of bombardment. Since the radiations associated with 4.4-hr. Br^{80*} are detected with efficiencies of one percent or less in our counting arrangement, this nuclide is detected only through its daughter, 18-min. Br^{80}. Application of the usual radioactive rate laws indicates that approximately 97 percent of the observed activity is due to 18-min. Br^{80} formed directly rather than by formation and decay of Br^{80*}.

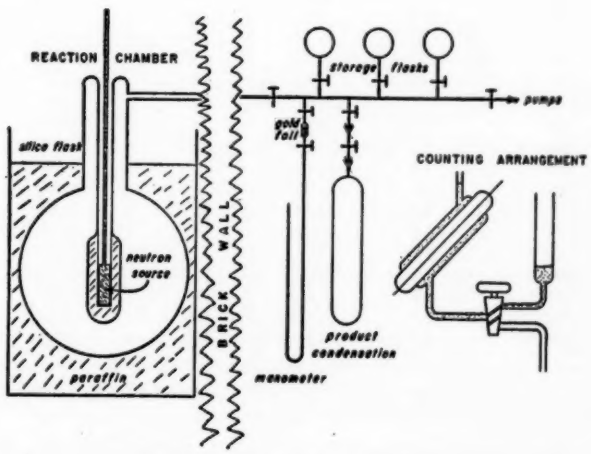

FIG. 1. Arrangement of apparatus.

* Presented at the 115th meeting of the American Chemical Society, San Francisco (March, 1949).

† A contribution from the Radiation Chemistry Project, originally operated under Department of the Navy, ONR Contract 165 Task Order II, now operated under AEC Contract At(11-1)-38.

[1] S. Wexler and T. H. Davies, Conference on Hot Atom Chemistry, Brookhaven National Laboratories (August 19–20, 1948).
[2] W. F. Libby, J. Am. Chem. Soc. **69**, 2523 (1947).
[3] Willard, J. Phys. Colloid Chem. **52**, 585 (1948).
[4] H. Suess, Zeits. f. physik. Chemie **B45**, 297, 312 (1939).

TABLE II. Experimental data.

Experiment No.	Pressure of C_2H_5Br (mm Hg)	Pressure of C_2H_4 (mm Hg)	Pressure of HBr (mm Hg)	ρ
21	303	28.9	18.7	0.802[a]
22	303	29.1	18.5	0.748[b]
23	303	29.5	18.5	0.727[b]
24	304	29.5	18.9	0.716[b]
25	298	29.5	18.9	0.690[b]
26	294	29.2	59.2	0.649[b]
28	240	29.5	96.	0.685[b]
29	263	29.4	60.0	0.690
33	202	28.5	19.5	0.790
34	351	28.6	19.0	0.758
35	202	28.4	18.8	0.758
36	302	28.4	19.5	0.767
37	302	29.1	50.3	0.757
38	272	29.4	134.5	0.798
39	311	55.4	18.7	0.470
40	263	145.3	18.7	0.315
41	278	116.0	18.5	0.297
42	293	91.3	19.4	0.317
43	264	142.7	18.6	0.277
44	255	145.7	18.8	0.259
45–1	201	—	(Wash only)	0.535[c]
45–2	203	—	(Wash only)	0.44[c]
46–1	198	38	(Wash only)	2.25[c]
46–2	205	38	(Wash only)	2.28[c]
47–1	201	—	15.6	9.90
47–2	203	—	43	10.0
48	210	—	15.3	11.0[d]
49–1	197	—	203	30
49–2	342	—	10.5	4.50
50	190	—	123	7.3
51	201	—	61	12.0
53	185	—	130	18.2
54	217	—	137	32.3
55	201	—	14.8	13.5
56	137	—	17.0	16.3
57	199	—	16.1	17.6
58	206	—	16.8	23.0
66	204	29.7	16.4	0.705
67	204	34.2	27.2	0.506
68	178	28.2	29.6	0.538
71	8	24.7	164	0.897
73	15	50.5	151	0.598
74	10	14.4	178	1.53
75	9	23.5	180	1.12
76	9	38.6	190	0.695
77	9	103.4	178	0.440
78	8	69.5	183	0.559
79	9	73.0	336	0.597
80	12	53.2	338	0.738
81	8	148.0	148	0.354
82	8	28.7	332	1.047
83	12	81.0	330	0.562
84	13	13.8	340	1.09
85	13	121.8	180	0.366
86	13	119.0	336	0.443
87	14	137.0	334	0.500
88	14	136.0	187	0.382
89	16	140.0	334	0.417
90	16	136.0	187	0.369
91	7	4.3	201	4.68
92	12	4.2	179	4.91
93	12	4.34	339	0.548

[a] Air added. [b] Oxygen added. [c] See text. [d] Illuminated with ultraviolet light during neutron bombardment.

The apparatus used in this work is indicated in Fig. 1. The reaction vessel consisted of a 1.5-liter silica flask, with a re-entry in the neck for insertion of the neutron source. Additional paraffin was used around the flask for further moderation and reflection of neutrons. The reaction vessel was connected to a vacuum system containing pumps, reagent storage flasks, and a mercury manometer protected by a gold foil trap to exclude mercury from the system. A large (500 ml) product condensation vessel served as the receiver for the organic-inorganic mixture after bombardment.

Activity analysis was performed in a liquid sample Geiger counter with a wall thickness of about 30 mg/sq. cm. The liquid samples were delivered to the counter through a microseparatory funnel and occupied an annular space about the counter with a volume of a few cubic centimeters. The electronic circuit used to operate the Geiger counter was a Higinbotham-type scale-of-64 with the customary high voltage, recording, and timing apparatus.

The gaseous reagents were measured into the reaction chamber by direct pressure measurement or by expansion from a calibrated volume. After sufficient time for thorough mixing by diffusion and convection, the neutron source was inserted in the central position for exactly 15 min. During this exposure period the condensation flask, containing a few cubic centimeters of water and of ethyl bromide (carefully measured) at liquid air temperature, was evacuated to prepare for condensation of the reaction products.

At the end of the bombardment period, the reaction vessel was opened to the condensation vessel, where the reaction products condensed at liquid air temperature. This vessel was closed, removed from the vacuum system, and warmed to room temperature. Since hydrogen bromide and ethylene volatilize at a lower temperature than that at which water and ethyl bromide liquefy, the volume of the condensation vessel must be large enough to avoid excessive pressure during the warming process. When room temperature was reached the condensation vessel contained a few cubic centimeters each of ethyl bromide and aqueous hydrogen bromide and the bromine activity associated with each compound.

The two-liquid mixture obtained was pipetted into the microseparatory funnel where the ethyl bromide was usually the lower layer. A portion of each layer was admitted to the counting chamber for activity analysis. Since the counting chamber was completely filled for each determination, the ratio of observed count rates, each multiplied by the total volume of the phase, represents the ratio of activities in the two phases. Corrections for any density variations in the phases and for decay of 18-min. activity were applied to all analyses.

EXPERIMENTAL RESULTS

The experiments summarized in Table II illustrate the partition of active bromine between organic and inorganic forms under various conditions. In all experi-

ments the sum of the count rates in the two phases was approximately 1000 counts/min. and the activity of each phase was normally observed over a period of 2 to 5 min. The temperature of the reacting gases was that of the room (approximately 22°C) in all cases.

Experiments 21–38 were performed to determine the sensitivity of the ratio of inorganic to organic activity (hereafter designated by ρ) to variations in certain experimental conditions. It is evident that the presence of oxygen does not affect ρ appreciably and that moderate variations in the pressures of ethyl bromide and hydrogen bromide are similarly ineffective. Later experiments show, however, that large changes in the ratio of these two reagents alter ρ appreciably. The reproducibility of this group of experiments (average deviation = five percent) is considered typical.

Preliminary experiments demonstrated that when hydrogen bromide was not present in the reaction vessel appreciable activity remained after the gases were withdrawn. This was demonstrated by subsequent admission of hydrogen bromide, which acquired activity, presumably by exchange with active bromide deposited on the walls of the reaction vessel. A few millimeters pressure of hydrogen bromide used in this "washing" technique sufficed to remove activity and subsequent washes were inactive. This efficiency in removal leads us to believe that "wall effects" cannot be serious in mixtures containing hydrogen bromide. Furthermore, the independence of ρ upon hydrogen bromide pressure (shown in experiments 21–38) was substantially confirmed at pressures as low as 5 mm. Only in experiments 45-1–46-2 are "wall effects" considered important and in these cases the inorganic activity may have consisted in part of atomic or molecular forms on the walls of the reaction vessel.

Experiments 39–44 and 66–68 explore the variation in ρ with changing ethylene pressure P. It is found that these data may be described by a linear equation of the type

$$\rho P = aP + b$$

where a and b are constants. This behavior is illustrated in Fig. 2. In experiments 71–93 the ethylene dependence is again explored, but in these cases the target compound is hydrogen bromide rather than ethyl bromide, that is, the active bromine originates largely in the former substance since it contains most of the stable bromine present in the system. A small amount of ethyl bromide was added to the reaction mixture to act as carrier for active organic bromide. A similar dependence upon ethylene pressure is observed (see Fig. 2) although the values of the constants a and b are different. There is also a small, but definite dependence on the hydrogen bromide pressure. The experiments fall into two groups, one of which has a hydrogen bromide pressure of approximately 180 mm and the other a pressure of approximately 330 mm. For these two groups the values of a (slope) are equal, but the values of b (intercept) differ. Table III summarizes the characteristics of these curves as determined by least-square treatment.

Experiments 47–58 show the presence of a small amount of organic activity even when large amounts of hydrogen bromide and no ethylene are present during the bombardment. The large variations in ρ observed in some of these experiments performed under nearly identical conditions are due in part to the extreme inequality of the partition between the two forms. The organic activity in these experiments was sometimes less than 100 counts/min. No quantitative interpretation of this behavior has been attempted.

Experiment 48, in which the reaction vessel was illuminated with an intense mercury resonance lamp during neutron bombardment, was designed to observe the effect of a large change in the concentration of organic radicals and atoms. Such particles, produced by the gamma radiation from the neutron source and in much larger quantities by the ultraviolet light, do not appear to affect the activity distribution.

DISCUSSION

The essential features of one reaction mechanism capable of yielding the observed functional form of the activity partition were stated originally by Suess[4] and treated formally by us in a preliminary communication.[6] While the experimental data obtained by Suess were not sufficiently precise to permit a test of these kinetic postulates our preliminary experiments indicated the validity of the form $\rho P = aP + b$. The values of slope and intercept obtained in the earlier work are distinctly different from those reported here, but this may be largely attributed to more careful attention to experimental conditions and to various corrections for concentrations and counting in the present work.

Reaction mechanisms proposed for this system must account for two major experimental facts: (1) the lack of hydrogen bromide dependence with ethyl bromide

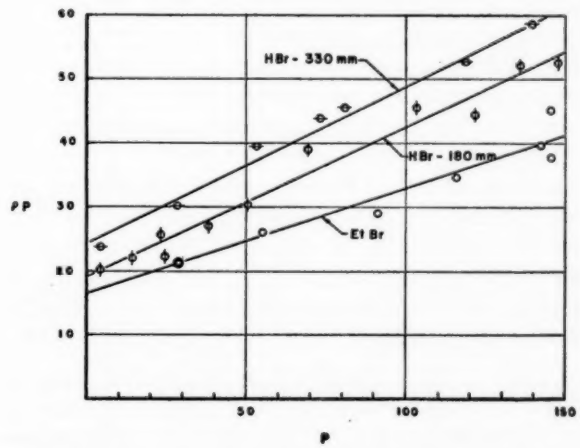

FIG. 2. Ethylene dependence of activity partition.

[6] W. H. Hamill and R. R. Williams, J. Chem. Phys. **16**, 1171 (1948).

target (and the minor dependence with hydrogen bromide target) and (2) the fact that the fraction of organic activity does not approach unity at high ethylene pressures. The fraction of inorganic activity at infinite ethylene pressure is given by the slopes (see Table III) of the lines in Fig. 2.

The lack of dependence on hydrogen bromide pressure means either that this reagent is not directly involved in a rate-determining process or that it is equally involved in the production of both inorganic and organic activity. In view of the efficiency of this reagent in fixing activity in inorganic form both during (experiments 47–58) and after (experiments 45 and 46) bombardment the former explanation is rejected and the exchange of active bromine atoms with hydrogen bromide is considered an important reaction [reaction (3) below]. On this basis the rate of formation of inorganic activities is proportional to the hydrogen bromide concentration. The corresponding process leading to organic activity is described by reaction (6). Provided we assume that the specific rate of dissociation of the radical $C_2H_4Br^*$ is much greater than the specific rate of fixation [$k_5 \gg k_6(\mathrm{HBr})$], then the rate of formation of organic activity is also proportional to the hydrogen bromide concentration.

The failure to approach 100 percent organic activity at high ethylene pressures may also be accounted for in at least two ways. Suess[4] proposed that hydrogen bromide might undergo an exchange reaction with the radical $C_2H_4Br^*$ thus:

$$C_2H_4Br^*+HBr\rightarrow C_2H_4Br+HBr^*$$

yielding inorganic activity. This process would compete with reaction (6) and divert a constant proportion of the active bromine to inorganic form even at high ethylene pressures. Alternatively, we propose a reaction which depends for its efficiency upon the unique manner of formation of bromine atoms and which has been capable of independent experimental verification (see below). The bromine particles initially liberated by the neutron-capture process have very great kinetic energy. During the early collisions of these "hot atoms" with the molecules of the system processes may occur whose rates are normally insignificant at room temperature. We propose that a certain proportion of the "hot atoms" will pick up a hydrogen atom from some molecule in the system and thus become inorganic activity [reaction (2a)] while the remainder are moderated to thermal velocities [reaction (2)] and react according to reactions (3)–(6). This proposal amounts to the diversion of a fixed fraction of the bromine activity irrespective of the ethylene and hydrogen bromide concentrations and is represented by reaction (2a).[7]

TABLE III. Characteristics of ethylene dependence (see Fig. 2).

Target substance	Slope (a)	Intercept (b)
C_2H_5Br	0.15	17
HBr (180 mm)	0.23	19
HBr (330 mm)	0.24	24

The reactions proposed above are presented here:

$$\text{either}\quad \left\{\begin{array}{l} C_2H_5Br+\text{neutron}\xrightarrow{k_1}\mathbf{Br^*}+\text{fragments} \\ \text{or} \\ HBr+\text{neutron}\xrightarrow{k_1}\mathbf{Br^*}+H \end{array}\right. \qquad (1)$$

$$\mathbf{Br^*}+RH\xrightarrow{k_2}Br^*+RH \qquad (2)$$

$$\mathbf{Br^*}+RH\xrightarrow{k_{2a}}\underline{HBr}^*+R \qquad (2a)$$

$$Br^*+HBr\xrightarrow{k_3}\underline{HBr}^*+Br \qquad (3)$$

$$Br^*+C_2H_4\underset{k_5}{\overset{k_4}{\rightleftharpoons}}C_2H_4Br^* \qquad (4)\text{ and }(5)$$

$$C_2H_4Br^*+HBr\xrightarrow{k_6}\underline{C_2H_5Br}^*+Br. \qquad (6)$$

The asterisk refers to active bromine and the bold-face type indicates a "hot atom." The ultimate inorganic and organic forms are underlined. Since in the macroscopic sense the concentrations of the reagents do not change during the course of the experiment we may divide the rate of formation of HBr*, given by

$$[d(\mathrm{HBr}^*)]/dt=k_{2a}(\mathbf{Br^*})(RH)+k_3(Br^*)(HBr)$$

by the rate of formation of $C_2H_5Br^*$, given by

$$[d(C_2H_5Br^*)]/dt=k_6(C_2H_4Br^*)(HBr).$$

Applying steady-state treatment to the concentrations of **Br***, Br*, and $C_2H_4Br^*$, the following expression may be obtained without further approximation where P is the ethylene pressure.

$$\rho P=\frac{k_3}{k_4}\left[\frac{k_5+k_6(HBr)}{k_6}\right]\left[1+\frac{k_{2a}}{k_2}\right]+\frac{k_{2a}}{k_2}P$$

Finally, if $k_5 \gg k_6(HBr)$ then the expression reduces to the form

$$\rho P=\frac{k_3k_5}{k_4k_6}\left(1+\frac{k_{2a}}{k_2}\right)+\frac{k_{2a}}{k_2}P$$

which corresponds to the experimental observations.

The most obvious result obtained by correlation of these expressions with the experimental observations is the value of k_{2a}/k_2, which is given by the slopes of the lines in Fig. 2. In the systems containing largely ethyl bromide this value is 0.15, while in systems containing largely hydrogen bromide the value is 0.23–0.24, indicating a larger proportion of hot atom reactions in the

[7] More detailed consideration of the proposed "hot atom" reaction is being undertaken by Dr. John L. Magee and will be subsequently published in this Journal.

latter case. A corresponding, but much smaller, change in intercepts is to be expected. From the change in slopes, a change of approximately five percent in intercepts would be predicted. This is too small to be quantitatively verified with the present data.

We wish to point out that in the case of neutron capture by hydrogen bromide, the proposal of a "hot atom reaction" forming hydrogen bromide at a rate independent of the ethylene pressure is experimentally indistinguishable from a failure to rupture the H—Br bond in the initial act. The latter possibility was pointed out by Suess[4] who showed that a maximum of only 1/80 of the gamma-recoil energy appears as internal energy (vibration and rotation) of the hydrogen bromide molecule. The remainder is present as translational energy of the whole molecule. Subsequent collisions would be likely to bring about dissociation, but the possibility remains that some unknown fraction of the activated hydrogen bromide molecules may not dissociate. One might attribute the difference in k_{2a}/k_2 between ethyl bromide and hydrogen bromide to this effect and in this event would conclude that the H—Br bond fails to rupture in approximately seven percent of the cases. Further experiments to test this point are now in progress.

The distinct difference in intercepts between the two series of experiments using hydrogen bromide at different pressures is probably due to the neglected hydrogen bromide term. While the term k_6(HBr) is apparently negligible at the low pressures used with the ethyl bromide target experiments, it seems to be of some small significance at higher pressures of hydrogen bromide. We do not have sufficient data to test this term quantitatively. On the basis of the scheme given we may, however, compute an approximate value of k_5/k_6 from the change in intercepts between the two series of hydrogen bromide experiments. Using the more precise form of the equation for ethylene dependence, we have

$$\frac{k_5+k_6(180)}{k_5+k_6(330)}=\frac{19}{24}$$

$$\frac{k_5}{k_6}\approx 400 \text{ mm.}$$

Using a value of 10^{13} sec.$^{-1}$ for the frequency factor of the quasiunimolecular radical dissociation (5) and a value of 10^6 mm^{-1} sec.$^{-1}$ for the frequency factor of the bimolecular reaction, we may estimate the difference in activation energies for reactions (5) and (6) as

$$\frac{k_5}{k_6}=\frac{10^{13}}{10^6}\exp\frac{-(E_5-E_6)}{RT}$$

from which we may estimate that

$$E_5-E_6\approx 5 \text{ kcal./mole.}$$

This is not incompatible with the results of Schmitz, Schumacher, and Jager,[8] who studied the photobromination of ethylene. They were able to deduce a value for the difference in activation energies for the reactions

$$C_2H_4Br\rightarrow C_2H_4+Br \qquad (5)$$

$$C_2H_4Br+Br_2\rightarrow C_2H_4Br_2+Br \qquad (6')$$

and found

$$E_5-E_6'=6.1 \text{ kcal./mole.}$$

We may further obtain an approximate ratio of the rate constants k_3 and k_4 by noting that the intercept of all lines in Fig. 2 has a value of approximately 20. Since k_{2a}/k_2 is small in comparison to unity, we may substitute in the expression for ρP and obtain

$$k_3/k_4\approx 0.05.$$

If this difference in rate constants were attributed entirely to a difference in activation energies for reactions (3) and (4) we would obtain

$$E_3-E_4\approx 2 \text{ kcal./mole.}$$

ADDITIONAL EXPERIMENTAL TESTS

The "hot atom" hypothesis proposed in the preceding section to account for the independent formation of a small amount of active hydrogen bromide suggests an experimental test consisting of dilution of the reaction mixture with a chemically inert substance. This should consequently reduce the yield of inorganic activity. Four experiments of this type are described in Table IV and compared with similar experiments in the absence of the inert gas, which was argon. In each case there was observed a decrease in the fraction of inorganic activity, in qualitative confirmation of the "hot atom" hypothesis.

The assumption that the radical C_2H_4Br dissociates more rapidly than it is fixed by hydrogen bromide suggested experiments with olefins which could register such a sequence through the possibility of isotopic exchange. The allylic and vinylic bromides may, upon addition of bromine atoms, form radicals in which two bromine atoms occupy equivalent positions, as shown below in the case of α,β-dibromoethylene.

$$\begin{array}{c} H\ H \\ Br^*+C=C \\ Br\ Br \end{array} \rightarrow \begin{array}{c} H\ H \\ Br^*C-C\cdot \\ Br\ Br \end{array} \rightarrow \begin{array}{c} H\ H \\ C=C+Br. \\ Br^*\ Br \end{array}$$

Dissociation of the radical may leave the radioactive bromine in the bromo-olefin, but if fixation by hydrogen bromide is rapid, the radioactive form will be the addition product 1,1.2-tribromoethane.

Small pressures of α,β-dibromoethylene were added to reaction mixtures similar to those described in Table II. After neutron bombardment, the activity

[8] Schmitz, Schumacher, and Jager, Zeits. f. physik. Chemie **B51**, 281 (1942).

TABLE IV. Effect of argon on the activity partition.

C_2H_4 (P in mm Hg)	(P in mm Hg)	ρ Observed	ρ Calculated without A
26	460	0.47	0.82
28.2	526	0.54	0.79
34.2	532	0.52	0.68
45	478	0.28	0.54
Ethyl bromide = 200 mm Hg		Hydrogen bromide = 30–50 mm Hg	

distribution ρ was determined in the usual fashion. Table V describes these experiments.

The presumption that the organic activity obtained through use of the bromo-olefin was due to exchange rather than addition was confirmed in two experiments using 300 mm hydrogen bromide, 10 mm of the bromo-olefin and 1 mm of its addition product as the mixture for neutron bombardment. The two organic substances, with added carrier, were partially separated by distillation and the activity of each was measured. Using a density analysis to determine the composition of each fraction, it was determined that the tribromoethane activity constituted 0 ± 5 and 5 ± 5 percent of the organic activity in these experiments. These results confirm the presumption that the bromo-olefine exchanges efficiently with atomic bromine.

α,β-dibromoethylene appears to be an extremely efficient reagent for atomic bromine, since the yield of organic activity does not increase significantly after the pressure of the reagent reaches 5 mm in the case of hydrogen bromide "target." Similar results are found with allyl bromide and 2-bromopropene. We conclude that a few millimeters pressure of the bromo-olefin is sufficient to pick up all bromine atoms which are moderated to thermal velocities and that the active hydrogen bromide appearing at this concentration of bromo-olefin is the result of the "hot atom" reaction (2a) proposed in the kinetic scheme. Table V shows that the average value of ρ obtained from these experiments with bromo-olefines (discarding the first, which has an extremely low pressure of bromo-olefin) agrees well with the values of k_{2a}/k_2 estimated from the slopes of the lines in Fig. 2 (see Table III). When hydrogen bromide is the major constituent of the reaction mixture, we find $k_{2a}/k_2=0.235$ from Fig. 2 and $\rho=0.205$ in the bromo-olefin experiments. When ethyl bromide is the major constituent, we find $k_{2a}/k_2=0.15$ from Fig. 2

TABLE V. Activity distribution in the presence of α,β-dibromoethylene.

Ethyl bromide in mm Hg	Hydrogen bromide in mm Hg	Ethylene in mm Hg	α,β-dibromo-ethylene in mm Hg	ρ Inorganic/organic
[a]	170	0	0.5	0.33
[a]	180	0	5	0.22
[a]	170	0	24	0.19
200	[a]	0	10	0.14
200	[a]	100	10	0.15

[a] Substance used as "wash" only.

and $\rho=0.145$ from the bromo-olefin experiments. Thus it appears that these experiments support both the "hot atom" hypothesis and the radical dissociation hypothesis.

It is interesting to note that the high efficiency of the bromo-olefins is compatible with the value of k_3/k_4 estimated from the ethylene experiments. There the rate constant for addition of bromine atoms to the double bond appeared to be approximately twenty times as great as that for exchange with hydrogen bromide. It would appear that the comparable rate constant in the case of α,β-dibromoethylene is at least one hundred times as great as that for the hydrogen bromide exchange.

CONCLUSION

The kinetic scheme presented above is in satisfactory agreement with the observed dependence of the activity partition on the ethylene pressure. The scheme correctly allows for a small hydrogen bromide dependence, but this could not be quantitatively evaluated. Two critical features of the reaction mechanism were subjected to further experimental tests. The contribution of a "hot atom" reaction forming hydrogen bromide appears to be confirmed by experiments conducted in the presence of argon gas. The assumption that the dissociation of the radical C_2H_4Br is more rapid than its fixation by hydrogen bromide was tested by use of bromo-olefins. These compounds showed high efficiency for exchange with atomic bromine and no detectable rate of addition in the presence of hydrogen bromide. The efficiency of this exchange has suggested further kinetic studies of such systems, which will be reported in a later communication.

Variations in Absorption Spectrum of the Nitrate Group

LEONARD I. KATZIN
Chemistry Division, Argonne National Laboratory, Chicago, Illinois
(Received February 24, 1950)

Lithium, magnesium, calcium, aluminum, manganous, cobaltous, nickelous, cupric, zinc, cadmium and thorium nitrates, and nitric acid, show an absorption in tertiary butyl alcohol solution which is different from that of dilute aqueous solutions of nitrates. The most marked effects are shown by the transition elements with partially completed *d* shells. The variety of the spectra indicate that a single change, such as the rearrangement of the normally planar nitrate ion into a pyramidal form, cannot account for nitrate spectrum changes.

DILUTE aqueous solutions of nitrates show a similar absorption in the ultraviolet which is attributable to the nitrate ion. There is a rounded peak at 300 millimicrons with a molal extinction coefficient approximating 7, and a sharply rising "end-absorption" as one progresses to shorter wave-lengths from about 265 millimicrons. The behavior of this peak under a number of conditions was studied by Schaefer.[1] The conclusion drawn was that the spectrum is a characteristic of the nitrate ion, whether in aqueous solution or in a melt of the solid.

Some salts show variations from Beer's Law under conditions of high concentration in water, or when alcohol is present in high concentrations. In the early days of absorption spectroscopy it was customary to attribute such deviations to "physical" influences in the environment of the absorbing entity. Schaefer[2] championed the view that every deviation from Beer's Law rests in chemical rather than physical alterations. For the case of the nitrate group, he showed that the absorption of 98.6 percent nitric acid, ethyl nitrate, and nitric acid in ethyl ether resemble each other, and are different from that of nitrate ion. This paper was followed by systematic studies of a number of salts, mostly nitrates.[3]

A summary by von Halban,[4] discussing data in publications by himself, Ebert, and Eisenbrand, reviewed the alterations of the nitrate ion spectrum in aqueous solution as a function of salt concentration. He pointed out the specific nature of the cation effects in the concentrated solutions, driving the absorption peak to higher extinction and lower wave-length values, and that the alterations could be shown not to be due to formation of nitric acid. In the specific case of nitric acid, he pointed out that the spectrum in concentrated acid was neither the spectrum of the nitrate ion, nor that of nitric acid in hexane, in which a spectrum similar to that of nitrate esters was found. Besides bringing in the factor of ionic deformability in explaining the results with the various salts, he pointed out the transition nitrate ion-hydronium nitrate-HNO_3 involved in the series of nitric acid spectra, and the applicability of similar stages to the spectra of the other nitrates.

Kortüm,[5] from similar studies of nitrate absorption in concentrated salt solutions, also pointed out the possibility of a water-anion interaction in the coordination sphere of a cation in concentrated aqueous solution. He voiced the further possibility that a change in the shape of the normally planar nitrate ion might be involved. Holleck[6] interpreted the phenomenon of catalysis of nitrate reduction at the dropping mercury electrode through polyvalent cations such as lanthanum as due to a change in shape of the planar nitrate group to the chemically less stable pyramidal form, citing the optical findings of von Halban and co-workers as evidence for this change in shape. From his reduction results, Holleck estimated the degree of transformation to the pyramidal form to be of the order of 95 percent for solutions in water 0.1*N* in lanthanum chloride.

Studies in this laboratory of the absorption of cobaltous nitrate dissolved in tertiary butyl alcohol[7] have shown a characteristic change in the nitrate absorption which far exceeds the difference between the spectra of nitrate ion and HNO_3. The absorption is shifted to shorter wave-lengths, the peak coming at about 285 millimicrons, and the molal extinction coefficient at this wave-length is about 112. A survey was therefore made of the absorption spectra of a number of nitrates soluble in tertiary butyl alcohol. Curves are shown in Fig. 1 for lithium, magnesium, calcium, aluminum, manganous, cobaltous, nickelous, cupric, zinc, cadmium, and thorium nitrates, and nitric acid, in tertiary butyl alcohol. There is also a reference curve of lithium nitrate in 50 percent tertiary butyl alcohol (lithium or other nitrate in dilute water solution is indistinguishable). The logarithm of the formal extinction coefficient (calculated per nitrate) is plotted against the wave-length to facilitate comparison of the curves even with large differences in extinction coefficient. The curves have been corrected for the absorption of solvent and of cation, the latter being significant only for the cupric case. The curves plotted are representa-

[1] K. Schaefer, Zeits. f. wiss. Phot. **8**, 212–234 (1910).
[2] K. Schaefer, Zeits. allgem. anorg. Chemie **97**, 285–311 (1916).
[3] K. Schaefer, Zeits. wiss. Phot. **17**, 193–217 (1918).
[4] H. von Halban, Zeits. Elektrochemie **34**, 489–497 (1928).
[5] G. Kortüm, Zeits. Elektrochemie **50**, 144–149 (1944).
[6] L. Holleck, Zeits. f. physik. Chemie **194**, 140–169 (1944).
[7] L. I. Katzin and E. Gebert, J. Am. Chem. Soc. (to be published).

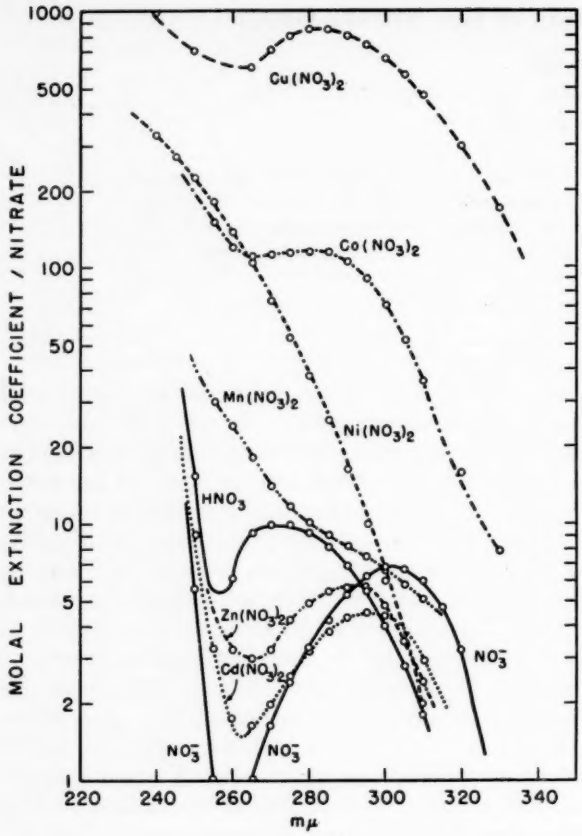

FIG. 1a.

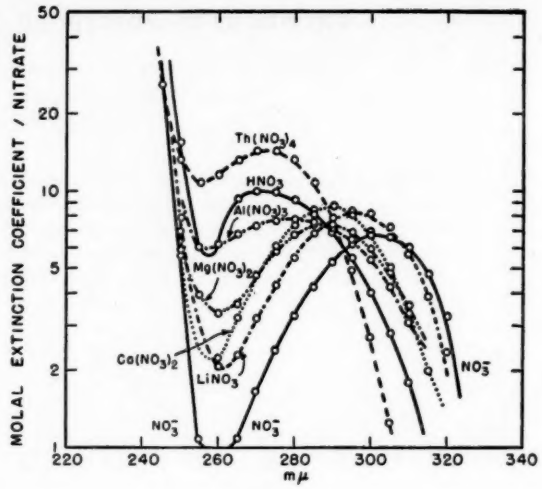

FIG. 1b.

tive members chosen from several runs, and the extinction coefficients at a given wave-length are good to at least 2 percent. The relations of points on a given curve are much more exact than this.

The striking feature of Fig. 1 is that all of the absorption curves for nitrate salts in tertiary butyl alcohol differ markedly from that of free nitrate ion. Furthermore, the spectra cannot be attributed to a mixture of the spectra of nitrate ion and nitric acid. A whole series of nitrates shows spectra more intensely absorbing than that of nitric acid, at the wave-length of its peak (270–275 millimicrons). These nitrates are the transition element nitrates: manganous, cobaltous, nickelous and cupric; and thorium nitrate.

From these observations it is seen that there exists a large range of spectral changes which can be induced in the absorption of the nitrate group. It therefore seems clear that one cannot follow Holleck[6] in ascribing the relatively minor spectral changes found in aqueous solution to changes in configuration of the nitrate group from planar to pyramidal. To ascribe the spectral alterations to ion shape changes would necessitate as many shapes as there are spectra. It therefore seems reasonable to consider the spectral alterations to be due entirely to shifts in electron orbits without alteration of the planar distribution of the atoms.

It seems significant that the most marked changes are found for the nitrates of the transition elements whose ions contain partially completed shells of outer electrons. This is true for the manganous, cobaltous, nickelous and cupric nitrates. Zinc and cadmium are also transition elements, but the zinc ion has full orbitals through the *3d* shell, and cadmium has full orbitals through the *4d* shell. The spectral effects for the nitrates of these metals are very small. In addition, both of these ions have colorless solutions. Manganous, cobaltous, nickelous and cupric solutions are colored, and the last three at least show a noticeable difference in color between the aqueous and tertiary butyl alcohol solutions of the nitrates.

The simple charged ions of the other metals tested in these investigations—lithium, magnesium, aluminum, calcium, and thorium—all possess noble gas configurations, with completed electron shells. One may postulate for these (including hydrogen ion) that the effect on the nitrate spectrum is a function of electrostatic charge and effective ionic radius. Thus, hydrogen, with the smallest ionic radius, and thorium, with the greatest ionic charge, show the largest effects on the nitrate ion spectrum. The zinc and cadmium salts, because of the completed shells, might also be considered with this group.

It has been shown in the case of cobaltous nitrate that there is complex formation between the metal atom and the nitrate groups.[7] In the cases of nickelous and cupric ions, addition of a small proportion of lithium nitrate to the metal perchlorate solutions in alcohol gives essentially the same spectrum as is shown by the bivalent metal nitrate solution alone, in complete parallel to the behavior of the cobalt case. In the case of the manganous salt, the only spectral data are for the addition of lithium nitrate to manganous perchlorate solution, since the solid manganous nitrate is unavailable commercially. The difference of the spectrum from that of lithium nitrate in tertiary butyl alcohol is evidence that nitrate has been transferred

to the manganous atom, although the completeness of the transfer cannot be assessed. Evidence from the cobalt nitrate studies has shown that lithium nitrate in tertiary butyl alcohol is essentially completely non-dissociated, so that the proportion of transfer is a measure of relative firmness of binding of the nitrate group to the metal atom. These data serve to confirm the suggestion of Kortüm[5] and that implied in the earlier work of von Halban and co-workers,[4] that co-ordinative binding of the anion may be the influence in the spectral changes found in concentrated nitrate solutions.

For the case of nitric acid in dioxane solution, von Halban and Litmanowitsch[8] showed unmistakably individual spectra for HNO_3, H_3ONO_3 (hydronium nitrate) and nitrate ion. Similar findings have been made for other absorbing anions such as picrate,[9] with the tendency for the spectra of the free anion and the electrostatically associated hydronium acid to be quite similar. A parallel type of absorption change has been found for both the cobalt and the nitrate groups in cobaltous nitrate in organic solvents.[7] Semiquantitatively similar color changes of the cupric and nickelous nitrate solutions, as well as the change in the absorption of lithium nitrate with water content of the tertiary butyl alcohol solution, indicate the phenomenon is probably general.

[8] H. von Halban and M. Litmanowitsch, Helv. Chim. Acta **31**, 1963–71 (1948).
[9] F. Bortini, Zeits. f. physik. Chemie **87**, 104–115 (1914).

EXPERIMENTAL

A model DU Beckman quartz prism spectrophotometer was used. The hydrated nitrates were dissolved in anhydrous tertiary butyl alcohol. In most cases the concentration of the stock solution was checked by analysis. In some cases a water analysis of the solid starting material served to give the hydration correction. The copper nitrate was made up in tertiary butyl alcohol containing about half its concentration of nitric acid, to avoid solution instability which was occasionally manifested in the absence of this precaution. The acidified alcohol was also used for the aluminum nitrate solution. In some experiments, perchlorate solutions were used, and a small proportion of lithium nitrate added. In the case of cobalt, copper and nickel solutions, the spectra thus obtained were essentially identical to those made by dissolving the nitrate salt. In the case of the manganous solution, the solid nitrate was not available, so only the perchlorate-nitrate curve was used. In all cases, blanks were properly made up to give correction for added nitric acid or metal perchlorate. The latter was significant only for the case of copper.

Grateful acknowledgment is made of the technical assistance of Miss Elizabeth Gebert.

THE JOURNAL OF CHEMICAL PHYSICS VOLUME 18, NUMBER 6 JUNE, 1950

Statistical Mechanics of Adsorption. X. Thermodynamics of Adsorption on an Elastic Adsorbent

TERRELL L. HILL
Naval Medical Research Institute, Bethesda, Maryland
(Received February 2, 1950)

Thermodynamic equations are derived which should be useful in the analysis of experimental data and theoretical models referring to the adsorption of a one-component gas on an elastic adsorbent. This problem is closely related to the thermodynamics of adsorption of a solute from a liquid solution onto an elastic adsorbent immersed in the solution (e.g., a myosin thread).

I. INTRODUCTION

STUDIES on (a) the adsorption of gases by rubber, textiles, proteins and other elastomers *not* under tension and on (b) the effect of the presence of a gas (constant pressure) on the length-tension curve of certain elastomers are, of course, well known. An obvious extension of this work is to measure adsorption isotherms with the adsorbent under tension. Such measurements should, for example, contribute to our knowledge of how the structure of certain proteins changes with extension.

The author is unaware of published investigations of this type. In anticipation of future experimental and theoretical efforts in this direction, we attempt here a brief thermodynamic analysis of the problem. The methods are essentially those of paper IX[1] of this series; we omit the straightforward extension to adsorption from a mixture of gases.[1]

Aside from intrinsic interest, gas adsorption is, of course, closely related thermodynamically to adsorption from a liquid solution, so that many equations given here will be approximately valid for a solution, replacing gas pressure by concentration or activity of the solute. There have been recent suggestions[2–5] that muscular contraction may involve "adsorption" of ions from solu-

[1] T. L. Hill, J. Chem. Phys. **18**, 246 (1950).
[2] J. Riseman and J. G. Kirkwood, J. Am. Chem. Soc. **70**, 2820 (1948), and references contained therein.
[3] A. Katchalsky, Experientia **5**, 319 (1949).
[4] W. Kuhn, Experientia **5**, 318 (1949).
[5] J. Botts and M. F. Morales (in preparation).

tion onto the protein myosin.[6a] The general type of question of interest is: At constant tension, say, how does the length of the adsorbent change with amount of material adsorbed?

Although this paper is primarily thermodynamic, we might mention here a few of the possible effects of (a) stretching and of (b) adsorbed molecules on the nature of the adsorbent. (a) An increase in length of the adsorbent may: (1) increase or decrease the number of adsorption sites or the "surface area" (e.g., the B.E.T. constant $v_m = v_m(L)$); (2) alter the adsorption energy distribution of sites (e.g., the B.E.T. constant $c = c(L)$); (3) increase or decrease the distances between sites, thus changing the energy of interaction of adsorbed molecules (this is the effect discussed by Riseman and Kirkwood[2]). (b) At constant length, the presence of adsorbed molecules can change the structure of the adsorbent owing to (1) interactions between adsorbed molecules and adsorbent or to (2) interactions between adsorbed molecules themselves (see (a) (3)). As a very simple illustration, a case of a dependence of surface area on length is included as Appendix I. We hope to examine statistical models in more detail elsewhere.

The adsorbents of interest are generally characterized by a molecular chain or network type of structure. It is clear that the concept of "surface area" has little meaning here (and we shall generally avoid it below); indeed, the "volume" of the condensed phase (adsorbent plus adsorbed molecules) is similarly only vaguely defined.[1] Despite this latter difficulty, in the present paper we *assume* a well-defined volume of the condensed phase as an excellent approximation in gas adsorption. In a later paper, including adsorption from solution where the volume problem is of more consequence, we shall use more care in this connection. We might also remark here that the surface thermodynamics of Gibbs seems of little use when applied to systems involving molecular networks,[6b] since there is no "surface."

II. SOLUTION THERMODYNAMICS

In this section we extend the methods of ordinary solution thermodynamics to a condensed phase with length L, tension Z, energy E, volume V, entropy S, temperature T, hydrostatic pressure P, and containing N adsorbed molecules and N_A adsorbent molecules.[1,7]

We must now make an arbitrary choice of either L or Z as an intensive variable, the other being extensive. If Z is intensive, increases in N_A are made by increasing L at constant Z; if L is intensive, increases in N_A are made keeping L constant (e.g., increasing the diameter of a cylindrical elastic thread), Z being proportional to N_A. In analogy with the pair $P-V$, we shall designate Z as intensive.[8]

General Equations

We have

$$dE = TdS - PdV + ZdL + \mu dN + \mu_A dN_A, \tag{1}$$

$$E = TS - PV + ZL + \mu N + \mu_A N_A, \tag{2}$$

where μ and μ_A are chemical potentials. We define

$$F \equiv N\mu + N_A\mu_A \tag{3}$$

$$= E - TS + PV - ZL, \tag{4}$$

so

$$dF = -SdT + VdP - LdZ + \mu dN + \mu_A dN_A. \tag{5}$$

Also, we define

$$\mathfrak{F} \equiv F + ZL = E - TS + PV \tag{6}$$

$$d\mathfrak{F} = -SdT + VdP + ZdL + \mu dN + \mu_A dN_A. \tag{7}$$

Now writing $l \equiv L/N_A$, where l is an intensive quantity, Eq. (7) becomes

$$d\mathfrak{F} = -SdT + VdP + ZN_A dl + \mu dN + (\mu_A + Zl)dN_A. \tag{8}$$

From Eqs. (5) and (7), using derivatives such as $\partial^2\mathfrak{F}/\partial T\partial L$ in the standard way, we can write

$$(\partial Z/\partial T)_{P,\,L,\,N,\,N_A} = -(\partial S/\partial L)_{T,\,P,\,N,\,N_A} \tag{9}$$

and other relations[9] showing the change of Z or L with T, P or N. We are, however, more interested in the system in which the condensed phase is in equilibrium with gas at pressure p. From Eq. (5) we have

$$\begin{aligned} d\mu &= -\bar{S}^Z dT + \bar{V}^Z dP - \bar{L}^Z dZ + (\partial\mu/\partial\Gamma)_{T,\,P,\,Z} d\Gamma \\ &= d\mu_G = -S_G dT + V_G dp, \end{aligned} \tag{10}$$

where $\Gamma = N/N_A$,

$$\bar{S}^Z = (\partial S/\partial N)_{T,\,P,\,Z,\,N_A}, \text{ etc.},$$

and

$$S_G = S_G/N_G, \text{ etc.}$$

Similarly, from Eq. (8),

$$\begin{aligned} d\mu &= -\bar{S}^l dT + \bar{V}^l dP + N_A\bar{Z}^l dl + (\partial\mu/\partial\Gamma)_{T,\,P,\,l} d\Gamma \\ &= -S_G dT + V_G dp, \end{aligned} \tag{11}$$

where[10]

$$\bar{S}^l = (\partial S/\partial N)_{T,\,P,\,l,\,N_A}, \text{ etc.}$$

[6a] Dr. K. S. Cole has pointed out to the writer that the adsorption of a solute onto an insoluble surface film is a closely related system, length and tension being replaced by area and surface pressure of the film.

[6b] If anything, a "linear thermodynamics" would be more appropriate.

[7] In networks, again, "molecule" may be vague, but any arbitrary convention is satisfactory.

[8] The choice is completely arbitrary for our purposes and does not affect our results, the addition of N_A involving only a mental process in either case. However, if we were interested in equilibria between the condensed phase and another phase containing *adsorbent* molecules, (say in solution) the choice would no longer be arbitrary (i.e., the meaning of μ_A depends on the choice).

[9] D. R. Elliott and S. A. Lippman, J. App. Phys. **16**, 50 (1945).

[10] We remark in passing that, for example,

$$S = N\bar{S}^Z + N_A\bar{S}_A{}^Z = N\bar{S}^l + N_A\bar{S}_A{}^l$$

but $\bar{S}^Z \neq \bar{S}^l$, where $\bar{S}_A{}^Z = (\partial S/\partial N_A)_{T,\,P,\,Z,\,N}$, etc.
This is an obvious modification of (in ordinary thermodynamics)

$$S = S(T, P, N_1, \cdots N_n) = \Sigma_i N_i(\partial S/\partial N_i)_{T,\,P,\,Nj} = \Sigma_i N_i(\partial S/\partial N_i)_{x,\,y,\,Ni}$$

$$(\partial S/\partial N_i)_{T,\,P,\,Nj} \neq (\partial S/\partial N_i)_{x,\,y,\,Nj},$$

where x and y are *any* two intensive variables for the system.

From Eqs. (10) and (11) we can now obtain, for example,[11]

$$(\partial p/\partial T)_{\Gamma,Z}=(S_G-\bar{S}^Z)/(V_G-\bar{V}^Z), \quad (P=p) \tag{12a}$$

$$(\partial \ln p/\partial T)_{\Gamma,Z}\cong(S_G-\bar{S}^Z)/kT = (H_G-\bar{H}^Z)/kT^2\equiv q_{st(Z)}/kT^2, \tag{12b}$$

$$(\partial Z/\partial T)_{\Gamma,p}=(S_G-\bar{S}^Z)/\bar{L}^Z, \quad (P=p) \tag{13}$$

$$(\partial\mu/\partial\Gamma)_{T,P,Z}=V_G(\partial p/\partial\Gamma)_{T,P,Z}, \tag{14}$$

$$(\partial l/\partial\Gamma)_{T,P,Z}=-V_G(\partial p/\partial Z)_{T,P,\Gamma}, \tag{15a}$$

$$(\partial l/\partial\Gamma)_{T,Z}\cong-kT(\partial \ln p/\partial Z)_{T,\Gamma}, \tag{15b}$$

$$(\partial p/\partial T)_{\Gamma,l}=(S_G-\bar{S}^l)/(V_G-\bar{V}^l), \quad (P=p) \tag{16a}$$

$$(\partial \ln p/\partial T)_{\Gamma,l}\cong(S_G-\bar{S}^l)/kT = (H_G-\bar{\mathfrak{H}}^l)/kT^2\equiv q_{st(l)}/kT^2, \tag{16b}$$

$$(\partial l/\partial T)_{\Gamma,p}=-(S_G-\bar{S}^l)/N_A\bar{Z}^l, \quad (P=p) \tag{17}$$

$$(\partial\mu/\partial\Gamma)_{T,P,l}=V_G(\partial p/\partial\Gamma)_{T,P,l}, \tag{18}$$

$$(\partial Z/\partial\Gamma)_{T,P,l}=V_G(\partial p/\partial l)_{T,P,\Gamma}, \tag{19a}$$

$$(\partial Z/\partial\Gamma)_{T,l}\cong kT(\partial \ln p/\partial l)_{T,\Gamma}, \tag{19b}$$

where

$$H_G=E_G+pV_G,$$
$$H=E+PV-ZL,$$
$$\mathfrak{H}=E+PV.$$

Equations (12) and (16) are isosteric Clausius-Clapeyron equations (q_{st} being the isosteric heat of adsorption). Equations (13) and (17) are similar to Eq. (9), etc., but apply to the equilibrium system. Equations (15) and (19) involve the important derivatives giving the change of length (tension constant) or tension (length constant) with amount of adsorbed material (see Section I and Appendix II). Equations (14) and (18) are employed below.

A Clausius-Clapeyron equation of special type is

$$\left(\frac{\partial p}{\partial T}\right)_{Z,l}=\frac{S_G-\bar{S}^x+(\partial\mu/\partial\Gamma)_{T,P,x}(\partial\Gamma/\partial T)_{P,Z,l}}{V_G-\bar{V}^x-(\partial\mu/\partial\Gamma)_{T,P,x}(\partial\Gamma/\partial P)_{T,Z,l}}. \quad (P=p,\ x=Z \text{ or } l) \tag{20}$$

This equation is of interest because the left-hand member can be evaluated *without* adsorption (Γ) measurements. A theoretical adsorption model can thus be tested by calculating the right-hand member of Eq. (20) from the theory and the left-hand member from Z, l, p, T measurements (which are relatively easy compared to Γ measurements).

Length-Tension Relation

As one expects, any alteration of the adsorbing properties of the adsorbent (and hence of the adsorption isotherm) caused by stretching (even if the adsorbed molecules themselves do not perturb the adsorbent appreciably[1]) will lead to a thermodynamically related alteration in the dependence of Z on L. That is, the adsorption isotherm $\Gamma=\Gamma(p, l, T)$ and the length-tension curve $Z=Z(l, \Gamma, T)$ are not independent.

Thus, on integrating Eq. (19a),

$$Z(\Gamma,T,P,l)=Z(0,T,P,l)+\int_0^\Gamma v_G(\partial p/\partial l)_{T,P,\Gamma}d\Gamma \quad (T,P,l \text{ constant}) \tag{21a}$$

$$Z(\Gamma,T,l)\cong Z(0,T,l)+kT\int_0^\Gamma(\partial \ln p/\partial l)_{T,\Gamma}d\Gamma. \quad (T,l \text{ constant}). \tag{21b}$$

Equation (21) shows how the length-tension relation for $\Gamma>0$ depends on the length-tension curve for the pure adsorbent ($\Gamma=0$) and on the equilibrium adsorption isotherm data in the form $p=p(\Gamma, l, T)$.

A Theorem on Slopes

Consider an equilibrium state characterized by Γ, Z, l, p, T and P ($\neq p$ for generality). If the system is now allowed to pass through neighboring equilibrium states, on the one hand keeping Z, T and P constant, and, on the other hand, keeping l, T and P constant, then

$$(\partial\Gamma/\partial p)_{T,P,Z}>(\partial\Gamma/\partial p)_{T,P,l} \tag{22a}$$

or, approximately,

$$(\partial\Gamma/\partial p)_{T,Z}>(\partial\Gamma/\partial p)_{T,l}. \tag{22b}$$

That is, whenever two isotherms pertaining to the same system at the same temperature intersect (in the same state), one isotherm being at constant l and the other at constant Z, then, at the point of intersection, the slope of the Z-isotherm is greater than the slope of the l-isotherm. An obvious corollary is that if both isotherms are extended above and below the intersection point, there are no further intersections (except at the origin), and the l-isotherm is everywhere above the Z-isotherm at pressures below the intersection point while the reverse is true above the intersection point.

We now prove Eq. (22a). Consider

$$\mu=\mu[T,P,\Gamma,l(T,P,\Gamma,Z)]. \tag{23}$$

From Eq. (8),

$$(\partial\mu/\partial l)_{T,P,\Gamma}=(\partial Z/\partial\Gamma)_{T,P,l}. \tag{24}$$

Using Eqs. (23) and (24),

$$(\partial\mu/\partial\Gamma)_{T,P,Z}=(\partial\mu/\partial\Gamma)_{T,P,l}+(\partial Z/\partial\Gamma)_{T,P,l}(\partial l/\partial\Gamma)_{T,P,Z}. \tag{25}$$

Now we can also write

$$(\partial l/\partial Z)_{T,P,\Gamma}=-(\partial\Gamma/\partial Z)_{T,P,l}(\partial l/\partial\Gamma)_{T,P,Z}. \tag{26}$$

[11] Throughout the paper "approximate" equations with the symbol $\cong$ are in general more than accurate enough for practical use (see reference 1).

We make the trivial restriction that the only systems contemplated here have the property that the left-hand member of Eq. (26) is positive.[12] Hence the two derivatives in the right-hand member of this equation must have opposite signs. Therefore, from Eq. (25),

$$(\partial\mu/\partial\Gamma)_{T,P,l} > (\partial\mu/\partial\Gamma)_{T,P,Z}.$$

Finally, using Eqs. (14) and (18), we obtain Eq. (22a) (also, the difference $(\partial p/\partial\Gamma)_{T,P,l} - (\partial p/\partial\Gamma)_{T,P,Z}$ can easily be written explicitly from these equations).

Appendix I illustrates some of the above relations for a special case. Also, a related theorem is obtained in the next section.

III. ADSORPTION THERMODYNAMICS[13]

We use here the adsorption thermodynamics approach of paper IX[1] (a) to find the significance of the "Gibbs adsorption isotherm" integral as applied to the present problem and (b) to obtain appropriate equations for the special case[1,14] in which adsorbed molecules do not perturb the adsorbent appreciably.

General Equations

We subtract from Eq. (1)

$$dE_{0l} = TdS_{0l} - PdV_{0l} + Z_{0l}dL + \mu_{0l}dN_A, \quad (27)$$

which refers to the *pure* adsorbent ($N=0$) of Eq. (1) at the *same* T, P, L and N_A. This gives

$$dE_l = TdS_l - PdV_l + Z_l dL - \Phi_l dN_A + \mu dN, \quad (28)$$

where

$$E_l = E - E_{0l}, \quad Z_l = Z - Z_{0l},$$
$$S_l = S - S_{0l}, \quad \Phi_l = \mu_{0l} - \mu_A.$$
$$V_l = V - V_{0l},$$

The point of this operation is, as before,[1] to make a transformation to a pseudo one-component system (N). Integrating Eq. (28),

$$E_l = TS_l - PV_l + Z_l L - \Phi_l N_A + \mu N. \quad (29)$$

We define

$$F_l \equiv \mu N = E_l - TS_l + PV_l - Z_l L + \Phi_l N_A, \quad (30)$$

so that

$$dF_l = -S_l dT + V_l dP - LdZ_l + N_A d\Phi_l + \mu dN. \quad (31)$$

Using

$$-LdZ_l = N_A Z_l dl - N_A d(lZ_l),$$

we have

$$dF_l = -S_l dT + V_l dP + N_A Z_l dl + N_A d\Phi' + \mu dN, \quad (32)$$
$$d\mu = -S_l dT + V_l dP + (Z_l/\Gamma)dl + (1/\Gamma)d\Phi'$$
$$= d\mu_G = -S_G dT + V_G dp, \quad (33)$$

where

$$\Phi' \equiv \Phi_l - lZ_l; \quad S_l = S_l/N, \text{ etc.} \quad (34)$$

From Eq. (33) we can now deduce, for example,

$$(\partial p/\partial T)_{\Phi',l} = (S_G - S_l)/(V_G - V_l) \quad (P=p) \quad (35a)$$
$$\cong (S_G - S_l)/kT \quad (35b)$$

$$\Phi' = \int_0^p \Gamma V_G dp \quad (P, T, l \text{ constant}) \quad (36a)$$

$$\cong kT \int_0^p \Gamma d \ln p. \quad (T, l \text{ constant}) \quad (36b)$$

Alternatively, we can subtract from Eq. (1)

$$dE_{0Z} = TdS_{0Z} - PdV_{0Z} + ZdL_{0Z} + \mu_{0Z}dN_A, \quad (37)$$

which refers to the *pure* adsorbent ($N=0$) of Eq. (1) at the *same* T, P, Z and N_A. This gives

$$dE_Z = TdS_Z - PdV_Z + ZdL_Z - \Phi_Z dN_A + \mu dN, \quad (38)$$

where

$$E_Z = E - E_{0Z}, \text{ etc.}; \quad \Phi_Z = \mu_{0Z} - \mu_A.$$

Then

$$d\mu = -S_Z dT + V_Z dP - L_Z dZ + (1/\Gamma)d\Phi_Z$$
$$= -S_G dT + V_G dp, \quad (39)$$
$$S_Z = S_Z/N, \text{ etc.},$$

and

$$(\partial p/\partial T)_{\Phi Z,\, Z} = (S_G - S_Z)/(V_G - V_Z) \quad (P=p) \quad (40)$$

$$\Phi_Z = \int_0^p \Gamma V_G dp \quad (P, T, Z \text{ constant}) \quad (41a)$$

$$\cong kT \int_0^p \Gamma d \ln p. \quad (T, Z \text{ constant}) \quad (41b)$$

Equations (36) and (41) are analogues of the "Gibbs adsorption isotherm" in integral form.

A Theorem on Areas

According to the results of the preceding section, if Φ' and Φ_Z are calculated for the same equilibrium state Γ, Z, l, p, T (i.e., by plotting Γ/p against p and integrating from $p=0$ up to the intersection point at $p=p$, following Eqs. (36b) and (41b), then, since in this range the l-isotherm is above the Z-isotherm, we shall certainly find that $\Phi' > \Phi_Z$.

We verify the above deduction by calculating $\Phi' - \Phi_Z$ explicitly. Thus, by definition,

$$\Phi' - \Phi_Z = (\mu_{0l} - \mu_A) - l(Z - Z_{0l}) - (\mu_{0Z} - \mu_A)$$
$$= \mu_{0l} - \mu_{0Z} - l(Z - Z_{0l}). \quad (42)$$

For pure adsorbent at P and T,

$$dE_0 = TdS_0 - PdV_0 + Z_0 dL_0 + \mu_0 dN_A,$$
$$d\mu_0 = -(S_0/N_A)dT + (V_0/N_A)dP - l_0 dZ_0, \quad (43)$$
$$d\mu_0 = -l_0 dZ_0. \quad (T, P \text{ constant}).$$

Since μ_{0l} and μ_{0Z} refer to the same T and P, from Eqs.

[12] This is analogous to the familiar $(\partial V/\partial P)_{T,N_i} < 0$ in ordinary thermodynamics. Another such relation in the present problem is, of course, $(\partial\Gamma/\partial p)_{T,x} > 0$, where $x = l$ or $x = Z$. See also Appendix II.

[13] The reason for this terminology is mentioned in reference 1.

[14] T. L. Hill, J. Chem. Phys. 17, 520 (1949).

(42) and (43)

$$\Phi'-\Phi_Z=-\int_{l_{0Z},\,Z}^{l,\,Z_{0l}} l_0 dZ_0-l(Z-Z_{0l})$$

$$=\int_{l_{0Z},\,Z}^{l,\,Z_{0l}}(l-l_0)dZ_0=\int_{l_{0Z},\,Z}^{l,\,Z_{0l}}(Z_0-Z)dl_0.$$

(P, T constant) (44)

Using

$$(\partial l_0/\partial Z_0)_{P,T}>0,$$

it is easy to see from the areas involved in a Z_0-l_0 plot that[15] $\Phi'-\Phi_Z>0$ whether $l<l_{0Z}$ or $l>l_{0Z}$. Equation (44) thus provides an additional (see Eq. (21)) connection between adsorption isotherm measurements (to evaluate $\Phi'-\Phi_Z$) and the length-tension curves of the pure adsorbent and of the adsorbent with $N>0$.

The physical significance of Eq. (44) is perhaps more obvious in the following alternative derivation. From the definition of $\mathfrak{F}$ in Eq. (6) it follows that $\Delta\mathfrak{F}$ for a reversible isothermal-isobaric process is equal to the work done on the system, apart from that arising from volume changes. Therefore, a computation of $\Delta\mathfrak{F}$ under these conditions attaches the physical significance of "work" to the various terms involved. We consider two alternative paths in going from the state ($\Gamma=0$, $p=0$, Z, $l=l_{0Z}$, T, P) to the state (Γ, p, Z, l, T, P):

$$\begin{array}{ccc} & (\Gamma=0,\ p=0,\ Z=Z_{0l},\ l,\ T,\ P) & \\ \nearrow^{\mathrm{IA}} & & \searrow_{\mathrm{IB}} \\ (\Gamma=0,\ p=0,\ Z,\ l=l_{0Z},\ T,\ P) & \xrightarrow{\mathrm{II}} & (\Gamma,\ p,\ Z,\ l,\ T,\ P). \end{array}$$

We now compute the various terms in

$$\Delta\mathfrak{F}_{\mathrm{II}}=\Delta\mathfrak{F}_{\mathrm{IA}}+\Delta\mathfrak{F}_{\mathrm{IB}}. \tag{45}$$

From Eq. (8),

$$\Delta\mathfrak{F}_{\mathrm{IA}}=N_A\int_{l_{0Z},\,Z}^{l,\,Z_{0l}} Z_0 dl_0=W_1 \quad (P,\ T \text{ constant}) \tag{46}$$

$$\Delta\mathfrak{F}_{\mathrm{IB}}=\int_0^N \mu dN=W_2 \quad (P,\ T,\ l \text{ constant}) \tag{47}$$

$$\Delta\mathfrak{F}_{\mathrm{II}}=N_A Z\int_{l_{0Z}}^{l} dl+\int_0^N \mu dN=W_3+W_4.$$

(P, T, Z constant) (48)

In words, the work W_1 necessary to stretch the pure adsorbent from l_{0Z} to l plus the work W_2 necessary to adsorb N molecules (l constant) is equal to the work W_3 necessary to stretch the adsorbent from l_{0Z} to l at tension Z (=constant) plus the (simultaneous) work W_4 necessary to adsorb N molecules (Z constant). Since[15] $W_1>W_3$, $W_4>W_2$. After integration by parts and use of $d\mu=V_G dp$ and Eqs. (36a) and (41a), Eq. (45) reduces to Eq. (44).

[15] For example, consider the case $l>l_{0Z}$. In the integration of the right-hand integral of Eq. (44), as l_0 increases from l_{0Z} to l, Z_0 increases ($\partial l_0/\partial Z_0>0$) from Z to Z_{0l}. In other words, in the range of integration, $Z_0\geq Z$, and hence the integral is positive. A similar argument can be given for $l<l_{0Z}$.

Special Case

There is a special case which should be of value as a good approximation for some systems: the adsorbent is unperturbed by adsorbed molecules (e.g., no swelling); $\mathfrak{A}_0=\alpha N_A$; and $\mathfrak{A}=\mathfrak{A}_0 f(l)$; where α is a constant, $\mathfrak{A}_0$ is the "surface area" when $Z=0$ and $\Gamma=0$, and $\mathfrak{A}$ is the surface area in general. This corresponds exactly to the case discussed at length in paper V,[14] with the added complication that the surface area (and, in general, other properties of the adsorbent potential field) depends on length.

Let A_s, S_s, V_s, etc. refer to the thermodynamic functions of the assembly of adsorbed molecules in the external field presented by the adsorbent. Let φ be the surface pressure (e.g., if the adsorbed phase is a two-dimensional gas, then φ is the kinetic theory or statistical mechanical "pressure"—force per unit length exerted on a surface piston). Consider

$$A_s=A_s(T,\ V_s,\ l,\ \mathfrak{A},\ N).$$

Then[14]

$$dA_s=-S_s dT-PdV_s+cdl-\varphi d\mathfrak{A}+\mu dN, \tag{49}$$

where $c\equiv(\partial A_s/\partial l)_{T,\ V_s,\ \mathfrak{A},\ N}$. Using $\mathfrak{A}=\mathfrak{A}_0 f(l)$,

$$dA_s=-S_s dT-PdV_s+[c-\varphi\mathfrak{A}_0(df/dl)]dl$$
$$-(\varphi\mathfrak{A}/\mathfrak{A}_0)d\mathfrak{A}_0+\mu dN. \tag{50}$$

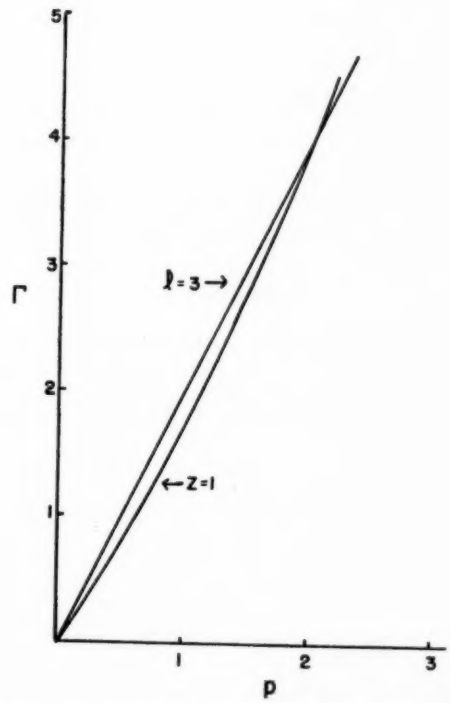

FIG. 1. Adsorption isotherms at constant length and tension for a simple numerical example (Appendix I).

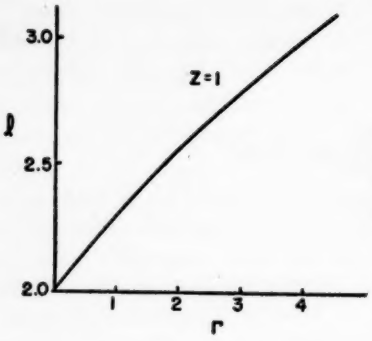

FIG. 2. Change of length of adsorbent at constant tension caused by adsorption, in a simple numerical example (Appendix I).

This is to be compared, term by term, with

$$dA_l = -S_l dT - P dV_l + N_A Z_l dl - \Phi' dN_A + \mu dN. \quad (51)$$

Hence, in this special case we can make the associations

$$\begin{aligned} S_l &= S_s, \quad N_A Z_l = c - \varphi \mathfrak{A}_0 (df/dl), \\ V_l &= V_s, \quad \Phi' N_A = \varphi \mathfrak{A}. \end{aligned} \quad (52)$$

IV. CALORIMETRY

We merely list certain results here since the extension of papers V and IX is straightforward.

Calorimetric heats of adsorption can be measured at constant l or Z. Following paper IX, one finds

$$Q_x = N(E_G - E_x), \quad (53)$$

$$q_{d(x)} = E_G - \bar{E}^x, \quad (54)$$

$$q_{st(l)} = q_{d(l)} + kT, \quad (55)$$

$$q_{st(Z)} = q_{d(Z)} + kT + Z\bar{L}^Z, \quad (56)$$

$$= q_{d(Z)} + kT - ZkT(\partial \ln p/\partial Z)_{T,\Gamma}, \quad (57)$$

$$q_{ith(x)} = q_{d(x)} + kT + V_G(\partial p/\partial N)_{T,x}, \quad (58)$$

where $x = l$ or Z, Q is the integral heat of adsorption, q_d the differential heat of adsorption and q_{ith} the isothermal heat of adsorption.

I have had the benefit of very helpful discussions with Dr. M. F. Morales, Miss Jean Botts, and Dr. K. S. Cole.

APPENDIX I

We discuss an extremely simple case as an example. For a very dilute adsorbate (perfect two-dimensional gas or dilute Langmuir adsorbate) assume that the adsorbate does not perturb the adsorbent, that the surface area (or number of sites) depends on l according to $\mathfrak{A} = \alpha N_A[1+\beta_2(l-l^0)]$, that this is the only effect of l on the adsorbing properties of the adsorbent, and that the length-tension curve for the pure adsorbent is $Z_0 = \beta_3(l_0 - l^0)$. The adsorption isotherm is then of the form $N = \beta_1' \mathfrak{A} p$ or

$$N/N_A = \Gamma = \beta_1[1+\beta_2(l-l^0)]p. \quad (\beta_1 = \alpha\beta_1') \quad (59)$$

l^0 is the "rest" length of the pure adsorbent, β_1 and β_3 are positive constants and β_2 is a constant which can be positive or negative.

Using Eqs. (21b) and (59), the general length-tension relation is

$$Z = \beta_3(l-l^0) - kT\beta_2\Gamma/[1+\beta_2(l-l^0)] \quad (60)$$

$$= \beta_3(l-l^0) - kT\beta_1\beta_2 p. \quad (61)$$

Putting Eq. (59) into Eq. (61) gives $\Gamma = \Gamma(Z, p)$:

$$\Gamma = [Z + (\beta_3/\beta_2) + kT\beta_1\beta_2 p]\beta_1\beta_2 p/\beta_3. \quad (62)$$

Then, from Eqs. (59), (62), (36b) and (41b),

$$\Phi' = kT\Gamma, \quad (63)$$

$$\Phi' - \Phi_Z = (kT\beta_1\beta_2 p)^2/2\beta_3 > 0. \quad (64)$$

The same result is found using Eq. (44) (as a check).

Also, from Eqs. (59) and (62),

$$(\partial\Gamma/\partial p)_Z - (\partial\Gamma/\partial p)_l = kT\beta_1^2\beta_2^2 p/\beta_3 > 0. \quad (65)$$

In Figs. 1 and 2, we show the adsorption isotherms and the dependence of l on Γ at constant Z (Eq. (60)) for a simple numerical example, taking (in arbitrary units) $l^0 = kT = \beta_1 = \beta_3 = 1$ and $\beta_2 = \frac{1}{2}$. The constant values of l and Z used are $l = 3$ and $Z = 1$. In this case the surface area is thus assumed to increase with increasing l. Hence adsorbing molecules onto the adsorbent will tend to increase l (Z constant) because the concomitant area increase will decrease the free energy of the adsorbed molecules (on the other hand it takes work to stretch the adsorbent so the actual increase in l represents a compromise—the state of minimum *total* free energy of the condensed phase).

A more general approach to theoretical models, which is hardly necessary here, is by way of statistical mechanics. This leads to an expression for A. One finds Z (e.g., Eq. (60)) then from

$$dA = -SdT - PdV + ZdL + \mu dN + \mu_A dN_A, \quad (66)$$

$$Z = (\partial A/\partial L)_{T,\,V,\,N,\,N_A}, \quad (67)$$

and the adsorption isotherm using

$$\mu = (\partial A/\partial N)_{T,\,V,\,L,\,N_A} = \mu_G(p, T). \quad (68)$$

We have verified the equations of Appendix I in this way for a perfect two-dimensional gas as adsorbate.

APPENDIX II

There are twelve possible derivatives involving p, Z, Γ and l (P, T constant). It is of some interest to catalog them according to sign, using the important derivative $(\partial l/\partial\Gamma)_Z$ as a reference. Omitting proofs:

(1) $(\partial\Gamma/\partial p)_Z$, $(\partial\Gamma/\partial p)_l$, $(\partial l/\partial Z)_p$, $(\partial l/\partial Z)_\Gamma$ are positive;

(2) $(\partial l/\partial p)_Z$, $(\partial l/\partial\Gamma)_p$, $(\partial Z/\partial\Gamma)_p$ have the same sign as $(\partial l/\partial\Gamma)_Z$;

(3) $(\partial Z/\partial p)_\Gamma$, $(\partial Z/\partial p)_l$, $(\partial Z/\partial\Gamma)_l$, $(\partial l/\partial p)_\Gamma$ have the opposite sign as $(\partial l/\partial\Gamma)_Z$.

The Relative Rates of the Reactions of Hydrogen Iodide and Deuterium Iodide with Methyl Iodide

THOMAS W. NEWTON*
Department of Chemistry, University of Wisconsin, Madison, Wisconsin
(Received October 4, 1949)

The relative rates of the reactions of hydrogen iodide and deuterium iodide with methyl iodide were studied by a competitive method at 310° and 250°C. The analysis of hydrogen-deuterium mixtures was accomplished by means of a simple viscometer with an accuracy of 0.5 percent. It was found that hydrogen iodide reacts about 1.4 times as fast as deuterium iodide at both temperatures. These results are discussed in terms of Eyring's theory of absolute reaction rates and a simple model.

INTRODUCTION

THIS paper is the second in a series concerned with the effect of substituting deuterium for hydrogen on the rates of gas reactions. In the first paper[1] work on the relative rates of photo-chlorination of chloroform and deuterochloroform was reported. The investigation of the isotope effect on the reaction between hydrogen iodide and methyl iodide is reported in this paper.

The effect of isotopic substitution is interesting because coupled with the theory of absolute reaction rates it gives some information about the activated complex.

The kinetics of the reaction between hydrogen iodide and methyl iodide,

$$HI+CH_3I=CH_4+I_2, \qquad (1)$$

was studied by Ogg[2] who found that the reaction proceeds by two parallel paths. One of these is the direct bimolecular reaction between the two reactant molecules, while the other consists of consecutive reactions involving methyl radicals and iodine atoms. In the present work no attempt was made to determine the rate of the reaction; instead the ratios of the rates of the reactions involving the two isotopic species were determined. The isotopic effect in the direct bimolecular reaction was larger than in the reaction by the second path and was the only one determined at all precisely in this investigation.

APPARATUS

The reactions were run in fifty ml sealed glass bulbs equipped with break-seals. They were heated either in an electrically heated bath of fused sodium and potassium nitrates or in an electric oven. The salt bath was regulated manually at 310°C within plus or minus 1°C. The oven was equipped with a regulator which held the temperature within 0.5° of 250°C. The temperatures were measured with a mercury in glass thermometer; this thermometer was not calibrated because the temperature coefficient of the rate ratio was very small.

The reaction bulbs were filled and emptied with a glass gas handling apparatus capable of evacuation to 10^{-5} mm Hg. (See Fig. 1.) Since hydrogen iodide and iodine attack mercury rapidly the single membrane gauge described by Moquin and Garman[3] was used as a null instrument for the pressure determinations. One side of the membrane was silvered so that with the aid of a lens an image of a single filament was projected onto a screen. With the same pressure on both sides the membrane was flat and the image of the filament was observed as a thin straight line. With unequal pressures the image was broader and blurred. The author believes that this device deserves more attention than it has received since it is sensitive, rugged and easy to construct. Several have been made which will withstand a pressure difference of one atmosphere from either side and yet will operate with a sensitivity of greater than 0.5 mm Hg.

At several stages during the runs it was necessary to separate a condensable gas from a stream of a non-condensable one. For this purpose the device described by Bates and Salley[4] was used. This consisted of five U-tubes arranged to fit in the same Dewar flask.

The samples of hydrogen and deuterium iodides were reduced by mercury to hydrogen-deuterium mixtures in small bulbs equipped with seal-offs and break-seals.

The analysis of the hydrogen-deuterium mixtures was accomplished by means of a simple viscometer shown in Fig. 2. The volume of the gas bulb was about 10 ml and

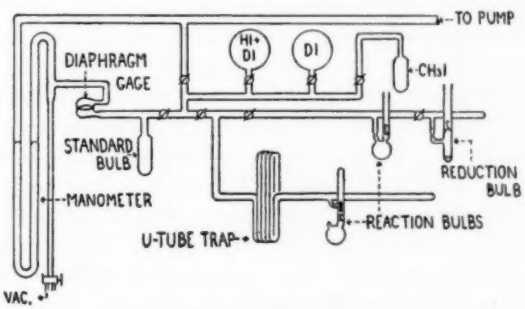

FIG. 1. Gas handling apparatus.

* National Research Council Fellow in Chemistry. Present address: P. O. Box 1663, Los Alamos, New Mexico.

[1] T. W. Newton and G. K. Rollefson, J. Chem. Phys. **17**, 718 (1949).

[2] R. A. Ogg, Jr., J. Am. Chem. Soc. **56**, 526 (1934). It should be mentioned that a decimal error occurs in this article; the values of K and K_1 are too large by a factor of ten.

[3] Moquin and Garman, Ind. Eng. Chem. (Anal. Ed.) **9**, 287 (1937).

[4] Bates and Salley, J. Am. Chem. Soc. **55**, 110 (1933).

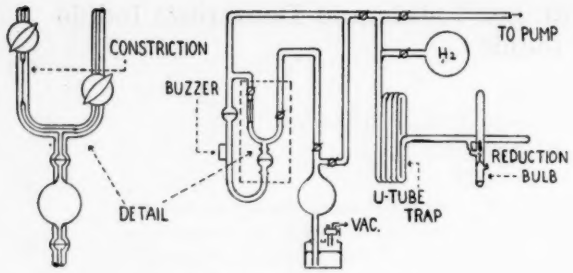

FIG. 2. Viscometer apparatus.

the pressure of the gas in the filled bulb was 15 cm Hg. Thus the gas needed for analysis amounted to about 2 ml at atmospheric pressure. A buzzer was fastened to the side of the viscometer to prevent sticking of the mercury. Without this buzzer the times of flow were very erratic. The system described by Nash[5] was used to increase the speed of the mercury at the timing points above and below the bulb. The timing was done with a stop-watch. With this system it was found that the six minute time of flow for deuterium was reproducible to within 0.5 second. The time of flow for tank hydrogen was found to be about 4.3 minutes. Synthetic mixtures were prepared by the reduction of mixtures of hydrogen iodide and deuterium iodide. It was found that the fraction of deuterium in these mixtures was a linear function of $(t_S/t_H)^2$ where t_H is the flow time for tank hydrogen and t_S is the time of flow for the sample. The calibration curve: $(t_S/t_H)^2$ *versus* fraction deuterium is linear as was to be expected since the time of flow is proportional to the viscosity and the viscosity is proportional to the square root of the mean molecular weight of the sample. The precision of the method depends on the reproducibility of the timing and amounts to about 0.5 percent of the total sample. This is about the same precision as was obtained with the thermal conductivity gauge used in the previous work on the chlorination of chloroform. The viscometer was used here since it requires no auxiliary electrical equipment and is easier to construct.

MATERIALS

Hydrogen.—Hydrogen was taken from a tank and purified by slow passage through a U-tube trap dipping into liquid air.

Deuterium.—Deuterium gas was obtained from the Stuart Oxygen Company of San Francisco on an allocation from the Atomic Energy Commission; it was reported to have a purity of greater than 99.5 percent. It was purified in the same manner as the hydrogen.

Iodine.—Iodine was resublimed from potassium iodide, then dried in a sealed tube containing resublimed phosphorous pentoxide. After some of the runs the iodine was recovered for reuse.

Hydrogen and Deuterium Iodides.—These were prepared by heating hydrogen or deuterium with iodine in a sealed bulb which contained a glowing platinum coil. The iodides were then purified by distilling while pumping from a trap in dry ice to a trap in liquid air. After several such distillations they were stored in black painted bulbs at room temperature. The stop-cocks on these bulbs were greased with Apiezon *N*; this caused no apparent decomposition of the hydrogen iodide.

Methyl Iodide.—Eastman Kodak methyl iodide was washed with a potassium carbonate solution and dried with anhydrous potassium carbonate. It was then distilled using a small Vigreaux column with a reflux ratio of about ten to one. The middle cut which boiled over a range of 0.1° was taken. The material was degassed by subjecting it to three bulb to bulb distillations on the vacuum line. It was finally treated for several days under vacuum with vacuum resublimed phosphorous pentoxide. It was stored in a bulb fastened to the vacuum line and kept at temperatures between 0° and −78°C.[6]

DETAILS OF A TYPICAL RUN

Reactant gases were distilled from the storage bulbs into a 35.5-ml standard bulb. The pressure of the gas in this bulb was determined by the use of the diaphragm gauge and the manometer. The temperature of the bulb was recorded so that the pressure reading could be reduced to 25°C. After distilling both gases into the reaction bulb it was sealed off. Before filling the bulb, it and the line were thoroughly evacuated and rinsed with some of hydrogen iodide-deuterium iodide mixture. The iodine which was added in some of the runs was distilled in from small ampules with breakable tips. The reaction bulbs were heated long enough for fifty to seventy-five percent of the hydrogen iodide to be consumed. The rate of the reaction of hydrogen iodide with methyl iodide is much greater than the rate of decomposition of hydrogen iodide; so no appreciable decomposition of the hydrogen iodide occurred. After the reaction bulb had been heated the desired length of time it was resealed to the vacuum line. The line was evacuated, flamed and rinsed as before. Upon opening the bulb the methane was pumped away while the rest of the reactants and products were caught in the U-tube trap. The pressure of the remaining gas was then determined as before in the standard bulb. The vapor pressure of the iodine present was small enough to be neglected. Liquid air was put around a reduction bulb and the hydrogen iodide-deuterium iodide mixture was collected there after passing it slowly through the U-trap cooled to −120°C by means of freezing ethyl bromide. This treatment removed the iodine and methyl iodide. The reduction bulb was then sealed off and shaken vigorously at room temperature. This causes the complete reduction of the mixture by the mercury. This and similar samples were

[5] L. K. Nash, Anal. Chem. **20**, 258 (1948).

[6] Dr. Jacob Bigeleisen has pointed out that the impurity, methylal, which is found in Eastman Kodak methyl iodide, probably would not be completely removed by the purification procedure used, but also that a trace of this substance would not affect the kinetic results.

sealed to the viscometer apparatus for analysis. The samples were pumped into the viscometer through a U-trap cooled with liquid air to remove traces of condensable impurities. Each sample was run at least twice and the results were averaged. Hydrogen from the storage bulb was run before and after every two samples to check on possible slight plugging of the capillary.

CALCULATIONS AND RESULTS

As shown in the previous paper,[1] the ratio of the bimolecular rate constants is given by the expression:

$$k_1/k_2=\log(HI_0/HI_f)/\log(DI_0/DI_f),$$

where HI_0 is the amount of hydrogen iodide present at the start of the reaction and HI_f is the amount present at the end. DI_0 and DI_f are the similar quantities for deuterium iodide. These four quantities are easily calculated from the isotopic analyses and the initial and final amounts of hydrogen iodide-deuterium iodide mixtures. The final amount of mixture is calculated from the initial amount of methyl iodide and the amounts of the reactants left after the reaction. The data taken and the calculated values of the rate constant ratios are given in Table I.

Ogg[2] has shown that the rate of reaction (1) is given by the expression:

$$-d(HI)/dt=k_1(HI)(CH_3I)+(k'/[(HI)+(I_2)])(HI)(CH_3I).$$

As indicated by the rate law, the reaction probably goes by two paths, one a bimolecular reaction and the other a series of consecutive reactions which is inhibited by iodine. In the runs with no added iodine the two paths contributed about equally to the reaction, but where iodine was added enough was used to cut the contribution of the second path about in half. As the data in Table I show, there is no significant difference in the rate ratios between the runs with added iodine and those without. Thus it can be shown that these rate ratios are very nearly equal to the ratio of the rate constants of the two bimolecular reactions:

$$HI+CH_3I=CH_4+I_2;\ k_1 \qquad (1)$$

and

$$DI+CH_3I=CH_3D+I_2;\ k_2. \qquad (2)$$

The spread of the data at the two temperatures is consistent with the uncertainty in the isotopic analysis. Insofar as the errors in the analysis were random, the average of the ratio values at each temperature are quite accurate. However a possible systematic error might have entered when the correction for the small amount of isotopic contamination was applied. The approximate amount of such contamination was determined in the following experiments. Part of a sample of hydrogen iodide-deuterium iodide was distilled directly into a reduction bulb and part directly into a reaction bulb, which was heated as in an ordinary run. Five such experiments were done, some with added iodine and some without. The analyses of the five samples which had been distilled directly into reduction bulbs showed that the average fraction of deuterium iodide was 0.412. The mean and maximum deviations from this value were 0.001 and 0.003. Heating in the reaction bulbs caused a decrease in the fraction of deuterium iodide in the mixture. This decrease was found to depend on the amount of hydrogen iodide-deuterium iodide used; so the results were calculated on the basis of the amount of mixture used in the rate ratio runs. The average correction was found to be 0.002 with mean and maximum deviations of 0.0007 and 0.0015 respectively. The presence of iodine made no significant difference. The methyl iodide could have caused isotopic contamination by exchanging hydrogens with the deuterium iodide or it might have contained a trace of an exchangeable impurity. To check on this source of contamination a mixture of deuterium iodide and hydrogen iodide which was about 0.98 deuterium iodide was allowed to react with one-half the equivalent amount of

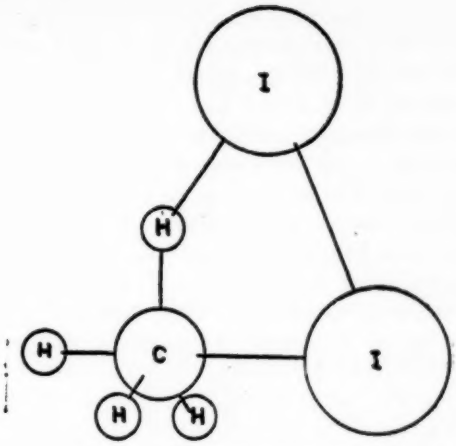

FIG. 3. Model of activated complex.

TABLE I. Data and results.

Initial (HI+DI)*	Initial fraction (DI)**	Initial (CH_3I)*	Final (HI+DI +CH_3I)*	Final fraction (DI)	Rate ratio	
(runs at 310°C with added iodine)						
43.30 cm	0.512	28.55 cm	19.90 cm	0.594	1.43	
38.50	0.512	22.60	19.70	0.578	1.42	
48.15	0.402	33.54	23.65	0.479	1.41	
46.40	0.402	29.41	19.98	0.472	1.38	
47.67	0.402	32.85	19.10	0.492	1.45	
46.53	0.402	30.77	20.04	0.487	1.45	ave: 1.42
(runs at 310°C without added iodine)						
41.84	0.512	26.41	17.15	0.589	1.39	
46.90	0.512	31.40	17.60	0.593	1.37	
44.78	0.402	29.89	15.90	0.498	1.45	
46.11	0.402	30.39	16.97	0.491	1.43	
46.33	0.402	30.61	16.45	0.490	1.41	ave: 1.41
(runs at 250°C with added iodine)						
46.48	0.410	31.32	31.10	0.467	1.43	
45.90	0.410	31.50	24.86	0.483	1.43	
39.33	0.410	25.14	27.88	0.461	1.42	ave: 1.43
(runs at 250°C without added iodine)						
46.15	0.410	31.69	21.79	0.492	1.44	
46.91	0.410	32.18	21.98	0.493	1.45	
44.34	0.410	28.64	25.23	0.470	1.38	ave: 1.42

* Amounts of reactants are given in cm Hg in the 35.5 ml standard bulb at 25°C.
** Corrected for isotopic contamination.

methyl iodide. After the reaction it was found that the fraction of deuterium iodide was unchanged within the experimental error of the analysis. This indicated that a small amount of exchange had occurred, since if none had occurred the fraction of deuterium in the mixture after reaction would have been a little higher than the starting value. The amount of exchange was such that the apparent starting composition was about 0.008 less than the actual starting composition. Unfortunately it was impossible to determine this value very precisely. Experiments run at 250° and 310°C indicated about the same amount of exchange. The activation energy for the exchange reaction is probably higher than that of the reaction to give methane and iodine, since the exchange reaction is only about one percent as fast. Thus it is unlikely that the amount of exchange was really the same at the two temperatures. A relatively large amount (two percent) of exchangeable impurity in the methyl iodide would give the same exchange at the two temperatures. This amount of impurity seems unlikely; so the calculations were made assuming that exchange occurred at 310°C but that it was negligible at 250°C. In applying this correction to the rate ratio runs allowance was made for the fact that greater concentrations of reactants were present and the fact that the hydrogen iodide-deuterium iodide mixture had a smaller fraction of deuterium iodide.

The uncertainty of the exchange correction does not affect the values of the rate ratios very much; thus if the same correction was applied at the two temperatures, the average value at 250°C would have been 1.49 instead of 1.42.

DISCUSSION

It is of interest to discuss the experimental results in terms of Eyring's[7] formulation of the absolute reaction rate and a reasonable model of the activated complex. According to that formulation

$$k_1/k_2=(\kappa_1/\kappa_2)(F_1^{\ddagger}/F_2^{\ddagger})(F_2/F_1)\exp[(E_2-E_1)/RT] \quad (3)$$

where the subscripts 1 and 2 refer to reactions (1) and (2). The $F^{\ddagger}$'s are the total partition functions of the activated complexes neglecting the imaginary frequencies in the reaction coordinates, and the F's are the total partition functions of the hydrogen iodide and deuterium iodide. (κ_1/κ_2) is the ratio of the transmission coefficients and (E_2-E_1) is the zero point energy difference between the initial molecules minus the zero point energy difference between the two activated complexes.

In order to calculate k_1/k_2 from Eq. (3) it is necessary to know the moments of inertia and the significant vibration frequencies of the activated complexes and the ratio of the transmission coefficients. The moments of inertia can be estimated easily with sufficient precision from a reasonable model for the activated complex. Rough estimates of the vibration frequencies could be obtained with much labor by means of the semi-empirical method of Eyring and Polanyi.[8] The ratio of the transmission coefficients is often assumed to be unity although there is no theoretical justification for this in the case considered here.[9] The tunnel effect will not be considered explicitly here; it is usually small and may be considered to be part of the transmission coefficient.

The experimental results of this investigation will be used to assign limits to the transmission coefficient ratio and to the vibration frequencies of the complex which are changed when deuterium is substituted for hydrogen.

The model chosen for this particular case is a four-membered ring as shown in Fig. 3. The bond distances are assumed to be proportional to ordinary covalent bond distances. The only vibration frequencies which need be considered are those which are altered appreciably when deuterium is substituted for hydrogen in the complex. Since the hydrogen is part of a ring of much heavier members (a methyl group and two iodine atoms), as an approximation only three of the fifteen modes of vibration will be changed significantly when deuterium is substituted for hydrogen. One of these three modes is along the decomposition coordinate of the complex and does not enter the calculation.

The partition function ratios in Eq. (3) can be factored into translational, rotational, vibrational and electronic parts. The translational part is very close to unity since the masses of the reactant and activated complex molecules are essentially unchanged when hydrogen is replaced by deuterium. The electronic factor is also very close to unity, since the fraction of molecules in any particular electronic state will not be changed by isotopic substitution.

The rotational part is given by

$$[(ABC)_1^{\ddagger}/(ABC)_2^{\ddagger}]^{\frac{1}{2}}(I_2/I_1)$$

where the $(ABC)^{\ddagger}$'s are the products of the moments of inertia of the two activated complexes and I_1 and I_2 are the moments of inertia of hydrogen iodide and deuterium iodide. The root of the quantity in brackets will be close

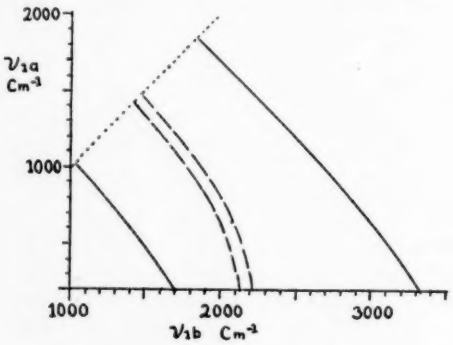

FIG. 4. Range of significant frequencies.

[7] Glasstone, Laidler, and Eyring, *Theory of Rate Processes*, (McGraw-Hill Book Company, Inc., New York, 1941), p. 190.

[8] Reference 7, p. 91.

[9] See J. O. Hirschfelder and E. Wigner, J. Chem. Phys. **7**, 616 (1939) and H. M. Hulbert and J. O. Hirschfelder, J. Chem. Phys. **11**, 276 (1943).

TABLE II. Calculated values of the rate ratios for several possible frequencies and transmission coefficient ratios.

ν_{1a}	ν_{1b}	Deuterium substitution (k_1/k_2)				Tritium substitution (k_1/k_3)			
cm^{-1}		κ_1/κ_2	523°K	583°K	Change in 60°	κ_1/κ_2	523°K	583°K	Change in 60°
200	1700	0.85	1.44	1.40	−3%	<0.85	<1.88	<1.80	−4.4%
1000	1100	0.80	1.43	1.39	−2.8%	<0.80	<1.92	<1.82	−6%
400	2100	1.00	1.45	1.43	−1.5%	1.00	1.76	1.74	−1%
1400	1500	1.00	1.41	1.42	+0.6%	1.00	1.71	1.72	+0.6%
200	3400	1.58	1.40	1.44	+2.8%	>1.58	>1.38	>1.47	+6.2%
1800	1900	1.30	1.39	1.45	+4.0%	>1.30	>1.51	>1.59	+4.8%

to unity for any reasonable model of the activated complex. The model chosen here makes this quantity about 0.98. Since (I_2/I_1) is very nearly 2.00 the rotational factor is about 1.96.

The vibrational part of (F_2/F_1) is given by:

$$[1-\exp(-h\nu_1/kT)]/[1-\exp(-h\nu_2/kT)].$$

This quantity is very nearly unity because the vibration frequencies of hydrogen iodide and deuterium iodide are too large to be appreciably excited at the temperatures involved.

The vibrational part of $(F_1^{\ddagger}/F_2^{\ddagger})$ is given by the product of two terms similar to the reciprocal of the one given for (F_2/F_1), one term each for the two significant vibrations of the activated complex.

Thus according to Eq. (3) and the above considerations

$$k_1/k_2=1.96(\kappa_1/\kappa_2)\exp[(E_2-E_1)/RT]\times\frac{[1-\exp(-h\nu_{2a}/kT)][1-\exp(-h\nu_{2b}/kT)]}{[1-\exp(-h\nu_{1a}/kT)][1-\exp(-h\nu_{1b}/kT)]}, \quad (4)$$

where

$$(E_2-E_1)/RT=(h/2kT)(\nu_{10}-\nu_{20})-(\nu_{1a}-\nu_{2a})-(\nu_{1b}-\nu_{2b})$$

and

$$\nu_{2i}=\nu_{1i}(2)^{-\frac{1}{2}}, \quad i=0,\ a \text{ and } b$$

since the interaction potential energy surface is not changed when deuterium is substituted for hydrogen. In the above expressions the subscripts 1 and 2 refer to hydrogen and deuterium, the subscript 0 refers to the vibration of hydrogen iodide or deuterium iodide, and the subscripts a and b refer to the two significant frequencies of the activated complex. For example ν_{2b} is the frequency of one of the significant vibrations in the deuterium substituted complex.

The experimental data indicate that $k_1/k_2=1.42\pm0.03$ at both 523°K and 583°K. In Fig. 4 the values of ν_{1a} and ν_{1b} consistent with the experimental data are shown between the solid lines. Under the special assumption that the transmission coefficient ratio is unity the possible frequency pairs are limited to those shown between the dashed lines.

The first part of Table II shows calculated values of k_1/k_2 for some of the possible values of ν_{1a}, ν_{1b} and κ_1/κ_2. More precise measurements over a wider temperature interval would be helpful in narrowing the range of frequencies and transmission coefficient ratios consistent with experiment.

Measurements of the relative rates of reaction of hydrogen iodide and tritium iodide with methyl iodide would be very interesting. The second part of Table II shows the predicted values of k_1/k_3 under some of the possible values of ν_{1a} and ν_{1b}, values of κ_1/κ_3 are unknown but it is reasonable to assume that $|1-(\kappa_1/\kappa_3)|>|1-(\kappa_1/\kappa_2)|$.

Thus if κ_1/κ_2 is unity, k_1/k_3 should be about 1.7 and have a very small temperature coefficient. If κ_1/κ_2 is large (1.3 to 1.6) k_1/k_3 should have a small positive temperature coefficient, but if κ_1/κ_2 is small (0.8 to 0.85) k_1/k_3 should have a small negative temperature coefficient. As Table II shows, these small temperature coefficients should be detectable if the precision in the tritium experiments were the same as in the deuterium ones.

ACKNOWLEDGMENTS

The author gratefully acknowledges the many helpful discussions with and the interest of Professor Farrington Daniels, in whose laboratory this work was done. He also wishes to acknowledge helpful discussions with Professors J. O. Hirschfelder, C. F. Curtiss, and E. L. King.

The assistance of the National Research Council in providing the author with a fellowship is also gratefully acknowledged.

Self-Quenching and Sensitization of Fluorescence of Chlorophyll Solutions*

W. F. WATSON† AND ROBERT LIVINGSTON
School of Chemistry, Institute of Technology, University of Minnesota, Minneapolis, Minnesota
(Received January 16, 1950)

The intensity of fluorescence of solutions of chlorophyll (either *a* or *b*) is sensibly independent of concentration, for values less than $2\times10^{-3}m$. At higher concentrations, the fluorescence decreases with increasing concentration, conforming to the empirical equation, $I_{f,\max}/I_f=1+4300m^2$. The absorption spectrum of chlorophyll *a* is the same at $0.02m$ as it is for very dilute solutions. These results, as well as the observed temperature coefficient of the fluorescent intensity, indicate that the self-quenching of chlorophyll solutions is not due to the formation of non-fluorescent dimers nor to collisions of the second kind, but is very probably related to the resonance exchange of excitation (16, 17) between an excited and normal chlorophyll molecule.

Measurements of the fluorescence intensity of solutions containing mixtures of chlorophylls *a* and *b* indicate that chlorophyll *b* can sensitize the fluorescence of chlorophyll *a*, and that the fluorescence of chlorophyll *b* is more strongly quenched by *a* than it is by itself.

As part of an attempt to study the optical and photochemical properties of chlorophyll, we have measured the intensity of fluorescence of solutions of chlorophylls under a variety of conditions. In concentrated solutions of either chlorophyll *a* or *b*, self-quenching (i.e., concentration quenching) occurs to an extent which is comparable to that previously observed for solutions of other complex molecules. Chlorophyll *b* sensitizes the fluorescence of chlorophyll *a* in solution which contain both substances. In concentrated solutions this sensitized fluorescence is largely masked by a strong quenching of chlorophyll *b* by chlorophyll *a*.

SELF-QUENCHING

Experimental Methods and Materials

The fluorimeter was essentially similar to that recently described by Livingston, Watson, and McArdle.[1] The exciting light was rendered parallel by spherical condensing lenses and a series of diaphragms. It illuminated about 1 cm² of the front face of the cell. The photo-cell was at a distance of about 10 cm from the front face of the vessel which contained the solution, and was so situated that the angle between lines, joining the center of the fluorescence vessel with the light source and with the photo-cell, was less than 30°. The exciting light consisted either of λ4358A (containing some 4036A) or else of a narrow band[2] with its maximum at 6450A. The current for the mercury arc was stabilized with a Sola constant-voltage transformer; the current for the incandescent lamp was controlled manually with the aid of an ammeter and rheostat. To eliminate the effect of reabsorption of the fluorescent light, a Wratten filter (No. 88), which absorbs all radiation of wave-length less than 6800A, was placed in front of the photo-cell.[3,4]

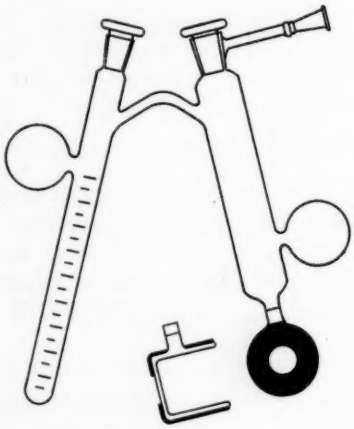

FIG. 1. Cell used in the fluorescent studies.

By the use of fluoresence cells of the modified Thunberg type[1] oxygen was removed from all of the solutions studied. Since the concentration of the chlorophyll in these solutions was varied over a wide range, it was necessary so to design the experiments as to minimize the "geometric" errors in the observed fluorescence resulting from the differing depths of penetration of the exciting light. This was done by placing the photo-cell in front of the fluorescence vessel at a distance great compared to the size of the fluorescent source and in a position where the fluorescent beam made an acute angle with a line normal to the face of the vessel, and by using thin vessels (1 or 2 mm thick). A simple graphical analysis of the geometric optics involved indicated that with this arrangement the maximum "geometric" error in the measured fluorescence was less than three percent. For concentrations of chlorophyll

* This work was supported jointly by the ONR (Contract N6ori-212, Task Order I. Project NR 059, 028) and by the Graduate School of the University of Minnesota to whom the authors are indebted.

† Present address: 48 Tewin Road, Welwyn Garden City, Herts., England.

[1] Livingston, Watson, and McArdle, J. Am. Chem. Soc. **71**, 1541 (1949). Figures 5 and 6 were inadvertently exchanged in this paper.

[2] R. Livingston and C. L. Ke, J. Am. Chem. Soc. **72**, 909 (1950).

[3] Compare W. Watson and R. Livingston, Nature **162**, 452 (1948).

[4] The efficiency of this filter in eliminating the effect of reabsorption was tested by placing a cuvette (1 cm thick) between the photo-cell and the fluorescence vessel and filling the cuvette with a solution of chlorophyll. Since the response of the galvanometer, actuated by the photo-cell and its amplifier, did not change as the concentration of the chlorophyll solution in the cuvette was varied, we may conclude that reabsorption of the fluorescent light did not affect the present measurements.

TABLE I. Fluorescence intensity as a function of chlorophyll concentration. (Incomplete absorption of exciting light.)

Solvent	Chlorophyll conc. $m \times 10^4$	I_F	I_F/I_A
	(Chlorophyll *a*)		
Ether	0.076	11	1.0
Ether	0.171	26	1.00
Ether	0.263	37.5	1.07
Ether	0.299	39.5	1.01
Ether	0.372	45	0.99
Ether	0.482	52	0.94
Methanol	0.086	8	1.0
Methanol	0.274	26	1.00
Methanol	0.438	35	1.00
Methanol	0.580	42	0.98
Acetone	0.45	38	0.98
Acetone	0.95	63	1.00
Acetone	3.32	82	0.92
Acetone	5.48	95	1.02
Acetone	6.78	104	1.05
	(Chlorophyll *b*)		
Acetone	0.24	22	0.85
Acetone	0.52	44.5	0.94
Acetone	1.49	81.5	0.94
Acetone	2.11	93	1.01
Acetone	2.38	96	1.01
Acetone	3.00	100	1.02
Acetone	4.27	104	1.05
Acetone	6.63	110	1.10

TABLE II. Fluorescence intensity as a function of chlorophyll *a* concentration. (Complete absorption.)

Chlorophyll *a* in ether $m \times 10^{-4}$	I_F	Chlorophyll *a* in acetone $m \times 10^{-4}$	I_F
4.39	78	6.78	75
5.67	79	8.00	76
7.32	80	12.5	76
8.72	81	17.6	76
9.86	81		
10.00	80		

less than $10^{-3}m$ the fluorescence vessel illustrated by Fig. 1 was used. The Dewar-seal type of vessel was used to avoid the difficulty of making and working with a thin disk-shaped cell with plane windows. Except for a circle of 1-cm² area, the front face of the cell was covered with a black mask. The graduated tube, attached to the Thunberg tube, served as a reservoir for stock solution.

At the beginning of each run the graduated side tube was filled with a known volume of stock solution and about 10 ml of solvent was placed in the fluorescence cell. The vessel was then evacuated and solvent distilled from both arms of the vessel until the volume of solvent in the fluorescence cell reached the calibrated value of 8.3 ml. The resulting concentration of the stock solution was computed from the ratio of its initial and final volume and from its initial concentration. A series of solutions of successively increasing concentration were then prepared by pouring measured volumes of the stock solution from the graduated side tube into the fluorescence cell. In this way it was possible to start with one filling of the cell and one evacuation, and to

TABLE III. Self-quenching of the fluorescence of chlorophyll solutions in acetone.

Solutions of chlorophyll *a* (in ether)		Solutions of chlorophyll *b* (in ether)	
$m \times 10^3$	$I_F/I_{F,max}$	$m \times 10^3$	$I_F/I_{F,max}$
0.91	1.00	0.95	1.00
1.32	1.00	1.46	1.00
2.4	0.96	2.1	1.00
3.9	0.94	2.2	1.00
5.1	0.93	3.9	0.97
6.0	0.83	5.2	0.87
6.8	0.83	8.0	0.73
6.9	0.83	10.3	0.61
10.7	0.68	13.2	0.51
11.6	0.62	20.6	0.35
11.7	0.62	(in acetone)	
17.4	0.47		
18.1	0.44	2.9	1.00
19.7	0.39	4.6	0.86
23.5	0.31	7.7	0.77
42.7	0.18	13.0	0.65
43.1	0.13	23.1	0.45
66.0	0.07	1.8*	1.00
		2.4*	1.00
		3.3*	0.95
		3.7*	0.91
		5.2*	0.89
		5.2*	0.80
		10.6*	0.73

* In these experiments the exciting light was a narrow band in the red. The intensity maximum of the absorbed light corresponded to λ6425A. In all other experiments exciting light of λ4358A was used.

prepare several solutions of different known concentrations and to measure their fluorescence. The limitation on the amount of chlorophyll available made the use of this cell, which required at least 8.3 cc of solution, impracticable for solutions more concentrated than $10^{-3}m$. A second vessel with a disk-shaped cell 1 mm thick and about 1 cm² in area was used for these concentrated solutions. Several concentrations were obtained from a single filling of the cell by evaporating successively several known amounts of solvent from the cell. While the manipulative technic required to fill and to degas this cell was more difficult, the reproducibility of the results obtained with it showed that it was satisfactory.

To measure the absorption spectra of concentrated solutions of chlorophyll with the Beckman spectrophotometer, it was necessary to use cuvettes much thinner than the standard 1-cm Beckman cells. An adjustable thin cell was constructed of two optically flat plates of quartz separated by thin metal spacers. The front wall of the cell was pressed against a rigid metal frame by light set screws, uniformly spaced on a frame behind the back plate of the cell. Lead spacers, similar to those used in infra-red spectroscopy, were used for thicknesses down to 0.05 mm. Thin aluminum foil was used for the thicknesses down to approximately 0.01 mm. When non-volatile solvents (such as dibutyl ether) were used, it was observed that squeezing the plates with light pressure resulted in a reasonably uniform layer approximately 0.0004 mm thick. The cell was filled by capillary action, and was emptied by touching its edge with a shred of filter paper. The cell

and its mount fitted into a special Beckman carriage, which also carried a standard comparison cell.

The chlorophylls and solvents used in these experiments were purified by methods which have been described previously.[1]

Results and Computations (Dilute Solutions)

It has been demonstrated for a wide variety of dyes[5,6] and of aromatic hydrocarbons,[7,8] that the intensity of the fluorescence of their solutions decreases as the concentration increases, commonly the effect is first noticeable at concentrations greater than $10^{-3}m$.

Since it has been reported[9] that chlorophyll solutions exhibit marked self-quenching in solutions as dilute as $10^{-4}m$, it appeared to be necessary to re-examine the fluorescence intensity of relatively dilute chlorophyll solutions taking precautions to eliminate the reabsorption of the emitted light and to minimize the effect of

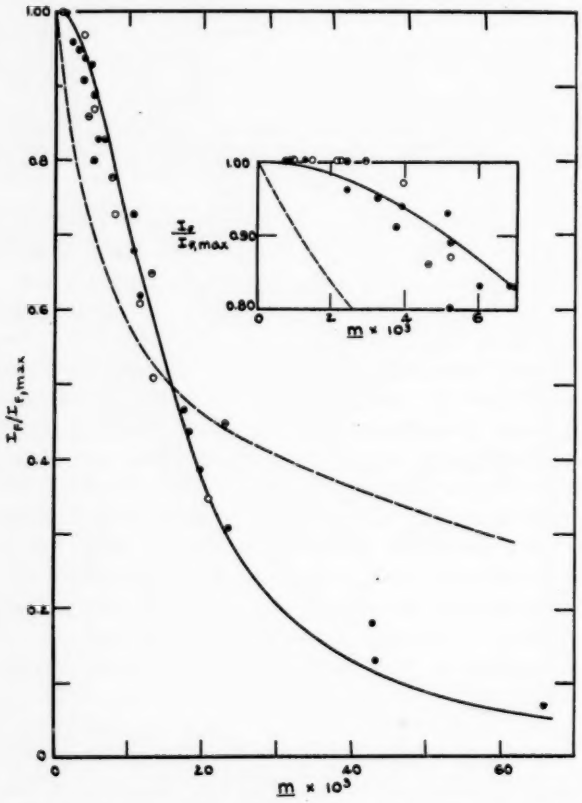

FIG. 2. Concentration quenching of chlorophyll solutions. ●—chlorophyll *a* (in ether) with λ4358A; ○—chlorophyll *b* (in ether), with λ4358A; ⊗—chlorophyll *b* (in acetone), with λ6425A; ⊖—chlorophyll *b* (in acetone) with λ4358A.

TABLE IV. Effect of temperature on the fluorescence intensities of dilute and of concentrated chlorophyll solutions.

Solutions	Temperature range	$(I_F/I_{F,max})$ 30°C	$-\frac{1}{I_F}\left(\frac{\partial I_F}{\partial t}\right)$
$5\times10^{-6}m$ chlorophyll *a* in methanol	15–70°C	1	0.0027
$5\times10^{-6}m$ chlorophyll *a* in ether	−30–30°C	1	0.0041
$1.2\times10^{-2}m$ chlorophyll *b* in acetone	13–49°C	0.64	0.0083

geometric factors. The results of such measurements are listed in Tables I and II. The fluorescent intensities, I_F, are recorded in arbitrary units, as read from the galvanometer. The intensities of absorbed light, I_A, were computed for a 2-mm layer using the extinction coefficients published by Zscheile and Harris.[10] These data prove definitely that chlorophyll solutions do not exhibit detectable self-quenching at concentrations less than $10^{-3}m$. Similar (although less extensive) results were obtained with mixtures of chlorophylls *a* and *b*.

In a preliminary publication,[3] Watson and Livingston presented data showing that apparent concentration quenching will be observed if no precautions are taken to eliminate the reabsorption of the emitted light. In these measurements, which were made to test the hypothesis that the apparent self-quenching observed by Weiss and Weill-Malherbe[9] was due to reabsorption, the photo-cell was placed behind the cuvette and the Wratten filter No. 88 was replaced with a Corning filter No. 246. The data obtained in this way are qualitatively consistent with those of Weiss and Weill-Malherbe. To confirm this interpretation of the data, a numerical calculation was made of the intensity of fluorescence which should be observed (at several concentrations) with the latter arrangement of the fluorimeter. In this calculation the extinction coefficients[10] of chlorophyll solutions, the relative intensities of the fluorescent light as a function of wave-length and the spectral variation of the sensitivity of the photo-cell were taken into account.[11] The resulting computed curve is in good agreement with the experimental data; thereby, indirectly confirming the direct proof of Tables I and II that there is no detectable self-quenching of the fluorescence of chlorophyll in solutions of $10^{-3}m$ or less.

Results and Computations (Concentrated Solutions)

The self-quenching of chlorophyll solutions becomes evident at about $2\times10^{-3}m$. The results of measurements illustrating this quenching are listed in Table III. The experiments were performed separately with both chlorophyll *a* and *b*. The measurements were made at room temperature (from 25 to 30°C). The seven measurements, whose results are marked with asterisks, were performed using a narrow band of red light as the

[5] P. Pringsheim, *Fluorescence and Phosphorescence* (Interscience Publishers, Inc., New York, 1949), pp. 347–59.
[6] S. I. Vavilov and P. P. Feofilov, Doklady Akad. Nauk, U.R.S.S. **34**, 243 (1942).
[7] E. J. Bowen and A. H. Williams, Trans. Faraday Soc. **35**, 765 (1939).
[8] G. Körtum and B. V. Finckh, Zeits. f. physik. Chemie **B52**. 263 (1942).
[9] J. Weiss and H. Weill-Malherbe, J. Chem. Soc. (London) 544 (1944).
[10] F. Zscheile and D. G. Harris, Bot. Gazz. **104**, 515 (1943).
[11] F. Zscheile and D. G. Harris, J. Phys. Chem. **47**, 623 (1943).

exciting radiation. In all other experiments the incident light was of λ4358A. In all cases the absorption was complete. Within the limits of precision of the measurements, identical results were obtained with chlorophylls *a* or *b*, and with either λ4358A or with red light as the exciting radiation.

The data of Table III are plotted on Fig. 2. The solid-line curve on Fig. 2 (including the inset) is a graph of the empirical, one-constant equation

$$I_{F,\max}/I_F = 1+4300m^2.$$

With the possible exception of the three points at concentrations greater than $0.04m$, the deviations of the experimental points from the curve appear to be within the limits of experimental error. Of the three sets of measurements, the data for chlorophyll *a* are probably the most precise, and those for chlorophyll *b* excited with red light, the least.

Since the effect of temperature on self-quenching should serve to differentiate between alternative interpretations of the phenomenon, we have measured the intensity of fluorescence of concentrated (i.e., partially quenched) solutions at several temperatures. The fluorescence intensities of a $0.0116m$ solution of chlorophyll *b* in acetone where 15.5, 14.0, and 11.5 (arbitrary units) at 13, 30.5, and 49°C, respectively. A comparison of this effect of temperature to the temperature coefficient of dilute solutions of chlorophyll *a* (determined[1] under similar conditions) is summarized in Table IV. Although the data obtained for concentrated and dilute solutions are not strictly comparable (since neither the solvent nor the chlorophyll were the same), it seems safe to conclude that the fluorescence intensity of partially quenched solution decreases with increasing temperature at least as rapidly as that of an unquenched (dilute) solution.

To determine whether the fluorescence quenching was accompanied by a change in the absorption, measurements were made of the absorption spectra of quenched and unquenched solutions. These spectra were measured with a Beckman spectrophotometer over the wave-length range 4000–7000A. Since it was difficult to use volatile solvents in the special thin cell which these measurements required, dibutyl ether was used as a solvent. The absorption spectrum of chlorophyll *a* at a concentration $0.020m$ is identical with the spectrum at $0.0010m$, within the limits of precision of the measurements. The intensity of fluorescence of a $0.020m$ is less than half of that of a $0.0010m$ solution, which is not detectably quenched.

Discussion and Conclusions

It has been demonstrated[12,13] that the concentration quenching which occurs in solutions of certain dyes is due to reversible dimerization, the dimer being non-fluorescent and frequently exhibiting a changed absorption spectrum. An increase in temperature increases the degree of dissociation of the dimer and, therefore, tends to increase the intensity of a partially quenched solution. In the present case there is no evidence that the concentration quenching is due to dimerization.

While the fact that the quenched and unquenched solutions have identical absorption spectra makes it improbable that the quenching is due to dimerization, this should not be accepted as definite proof. The intensity of fluorescence is very probably more readily influenced by minor changes in the dye molecule or its environment than is its absorption spectrum. The relatively great negative temperature coefficient of the intensity of fluorescence of a partially quenched solution is perhaps sufficient evidence to rule out the possibility that the observed quenching is due to reversible dimerization. Furthermore, the quadratic dependence of the quenching upon the concentration is inconsistent with the dimerization mechanism, as can be simply shown as follows. If we let the symbols $[G]$, $[G_2]$, and m represent, respectively, the molarities of the monomer, the dimer, and the total (stoichiometric) chlorophyll, the following relations must hold:

$$m=[G]+2[G_2]$$

$$K=[G_2]/[G]^2=(m-[G])/(2[G]^2)$$

or

$$[G]=(1/4K)[(8Km+1)^{\frac{1}{2}}-1].$$

Since these solutions obey Beer's law, the molar extinction coefficient of the dimer must be twice that of the monomer. Therefore, since the dimer has been assumed to be non-fluorescent,

$$I_F=\varphi\frac{[G]}{[G]+2[G_2]}I_A=\varphi\frac{[G]}{m}I_A,$$

where φ is the fluorescent yield of the monomer and I_A is the intensity of the light absorbed by the solution. Combining these equations, we obtain

$$\frac{I_F}{\varphi I_A}=\left(\frac{I_F}{I_A}\right)\Big/\left(\frac{I_F}{I_A}\right)_{\max}=\frac{1}{4Km}[(8Km+1)^{\frac{1}{2}}-1].$$

The dotted line in Fig. 2 is a plot of the equation, where K has been chosen to make the equation agree with the data at the half-quenching point. It is obvious that the equation and the data are incompatible. These three lines of evidence establish definitely that the self-quenching observed in acetone solutions of chlorophyll is not due to the reversible formation of a non-fluorescent dimer.

It has long been recognized[14,15] that concentration quenching frequently is not the result of extensive

[12] W. Lewschin, Acta Physicochim. U.R.S.S. **1**, 685 (1935); **2**, 221 (1935).

[13] E. Rabinowitch and L. Epstein, J. Am. Chem. Soc. **63**, 69 (1941). See also reference 5, pp. 353–9.

[14] F. Perrin, Comptes Rendus **178**, 1978 (1924).

[15] J. Perrin, Comptes Rendus **184**, 1097 (1927).

dimerization but rather is due to some type of interaction between excited and (separate) normal dye molecules. The simplest example of such an interaction is a collision of the second kind between an excited and a normal molecule.[5,9] However, the quenching corresponding to such a process would follow a Stern-Volmer law, and the reciprocal of the fluorescence intensity would be a linear function of the first power of the concentration, rather than of the second power as was observed in the present case. More recently,[16,17] it has been suggested that self-quenching is closely related to the transfer of excitation between like molecules. In particular, Vavilov has proposed that whenever energy of excitation is transferred between molecules there is an intrinsic, finite probability that it will be degraded.[18] Introducing this postulate into an otherwise general analysis of the probability of transfer of excitation, Vavilov derives the following equation.

$$(I_F/I_A)_{\max}/(I_F/I_A) = [1+\alpha+\beta-\beta\exp(-\Omega_0 C)]\exp(\Omega_0 C),$$

where α, β, and Ω_0 are constants which are adjustable within limits, and C is the concentration of the dye. When $\Omega_0 C \ll 1$, the equation may be written in the following approximate form:

$$(I_F/I_A)_{\max}/(I_F/I_A) = 1+(\alpha+\Omega_0)C+(\alpha+\beta)\Omega_0 C^2+\beta\Omega_0^2 C^3.$$

While the simplest empirical equation which represents the quenching data is

$$(I_F/I_A)_{\max}/(I_F/I_A)=1+4300m^2,$$

they are equally consistent with the following equation, although not with a complete quadratic whose linear coefficient is appreciably greater than 5.

$$(I_F/I_A)_{\max}/(I_F/I_A)=1+5m+3800m^2.$$

Comparing this relation with Vavilov's expanded equation and expressing the concentrations as molecules per cc, we obtain $\alpha+\Omega_0=8.3\times10^{-21}$ cc/molecule and $(\alpha+\beta)\Omega_0=1.05\times10^{-40}$ (cc/molecule)^2. The present data do not permit the evaluation of all three constants.

TABLE V. Percent absorption of the actinic light by 1 mm thickness of equimolar solution of chlorophylls *a* and *b* in acetone.

$(m_a=m_b)\times10^4$	Total absorption, I_A (percent of I°)	Absorption by chlorophyll *a*, $I_{A,a}$ (percent of I°)	$\alpha=I_{A,a}/I_A$
0.51	21.2	2.8	0.132
1.51	46.0	6.8	0.148
3.20	68.4	11.6	0.169
9.08	96.1	18.3	0.190
29.1	100	21.0	0.210
104.5	100	21.0	0.210

[16] S. Vavilov, J. Phys. U.S.S.R. **7**, 141 (1943).
[17] T. Förster, Ann. d. Physik **2**, 55 (1948).
[18] For a more definite hypothesis see J. Franck and R. Livingston, Rev. Mod. Phys. **21**, 505 (1949).

However, if we assume that $\alpha \ll \Omega_0$, the corresponding values of $\Omega_0=8.3\times10^{-21}$cc/molecule and $\beta=1.32\times10^{-18}$ cc/molecule are within the range of values of these quantities which Vavilov obtained for glycerine solutions of certain dyes. In Vavilov's derivation the quantities α and β are related directly to the probabilities of transfer of energy with and without quenching, respectively.

SENSITIZED FLUORESCENCE

Experimental Methods and Materials

The same fluorimeter (including the Wratten filter No. 88) and fluorescent cells were used in these experiments as were described in the preceding section. However, a narrow band of light having its maximum at λ4750A was used as the exciting radiation. This light was isolated from the radiation of a 1000-watt, projection-type, incandescent lamp by the use of 2.5 cm of five percent copper sulfate solution, a Farrand interference filter (having its transmission maximum at 4750A) and a picric acid solution. The spectral distribution of intensity of this light source was obtained by graphical integration from the absorption spectrum of the combined filter and the intensity distribution of the source.[19] The absorption spectra of the components of the filter were measured with the Beckman spectrophotometer.

The materials used in this work were similar to those described in the first part of the paper. All measurements were made in acetone solutions at room temperature, which varied between 24 and 27°C.

Results and Computations

If the transfer of energy of excitation can occur between unlike molecules in liquid solutions,[17] chlorophyll *b* should be able to sensitize the fluorescence of chlorophyll *a*. The lowest singlet excited state is slightly (about 1 kcal./mole) above that of chlorophyll *a*, and the fluorescence band of chlorophyll *b* strongly overlaps the (red) absorption band of chlorophyll *a*.[10] However, the similarity of the two compounds introduces some difficulties into the observation of sensitized

TABLE VI. Fluorescence intensities in arbitrary units of separate solutions of chlorophylls *a* and *b*.

$m\times10^4$	$I^\circ_{F,a}$	$I^\circ_{F,b}$
0.71	3.5	7.0
1.01	4.0	8.5
2.10	9.0	14.0
2.12	9.0	14.5
3.01	13.0	18.0
6.30	24.5	23.0
6.40		22.5
9.08		25.5
18.9		28.5
$(m\gg2\times10^{-3})$	(84)	(29)

[19] W. E. Forsythe and E. Q. Adams, J. Opt. Soc. Am. **35**, 108 (1945).

fluorescence. To magnify the effect, exciting light of λ4750A which is absorbed chiefly by chlorophyll *b*, and a photo-cell filter (Wratten No. 88) which transmits preferentially the fluorescence of chlorophyll *a* were used. Since the exciting light was not monochromatic, it was necessary to resort to graphical integration to determine the fraction of the light absorbed by each component.

This was calculated from the computed spectral distribution of intensity of the (filtered) light source and the known absorption spectra[10] of chlorophylls *a* and *b*. The results of such computations for equimolar mixtures of chlorophylls *a* and *b* are summarized in Table V.

Using exciting light of λ4750A, the fluorescence intensities (in arbitrary but consistent units) of solutions of chlorophyll *a* and of chlorophyll *b* were measured with the fluorimeter as described in this paper. These results are summarized in Table VI. As is shown in Fig. 2, concentration quenching is negligible in all of these solutions with the exception of the most concentrated chlorophyll *b* solution. The intensity corresponding to this is about two percent quenched and the absorption of light is practically complete. Accordingly, the maximum intensity of fluorescence of chlorophyll *b* (for this apparatus and solvent) is 29. Since the extinction coefficient of chlorophyll *a* for λ4750A is relatively small, it is not practicable to determine its maximum intensity of fluorescence directly. When the exciting light is λ4358A the ratio of the maximum fluorescent intensity of chlorophyll *a* to that of chlorophyll *b* is 2.90. This factor is presumably independent of the wave-length of the exciting light in the range of wave-lengths used in the present experiments. Therefore,[20–22] the maximum fluorescent intensity, which would be exhibited by chlorophyll *a* solutions if concentration quenching did not occur, is $2.90\times29=84$. The results of a set of measurements made with solutions which contained equal concentrations of chlorophyll *a* and *b* in the dilute range (where concentration quenching in the separate solutions is negligible) are summarized in Table VII. The quantities listed in the second and third columns are ratios of the intensities of light absorbed severally by chlorophyll *a* or *b* (in the solution) to the total intensity of the incident light, I°. The values were interpolated from Table V. I_F is the measured intensity of fluorescence of the solution. The quantity, $I_{F,a}+I_{F,b}$, is the fluorescent intensity which the solution would have if there were neither concentration quenching nor energy exchange. It was computed from the relation, $I_{F,a}+I_{F,b}=(I_{A,a}/I^\circ)84+(I_{A,b}/I^\circ)29$. The last column gives the percentage excess of the measured fluorescence intensity over the computed intensity. The uncertainties indicated for these percentage differences are estimated values of their probable errors, based upon the assumption that the probable errors of I_F, $I_{F,a}$, and $I_{F,b}$ are each equal to 0.6. It is apparent that the results corresponding to the two lowest concentrations are without significance. However, the percent differences obtained for the more concentrated solutions are very probably too large to be due to experimental error, and they constitute reasonably definite evidence that the process of energy exchange from chlorophyll *b* to chlorophyll *a* has a fairly high probability of occurrence for these solutions.

The interpretation of the measurements of the fluorescence of concentrated solutions is complicated by the simultaneous occurrence with energy transfer of self-quenching and possibly of "cross-quenching" between chlorophylls *a* and *b*. It seems advisable, therefore, before discussing the data obtained with concentrated solutions, to examine the various possible ways in which a molecule may lose energy of excitation and how these several possibilities are interrelated. The following eleven steps include all of the obvious ways in which molecules of chlorophyll *a* or *b* (here designated as *A* and *B*) can lose or gain energy of excitation. Whether steps 4 or 6 go directly from the excited, singlet states to the ground states or involve an intermediate long-lived (triplet?) state[23] is immaterial to the present discussion. Both the resonance transfer[14–17,25] of excitation from *B* to *A* and the capture by *A* of a photon emitted by *B* contribute to step 11. However, the latter process is relatively unimportant since the maximum fluorescent yield of chlorophyll *b* is less than 0.1[24] and the probability of reabsorption of a photon is always less than unity and is especially small in dilute solutions where the fluorescent yield is at a maximum. Since the filter in front of the photo-cell excluded light of all wave-lengths which are appreciably absorbed by either chlorophyll *a* or *b*, the absorption of the fluorescent light by the components of the solution does not contribute to the observed self-quenching or cross-quenching of fluorescence; i.e., to steps 7, 8, 9, or 10.

1.	$h\nu+A\rightarrow A^*$	$v_1=\alpha I.$
2.	$h\nu+B\rightarrow B^*$	$v_2=\beta I.$
3.	$A^*\rightarrow A+h\nu_f$	$v_3=k_3a.$
4.	$A^*\rightarrow\!\!\!\rightarrow A$	$v_4=k_4a.$
5.	$B^*\rightarrow B+h\nu_f$	$v_5=k_5b.$
6.	$B^*\rightarrow\!\!\!\rightarrow B$	$v_6=k_6b.$
7.	$A^*\xrightarrow{A}A$	$v_7=f_7(A)\cdot a.$
8.	$A^*\xrightarrow{B}A$	$v_8=f_8(A,B)\cdot a.$
9.	$B^*\xrightarrow{B}B$	$v_9=f_9(B)\cdot b.$
10.	$B^*\xrightarrow{A}B$	$v_{10}=f_{10}(A,B)\cdot b.$
11.	$A+B^*\rightarrow A^*+B$	$v_{11}=f_{11}(A,B)\cdot b.$

[20] S. I. Vavilov, Phil. Mag. **43**, 307 (1922).
[21] E. J. Bowen, Proc. Roy. Soc. **A154**, 349 (1936).
[22] S. S. Solomin, Comptes Rendus Acad. Sci. U.R.S.S. **31**, 742 (1941).
[23] R. Livingston, Society of Dyers and Colourists **65**, 781 (1949).
[24] T. Prins, Nature **134**, 457 (1934).

TABLE VII. Fluorescence of equimolar mixtures of chlorophylls *a* and *b*.

$(m_a=m_b)\times10^4$	$I_{A,a}/I^\circ$	$I_{A,b}/I^\circ$	I_F	$I_{F,a}+I_{F,b}$	$\left(1-\frac{I_{F,a}+I_{F,b}}{I_F}\right)100$
0.35	0.020	0.120	6	5.2	13±16
0.51	0.028	0.184	7	7.7	−10±14
1.05	0.048	0.307	16.5	12.9	22±6
1.06	0.048	0.307	16	12.9	19±6
1.51	0.068	0.392	19	17.1	10±5
3.15	0.114	0.568	33	26.1	21±4
3.20	0.116	0.568	35	26.2	25±3
4.54	0.140	0.655	42	30.8	27±2
9.45	0.184	0.782	54	38.1	29±2
19.4	0.210	0.790	54.5	40.6	25±2

At constant temperature and in a given solvent, the rates, v_i, of the first six steps are undoubtedly represented by their respective rate equations as written. The total "intensity" (expressed as photons per cc per sec.) of the light absorbed by the solution is represented by I. The concentrations (in molecules per cc) of the excited molecules, A^* and B^*, are indicated by a and b, respectively. The fractions of the light absorbed by A and B are equal, respectively, to α and β. To keep the analysis as general as is possible, the rates of the last five steps are represented as unknown functions, $f_i(A, B)$, of the concentrations of A and B, although the rates are assumed to be directly proportional to the concentrations a or b.

Since we are considering these systems only when they are in true steady states, there is no approximation involved in writing $da/dt=db/dt=0$. It follows that $\alpha I+f_{11}(A, B)b=[k_3+k_4+f_7(A)+f_8(A, B)]a$ and $\beta I=[k_5+k_6+f_9(B)+f_{10}(A, B)+f_{11}(A, B)]b$. If we represent the probability of transfer of excitation from B to A by w_{11},

$$w_{11}=\frac{f_{11}(A, B)}{k_5+k_6+f_9(B)+f_{10}(A, B)+f_{11}(A, B)}$$

and $f_{11}(A, B)b=\beta I w_{11}$

$$\alpha I+\beta I w_{11}=[k_3+k_4+f_7(A)+f_8(A, B)]a.$$

The probability of an emission of a photon by A^* is

$$w_3=\frac{k_3}{k_3+k_4+f_7(A)+f_8(A, B)}.$$

Therefore $k_3a=w_3I(\alpha+\beta w_{11})$. Since the intensity of fluorescence for each component (A or B) is measured in arbitrary units, it cannot be set directly equal to the rate of the corresponding reaction steps. However, the directly measured fluorescence intensities $I_{F,a}$ and $I_{F,b}$, corresponding respectively to the emission from A and B in the solution, are proportional to the appropriate reaction rates.

$$I_{F,a}=rv_3 \quad \text{and} \quad I_{F,b}=sv_5$$

where r and s are constants, whose values are dependent upon the geometry of the fluorimeter and the transmissivity of the filter for the light emitted. If I_F is the total (measured) fluorescence of the solution, $I_F=I_{F,a}+I_{F,b}=rw_3I(\alpha+\beta w_{11})+s\beta I w_5$, where

$$w_5=\frac{k_5}{k_5+k_6+f_9(B)+f_{10}(A, B)+f_{11}(A, B)}.$$

For a solution containing A only, the measured intensity of the fluorescence is

$$I^\circ_{F,a}=rI^\circ_{A,a}\frac{k_3}{k_3+k_4+F_7(A)}$$

$$=rI^\circ_{A,a}w_3/(1-w_8)$$

where $I^\circ_{A,a}$ is the intensity of the light absorbed by the

TABLE VIII. Summary of sensitized fluorescence and cross-quenching.

$m_A\times10^4$	$m_B\times10^4$	I_F	I	α	$I^\circ_{A,a}$	$I^\circ_{F,a}$	$I^\circ_{A,b}$	$I^\circ_{F,b}$	Assume $w_8=0$		Assume $w_8=w_7$	
									w_{11}	w_{10}	w_{11}	w_{10}
1.05	1.05	16.5	0.35	0.140	0.050	4.1	0.310	8.8	0.24–0.50	0–0.50		
1.06	1.06	16	0.35	0.140	0.050	4.1	0.310	8.8	0.20–0.48	0–0.52		
1.51	1.51	19	0.46	0.148	0.076	6.3	0.389	11.1	0.10–0.41	0–0.59		
3.15	3.15	33	0.68	0.168	0.166	13.7	0.637	18.2	0.25–0.51	0–0.49		
3.20	3.20	35	0.69	0.169	0.167	13.8	0.645	18.4	0.30–0.54	0–0.46		
4.54	4.54	42	0.79	0.175	0.230	19.0	0.730	20.8	0.34–0.57	0–0.43		
19.4	19.4	54.5	1.00	0.21	1.00	82.5	1.00	29.0	0.34–0.57	0–0.43		
29.1	29.1	46.1	1.00	0.21	1.00	81.1	1.00	28.6	0.15–0.45	0–0.55		
49.3	49.3	31.1	1.00	0.21	1.00	76.5	1.00	25.8	0–0.25	0.26–0.75		
61.1	61.1	32.0	1.00	0.21	1.00	72.5	1.00	24.2	0–0.29	0.12–0.71		
104.5	104.5	15.5	1.00	0.21	1.00	57.1	1.00	19.8	0–0.08	0.77–0.92		
5.0	10.5	46	1.00	0.100	0.240	18.0	0.89	26	0.34–0.57	0–0.43	0.34–0.57	0–0.43
5.0	21.1	42	1.00	0.496	0.240	18.0	1.00	26	0.29–0.54	0–0.46	0.30–0.54	0–0.46
5.0	31.5	38.5	1.00	0.0334	0.240	18.0	1.00	25.5	0.24–0.50	0–0.50	0.25–0.51	0–0.49
5.0	41.9	37	1.00	0.0250	0.240	18.0	1.00	24	0.23–0.48	0–0.52	0.26–0.51	0–0.49
5.0	63.0	35	1.00	0.0167	0.240	18.0	1.00	21	0.24–0.45	0–0.55	0.30–0.53	0–0.47
5.0	84.0	31	1.00	0.0125	0.240	18.0	1.00	18.5	0.21–0.41	0–0.59	0.32–0.53	0–0.47
2.0	9.1	35	1.00	0.046	0.104	8.6	1.00	29	0.07–0.40	0–0.60		
4.0	9.1	40	1.00	0.093	0.202	16.6	1.00	29	0.13–0.43	0–0.57		
9.0	9.1	55	1.00	0.210	0.39	32	1.00	29	0.36–0.59	0–0.51		

solution of A and

$$w_8=\frac{f_8(A,B)}{k_3+k_4+f_7(A)+f_8(A,B)}.$$

Similarly,

$$I^\circ_{F,b}=sI^\circ_{A,b}\frac{w_5}{1-w_{10}-w_{11}}.$$

Therefore $rw_3=(I^\circ_{F,a}/I^\circ_{A,a})(1-w_8)$ and

$$sw_5=(I^\circ_{F,b}/I^\circ_{A,b})(1-w_{10}-w_{11})$$

and it follows that

$$\frac{I_F}{I}=\frac{I^\circ_{F,a}}{I^\circ_{A,a}}(\alpha+\beta w_{11})(1-w_8)+\frac{I^\circ_{F,b}}{I^\circ_{A,b}}\beta(1-w_{10}-w_{11}).$$

This is the general equation containing, in addition to several measurable quantities, three unknowns, w_8, w_{10}, and w_{11}. Since it appears that it would be stretching the precision of the data to try to determine all three of those unknowns, we shall assume a value for one of them. If it is assumed that concentration quenching is directly related to energy transfer[6-18,25] it follows that the efficiency of quenching of B^* by A will be much greater than A^* by B. The probability of the latter process is w_8. To simplify the treatment of the data, we shall assume that $w_8=0$. As a check on the validity of this assumption, we shall repeat the computations assuming that

$$w_8=\frac{f_7(A)}{k_3+k_4+f_7(A)},$$

which is an upper limit for w_8.

The data related to sensitized fluorescence and quenching are summarized in Table VIII. The values given in the columns headed I_f and I are directly measured quantities and correspond to the indicated molarities of chlorophylls a and b. The data listed in columns five through nine were obtained from Tables III, V, and VI by interpolation and by means of the safe assumption that for solutions of chlorophyll a (or b), too dilute to show concentration quenching, the intensity of fluorescence is directly proportional to the intensity of the absorbed light. The limiting values for w_{10} and w_{11}, given in the last four columns, were calculated by the methods described in the preceding section. The assumption that $w_8=0$ was tested only for those cases where it had the greatest effect upon the computed values. Even in these cases, it is apparent that this assumption does not change the general trend of these computed values. The values of the limits of w_{10} and w_{11}, corresponding to the experiments with equimolar solutions of chlorophylls a and b, are plotted as a function of the molarity in Fig. 3.

[25] T. Förster, Zeits. f. Electrochemie 53, 93 (1949).

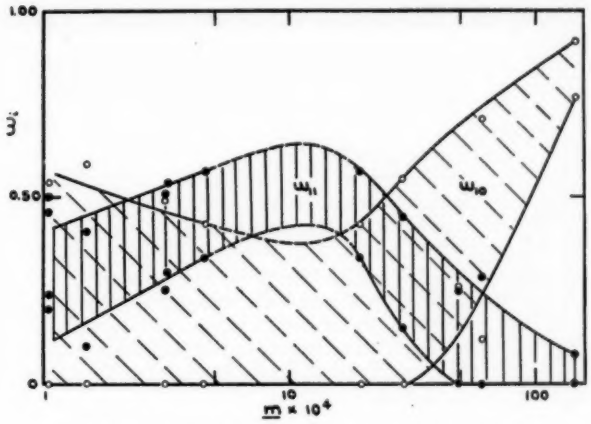

FIG. 3. Probabilities of excitation transfer in solutions of chlorophyll a and b.

There are several conclusions which can be drawn from these data: (1) Energy transfer from chlorophyll b to a becomes of relative importance in equimolar solutions at molarities greater than $2\times10^{-4}m$ (or possibly $1\times10^{-4}m$). This result is in surprisingly good agreement with the concentration of $8\times10^{-4}m$ which Förster has computed[17] as corresponding to the incidence of excitation transfer in chlorophyll solutions. (2) The quenching of chlorophyll b by chlorophyll a is more efficient than the self-quenching of either chlorophyll a or b. (3) The quenching of chlorophyll a by b is not more efficient than self-quenching and is probably of negligible importance. (4) The rate of quenching of chlorophyll b by a is a higher order function of concentration than is the rate of energy transfer between these molecules; indeed, the present data are consistent with the arbitrary hypothesis that the rate of quenching interactions is proportional to the second power of the dye and the rate of non-quenching transfers of excitation to the first power.

Recently Förster[25] has shown that the fluorescence of methanolic solutions of trypaflavine is quenched efficiently by rhodamine B. From a study of the quenching by mixtures of rhodamine B and potassium iodide and of the effect of viscosity upon the quenching by the several compounds, he demonstrates that the quenching of trypaflavine by rhodamine B is a statistical but non-diffusional process: i.e., that this quenching is not due to the formation of non-fluorescent addition compounds between the two dyes nor to collisions of the second kind. Due to experimental difficulties, he was unable to demonstrate that fluorescence of rhodamine B sensitized by trypaflavine occurred as the result of a direct exchange of excitation energy. The present results on chlorophylls a and b can be explained by a mechanism which is consistent with that put forward by Förster.[17,25]

On the Electrical Conductivity of Violanthrone, Iso-Violanthrone, and Pyranthrone

HIDEO AKAMATU AND HIROO INOKUCHI
Chemical Institute, Faculty of Science, Tokyo University, Tokyo
(Received February 16, 1950)

Violanthrone, iso-violanthrone, and pyranthrone have electrical conductance to a certain degree. This is due to the molecular structure of these compounds, which are made of the network planes of carbon atoms, and to the assumption that the π-electron contribute to the electrical conduction.

The electrical resistivity of violanthrone, iso-violanthrone, and pyranthrone was measured. The values at 15°C are as follows; 2.3×10^{10} ohm-cm, 5.7×10^{9} ohm-cm, and 3.9×10^{15} ohm-cm respectively. The resistivity decreases with increasing temperature in every case, and a good linear relationships is observed between the logarithm of the resistivity and the reciprocal of the temperature. As the activation energy of the electrical conductance, the following values were observed; 0.39 ev, 0.375 ev, and 0.53 ev respectively. The values for violanthrone and iso-violanthrone suggest that they can be assumed to be intrinsic semiconductors.

THE electrical conductivity of graphite[1] and carbon black has been attributed to their molecular structures which are made of network planes of the conjugated double bonds of carbon atoms with the π-electrons. There are some organic compounds which have similar molecular structures, for example, violanthrone, iso-violanthrone, and pyranthrone (Fig. 1). The analogy between the molecules of carbon black and these compounds has been pointed out by us in a previous paper,[2] although the molecules of these compounds do not form a layer lattice as do the carbon sheets in graphite. In spite of this difference there seems to be a possibility that these substances have electrical conductivity to a certain degree.

As single crystals are not available, we were obliged to deal with powdered specimens. The method was like that used by Brunner and Hammerschmid[3] for measuring the conductivity of powdered graphite. The specimen was packed in a good quality ebonite cylinder, and compressed between the metal ends. The electrical resistance was measured by the current produced for a known applied potential giving not over 800 volts per cm. The small current, less than 10^{-9} amp., was magnified 1500 times by a direct-current amplifier. Pressure was applied by a lever system. The highest value of the pressure was 300 kg/cm², and the dimensions of the specimen was between 0.1 and 0.3 cm in height and 0.5025 cm² in cross section. To control the temperature, the specimen holder was heated from outside by a small electrical oven. The surface of this oven was covered with copper plate, which was earthed to prevent any electrical disturbance.

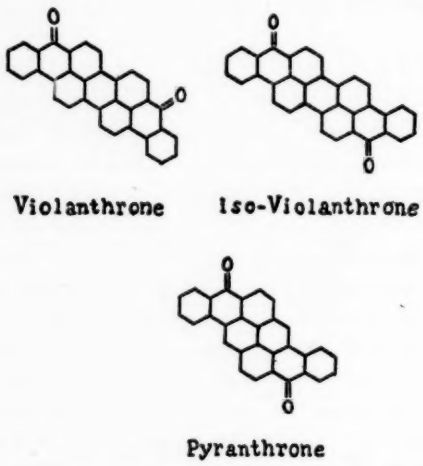

FIG. 1. Violanthrone, iso-violanthrone, and pyranthrone.

Violanthrone, iso-violanthrone, and pyranthrone were obtained by carefully purifying the commercial dyestuffs by the method already described by one of us.[2] The final products give many sharp x-ray diffraction powder pattern lines, and under the electron microscope they are found to be made up of flake-like needle crystals.

The relation between electrical resistivity ρ and pressure p is given in Fig. 2 for iso-violanthrone. The resistivity is approximately constant above 80 kg/cm² and values given below are for this range.

The temperature dependency of the electrical resistivity is shown in Figs. 3 and 4. The reproducibility of

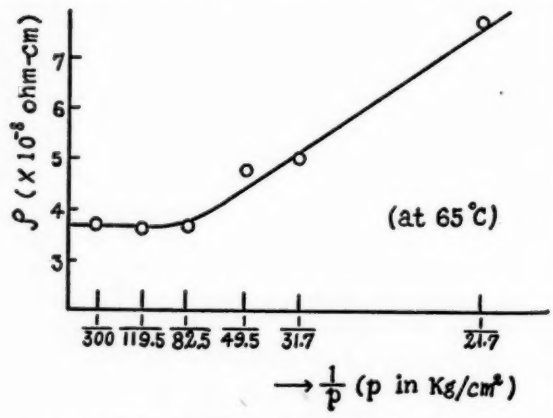

FIG. 2. The relation between resistivity and pressure for iso-violanthrone.

[1] P. R. Wallace, Phys. Rev. **71**, 622 (1947).
[2] H. Akamatu and K. Nagamatsu, J. Colloid Sci. **2**, 593 (1947).
[3] J. Brunner and H. Hammerschmid, Zeits. f. Elektrochemie **40**, 60 (1934).

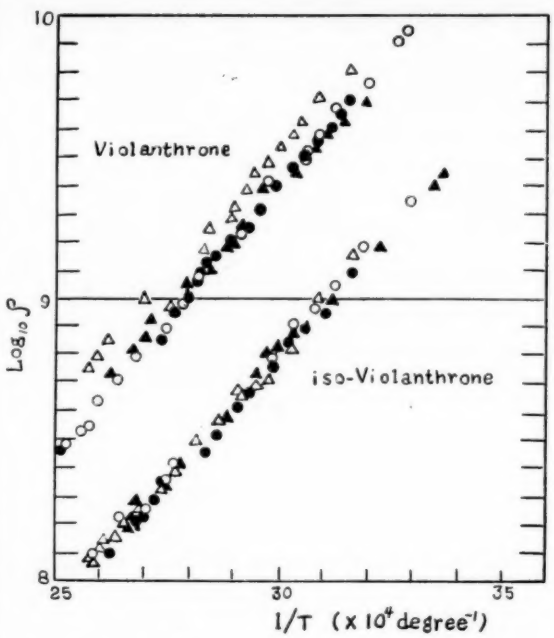

FIG. 3. The relation between resistivity and temperature for violanthrone and iso-violanthrone. △ 82.1 kg/cm², rising temp. ▲ 82.1 kg/cm², falling temp. ○ 119.5 kg/cm², rising temp. ● 119.5 kg/cm², falling temp.

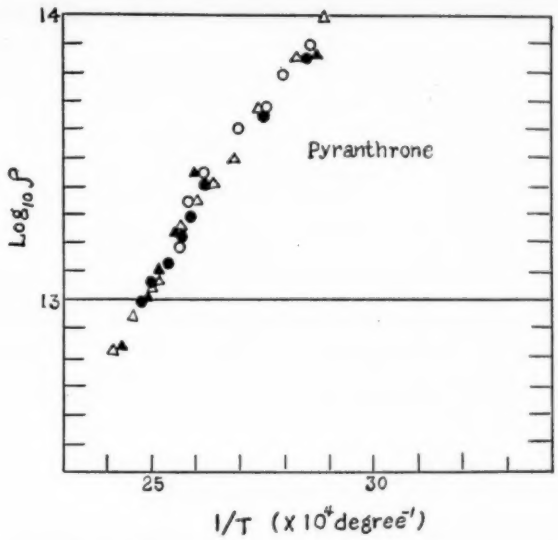

FIG. 4. The relation between resistivity and temperature for pyranthrone. The same symbols as in Fig. 3.

TABLE I. The values of ρ at 15°C, σ_0, E, and $\Delta\epsilon$ of violanthrone, iso-violanthrone, and pyranthrone.

	Violanthrone	Iso-violanthrone	Pyranthrone
ρ15°	2.3×10^{10} ohm-cm	5.7×10^{9} ohm-cm	3.9×10^{15} ohm-cm
E	0.39 ev	0.375 ev	0.53 ev
σ_0	3.4×10^{-4} ohm^{-1}-cm^{-1}	6.8×10^{-4} ohm^{-1}-cm^{-1}	4.1×10^{-7} ohm^{-1}-cm^{-1}
$\Delta\epsilon$	0.78 ev	0.75 ev	1.06 ev

the values observed was good, and hysteresis was not observed when the temperature was raised or dropped.

The temperature coefficient of the electrical resistivity was negative in every case, with a linear relation between $\log\rho$ and $1/T$ corresponding to $\rho=\rho_0\exp(E/kT)$, where E is the activation energy. Values of E, and of ρ at 15°C are given in Table I.

The purity of the specimen was proved by measurements of the resistivity after repeated sublimations, the value being highest after the first sublimation but thereafter constant. Thus initial impurities reduced the electrical conduction. The effect of moisture was also checked, but no important effect was observed. In the case of ionic conduction, it is known[4] that a relaxation time is frequently observed before the stationary current is established. No dependency of the current upon the time could be observed in our experiments. All of the observations seem to prove that the conduction is electronic.

The equation expressing resistivity can be rewritten as

$$\sigma=\sigma_0\exp(-\Delta\epsilon/2kT), \qquad (1)$$

where σ is the electrical conductivity and the formula is written intentionally analogous to that for semiconductors. Values of σ_0 and $\Delta\epsilon$ are given in Table I. By the theory of semiconductors, $\Delta\epsilon$ is the energy difference between the empty level and the occupied level of the crystal, and the observed values of $\Delta\epsilon$ are comparable to those of usual semiconductors, of the order of $10^{-1}\sim10^{-2}$ ev generally. Hence the electrical conductivity of these three compounds is similar to that of the usual semiconductors. If we assume that the observed resistivities are attributed largely to contact resistances at the boundaries of the crystallites, the crystals themselves must have considerably higher conductivities than the values observed. If these compounds can be assumed to be semiconductors, they must be so-called intrinsic semiconductor, because the presence of impurities is not necessary.

[4] M. F. Manning and M. E. Bell, Rev. Mod. Phys. 12, 215 (1940).

Infra-Red and Raman Spectra of Fluorinated Ethylenes. III. Tetrafluoroethylene*

J. Rud Nielsen and Howard H. Claassen
Department of Physics, University of Oklahoma, Norman, Oklahoma

and

D. C. Smith
Naval Research Laboratory, Washington, D. C.

(Received March 6, 1950)

The infra-red absorption spectrum of gaseous tetrafluoroethylene between 2 and 22μ has been investigated with a prism spectrometer of high resolution, and the region from 20 to 37μ has been surveyed with a KRS-5 prism. The Raman spectrum of C_2F_4 gas has been photographed with a three-prism glass spectrograph of linear dispersion 15 A/mm at 4358A, and semiquantitative polarization measurements have been made. All of the 12 fundamental vibration frequencies have been determined, although with some uncertainty for three frequencies obtained from combination bands. The spectra have been interpreted in detail.

INTRODUCTION

THE infra-red spectrum of tetrafluoroethylene has been studied by Torkington and Thompson.[1] The Raman spectrum has apparently not been previously investigated. If this molecule has the same symmetry as ethylene, as indicated by recent electron diffraction work by Isabella and Jerome Karle,[2] only five of the twelve fundamentals and none of the first overtones are active in infra-red absorption. Hence, Torkington and Thompson were not able to assign more than two or three of the fundamentals with any certainty.

EXPERIMENTAL

Two samples of tetrafluoroethylene were investigated. The infra-red spectrum of the first sample did not agree well with that shown by Torkington and Thompson; some of the bands had about the same intensity, others were several-fold weaker and a few definitely stronger. For this reason, and because of difficulties encountered in the interpretation of the spectra, it was concluded that the first sample and also that studied by Torkington and Thompson were impure. Through the courtesy of Dr. C. F. Hammer of the Plastics Department of E. I. du Pont de Nemours and Company, information was obtained about the impurities present, and later a purified sample was secured. The only impurity known to be present in the second sample is a very small amount of cyclic C_4F_8.

The infra-red spectrum of gaseous C_2F_4 was measured from 2 to 22.3μ in the manner described in the first paper of this series.[3] In addition, the region from 22 to 37.6μ was surveyed with a KRS-5 prism instrument at the National Bureau of Standards, through the courtesy of Dr. E. K. Plyler. The Raman spectrum of gaseous C_2F_4 at about seven atmospheres was studied with a Lane-Wells spectrograph, and polarization measurements were made on the first sample in the manner previously described.[4] In order to get as complete a Raman spectrum of the second sample as possible, this sample was exposed for 190 hours in the apparatus used for polarization measurements, with all but a few baffles removed.

RESULTS

The infra-red absorption spectrum from 2 to 22.3μ of the second sample of tetrafluoroethylene gas is shown in Fig. 1. The wave numbers for the observed absorption maxima or "shoulders" are given in the first column of Table I. In the second column are indicated the relative intensities as well as the band contours in Badger and Zumwalt's notation.[5] A microphotometer record of the Raman spectrum of the second sample of C_2F_4 gas is shown in Fig. 2. The observed Raman shifts are listed in the first column of Table II. In the second column are given rough estimates of the intensities of the bands and indications of unusual sharpness or diffuseness. In the third column are given results of the polarization measurements made on the impure sample. Because of the extreme weakness of the Raman bands, the polarization data are mostly qualitative.

INTERPRETATION

1. Determination of Fundamentals

The interpretation of the infra-red and Raman spectra of tetrafluoroethylene has proved to be a difficult problem. This has been in part caused by the presence of impurity bands in the spectra of the first sample. It has also been a result of the facts that two of the infra-red-active fundamentals lie beyond 22μ and two of the Raman-active fundamentals overlap, while a third is abnormally weak and diffuse.

The available electron diffraction data are consistent with the assumption that the C_2F_4 molecule is planar and of symmetry V_h. From Brockway and Livingston's[6]

* This work has been supported by the ONR under Contract N7 onr-398, Task Order I.

[1] P. Torkington and H. W. Thompson, Trans. Faraday Soc. **41**, 236 (1945).

[2] I. L. Karle and J. Karle, J. Chem. Phys. **18**, 565 (1950).

[3] Smith, Nielsen, and Claassen, J. Chem. Phys. **18**, 326 (1950).

[4] Nielsen, Claassen, and Smith, J. Chem. Phys. **18**, 485 (1950).

[5] R. M. Badger and L. R. Zumwalt, J. Chem. Phys. **6**, 711 (1938).

[6] L. O. Brockway and R. L. Livingston, University of Michigan Report M510 on Electron Diffraction Investigation of Fluorocarbons, June 30, 1944.

data: C=C distance=1.27A, CF distance=1.32A and FCF angle=110°, the following moments of inertia are obtained: 147, 261 and 408×10^{-40} g cm². The axis of smallest moment of inertia is the line through the two carbon nuclei. Recent work by Drs. Isabella and Jerome Karle[2] has given the dimensions: C=C distance=CF distance=1.31A and the FCF angle=114°. These data give the values 152, 254, and 406×10^{6} g cm² for the three moments of inertia.

From these moments of inertia the Badger-Zumwalt parameters are found to be $\rho=1.04$ and $S=-0.28$. From Badger and Zumwalt's curves for $\rho=5/4$ and $S=-\frac{1}{2}$ the approximate values 7.1, 5.7, and 6.5 cm^{-1}, are found for the separation $\nu-\nu_0$ of the maxima of the rotational branches from the band center for Types A, B and C bands, respectively.

If the C_2F_4 molecule is planar and of symmetry V_h the normal vibrations divide themselves into symmetry species in the following manner: $3A_g+1A_u+2B_{1g}+1B_{1u}+1B_{2g}+2B_{2u}+2B_{3u}$. The three fundamentals belonging to A_g are active only in the Raman effect and give rise to polarized bands. The two fundamentals belonging to B_{1g} and the one belonging to B_{2g} give depolarized Raman bands and are inactive in the infra-red. The normal vibration belonging to A_u is inactive both in the Raman effect and in infra-red absorption. The fundamental belonging to B_{1u} is active only in the infra-red and gives rise to a band with Type C contour. The two

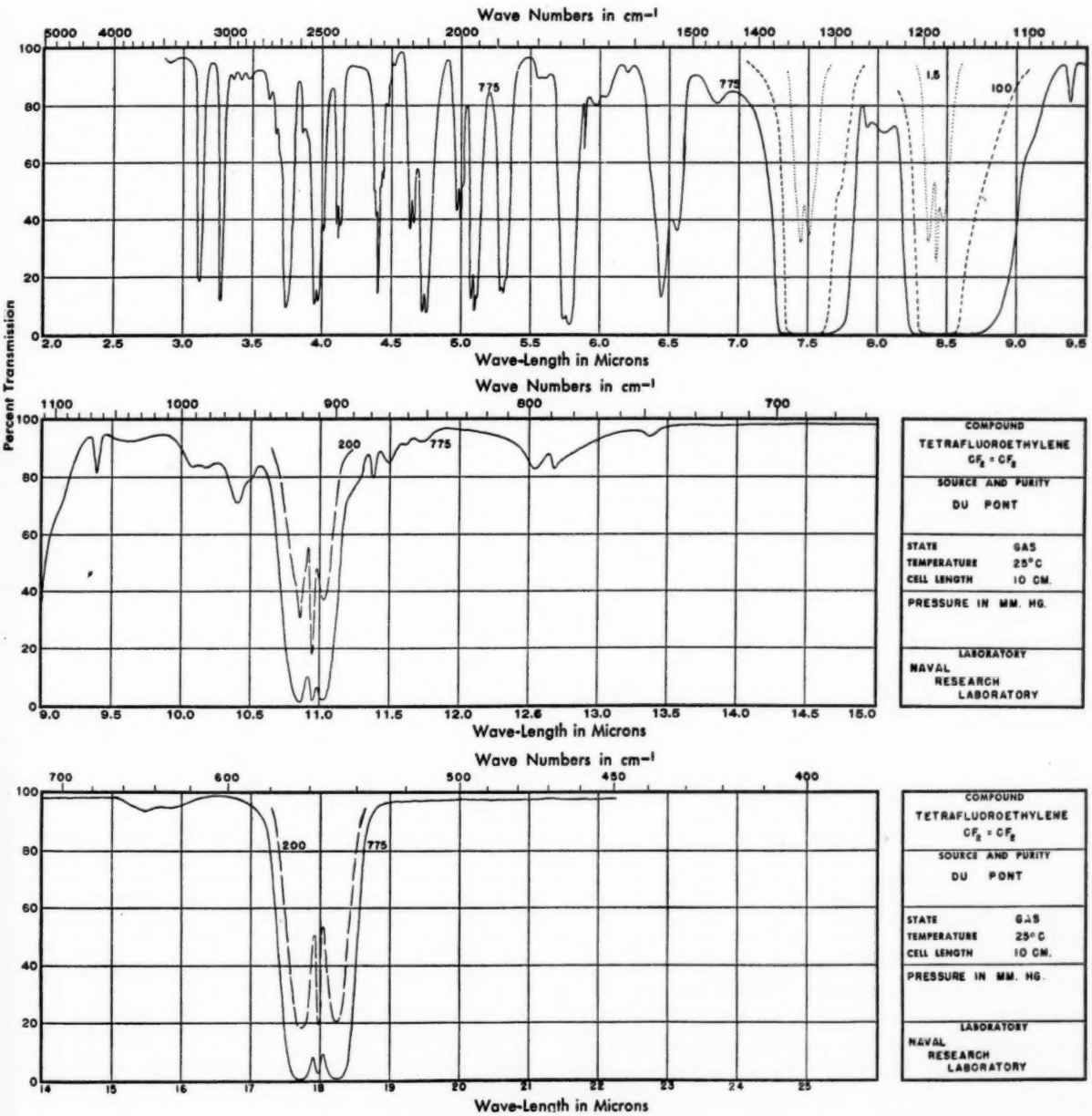

FIG. 1. Infra-red spectrum of tetrafluoroethylene gas.

TABLE I. Infra-red spectrum of tetrafluoroethylene (gas).

Wave number	Description		Interpretation
370* cm^{-1}			$778-407=371(B_{1u})$
407*	s	Type *A* or *C*	B_{1u} Fundamental
549			
558	s	Type *A*	B_{3u} Fundamental
566			
~631	vvw	Type *B*	$245+394=639(B_{2u})$;
~647	vvw		$1186-544=642(B_{2u})$
747	vvw		$210+544=754(B_{1u})$
789	vvw		$245+544=789(B_{3u})$; $1340-558=782(B_{2u})$
~796	vvw		$394+407=801(B_{1u})$; $1337-544=793(B_{3u})$
852	vvw		
862	vvw		$210+245+407=862(B_{3u})$
871	vvw		
879	vw	Type *A* or *C*	$510+778-407=881(B_{3u})$;
~886	vvw		$407+2\times245=897(B_{1u})$
907			
913	s	Type *A*	$407+510=917(B_{3u})$
921			
~953	vvw		$394+558=952(B_{3u})$; $1337-394=943(B_{2u})$
~960	vw		Cyclic C_4F_8 impurity
982	vvw	Type *B*?	$558+2\times210=978(B_{3u})$
992	vvw		$407+2\times245=897(B_{1u})$
1040			
1065	vvw	Type *C*	$510+558=1068(B_{1u})$
1090			
1181			
1186	vs	Type *A*	B_{3u} Fundamental
1195			
~1239	vvw		Cyclic C_4F_8 impurity
1261	vvw		$210+510+544=1264(B_{3u})$; $245+2\times510=1265(B_{2u})$
~1295			$245+510+544=1299(B_{1u})$
1332	vs	Type *B*	B_{2u} Fundamental
1342	vs		
~1460	vw d		$1872-407=1465(B_{1u})$; $407+510+544=1461(B_{2u})$; $394+510+558=1462(B_{1u})$
1524	m		$407+2\times558=1523(B_{1u})$
1550	m		$210+1340=1550(B_{1u})$
1613	vvw		$1186+2\times210=1606(B_{1u})$
~1656	vvw		$558+2\times544=1646(B_{3u})$
~1675	vvw		$3\times558=1674(B_{3u})$; $1186+2\times245=1676(B_{3u})$
1696	vw	Type *C*	$510+1186=1696(B_{1u})$
~1729	s	Type *B*	$394+1337=1731(B_{2u})$;
~1741	s		$544+1186=1730(B_{2u})$
~1790	vvw	Type *B*	$210+407+1186=1803(B_{2u})$
~1800	vvw		
~1880	m		$544+1337=1881(B_{3u})$
1885	m		
1888	m		
1893	m		$558+1340=1898(B_{2u})$
1954	m		
1962	m	Type *A*	$778+1186=1964(B_{3u})$
1969	m		
1997			
2002	m	Type *A*	$1186+2\times407=2000(B_{3u})$
2011			
2105	s	Type *B*	$778+1337=2115(B_{2u})$;
2116	s		$245+1872=2117(B_{2u})$
2147	m	Type *B*	$1337+2\times407=2151(B_{2u})$
2156	m		
2213	vvw		$1186+2\times510=2206(B_{3u})$
2240	vvw		
2255	vw		$407+510+1340=2257(B_{2u})$
2261	w		
2274	m	Type *C*	$407+1872=2279(B_{1u})$
2279	w		
2287	vw		$407+544+1340=2291(B_{1u})$; $394+558+1340=2292(B_{2u})$
2421	w		
2427	m		$558+1872=2430(B_{3u})$
2434	w		
2498	vw		$394+778+1337=2509(B_{2u})$; $245+394+1872=2511(B_{2u})$; $544+778+1186=2508(B_{2u})$
2523	m	Type *B*	$1186+1340=2526(B_{2u})$
2534	m		
2588	vvw		$210+510+1872=2592(B_{2u})$
2648	vw		
2672	m		$1337+1340=2677(B_{3u})$
2680	vw		
2723	vvw		$210+1186+1337=2733(B_{1u})$; $1186+2\times778=2742(B_{3u})$
2762	vvw		$245+1186+1337=2768(B_{3u})$
2880	vvw		$1337+2\times778=2893(B_{2u})$; $245+778+1872=2895(B_{2u})$
2924	vvw		$558+2\times1186=2930(B_{3u})$; $245+2\times1340=2925(B_{2u})$; $394+1186+1340=2920(B_{2u})$
2976	vvw		$544+558+1872=2974(B_{2u})$
~3058	m		$1186+1872=3058(B_{2u})$
~3205	m		$1337+1872=3209(B_{2u})$

TABLE I.—*Continued.*

* Observed by Dr. E. K. Plyler of the National Bureau of Standards.

fundamentals belonging to B_{2u} are infra-red-active and give bands of contour Type *B*. The two vibrations belonging to B_{3u} give Type *A* infra-red bands. Neither the B_{2u} nor the B_{3u} vibrations are Raman-active.

The three strong or medium Raman bands at 1872, 819 and 778 cm^{-1} are definitely polarized. The polarization exposures indicate that also the weak band at 394 cm^{-1} is polarized. Moreover, the still weaker sharp Raman band at 1019 cm^{-1} has a contour indicating that it is totally symmetrical. The band at 1872 cm^{-1} is certainly an A_g fundamental. Since all of the olefinic fluorocarbons that have been investigated have a frequency in this region, this fundamental can presumably be characterized roughly as a C=C stretching mode. The Raman band at 778 cm^{-1}, which is highly polarized and the most intense band in the spectrum, certainly represents an A_g fundamental. It probably involves largely a symmetrical CF stretching but undoubtedly also CF_2 deformation and a certain amount of C=C stretching. On the assumption that the C_2F_4 molecule has the symmetry V_h, there should be only one more A_g fundamental. The polarized Raman bands at 819 and 1019 cm^{-1} can both be interpreted as overtones. The high intensity of the former may be explained as resulting from its proximity to the A_g fundamental at 778

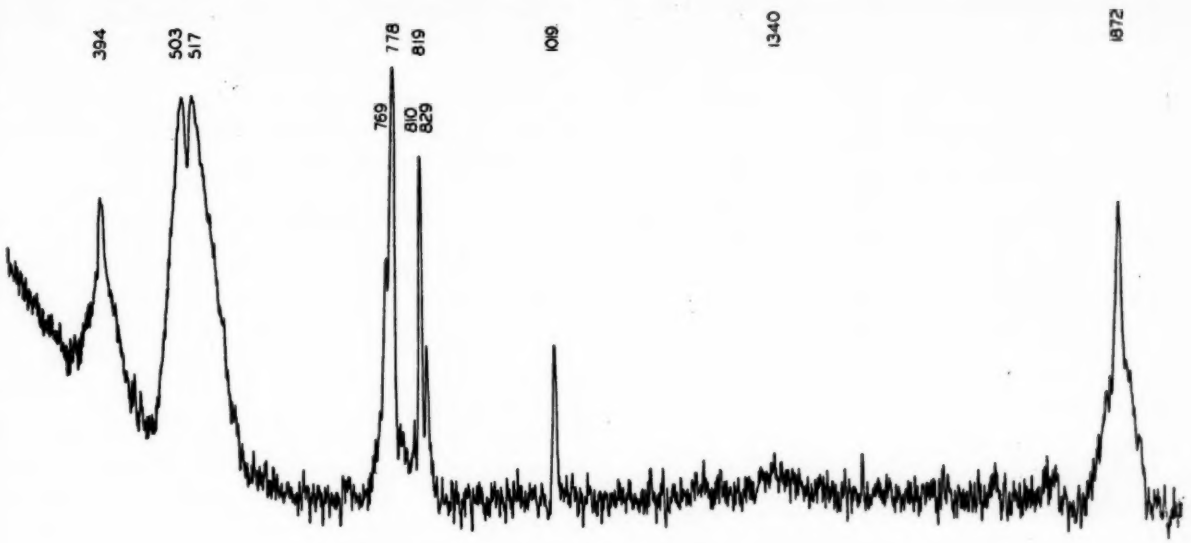

FIG. 2. Raman spectrum of tetrafluoroethylene gas.

cm^{-1}. Thus, the third A_g fundamental must undoubtedly be identified with the rather weak Raman band at 394 cm^{-1}. It may be designated roughly as a symmetrical CF_2 deformation mode.

Three fundamentals should give depolarized Raman bands. Two of these, associated with in-plane rocking (B_{1g}) and out-of-plane wagging (B_{2g}) motions in which the two carbon atoms, moving out of phase with each other, have greater amplitude than the fluorine atoms, may be expected to lie in the neighborhood of 500 cm^{-1}. At first they were identified with a broad asymmetrical depolarized doublet appearing at 503 and 517 cm^{-1}. This interpretation, however, led to difficulties in accounting for overtone and combination bands. It was then recalled that the theory of interaction between vibration and rotation predicts a doublet structure for the B_{2g} fundamental,[7] and the two maxima were interpreted as the rotational branches of this fundamental the center of which was taken to be at 510 cm^{-1}. Because of the apparent broadening of the doublet band towards high wave numbers it was assumed that the B_{1g} rocking frequency lies somewhat higher than the B_{2g} fundamental. The value of 544 cm^{-1} was subsequently determined from infra-red combination bands. It is neither as accurate nor as certain as the directly determined fundamentals.

The other B_{1g} fundamental, which may be characterized roughly as an unsymmetrical CF stretching vibration, would be expected to lie in the region between 1100 and 1400 cm^{-1}. It was first identified with a weak band at 1225 cm^{-1}. However, when the purer sample of C_2F_4 became available this band was found to have been caused by an impurity. An attempt was therefore made to determine this fundamental from the five binary infra-red combination bands in which it should occur. Four of these bands were identified with a fair degree of certainty, and the frequency 1340 cm^{-1} was determined. Afterward, when a 190-hour exposure was made with the pure sample of C_2F_4, a weak and extremely diffuse Raman band with a maximum at 1340±10 cm^{-1} was observed. There can be no doubt that it represents the high B_{1g} fundamental. Its low intensity may be an indication of the highly ionic character of the CF bonds in C_2F_4.

The two fundamentals of species B_{3u} should give rise to Type A infra-red absorption bands. As may be seen from Fig. 1, three strong bands of this contour type have been observed. Those at 558 and 1186 cm^{-1} are undoubtedly the B_{3u} fundamentals. The former may be characterized roughly as a CF_2 deformation, the other as a symmetrical CF stretching mode in which the motions in the two CF_2 groups are out of phase. The Type A band at 913 cm^{-1}, which is somewhat less intense than the band at 558 and much weaker than the band at 1186 cm^{-1}, has been interpreted as a combination band.

TABLE II. Raman spectrum of tetrafluoroethylene (gas).

Wave number	Description		Depolarization	Interpretation
394 cm^{-1}	w		p?	A_g Fundamental
503	m	d	0.88	B_{2g} Fundamental
517	m	d	0.84	
769.4	vw	sh		$788+\nu_i-\nu_i(A_g)$; $210+558=768(B_{3g})$
777.9	s	sh	<0.2	A_g Fundamental
809.7	vvw	sh		$2\times394=788(A_g)$; $2\times407+\nu_j-\nu_j$
818.9	m	sh	<0.4	$2\times407=814(A_g)$
828.7	vw	sh		$2\times407+\nu_k-\nu_kA_g$
1018.5	w	sh		$2\times510=1020(A_g)$
1340	vw	vd		B_{1g} Fundamental
1872	m		p	A_g Fundamental

[7] See G. Herzberg, *Infrared and Raman Spectra of Polyatomic Molecules* (D. Van Nostrand & Company, New York, 1945), p. 491.

TABLE III. Fundamental vibration frequencies for C_2F_4 (gas).

Symmetry species	Approximate character	Wave number	Spectrum in which observed
A_g	CF_2 Deformation	394 cm^{-1}	R
A_g	CF Stretching	777.9	R
A_g	C:C Stretching	1872	R
A_u	Twisting	~210	I combinations
B_{1g}	CF_2 Rocking	~544	I combinations
B_{1g}	CF Stretching	~1340	R
B_{1u}	CF_2 Wagging	407	I
B_{2g}	CF_2 Wagging	510	R
B_{2u}	CF_2 Rocking	~245	I combinations
B_{2u}	CF Stretching	1337	I
B_{3u}	CF_2 Deformation	558	I
B_{3u}	CF Stretching	1186	I

The very intense infra-red band at 1337 cm^{-1} has a Type B contour with about the predicted separation between the rotational branches. It must be one of the two B_{2u} fundamentals and may be characterized as an unsymmetrical CF stretching mode. The other B_{2u} fundamental, which may be characterized roughly as a CF_2 rocking vibration in which the two carbon atoms are displaced in the same direction, should lie at considerably lower wave numbers. Since no other Type B band of reasonable intensity had been observed above 450 cm^{-1}, it was concluded that the second B_{2u} fundamental lies beyond the long wave-length limit of the region observable with a potassium bromide prism. Moreover, when it was found that the only observed Type C bands that might be identified with the single fundamental of species B_{1u} were caused by impurities, it became clear that this fundamental also lies outside the range of the potassium bromide prism. Arrangements were therefore made to survey the infra-red spectrum with a KRS-5 prism at the National Bureau of Standards. Two bands were observed, a strong band at 407 cm^{-1} and a faint band at 370 cm^{-1}. The latter can readily be interpreted as a difference band, 778–407 cm^{-1}. The band at 407 cm^{-1} was first reported to have doublet structure and was therefore interpreted as the missing B_{2u} fundamental. However, when attempts were made to identify certain combination bands this assignment proved unsatisfactory. The data obtained at the Bureau of Standards were then examined, and it was found that the band at 407 cm^{-1} definitely has a PQR structure. Thus, although the resolution was too low to differentiate between Type A and Type C contours, it is clear that 407 cm^{-1} must be the B_{1u} rather than the B_{2u} fundamental. The latter then must lie below 266 cm^{-1}, the smallest wave number reached by the KRS-5 instrument. Attempts to determine it from infra-red combination bands have led to the value 245 cm^{-1}.

The single fundamental of species A_u, which represents a torsional oscillation, is inactive as well in the infra-red as in the Raman effect but should occur in three infra-red binary combination bands. Two of these have been identified with fair certainty and the frequency 210 cm^{-1} obtained.

The values obtained for the fundamental vibration frequencies for tetrafluoroethylene are listed in the third column of Table III. In the second column the general nature of the vibrations is roughly indicated. In the fourth column is given the spectrum from which each fundamental has been determined.

2. Interpretation of the Spectra

On the basis of the fundamental vibration frequencies listed in Table III it has been possible to interpret satisfactorily all of the observed infra-red absorption maxima and Raman bands. The interpretations are given in the third column of Table I and the fourth column of Table II.

Of the 29 binary sum bands that are infra-red active 20 have been observed. Three are masked by fundamentals, four overlap with other binary combination bands, and two are apparently too weak for observation. Only two absorption maxima are interpreted as binary difference bands. However, some of the bands interpreted as sum bands could be interpreted as difference bands. Thus, the Type B band at 639 cm^{-1} could be interpreted as $1186-544=642(B_{2u})$, the band at 789 cm^{-1} could be $1337-544=787(B_{3u})$ or $1340-558=782(B_{2u})$, and the band at 796 cm^{-1} could be $1186-394=792(B_{3u})$. Some 20 bands are interpreted as ternary combination bands.

The agreement between the calculated and observed frequencies is very close in all cases, except for the band at 879 cm^{-1} which is interpreted as a ternary combination involving twice the rather inaccurately determined fundamental 245 cm^{-1}. Many of the absorption maxima, especially at high frequencies, can be interpreted in more than one way. A number of the alternative interpretations are included in Table I, especially in cases where they are nearly as plausible as the preferred interpretations or where the band contour indicates an overlapping of two or more bands. In the case of a few bands, notably the doublet bands at 1735, 2111, and 2152 cm^{-1}, two interpretations appear equally satisfactory in the absence of theoretical intensity estimates. No evidence is found of Fermi coupling in these cases.

The remarkably high intensity of the binary band at 913 cm^{-1} has already been mentioned. The ternary bands at 2002 and 2152 cm^{-1} also seem to have surprisingly high intensity. Other bands are equally conspicuous by their low intensity. While the correlation between the observed contour and the assigned species is very good on the whole, there are some exceptions, and a number of bands do not have typical contours. Most of these bands, however, are very weak and overlap with other bands.

The interpretation given in Table II of some of the Raman bands not taken to be fundamentals suffers from certain ambiguities. The band at 819.9 cm^{-1} is undoubtedly an overtone, probably of 407 cm^{-1} but possibly of 394 cm^{-1}, which has been enhanced by Fermi coupling with the totally-symmetrical fundamental at

777.9 cm^{-1}. The band at 809.7 cm^{-1} has been interpreted as 2×394, the rather large difference between calculated and observed frequency being ascribed to the proximity to the A_g fundamental. However, this band could be an upper-stage band corresponding to 819 cm^{-1}.

The interpretation of the faint sharp band at 769.4 cm^{-1} as an upper-stage band, $778+\nu_i-\nu_i$, seems more plausible than its interpretation as the B_{3g} combination, $210+558$ cm^{-1}. The faint sharp Raman band at 828.7 cm^{-1} has been interpreted as an upper-stage band, $2\times407+\nu_k-\nu_k$, rather than as the B_{3g} difference band $1340-510$ cm^{-1}, because the corresponding sum band has not been observed. If the preferred interpretations are correct, the group of Raman bands, 769, 778, 819, and 829 cm^{-1}, are related to each other in much the same manner as similar groups in the spectra of CO_2 and CS_2.

ACKNOWLEDGMENTS

The writers wish to express their indebtedness to Dr. C. F. Hammer and E. I. du Pont de Nemours and Company for the samples; to Doctors Isabella and Jerome Karle for electron diffraction data; and to Dr. E. K. Plyler and the National Bureau of Standards for data in the long wave-length region.

THE JOURNAL OF CHEMICAL PHYSICS VOLUME 18, NUMBER 6 JUNE, 1950

The Statistical Mechanical Theory of Transport Processes. IV. The Equations of Hydrodynamics*

J. H. Irving and John G. Kirkwood
Gates and Crellin Laboratories of Chemistry No. 1343, Pasadena, California
(Received November 21, 1949)

The equations of hydrodynamics—continuity equation, equation of motion, and equation of energy transport—are derived by means of the classical statistical mechanics. Thereby, expressions are obtained for the stress tensor and heat current density in terms of molecular variables. In addition to the familiar terms occurring in the kinetic theory of gases, there are terms depending upon intermolecular force. The contributions of intermolecular force to the stress tensor and heat current density are expressed, respectively, as quadratures of the density and current density in the configuration space of a pair of molecules.

INTRODUCTION

THIS paper will be concerned with a derivation of the equations of hydrodynamics from the principles of the classical statistical mechanics. In particular, the equation of continuity, the equation of motion, and the equation of energy transport will be derived. By so doing, the stress tensor and heat current density can be expressed in terms of molecular variables. The stress tensor consists of a kinetic part (which occurs in the kinetic theory of gases) and another term (dominant for a liquid) which will be expressed as a quadrature involving the potential of intermolecular force and the density of pairs of molecules. The heat current density is the sum of the familiar kinetic part and a quadrature involving the potential of intermolecular force and the density and current density in the configuration space of a pair of molecules. The results were previously stated in the first article of this series,[1] when this derivation was promised.

To obtain explicit expressions for the pair probability density and probability current density one would in principle need to solve the Liouville equation [Eq. (2.2)] for the probability distribution in Gibbs phase space and then perform repeated integrations. Since this program is untenable for a liquid, various attempts have been made to obtain a closed equation satisfied approximately by the probability distribution function in the phase space of a pair of molecules. One such equation has been derived by Born and Green[2] using a generalized "superposition" assumption. Another, a generalization of the well-known Fokker-Planck equation of stochastic theory, has been derived by Kirkwood[1] by introducing the concepts of time smoothing and a friction constant. This latter equation has been applied to obtain an expression for the stress tensor linear in gradients of fluid velocity and, thereby, expressions (in terms of molecular variables) for coefficients of shear and volume viscosity.[3] The same equation generalized to non-uniform temperatures, after linearizing in the temperature gradient, leads to an explicit expression for the heat current and thereby to an expression for the coefficient of thermal conductivity.[4] We shall assume, for purposes of mathematical simplicity, a single component, single phase fluid system consisting of molecules which interact under central forces only. It is not difficult to generalize the treatment to a multiple component or multiple

* This work was supported by the U. S. ONR under Contract N6onr-244 with the California Institute of Technology.
[1] J. G. Kirkwood, J. Chem. Phys. **14**, 180 (1946).
[2] M. Born and H. S. Green, Proc. Roy. Soc. **A188**, 10 (1946).
[3] Kirkwood, Buff, and Green, J. Chem. Phys. **17**, 988 (1949).
[4] Kirkwood, Standart, and Irving (in preparation). The numerical evaluation awaits a more precise computation of the theoretical radial distribution function.

phase system or to include molecular interaction depending upon rotational or internal degrees of freedom. Before entering upon the statistical mechanical theory, we shall first review the phenomenological theory of the hydrodynamical equations.

I. THE PHENOMENOLOGICAL THEORY

We imagine a continuous fluid consisting of a single chemical component with mass density $\rho(\mathbf{r};t)$ and local velocity $\mathbf{u}(\mathbf{r};t)$ at the point $\mathbf{r}$ and at the time t. We now imagine ω to be a fixed region somewhere in the interior of the fluid. The mass of the fluid within ω is given by

$$\int_\omega \rho(\mathbf{r};t)d\omega.$$

Its rate of change, since ω is fixed (not moving with the fluid), is

$$\int_\omega \frac{\partial}{\partial t}\rho(\mathbf{r};t)d\omega.$$

This increase of mass must be entirely due to influx of fluid through the boundary S of ω, i.e.,

$$\int_\omega \frac{\partial}{\partial t}\rho d\omega = -\int_S \rho\mathbf{u}\cdot d\mathbf{S} = -\int_\omega \nabla_\mathbf{r}\cdot[\rho\mathbf{u}]d\omega$$

where the surface integral has been converted to a volume integral by Gauss' theorem. Since ω is quite arbitrary, upon equating integrands, we get the continuity equation

$$\frac{\partial}{\partial t}\rho(\mathbf{r};t) = -\nabla_\mathbf{r}\cdot[\rho(\mathbf{r};t)\mathbf{u}(\mathbf{r};t)]. \tag{1.1}$$

The hydrodynamical equation of motion may be derived by equating the rate of change of momentum within ω,

$$\int_\omega \frac{\partial}{\partial t}[\rho(\mathbf{r};t)\mathbf{u}(\mathbf{r};t)]d\omega$$

plus the rate of flow of momentum out through the surface of ω,

$$\int_S \rho(\mathbf{r};t)\mathbf{u}(\mathbf{r};t)\mathbf{u}(\mathbf{r};t)\cdot d\mathbf{S} = \int_\omega \nabla_\mathbf{r}\cdot[\rho\mathbf{u}\mathbf{u}]d\omega$$

to the sum of the forces acting on the fluid within ω. These forces are the body force

$$\int_\omega \mathbf{X}(\mathbf{r};t)d\omega,$$

where $\mathbf{X}$ is the force per unit volume due to external sources, and the surface force.

$$\int_S \boldsymbol{\sigma}(\mathbf{r};t)\cdot d\mathbf{S} = \int_\omega \nabla_\mathbf{r}\cdot\boldsymbol{\sigma}d\omega,$$

where $\boldsymbol{\sigma}$ is the symmetric stress tensor.

Since ω is arbitrary, the resulting differential equation is

$$\frac{\partial}{\partial t}[\rho\mathbf{u}]+\nabla_\mathbf{r}\cdot[\rho\mathbf{u}\mathbf{u}] = \mathbf{X}+\nabla_\mathbf{r}\cdot\boldsymbol{\sigma}. \tag{1.2}$$

We now introduce the internal energy density, $E(\mathbf{r};t)$, consisting of three parts—the interaction potential energy density, $E_V(\mathbf{r};t)$, due to interactions between fluid particles; the kinetic energy density, $E_K(\mathbf{r};t)$; and the potential energy density, $E_\psi(\mathbf{r};t)$, due to external sources, assumed to be conservative.

$$E = E_V+E_K+E_\psi. \tag{1.3}$$

The rate of change of internal energy within ω is

$$\int_\omega \frac{\partial}{\partial t}E(\mathbf{r};t)d\omega.$$

The rate of flux of energy from ω is

$$\int_S [E(\mathbf{r};t)\mathbf{u}(\mathbf{r};t)+\mathbf{q}(\mathbf{r};t)]\cdot d\mathbf{S} = \int_\omega \nabla_\mathbf{r}\cdot[E\mathbf{u}+\mathbf{q}]d\omega$$

where $E\mathbf{u}$ is the convective energy current and $\mathbf{q}$ is the conductive heat current. The work done per unit time by the fluid within ω on the rest of the system is

$$-\int_\omega \mathbf{u}\cdot\boldsymbol{\sigma}\cdot d\mathbf{S} = -\int_S \nabla_\mathbf{r}\cdot(\mathbf{u}\cdot\boldsymbol{\sigma})d\omega.$$

According to the law of conservation of energy, the sum of these three rates must vanish. Since ω is arbitrary, the sum of the integrands must also vanish, giving the energy transport equation

$$(\partial/\partial t)E+\nabla_\mathbf{r}\cdot[E\mathbf{u}+\mathbf{q}-\mathbf{u}\cdot\boldsymbol{\sigma}] = 0. \tag{1.4}$$

II. STATISTICAL MECHANICAL THEORY—THE DISTRIBUTION FUNCTION AND EXPECTATION VALUES

In the statistical mechanical theory we no longer consider a continuous fluid, but rather we treat a system consisting of N molecules, each having three degrees of translational freedom (but for the sake of simplicity, no other degrees of freedom). We denote the positions of these molecules by the sequence of three-vectors $\mathbf{R}_1, \mathbf{R}_2, \cdots, \mathbf{R}_N$, and their momenta by $\mathbf{p}_1, \mathbf{p}_2, \cdots, \mathbf{p}_N$. According to Gibbs, the instantaneous state of the system may be represented by a point in the $6N$-dimensional phase space representing the $3N$ coordinates and $3N$ momenta of the system. We may consider our representative system as drawn randomly from an ensemble of similar systems, the state of each being confined to that portion of phase space consistent with the macroscopic restraints imposed in the preparation of the system.†

† See reference 1 for a discussion of the process of measurement.

The probability distribution function (relative density of representative points in phase space) we denote by

$$f(\mathbf{R}_1, \cdots, \mathbf{R}_N; \mathbf{p}_1, \cdots, \mathbf{p}_N; t),$$

satisfying the normalization condition

$$\int\cdots\int_{6N \text{ fold}} f d\mathbf{R}_1\cdots d\mathbf{R}_N d\mathbf{p}_1\cdots d\mathbf{p}_N = 1 \qquad (2.1)$$

where $d\mathbf{R}_k$ stands for a volume element in the configuration space and $d\mathbf{p}_k$ a volume element in the momentum space of the kth molecule. f changes in time according to the well-known Liouville equation

$$\frac{\partial f}{\partial t} = \sum_{k=1}^{N}\left[-\frac{\mathbf{p}_k}{m_k}\cdot\nabla_{\mathbf{R}_k} f + \nabla_{\mathbf{R}_k} U\cdot\nabla_{\mathbf{p}_k} f\right] \qquad (2.2)$$

where U is the potential energy of the entire system.

Any dynamical variable, $\alpha(\mathbf{R}_1, \cdots, \mathbf{R}_N; \mathbf{p}_1, \cdots, \mathbf{p}_N)$, has an expectation value given at time t by

$$\langle\alpha; f\rangle = \int\cdots\int_{6N \text{ fold}} \alpha(\mathbf{R}_1, \cdots, \mathbf{p}_1\cdots) f(\mathbf{R}_1, \cdots \mathbf{p}_1, \cdots; t) \times d\mathbf{R}_1\cdots d\mathbf{R}_N d\mathbf{p}_1\cdots d\mathbf{p}_N. \qquad (2.3)$$

We thus denote by $\langle\alpha; f\rangle$ the expectation value of α for a distribution function f. (It is merely the inner product of α and f taken over phase space.)

Providing α does not depend on time explicitly, the rate of change of the expectation value of α is given by

$$\frac{\partial}{\partial t}\langle\alpha; f\rangle = \left\langle\alpha; \frac{\partial f}{\partial t}\right\rangle = \sum_{k=1}^{N}\left[\left\langle\alpha; -\frac{\mathbf{p}_k}{m_k}\cdot\nabla_{\mathbf{R}_k} f\right\rangle + \langle\alpha; \nabla_{\mathbf{R}_k} U\cdot\nabla_{\mathbf{p}_k} f\rangle\right]. \qquad (2.4)$$

By Green's theorem applied in the space of $\mathbf{R}_k$

$$\left\langle\alpha; -\frac{\mathbf{p}_k}{m_k}\cdot\nabla_{\mathbf{R}_k} f\right\rangle = \left\langle\frac{\mathbf{p}_k}{m_k}\cdot\nabla_{\mathbf{R}_k}\alpha; f\right\rangle \qquad (2.5)$$

providing the integrated part vanishes; i.e., providing the system is bounded or f falls off sufficiently rapidly as $\mathbf{R}_k \to \infty$. Likewise, since $\nabla_{\mathbf{R}_k} U$ is independent of momentum $\mathbf{p}_k$, and since f falls off rapidly as $\mathbf{p}_k \to \infty$, use of Green's theorem in the momentum space of $\mathbf{p}_k$ yields

$$\langle\alpha; \nabla_{\mathbf{R}_k} U\cdot\nabla_{\mathbf{p}_k} f\rangle = -\langle\nabla_{\mathbf{R}_k} U\cdot\nabla_{\mathbf{p}_k}\alpha; f\rangle. \qquad (2.6)$$

Thus, (2.4) becomes

$$\frac{\partial}{\partial t}\langle\alpha; f\rangle = \sum_{k=1}^{N}\left\langle\frac{\mathbf{p}_k}{m_k}\cdot\nabla_{\mathbf{R}_k}\alpha - \nabla_{\mathbf{R}_k} U\cdot\nabla_{\mathbf{p}_k}\alpha; f\right\rangle \qquad (2.7)$$

giving the rate of change of the expectation value of α as the expectation value of the dynamical variable

$$\sum_{k=1}^{N}\left[\frac{\mathbf{p}_k}{m_k}\cdot\nabla_{\mathbf{R}_k}\alpha - \nabla_{\mathbf{R}_k} U\cdot\nabla_{\mathbf{p}_k}\alpha\right].$$

We shall use (2.7) to derive the equations of hydrodynamics.

III. STATISTICAL MECHANICAL EXPRESSIONS FOR DENSITIES

The equations of hydrodynamics (1.1), (1.2), and (1.4) are concerned with densities in ordinary 3-space, e.g., mass density, momentum density, and energy density. We shall now express these as the expectation values of dynamical variables over an ensemble having distribution function f.

The probability per unit volume that the kth molecules be at $\mathbf{R}_k$ is

$$\int\cdots\int_{6N\text{-}3 \text{ fold}} f(\mathbf{R}_1, \cdots \mathbf{p}_1, \cdots; t) d\mathbf{R}_1\cdots \times d\mathbf{R}_{k-1} d\mathbf{R}_{k+1}\cdots d\mathbf{R}_N d\mathbf{p}_1\cdots d\mathbf{p}_N$$

where the integration is over all position vectors except $\mathbf{R}_k$ and over all momenta vectors. Introducing Dirac's δ-function, the probability per unit volume that the kth molecule be at $\mathbf{r}$ at time t is

$$\langle\delta(\mathbf{R}_k - \mathbf{r}); f\rangle = \int\cdots\int_{6N \text{ fold}} \delta(\mathbf{R}_k - \mathbf{r}) f(\mathbf{R}_1, \cdots; \mathbf{p}_1, \cdots; t) d\mathbf{R}_1\cdots d\mathbf{p}_N.$$

The total mass density at $\mathbf{r}$ due to all molecules is thus given at time t by

$$\rho(\mathbf{r}; t) = \sum_{k=1}^{N} m_k\langle\delta(\mathbf{R}_k - \mathbf{r}); f\rangle. \qquad (3.1)$$

The mean momentum of the kth molecule, providing it is at $\mathbf{r}$ and the locations of the others are unspecified, is given by the ratio

$$\frac{\displaystyle\int\cdots\int_{6N \text{ fold}} \mathbf{p}_k\delta(\mathbf{R}_k - \mathbf{r}) f(\mathbf{R}_1, \cdots; \mathbf{p}_1\cdots; t) d\mathbf{R}_1\cdots d\mathbf{p}_N}{\displaystyle\int\cdots\int_{6N \text{ fold}} \delta(\mathbf{R}_k - \mathbf{r}) f(\mathbf{R}_1, \cdots; \mathbf{p}_1, \cdots; t) d\mathbf{R}_1\cdots d\mathbf{p}_N} = \frac{\langle\mathbf{p}_k\delta(\mathbf{R}_k - \mathbf{r}); f\rangle}{\langle\delta(\mathbf{R}_k - \mathbf{r}); f\rangle}.$$

Consequently, $\langle\mathbf{p}_k\delta(\mathbf{R}_k - \mathbf{r}); f\rangle$ is the product of this mean momentum by the probability per unit volume that the kth molecule be at $\mathbf{r}$; i.e., it is the contribution of the kth molecule to the momentum per unit volume (mass current density). The total momentum density

at $\mathbf{r}$ is thus given at time t by

$$\rho(\mathbf{r};t)\mathbf{u}(\mathbf{r};t)=\sum_{k=1}^{N}\langle \mathbf{p}_k\delta(\mathbf{R}_k-\mathbf{r});f\rangle, \tag{3.2}$$

where $\mathbf{u}(\mathbf{r};t)$, thus defined, is the mean fluid velocity at $\mathbf{r}$.

There is no difficulty encountered in defining mass density or momentum density since the mass or momentum of any molecule may be considered as localized at that molecule. This is also true of kinetic energy density. Since the kinetic energy of the kth molecules is $p_k^2/2m_k$ (where p_k is the magnitude of the vector $\mathbf{p}_k$), its contribution to the kinetic energy density at $\mathbf{r}$ is $\langle(p_k^2/2m_k)\delta(\mathbf{R}_k-\mathbf{r});f\rangle$, and the entire kinetic energy density at $\mathbf{r}$ is given at the time t by

$$E_K(\mathbf{r};t)=\sum_{k=1}^{N}\left\langle\frac{p_k^2}{2m_k}\delta(\mathbf{R}_k-\mathbf{r});f\right\rangle. \tag{3.3}$$

The potential energy, U, of the system we shall assume to be of the form

$$U=\sum_{k=1}^{N}\psi_k(\mathbf{R}_k)+\tfrac{1}{2}\sum\sum_{j\neq k}V_{jk} \tag{3.4}$$

where $\psi_k(\mathbf{R}_k)$ is the potential energy of the kth molecule in an external field of force, and V_{jk} is the mutual potential between the jth and kth molecules.

The potential energy $\psi_k(\mathbf{R}_k)$ may quite naturally be considered localized at $\mathbf{R}_k$, the location of the kth molecule. Thus, the total potential energy density at $\mathbf{r}$ associated with the interaction of molecules with the external field is

$$\begin{aligned}E_\psi(\mathbf{r};t)&=\sum_{k=1}^{N}\langle\psi_k(\mathbf{R}_k)\delta(\mathbf{R}_k-\mathbf{r});f\rangle\\&=\sum_{k=1}^{N}\psi_k(\mathbf{r})\langle\delta(\mathbf{R}_k-\mathbf{r});f\rangle.\end{aligned} \tag{3.5}$$

Similarly the force on the kth molecule due to external sources is $-\nabla_{\mathbf{R}_k}\psi_k(\mathbf{R}_k)$, and the external force (body force) per unit volume at $\mathbf{r}$ is

$$\begin{aligned}X(\mathbf{r};t)&=-\sum_{k=1}^{N}\langle[\nabla_{\mathbf{R}_k}\psi_k(\mathbf{R}_k)]\delta(\mathbf{R}_k-\mathbf{r});f\rangle\\&=-\sum_{k=1}^{N}[\nabla_{\mathbf{r}}\psi_k(\mathbf{r})]\langle\delta(\mathbf{R}_k-\mathbf{r});f\rangle.\end{aligned} \tag{3.6}$$

The potential V_{jk}, depending on the location of both the jth and the kth molecule, is not so naturally localizable; it may only be considered as localized at a point in the six-dimensional configuration space of the pair. It is necessary, however, to define interaction potential energy density in 3-space, for this concept is required to give meaning to the internal energy density of the energy transport equation. For most systems of interest the potential V_{jk} is a short-range function of the molecular separation, R_{jk}, and consequently contributes negligibly to the potential energy unless molecules j and k are close, in which case, if the interaction potential energy be considered as distributed in any manner in the vicinity of the pair, it is sufficiently localized for macroscopic applications. This localization may be made quite precise (though arbitrary) by saying that half of the energy V_{jk} resides in each molecule of the pair. By this formal definition the total interaction potential energy residing in the kth molecule is

$$\frac{1}{2}\sum_{\substack{j=1\\j\neq k}}^{N}V_{jk}$$

and the total interaction potential energy density at $\mathbf{r}$ is

$$E_V(\mathbf{r};t)=\frac{1}{2}\sum\sum_{j\neq k}\langle V_{jk}\delta(\mathbf{R}_k-\mathbf{r});f\rangle. \tag{3.7}$$

As mentioned previously, the stress tensor and heat current density will be expressed as quadratures involving the pair density of molecules and the current density in pair space, respectively.

The pair density, $\rho^{(2)}(\mathbf{r},\mathbf{r}';t)$ is the probability per (unit volume)^2 that one molecule (any molecule) will be at $\mathbf{r}$ and another will be at $\mathbf{r}'$. It is given by

$$\rho^{(2)}(\mathbf{r},\mathbf{r}';t)=\sum\sum_{j\neq k}\langle\delta(\mathbf{R}_j-\mathbf{r})\delta(\mathbf{R}_k-\mathbf{r}');f\rangle. \tag{3.8}$$

The pair density is a symmetric function of its two arguments, $\mathbf{r}$ and $\mathbf{r}'$.

The particle current density in pair space is given by the six-component vector

$$\begin{aligned}\mathbf{j}^{(2)}(\mathbf{r},\mathbf{r}';t)=\sum\sum_{k\neq i}\Big\langle\Big(&\frac{\mathbf{p}_k}{m_k}\oplus\frac{\mathbf{p}_i}{m_i}\Big)\\&\times\delta(\mathbf{R}_k-\mathbf{r})\delta(\mathbf{R}_i-\mathbf{r}');f\Big\rangle.\end{aligned} \tag{3.9}$$

In this equation $(\mathbf{p}_k/m_k)\oplus(\mathbf{p}_i/m_i)$ is also a six-component vector, the velocity in the pair space of the kth and ith molecules. It is the direct sum of $\mathbf{p}_k/m_k$, lying entirely in the three-dimensional subspace of the kth molecule, and $\mathbf{p}_i/m_i$, lying in the subspace of the ith molecule. The six components of $\mathbf{j}^{(2)}$ may be labeled as the corresponding components of $\mathbf{r}\oplus\mathbf{r}'$. The first three components, i.e., the projection of $\mathbf{j}^{(2)}$ onto the space of its first argument, $\mathbf{r}$, is

$$\mathbf{j}_1^{(2)}(\mathbf{r},\mathbf{r}';t)=\sum\sum_{k\neq i}\left\langle\frac{\mathbf{p}_k}{m_k}\delta(\mathbf{R}_k-\mathbf{r})\delta(\mathbf{R}_i-\mathbf{r}');f\right\rangle. \tag{3.10}$$

It is this quantity which will arise in the expression for heat current. $\mathbf{j}_1^{(2)}(\mathbf{r},\mathbf{r}';t)$ may be interpreted as the particle current density at $\mathbf{r}$ (in ordinary physical space), if another particle is at $\mathbf{r}'$, multiplied by the particle

density at $\mathbf{r}'$. In contrast to the pair density, $\mathbf{j}_1^{(2)}(\mathbf{r}, \mathbf{r}'; t)$ is not a symmetrical function of $\mathbf{r}$ and $\mathbf{r}'$.

The densities which have been defined in this section are point functions. They are all ensemble averages of dynamical variables. It should be emphasized, however, that the conventional hydrodynamics is concerned with macroscopic observables. In measuring these observables one not only takes a statistical average over the systems of an ensemble (by repeating the observations many times) but two additional averages as well. The first is a spatial average over a microscopically large though macroscopically small domain, determined by the resolving power of one's measuring instruments. The second is a time average over an interval determined by the relaxation time of one's measuring instruments. The equation of hydrodynamics are thus relations among these measured averages, found to hold empirically.

In addition to the point function densities defined above, we shall later give a point function definition for stress tensor and heat current. It is interesting that these point functions, though averaged neither over space nor time, satisfy equations that are identical in form to the equations of hydrodynamics (at least to those hydrodynamical equations for a single component, single phase system, derived in Section I). In the following sections we shall derive the hydrodynamical-like equations satisfied by these point functions. To obtain the hydrodynamical equations themselves it is merely necessary to perform the appropriate space and time averages.

It will be noted that in defining the densities, heretofore, we have made no reference to the similarity of molecules. Nor are the derivations of the statistical mechanical expressions for the time rate of change of these densities facilitated by imposing the restriction of similar molecules. It is only when we are ready to define the point function stress tensor and heat current density that we must impose this restriction; for these functions are defined so as to satisfy the hydrodynamical equations of Section I, which are only valid for a single component, single phase system.

IV. THE EQUATION OF CONTINUITY

We now apply Eq. (2.7) to the derivation of the equation of continuity. To this end we take α to be

$$\alpha \equiv \sum_{j=1}^{N} m_j \delta(\mathbf{R}_j - \mathbf{r}). \tag{4.1}$$

Then, as required for (2.7),

$$\frac{\mathbf{p}_k}{m_k} \cdot \nabla_{\mathbf{R}_k} \alpha - \nabla_{\mathbf{R}_k} U \cdot \nabla_{\mathbf{p}_k} \alpha = \mathbf{p}_k \cdot \nabla_{\mathbf{R}_k} \delta(\mathbf{R}_k - \mathbf{r}) = -\nabla_{\mathbf{r}} \cdot [\mathbf{p}_k \delta(\mathbf{R}_k - \mathbf{r})]. \tag{4.2}$$

From the definition (3.1), Eqs. (4.1), (2.7), and (4.2), and finally the definition (3.2)

$$\frac{\partial}{\partial t} \rho(\mathbf{r}; t) = \frac{\partial}{\partial t} \langle \alpha; f \rangle = \sum_{k=1}^{N} \langle -\nabla_{\mathbf{r}} \cdot [\mathbf{p}_k \delta(\mathbf{R}_k - \mathbf{r})]; f \rangle = -\nabla_{\mathbf{r}} \cdot [\rho(\mathbf{r}; t) \mathbf{u}(\mathbf{r}; t)]$$

which is the equation of continuity, (1.1).

V. THE HYDRODYNAMICAL EQUATION OF MOTION (MOMENTUM TRANSPORT)

Before deriving the hydrodynamical equation of motion we wish to alter (2.7) to give the rate of change of the expectation value of a vector α having components α_ν. According to (2.7), for $\nu = 1, 2, 3$,

$$\frac{\partial}{\partial t} \langle \alpha_\nu; f \rangle = \sum_{k=1}^{N} \left\langle \frac{\mathbf{p}_k}{m_k} \cdot \nabla_{\mathbf{R}_k} \alpha_\nu - \nabla_{\mathbf{R}_k} U \cdot \nabla_{\mathbf{p}_k} \alpha_\nu; f \right\rangle.$$

These three equations ($\nu = 1, 2, 3$) may be written in diadic notation as

$$\frac{\partial}{\partial t} \langle \boldsymbol{\alpha}; f \rangle = \sum_{k=1}^{N} \left\langle \left(\frac{\mathbf{p}_k}{m_k} \cdot \nabla_{\mathbf{R}_k} \right) \boldsymbol{\alpha} - (\nabla_{\mathbf{R}_k} U \cdot \nabla_{\mathbf{p}_k}) \boldsymbol{\alpha}; f \right\rangle. \tag{5.1}$$

We now take $\boldsymbol{\alpha}$ to be

$$\boldsymbol{\alpha} = \sum_{j=1}^{N} \mathbf{p}_j \delta(\mathbf{R}_j - \mathbf{r}). \tag{5.2}$$

Then

$$\left(\frac{\mathbf{p}_k}{m_k} \cdot \nabla_{\mathbf{R}_k} \right) \boldsymbol{\alpha} - (\nabla_{\mathbf{R}_k} U \cdot \nabla_{\mathbf{p}_k}) \boldsymbol{\alpha} = \left(\frac{\mathbf{p}_k}{m_k} \cdot \nabla_{\mathbf{R}_k} \right) \mathbf{p}_k \delta(\mathbf{R}_k - \mathbf{r}) - (\nabla_{\mathbf{R}_k} U \cdot \nabla_{\mathbf{p}_k}) \mathbf{p}_k \delta(\mathbf{R}_k - \mathbf{r}) = -\nabla_{\mathbf{r}} \cdot \left[\frac{\mathbf{p}_k \mathbf{p}_k}{m_k} \delta(\mathbf{R}_k - \mathbf{r}) \right] - (\nabla_{\mathbf{R}_k} U) \delta(\mathbf{R}_k - \mathbf{r}). \tag{5.3}$$

From (3.4)

$$\nabla_{\mathbf{R}_k} U = \nabla_{\mathbf{R}_k} \psi_k(\mathbf{R}_k) + \sum_{\substack{j=1 \\ \neq k}}^{N} \nabla_{\mathbf{R}_k} V_{jk}. \tag{5.4}$$

From (5.2) and the definition of momentum density, (3.2), we have

$$\langle \boldsymbol{\alpha}; f \rangle = \rho(\mathbf{r}; t) \mathbf{u}(\mathbf{r}; t). \tag{5.5}$$

Substituting (5.5) and (5.3) into (5.1) and replacing $\nabla_{\mathbf{R}_k} U$ by its equivalent given in (5.4), we obtain, upon introducing $\mathbf{X}$, the body force defined in (3.6),

$$\frac{\partial}{\partial t} [\rho(\mathbf{r}; t) \mathbf{u}(\mathbf{r}; t)] = -\nabla_{\mathbf{r}} \cdot \sum_{k=1}^{N} \left\langle \frac{\mathbf{p}_k \mathbf{p}_k}{m_k} \delta(\mathbf{R}_k - \mathbf{r}); f \right\rangle + \mathbf{X}(\mathbf{r}; t) - \sum_{j \neq k} \sum \langle (\nabla_{\mathbf{R}_k} V_{jk}) \delta(\mathbf{R}_k - \mathbf{r}); f \rangle. \tag{5.6}$$

The first term on the right in Eq. (5.6) may be

modified by noting that

$$\sum_{k=1}^{N} m_k\left\langle\left(\frac{\mathbf{p}_k}{m_k}-\mathbf{u}\right)\left(\frac{\mathbf{p}_k}{m_k}-\mathbf{u}\right)\delta(\mathbf{R}_k-\mathbf{r});f\right\rangle$$

$$=\sum_{k=1}^{N}\left\langle\frac{\mathbf{p}_k\mathbf{p}_k}{m_k}\delta(\mathbf{R}_k-\mathbf{r});f\right\rangle-\mathbf{u}\sum_{k=1}^{N}\langle\mathbf{p}_k\delta(\mathbf{R}_k-\mathbf{r});f\rangle$$

$$-\sum_{k=1}^{N}\langle\mathbf{p}_k\delta(\mathbf{R}_k-\mathbf{r});f\rangle\mathbf{u}+\mathbf{u}\mathbf{u}\sum_{k=1}^{N}m_k\langle\delta(\mathbf{R}_k-\mathbf{r});f\rangle$$

$$=\sum_{k=1}^{N}\left\langle\frac{\mathbf{p}_k\mathbf{p}_k}{m_k}\delta(\mathbf{R}_k-\mathbf{r});f\right\rangle-\rho\mathbf{u}\mathbf{u} \tag{5.7}$$

where we have used (3.1) and (3.2).

The last term in (5.6) may be cast in a more convenient form by symmetrizing with respect to the dummy indices j and k.

$$-\sum_{j\neq k}\sum\langle(\nabla_{\mathbf{R}_k}V_{jk})\delta(\mathbf{R}_k-\mathbf{r});f\rangle$$

$$=-\frac{1}{2}\sum_{j\neq k}\sum\langle(\nabla_{\mathbf{R}_k}V_{jk})\delta(\mathbf{R}_k-\mathbf{r})$$

$$+(\nabla_{\mathbf{R}_j}V_{kj})\delta(\mathbf{R}_j-\mathbf{r});f\rangle=-\frac{1}{2}\sum_{j\neq k}\sum\langle(\nabla_{\mathbf{R}_k}V_{jk})$$

$$\times[\delta(\mathbf{R}_k-\mathbf{r})-\delta(\mathbf{R}_j-\mathbf{r})];f\rangle. \tag{5.8}$$

Where we have used Newton's third law:

$$\nabla_{\mathbf{R}_j}V_{kj}=-\nabla_{\mathbf{R}_k}V_{jk}.$$

The difference of the δ-functions may be expanded formally as a Taylor's series in the vector separation, $\mathbf{R}_{jk}=\mathbf{R}_k-\mathbf{R}_j$.

$$\delta(\mathbf{R}_k-\mathbf{r})-\delta(\mathbf{R}_j-\mathbf{r})$$

$$=-\mathbf{R}_{jk}\cdot\nabla_{\mathbf{r}}\delta(\mathbf{R}_j-\mathbf{r})+\tfrac{1}{2}(\mathbf{R}_{jk}\cdot\nabla_{\mathbf{r}})^2\delta(\mathbf{R}_j-\mathbf{r})-\cdots$$

$$+\frac{1}{n!}(-\mathbf{R}_{jk}\cdot\nabla_{\mathbf{r}})^n\delta(\mathbf{R}_j-\mathbf{r})+\cdots$$

$$=-\nabla_{\mathbf{r}}\cdot\left[\mathbf{R}_{jk}\left\{1-\frac{1}{2}\mathbf{R}_{jk}\cdot\nabla_{\mathbf{r}}+\cdots\right.\right.$$

$$\left.\left.+\frac{1}{n!}(-\mathbf{R}_{jk}\cdot\nabla_{\mathbf{r}})^{n-1}+\cdots\right\}\delta(\mathbf{R}_j-\mathbf{r})\right]. \tag{5.9}$$

Substituting (5.9) into (5.8) gives, after commuting $\nabla_{\mathbf{r}}$ with the integration over phase space:

$$-\sum_{j\neq k}\sum\langle(\nabla_{\mathbf{R}_k}V_{jk})\delta(\mathbf{R}_k-\mathbf{r});f\rangle$$

$$=\nabla_{\mathbf{r}}\cdot\left[\frac{1}{2}\sum_{j\neq k}\sum\left\langle(\nabla_{\mathbf{R}_k}V_{jk})\mathbf{R}_{jk}\left\{1-\frac{1}{2}\mathbf{R}_{jk}\cdot\nabla_{\mathbf{r}}\right.\right.\right.$$

$$\left.\left.\left.+\cdots+\frac{1}{n!}(-\mathbf{R}_{jk}\cdot\nabla_{\mathbf{r}})^{n-1}+\cdots\right\}\delta(\mathbf{R}_j-\mathbf{r});f\right\rangle\right]. \tag{5.10}$$

Substituting (5.7) and (5.10) into (5.6), we obtain

$$(\partial/\partial t)[\rho\mathbf{u}]+\nabla_{\mathbf{r}}\cdot[\rho\mathbf{u}\mathbf{u}]=\mathbf{X}+\nabla_{\mathbf{r}}\cdot\left[-\sum_{k=1}^{N}m_k\left\langle\left(\frac{\mathbf{p}_k}{m_k}-\mathbf{u}\right)\left(\frac{\mathbf{p}_k}{m_k}-\mathbf{u}\right)\delta(\mathbf{R}_k-\mathbf{r});f\right\rangle\right.$$

$$\left.+\frac{1}{2}\sum_{j\neq k}\sum\left\langle\left(\nabla_{\mathbf{R}_k}V_{jk}\right)\mathbf{R}_{jk}\left\{1-\frac{1}{2}\mathbf{R}_{jk}\cdot\nabla_{\mathbf{r}}+\cdots+\frac{1}{n!}(-\mathbf{R}_{jk}\cdot\nabla_{\mathbf{r}})^{n-1}+\cdots\right\}\delta(\mathbf{R}_j-\mathbf{r});f\right\rangle\right]. \tag{5.11}$$

Equation (5.11) has been derived without referring to the restriction of a single component, single phase system. In fact, the equation holds as well when there are non-central forces depending upon rotational or other internal degrees of freedom.‡

We now wish to compare (5.11) with (1.2), the hydrodynamical equation for a single component, single phase system. Consequently we must consider (5.11) when all particles are identical. We shall also limit the subsequent treatment to central forces depending on range only. Hence,

$$V_{jk}=V(R_{jk})$$

and

$$\nabla_{\mathbf{R}_k}V_{jk}=\frac{\mathbf{R}_{jk}}{R_{jk}}V'(R_{jk}).$$

We are now ready to define a point function stress tensor, $\boldsymbol{\sigma}$.

$$\boldsymbol{\sigma}(\mathbf{r};t)=\boldsymbol{\sigma}_K(\mathbf{r};t)+\boldsymbol{\sigma}_V(\mathbf{r};t) \tag{5.12}$$

‡ In the event that there are other degrees of freedom ξ_i having conjugate momenta η_i, then f is a distribution function in a phase space of higher dimensions, and the expectation value of a dynamical variable α is $\langle\alpha;f\rangle$, where the brackets now indicate integration over this entire phase space. The Liouville equation, (2.2), must be amended by adding to the right

$$\sum_i\left[-\frac{\partial H}{\partial\eta_i}\frac{\partial f}{\partial\xi_i}+\frac{\partial H}{\partial\xi_i}\frac{\partial f}{\partial\eta_i}\right],$$

where H is the Hamiltonian of the system. This changes the expression for $(\partial/\partial t)\langle\alpha;f\rangle$ by

$$\sum_i\left\langle\alpha;-\frac{\partial H}{\partial\eta_i}\frac{\partial f}{\partial\xi_i}+\frac{\partial H}{\partial\xi_i}\frac{\partial f}{\partial\eta_i}\right\rangle.$$

Providing α is independent of all ξ_i and η_i, this vanishes upon integrating the first term by parts with respect to ξ_i, and the second term with respect to η_i, assuming that the integrated parts also vanish (e.g., if ξ_i is cyclic and $f\to 0$ rapidly as $\eta_i\to\pm\infty$).

Consequently, the expression for the rate of change of the expectation value of a dynamical variable independent of internal degrees of freedom is unchanged by the existence of these internal degrees of freedom. Thus, the derivation of (5.11) is equally valid for central or non-central forces depending upon rotational or other internal degrees of freedom.

$$\boldsymbol{\sigma}_K(\mathbf{r};t)$$

$$=-\sum_{k=1}^{N} m\left\langle\left(\frac{\mathbf{p}_k}{m}-\mathbf{u}\right)\left(\frac{\mathbf{p}_k}{m}-\mathbf{u}\right)\delta(\mathbf{R}_k-\mathbf{r});f\right\rangle \quad (5.13)$$

$$\boldsymbol{\sigma}_V(\mathbf{r};t)=\frac{1}{2}\sum_{j\neq k}\sum\left\langle\frac{\mathbf{R}_{jk}\mathbf{R}_{jk}}{R_{jk}}V'(R_{jk})\left\{1-\frac{1}{2}\mathbf{R}_{jk}\cdot\nabla_{\mathbf{r}}+\cdots\right.\right.$$

$$\left.\left.+\frac{1}{n!}(-\mathbf{R}_{jk}\cdot\nabla_{\mathbf{r}})^{n-1}+\cdots\right\}\delta(\mathbf{R}_j-\mathbf{r});f\right\rangle. \quad (5.14)$$

With this definition Eq. (5.11) becomes identical in form to the hydrodynamical equation of motion, (1.2). It is an equation relating point function densities and the point function stress tensor. When appropriate space and time averages are taken, it becomes the hydrodynamical equation itself.

Since only the divergence of $\boldsymbol{\sigma}$ enters into the hydrodynamical equation of motion, $\boldsymbol{\sigma}$ itself is undetermined (so far as this equation goes) up to an arbitrary tensor of vanishing divergence. The stress tensor we have defined in Eqs. (5.12)–(5.14) is not only the most apparent choice to reduce (5.11) to the hydrodynamical equation of motion but also is the only choice in accord with the physical definition of the stress tensor as the force transmitted per unit area.

$\boldsymbol{\sigma}_k$ is the kinetic contribution to the stress tensor. $\boldsymbol{\sigma}_k\cdot d\mathbf{S}$, viewed from a coordinate system moving with the local velocity $\mathbf{u}$, is the momentum transferred per unit time across the area dS due to the macroscopically imperceptible spread of the fluid velocities about the mean fluid velocity. $\boldsymbol{\sigma}_k$ is the familiar expression for the stress tensor which arises in the kinetic theory of gases, when the intermolecular force can be neglected. It is dominated by $\boldsymbol{\sigma}_V$ in liquids.

$\boldsymbol{\sigma}_V$ is the contribution of intermolecular forces to the stress tensor. $\boldsymbol{\sigma}_V\cdot d\mathbf{S}$ represents the force acting across dS due to the interaction of molecules on opposite sides of dS. This fact is demonstrated in the Appendix.

We now set out to express $\boldsymbol{\sigma}_V$ as a quadrature involving the pair density defined in (3.8). First we introduce into (5.14) a new δ-function, $\delta(\mathbf{R}_{jk}-\mathbf{R})$, and integration over the new variable, $\mathbf{R}$.

$$\boldsymbol{\sigma}_V(\mathbf{r};t)=\frac{1}{2}\sum_{j\neq k}\sum\left\langle\int_{3\text{ fold}}\delta(\mathbf{R}_{jk}-\mathbf{R})\frac{\mathbf{RR}}{R}V'(R)\left\{1-\frac{1}{2}\mathbf{R}\cdot\nabla_{\mathbf{r}}\right.\right.$$

$$\left.\left.+\cdots+\frac{1}{n!}(-\mathbf{R}\cdot\nabla_{\mathbf{r}})^{n-1}+\cdots\right\}\delta(\mathbf{R}_j-\mathbf{r})d\mathbf{R};f\right\rangle.$$

We now commute the integration over $\mathbf{R}$ with the integration over phase and with the summation, and we factor out of the brackets and out of the sum all quantities which do not depend on the particle coordinates nor the indices j and k.

$$\boldsymbol{\sigma}_V(\mathbf{r};t)=\frac{1}{2}\int_{3\text{ fold}}\frac{\mathbf{RR}}{R}V'(R)$$

$$\times\left\{1-\frac{1}{2}\mathbf{R}\cdot\nabla_{\mathbf{r}}+\cdots+\frac{1}{n!}(-\mathbf{R}\cdot\nabla_{\mathbf{r}})^{n-1}+\cdots\right\}$$

$$\times\sum_{j\neq k}\sum\langle\delta(\mathbf{R}_{jk}-\mathbf{R})\delta(\mathbf{R}_j-\mathbf{r});f\rangle d\mathbf{R}.$$

The product $\delta(\mathbf{R}_{jk}-\mathbf{R})\delta(\mathbf{R}_j-\mathbf{r})$ is equivalent to the product $\delta(\mathbf{R}_j-\mathbf{r})\delta(\mathbf{R}_k-\mathbf{r}-\mathbf{R})$; consequently the sum may be identified as the pair density defined in (3.8). This gives

$$\boldsymbol{\sigma}_V(\mathbf{r};t)=\frac{1}{2}\int_{3\text{ fold}}\frac{\mathbf{RR}}{R}V'(R)\left\{1-\frac{1}{2}\mathbf{R}\cdot\nabla_{\mathbf{r}}+\cdots\right.$$

$$\left.+\frac{1}{n!}(-\mathbf{R}\cdot\nabla_{\mathbf{r}})^{n-1}+\cdots\right\}\rho^{(2)}(\mathbf{r},\mathbf{r}+\mathbf{R};t)d\mathbf{R}. \quad (5.15)$$

For a liquid, the pair density, $\rho^{(2)}(\mathbf{r},\mathbf{r}+\mathbf{R})$, considered as a function of the two independent coordinates $\mathbf{r}$ and $\mathbf{R}$, is a slow function of $\mathbf{r}$, although a sensitive function of the relative coordinate, $\mathbf{R}$. Since the change in the pair density due to changing the independent variable $\mathbf{r}$ by an amount $\mathbf{R}$, $\mathbf{R}\cdot\nabla_{\mathbf{r}}\rho^{(2)}(\mathbf{r},\mathbf{r}+\mathbf{R})$ is negligible with respect to $\rho^{(2)}(\mathbf{r},\mathbf{r}+\mathbf{R})$ for $\mathbf{R}$ of the order of the "range" of intermolecular force [range of $V'(R)$], all terms beyond the first in the brace of (5.15) may be neglected. Only at a boundary or interface is $\rho^{(2)}(\mathbf{r},\mathbf{r}+\mathbf{R})$ also sensitive to $\mathbf{r}$, in which case neglecting terms beyond the first may not be justified.

For a fluid with identical particles it is convenient to express the pair density as a product of singlet particle densities, $\rho(\mathbf{r};t)/m$ and $\rho(\mathbf{r}+\mathbf{R};t)/m$, and a correlation function, $g^{(2)}$.

$$\rho^{(2)}(\mathbf{r},\mathbf{r}+\mathbf{R};t)=\frac{1}{m^2}\rho(\mathbf{r};t)\rho(\mathbf{r}+\mathbf{R};t)g^{(2)}(\mathbf{r};\mathbf{R};t). \quad (5.16)$$

$g^{(2)}$ is expressed as a function of $\mathbf{r}$, the coordinate of the first of the pair (to which it is insensitive) and $\mathbf{R}$, the relative coordinate (to which it is sensitive).

When (5.16) is substituted into (5.15), neglecting all terms beyond the first in the brace and replacing the slowly varying mass density $\rho(\mathbf{r}+\mathbf{R};t)$ by $\rho(\mathbf{r};t)$, we obtain the approximation (very accurate for a bulk fluid phase).

$$\boldsymbol{\sigma}_V(\mathbf{r};t)=\frac{[\rho(\mathbf{r};t)]^2}{2m^2}\int_{3\text{ fold}}\frac{\mathbf{RR}}{R}V'(R)g^{(2)}(\mathbf{r};\mathbf{R};t)d\mathbf{R}. \quad (5.17)$$

The intermolecular force contribution to the macroscopic stress tensor may be obtained by taking the appropriate space and time averages of (5.17). The equation is invariant under averaging except that $g^{(2)}$ must be replaced by its average.

The pressure may be obtained by taking the diagonal sum of the stress tensor

$$P=-\tfrac{1}{3}\,\text{Trace}\,\boldsymbol{\sigma}. \tag{5.18}$$

From (5.13)

$$-\frac{1}{3}\,\text{Trace}\,\boldsymbol{\sigma}_K=\frac{2}{3}\sum_{k=1}^{N}\left\langle\frac{m}{2}\left|\frac{\mathbf{p}_k}{m}-\mathbf{u}\right|^2\delta(\mathbf{R}_k-\mathbf{r});f\right\rangle \tag{5.19}$$

and from (5.17)

$$-\tfrac{1}{3}\,\text{Trace}\,\boldsymbol{\sigma}_V=-\frac{[\rho(\mathbf{r};t)]^2}{6m^2}\int_{3\text{ fold}}RV'(R)g^{(2)}(\mathbf{r};\mathbf{R};t)d\mathbf{R}. \tag{5.20}$$

The sum occurring in (5.19) is [according to (3.3)] the kinetic energy density at $\mathbf{r}$ measured from a frame of reference moving with the mean velocity, $\mathbf{u}$. In equilibrium this is given by $(3/2)kT\times\rho/m$, the kinetic energy per molecule times the particle density. In an equilibrium state, $g^{(2)}$ and ρ are independent of $\mathbf{r}$ and $g^{(2)}$ is isotropic with respect to the relative coordinate, $\mathbf{R}$; i.e., $g^{(2)}$ is a function of the distance R only. Equations (5.18)–(5.20) thus give for the equilibrium pressure

$$P_{\text{eq}}=\frac{\rho}{m}kT-\frac{2\pi}{3}\left(\frac{\rho}{m}\right)^2\int R^3V'(R)g^{(2)}(R)dR. \tag{5.21}$$

This is the "equation of state" for a fluid which may be derived without regard to hydrodynamics by using the virial theorem.

VI. THE ENERGY TRANSPORT EQUATION

The derivation of the energy transport equation follows the lines of the preceding section. However, since the equations involved have more terms, confusion can be avoided by deriving separate expressions for the rate of change of the several parts of the energy density.

First we shall apply Eq. (2.7) taking

$$\alpha=\sum_{j=1}^{N}\frac{p_j^2}{2m_j}\delta(\mathbf{R}_j-\mathbf{r}). \tag{6.1}$$

The kinetic energy density, (3.3), is

$$E_K(\mathbf{r};t)=\langle\alpha;f\rangle. \tag{6.2}$$

As required by (2.7)

$$\begin{aligned}&\frac{\mathbf{p}_k}{m_k}\cdot\nabla_{\mathbf{R}_k}\alpha-(\nabla_{\mathbf{R}_k}U)\cdot\nabla_{\mathbf{p}_k}\alpha\\&=-\frac{p_k^2}{2m_k}\frac{\mathbf{p}_k}{m_k}\cdot\nabla_{\mathbf{r}}\delta(\mathbf{R}_k-\mathbf{r})-(\nabla_{\mathbf{R}_k}U)\cdot\frac{\mathbf{p}_k}{m_k}\delta(\mathbf{R}_k-\mathbf{r})\\&=-\nabla_{\mathbf{r}}\cdot\left[\frac{p_k^2}{2m_k}\frac{\mathbf{p}_k}{m_k}\delta(\mathbf{R}_k-\mathbf{r})\right]\\&\quad-\left[\nabla_{\mathbf{R}_k}\psi_k(\mathbf{R}_k)+\sum_{\substack{j=1\\j\neq k}}^{N}\nabla_{\mathbf{R}_k}V_{jk}\right]\cdot\frac{\mathbf{p}_k}{m_k}\delta(\mathbf{R}_k-\mathbf{r}),\end{aligned} \tag{6.3}$$

where we have used (5.4). When (6.2) and (6.3) are substituted into (2.7), we obtain

$$\begin{aligned}\frac{\partial}{\partial t}E_K(\mathbf{r};t)&=-\nabla_{\mathbf{r}}\cdot\sum_{k=1}^{N}\left\langle\frac{p_k^2}{2m_k}\frac{\mathbf{p}_k}{m_k}\delta(\mathbf{R}_k-\mathbf{r});f\right\rangle\\&\quad-\sum_{k=1}^{N}[\nabla_{\mathbf{r}}\psi_k(\mathbf{r})]\cdot\left\langle\frac{\mathbf{p}_k}{m_k}\delta(\mathbf{R}_k-\mathbf{r});f\right\rangle\\&\quad-\sum_{j\neq k}\sum\left\langle(\nabla_{\mathbf{R}_k}V_{jk})\cdot\frac{\mathbf{p}_k}{m_k}\delta(\mathbf{R}_k-\mathbf{r});f\right\rangle.\end{aligned} \tag{6.4}$$

Next we apply (2.7) using

$$\alpha=\sum_{j=1}^{N}\psi_j(\mathbf{r})\delta(\mathbf{R}_j-\mathbf{r}). \tag{6.5}$$

Then, according to (3.5), the energy density due to external fields is

$$E_\psi(\mathbf{r};t)=\langle\alpha;f\rangle \tag{6.6}$$

and

$$\begin{aligned}&(\mathbf{p}_k/m_k)\cdot\nabla_{\mathbf{R}_k}\alpha-(\nabla_{\mathbf{R}_k}U)\cdot\nabla_{\mathbf{p}_k}\alpha\\&\quad=\psi_k(\mathbf{r})(\mathbf{p}_k/m_k)\cdot\nabla_{\mathbf{R}_k}\delta(\mathbf{R}_k-\mathbf{r})\\&\quad=-\psi_k(\mathbf{r})\nabla_{\mathbf{r}}\cdot[(\mathbf{p}_k/m_k)\delta(\mathbf{R}_k-\mathbf{r})].\end{aligned} \tag{6.7}$$

Substituting (6.6) and (6.7) into (2.7) gives

$$\frac{\partial}{\partial t}E_\psi(\mathbf{r};t)=-\sum_{k=1}^{N}\psi_k(\mathbf{r})\nabla_{\mathbf{r}}\cdot\left\langle\frac{\mathbf{p}_k}{m_k}\delta(\mathbf{R}_k-\mathbf{r});f\right\rangle. \tag{6.8}$$

Finally, we shall apply (2.7) using

$$\alpha=\frac{1}{2}\sum_{i\neq j}\sum V_{ij}\delta(\mathbf{R}_j-\mathbf{r}). \tag{6.9}$$

The potential energy density due to molecular interaction is then, according to (3.7),

$$E_V(\mathbf{r};t)=\langle\alpha;f\rangle \tag{6.10}$$

and

$$\begin{aligned}&(\mathbf{p}_k/m_k)\cdot\nabla_{\mathbf{R}_k}\alpha-(\nabla_{\mathbf{R}_k}U)\cdot\nabla_{\mathbf{p}_k}\alpha\\&=\frac{\mathbf{p}_k}{2m_k}\cdot\left[\sum_{\substack{j=1\\j\neq k}}^{N}(\nabla_{\mathbf{R}_k}V_{kj})\delta(\mathbf{R}_j-\mathbf{r})+\sum_{\substack{i=1\\i\neq k}}^{N}(\nabla_{\mathbf{R}_k}V_{ik})\delta(\mathbf{R}_k-\mathbf{r})\right.\\&\quad\left.+\sum_{\substack{i=1\\i\neq k}}^{N}V_{ik}\nabla_{\mathbf{R}_k}\delta(\mathbf{R}_k-\mathbf{r})\right]\\&=\frac{\mathbf{p}_k}{2m_k}\cdot\sum_{\substack{j=1\\j\neq k}}^{N}(\nabla_{\mathbf{R}_k}V_{jk})[\delta(\mathbf{R}_j-\mathbf{r})+\delta(\mathbf{R}_k-\mathbf{r})]\\&\quad-\frac{1}{2}\nabla_{\mathbf{r}}\cdot\left[\sum_{\substack{j=1\\j\neq k}}^{N}V_{jk}\frac{\mathbf{p}_k}{m_k}\delta(\mathbf{R}_k-\mathbf{r})\right].\end{aligned} \tag{6.11}$$

When (6.10) and (6.11) are substituted into (2.7), we obtain

$$\frac{\partial}{\partial t}E_V(\mathbf{r};t)=\frac{1}{2}\sum_{j\neq k}\sum\left\langle(\nabla_{\mathbf{R}_k}V_{jk})\cdot\frac{\mathbf{p}_k}{m_k}[\delta(\mathbf{R}_j-\mathbf{r})+\delta(\mathbf{R}_k-\mathbf{r})];f\right\rangle$$
$$-\frac{1}{2}\nabla_{\mathbf{r}}\left[\sum_{j\neq k}\sum\left\langle V_{jk}\frac{\mathbf{p}_k}{m_k}\delta(\mathbf{R}_k-\mathbf{r});f\right\rangle\right]. \quad (6.12)$$

Adding up the rates given in (6.4), (6.8), and (6.12), we obtain the rate of change of the total internal energy density.

$$\frac{\partial}{\partial t}E(\mathbf{r};t)=-\nabla_{\mathbf{r}}\cdot\left[\sum_{k=1}^{N}\left\langle\frac{p_k^2}{2m_k}\frac{\mathbf{p}_k}{m_k}\delta(\mathbf{R}_k-\mathbf{r});f\right\rangle\right.$$
$$+\sum_{k=1}^{N}\psi_k(\mathbf{r})\left\langle\frac{\mathbf{p}_k}{m_k}\delta(\mathbf{R}_k-\mathbf{r});f\right\rangle$$
$$\left.+\frac{1}{2}\sum_{j\neq k}\sum\left\langle V_{jk}\frac{\mathbf{p}_k}{m_k}\delta(\mathbf{R}_k-\mathbf{r});f\right\rangle\right]$$
$$+\frac{1}{2}\sum_{j\neq k}\sum\left\langle(\nabla_{\mathbf{R}_k}V_{jk})\cdot\frac{\mathbf{p}_k}{m_k}[\delta(\mathbf{R}_j-\mathbf{r})-\delta(\mathbf{R}_k-\mathbf{r})];f\right\rangle. \quad (6.13)$$

From the definitions of the several parts of the energy density

$$\nabla_{\mathbf{r}}\cdot(E\mathbf{u})=\nabla_{\mathbf{r}}\cdot\left[\sum_{k=1}^{N}\left\langle\frac{p_k^2}{2m_k}\mathbf{u}\delta(\mathbf{R}_k-\mathbf{r});f\right\rangle\right.$$
$$+\sum_{k=1}^{N}\psi_k(\mathbf{r})\langle\mathbf{u}\delta(\mathbf{R}_k-\mathbf{r});f\rangle$$
$$\left.+\frac{1}{2}\sum_{j\neq k}\sum\langle V_{jk}\mathbf{u}\delta(\mathbf{R}_k-\mathbf{r});f\rangle\right]. \quad (6.14)$$

Adding (6.14) to (6.13), we obtain

$$\frac{\partial}{\partial t}E(\mathbf{r};t)+\nabla_{\mathbf{r}}\cdot(E\mathbf{u})$$
$$=-\nabla_{\mathbf{r}}\cdot\left[\sum_{k=1}^{N}\left\langle\frac{p_k^2}{2m_k}\left(\frac{\mathbf{p}_k}{m_k}-\mathbf{u}\right)\delta(\mathbf{R}_k-\mathbf{r});f\right\rangle\right.$$
$$+\sum_{k=1}^{N}\psi_k(\mathbf{r})\left\langle\left(\frac{\mathbf{p}_k}{m_k}-\mathbf{u}\right)\delta(\mathbf{R}_k-\mathbf{r});f\right\rangle$$
$$\left.+\frac{1}{2}\sum_{j\neq k}\sum\left\langle V_{jk}\left(\frac{\mathbf{p}_k}{m_k}-\mathbf{u}\right)\delta(\mathbf{R}_k-\mathbf{r});f\right\rangle\right]$$
$$+\frac{1}{2}\sum_{j\neq k}\sum\left\langle(\nabla_{\mathbf{R}_k}V_{jk})\cdot\frac{\mathbf{p}_k}{m_k}[\delta(\mathbf{R}_j-\mathbf{r})-\delta(\mathbf{R}_k-\mathbf{r})];f\right\rangle. \quad (6.15)$$

Equation (6.15) has been derived without any reference to the assumption of a single component, single phase system. The derivation is equally valid for central or non-central forces depending upon rotational or other internal degrees of freedom.

In order to reduce (6.15) to the point function counterpart of the hydrodynamical equation of energy transport for a single component, single phase system, (1.4), we must assume all molecules identical. We shall further impose the restriction that the intermolecular force shall be central, depending upon range only.

Under the assumption of identical molecules, the second term on the right of (6.15) vanishes, for it becomes

$$\frac{\psi(\mathbf{r})}{m}\left[\sum_{k=1}^{N}\langle\mathbf{p}_k\delta(\mathbf{R}_k-\mathbf{r});f\rangle-\mathbf{u}\sum_{k=1}^{N}m\langle\delta(\mathbf{R}_k-\mathbf{r});f\rangle\right]=0$$

by the definition (3.1) and (3.2).

To reduce (6.15) to the form of (1.4) it is necessary to define a point function heat current density, $\mathbf{q}(\mathbf{r};t)$, satisfying the equation:

$$\nabla_{\mathbf{r}}\cdot(\mathbf{q}-\mathbf{u}\cdot\boldsymbol{\sigma})=\nabla_{\mathbf{r}}\cdot\left[\sum_{k=1}^{N}\left\langle\frac{p_k^2}{2m}\left(\frac{\mathbf{p}_k}{m}-\mathbf{u}\right)\delta(\mathbf{R}_k-\mathbf{r});f\right\rangle\right.$$
$$\left.+\frac{1}{2}\sum_{j\neq k}\sum\left\langle V(R_{kj})\left(\frac{\mathbf{p}_k}{m}-\mathbf{u}\right)\delta(\mathbf{R}_k-\mathbf{r});f\right\rangle\right]$$
$$+\frac{1}{2}\sum_{j\neq k}\sum\left\langle\frac{V'(R_{kj})}{R_{kj}}\mathbf{R}_{kj}\cdot\frac{\mathbf{p}_k}{m}[\delta(\mathbf{R}_j-\mathbf{r})-\delta(\mathbf{R}_k-\mathbf{r})];f\right\rangle \quad (6.16)$$

where $\boldsymbol{\sigma}$ is the point function stress tensor defined in (5.12). We have used the relations:

$$V_{jk}=V(R_{kj})$$
$$\nabla_{\mathbf{R}_k}V_{jk}=\frac{\mathbf{R}_{jk}}{R_{jk}}V'(R_{jk})=-\frac{\mathbf{R}_{kj}}{R_{kj}}V'(R_{kj}).$$

Equation (6.16) merely specifies the divergence of the heat current, and leaves $\mathbf{q}$ itself undetermined up to the curl of an arbitrary vector field. We shall now find a particular solution of (6.16), and then we shall demonstrate that this solution agrees with the physical definition of the heat current density.

The last term of (6.16) may be converted into a divergence by replacing the difference of the δ-functions by the Taylor's series expansion given in (5.9), inter-

changing the roles of j and k.

$$\frac{1}{2}\sum_{j\neq k}\sum\left\langle\frac{V'(R_{kj})}{R_{kj}}\mathbf{R}_{kj}\cdot\frac{\mathbf{p}_k}{m}[\delta(\mathbf{R}_j-\mathbf{r})-\delta(\mathbf{R}_k-\mathbf{r})];f\right\rangle$$

$$=-\nabla_{\mathbf{r}}\cdot\left[\frac{1}{2}\sum_{j\neq k}\sum\left\langle\frac{V'(R_{kj})}{R_{kj}}\mathbf{R}_{kj}\mathbf{R}_{kj}\cdot\frac{\mathbf{p}_k}{m}\left\{1-\frac{1}{2}\mathbf{R}_{kj}\cdot\nabla_{\mathbf{r}}\right.\right.\right.$$

$$\left.\left.\left.+\cdots+\frac{1}{n!}(-\mathbf{R}_{kj}\cdot\nabla_{\mathbf{r}})^{n-1}+\cdots\right\}\delta(\mathbf{R}_k-\mathbf{r});f\right\rangle\right]. \quad (6.17)$$

From the definition of $\boldsymbol{\sigma}_k$ in (5.13),

$$\nabla_{\mathbf{r}}\cdot(\mathbf{u}\cdot\boldsymbol{\sigma}_K)$$

$$=\nabla_{\mathbf{r}}\cdot\left[\sum_{k=1}^{N}\left\langle\frac{m}{2}\left(-2\frac{\mathbf{p}_k}{m}\cdot\mathbf{u}+2u^2\right)\right.\right.$$

$$\left.\left.\times\left(\frac{\mathbf{p}_k}{m}-\mathbf{u}\right)\delta(\mathbf{R}_k-\mathbf{r});f\right\rangle\right]$$

$$=\nabla_{\mathbf{r}}\cdot\left[\sum_{k=1}^{N}\left\langle\frac{m}{2}\left(-2\frac{\mathbf{p}_k}{m}\cdot\mathbf{u}+u^2\right)\right.\right.$$

$$\left.\left.\times\left(\frac{\mathbf{p}_k}{m}-\mathbf{u}\right)\delta(\mathbf{R}_k-\mathbf{r});f\right\rangle\right] \quad (6.18)$$

since

$$\sum_{k=1}^{N}\left\langle\frac{m}{2}u^2\left(\frac{\mathbf{p}_k}{m}-\mathbf{u}\right)\delta(\mathbf{R}_k-\mathbf{r});f\right\rangle$$

$$=\frac{u^2}{2}\left[\sum_{k=1}^{N}\langle\mathbf{p}_k\delta(\mathbf{R}_k-\mathbf{r});f\rangle-\mathbf{u}\sum_{k=1}^{N}m\langle\delta(\mathbf{R}_k-\mathbf{r});f\rangle\right]=0$$

by (3.1) and (3.2).

When (6.17) is substituted into (6.16) and (6.18) added to this equation, we obtain

$$\nabla_{\mathbf{r}}\cdot(\mathbf{q}-\mathbf{u}\cdot\boldsymbol{\sigma}_V)$$

$$=\nabla_{\mathbf{r}}\cdot\left[\sum_{k=1}^{N}\left\langle\frac{m}{2}\left|\frac{\mathbf{p}_k}{m}-\mathbf{u}\right|^2\left(\frac{\mathbf{p}_k}{m}-\mathbf{u}\right)\delta(\mathbf{R}_k-\mathbf{r});f\right\rangle\right.$$

$$+\frac{1}{2}\sum_{j\neq k}\sum\left\langle V(R_{kj})\left(\frac{\mathbf{p}_k}{m}-\mathbf{u}\right)\delta(\mathbf{R}_k-\mathbf{r});f\right\rangle$$

$$-\frac{1}{2}\sum_{j\neq k}\sum\left\langle\frac{V'(R_{kj})}{R_{kj}}\mathbf{R}_{kj}\mathbf{R}_{kj}\cdot\frac{\mathbf{p}_k}{m}\left\{1-\frac{1}{2}\mathbf{R}_{kj}\cdot\nabla_{\mathbf{r}}+\cdots\right.\right.$$

$$\left.\left.\left.+\frac{1}{n!}(-\mathbf{R}_{kj}\cdot\nabla_{\mathbf{r}})^{n-1}+\cdots\right\}\delta(\mathbf{R}_k-\mathbf{r});f\right\rangle\right], \quad (6.19)$$

where $|(\mathbf{p}_k/m)-\mathbf{u}|$ is the magnitude of the vector $(\mathbf{p}_k/m)-\mathbf{u}$.

We shall now define the point function heat current density, the most apparent solution of (6.19), as

$$\mathbf{q}(\mathbf{r};t)=\mathbf{q}_K(\mathbf{r};t)+\mathbf{q}_V(\mathbf{r};t) \quad (6.20)$$

$$\mathbf{q}_K(\mathbf{r};t)=\sum_{k=1}^{N}\left\langle\frac{m}{2}\left|\frac{\mathbf{p}_k}{m}-\mathbf{u}\right|^2\left(\frac{\mathbf{p}_k}{m}-\mathbf{u}\right)\delta(\mathbf{R}_k-\mathbf{r});f\right\rangle \quad (6.21)$$

$$\mathbf{q}_V(\mathbf{r};t)=\mathbf{u}\cdot\left[\boldsymbol{\sigma}_V-\frac{1}{2}\sum_{j\neq k}\sum\langle V(R_{kj})\mathbf{1}\delta(\mathbf{R}_k-\mathbf{r});f\rangle\right]$$

$$+\frac{1}{2}\sum_{j\neq k}\sum\left\langle\left[V(R_{kj})\mathbf{1}-\frac{V'(R_{kj})}{R_{kj}}\mathbf{R}_{kj}\mathbf{R}_{kj}\left\{1+\cdots\right.\right.\right.$$

$$\left.\left.\left.+\frac{1}{n!}(-\mathbf{R}_{kj}\cdot\nabla_{\mathbf{r}})^{n-1}+\cdots\right\}\right]\cdot\frac{\mathbf{p}_k}{m}\delta(\mathbf{R}_k-\mathbf{r});f\right\rangle \quad (6.22)$$

where $\mathbf{1}$ is the unit tensor of the second rank.

$\mathbf{q}_V$ may be expressed in terms of the pair density and particle current density in pair space by introducing into (6.22) a new δ-function $\delta(\mathbf{R}_{kj}-\mathbf{R})$, and integrating over $\mathbf{R}$.

$$\mathbf{q}_V(\mathbf{r};t)=\mathbf{u}\cdot\left[\boldsymbol{\sigma}_V-\frac{1}{2}\sum_{j\neq k}\sum\left\langle\int_{3\text{ fold}}\delta(\mathbf{R}_{kj}-\mathbf{R})\right.\right.$$

$$\left.\times V(R)\mathbf{1}\delta(\mathbf{R}_k-\mathbf{r})d\mathbf{R};f\right\rangle\Big]+\frac{1}{2}\sum_{j\neq k}\sum\left\langle\int_{3\text{ fold}}\delta(\mathbf{R}_{kj}-\mathbf{R})\right.$$

$$\times\left[V(R)\mathbf{1}-\frac{V'(R)}{R}\mathbf{R}\mathbf{R}\left\{1+\cdots\right.\right.$$

$$\left.\left.+\frac{1}{n!}(-\mathbf{R}\cdot\nabla_{\mathbf{r}})^{n-1}+\cdots\right\}\right]\cdot\frac{\mathbf{p}_k}{m}\delta(\mathbf{R}_k-\mathbf{r})d\mathbf{R};f\Big\rangle.$$

Commuting the integrations over $\mathbf{R}$ with the phase integrals and the summations we obtain

$$\mathbf{q}_V(\mathbf{r};t)=\mathbf{u}\cdot\left[\boldsymbol{\sigma}_V-\frac{1}{2}\int_{3\text{ fold}}V(R)\mathbf{1}\sum_{j\neq k}\sum\langle\delta(\mathbf{R}_{kj}-\mathbf{R})\right.$$

$$\left.\times\delta(\mathbf{R}_k-\mathbf{r});f\rangle d\mathbf{R}\right]+\frac{1}{2}\int_{3\text{ fold}}\left[V(R)\mathbf{1}-\frac{\mathbf{R}\mathbf{R}}{R}V'(R)\right.$$

$$\left.\times\left\{1-\frac{1}{2}\mathbf{R}\cdot\nabla_{\mathbf{r}}+\cdots\frac{1}{n!}(-\mathbf{R}\cdot\nabla_{\mathbf{r}})^{n-1}+\cdots\right\}\right]$$

$$\cdot\left[\sum_{j\neq k}\sum\left\langle\frac{\mathbf{p}_k}{m}\delta(\mathbf{R}_{kj}-\mathbf{R})\delta(\mathbf{R}_k-\mathbf{r});f\right\rangle\right]d\mathbf{R}.$$

The product $\delta(\mathbf{R}_{kj}-\mathbf{R})\delta(\mathbf{R}_k-\mathbf{r})$ is equivalent to the product $\delta(\mathbf{R}_k-\mathbf{r})\delta(\mathbf{R}_j-\mathbf{r}-\mathbf{R})$. Consequently, referring to the definitions (3.8) and (3.10) and replacing $\boldsymbol{\sigma}_V$ by

its value given in (5.15), the above equation becomes

$$\mathbf{q}_V(\mathbf{r};t)=-\frac{1}{2}\mathbf{u}(\mathbf{r};t)\cdot\int_{3\text{ fold}}\left[V(R)\mathbf{1}-\frac{\mathbf{RR}}{R}V'(R)\right]\left\{1-\frac{1}{2}\mathbf{R}\cdot\nabla_{\mathbf{r}}+\cdots+\frac{1}{n!}(-\mathbf{R}\cdot\nabla_{\mathbf{r}})^{n-1}+\cdots\right\}\rho^{(2)}(\mathbf{r},\mathbf{r}+\mathbf{R};t)d\mathbf{R}$$

$$+\frac{1}{2}\int_{3\text{ fold}}\left[V(R)\mathbf{1}-\frac{\mathbf{RR}}{R}V'(R)\right]\left\{1-\frac{1}{2}\mathbf{R}\cdot\nabla_{\mathbf{r}}+\cdots+\frac{1}{n!}(-\mathbf{R}\cdot\nabla_{\mathbf{r}})^{n-1}+\cdots\right\}\cdot\mathbf{j}_1{}^{(2)}(\mathbf{r},\mathbf{r}+\mathbf{R};t)d\mathbf{R}. \quad (6.23)$$

In the interior of a fluid $\rho^{(2)}$ and $\mathbf{j}_1{}^{(2)}$, are very slow functions of $\mathbf{r}$; consequently, as explained in the preceding section, all terms in the brace beyond the first may be neglected. Equation (6.23) then reduces to

$$\mathbf{q}_V(\mathbf{r};t)=\frac{1}{2}\int_{3\text{ fold}}\left[V(R)\mathbf{1}-\frac{\mathbf{RR}}{R}V'(R)\right]\cdot[\mathbf{j}_1{}^{(2)}(\mathbf{r},\mathbf{r}+\mathbf{R};t)-\mathbf{u}(\mathbf{r};t)\rho^{(2)}(\mathbf{r},\mathbf{r}+\mathbf{R};t)]d\mathbf{R}. \quad (6.24)$$

What are the physical interpretations of the various terms comprising $\mathbf{q}$? The interpretation is somewhat easier viewed from a coordinate frame moving with the local velocity $\mathbf{u}$. $\mathbf{q}_K$ represents the current density of kinetic energy due to the macroscopically imperceptible random molecular motion. It is this term which occurs in the kinetic theory of gases. The terms in $\mathbf{q}_V$ involving $V(R)$ (but not its derivative) represent the current density of potential energy due to this same random motion. The terms in $\mathbf{q}_V$ involving $V'(R)$, when dotted into an element of area $d\mathbf{S}$, represent the work per unit time done on molecules on one side of dS by molecules on the other. Work is done on the former as they move (due to their macroscopically imperceptible random motion) through the force field of the latter.

COMPILATION OF RESULTS

The equations of phenomenological hydrodynamics for a single component, single phase system are relations among certain macroscopic observables—mass density, fluid velocity, body force density, energy density, stress tensor, and heat current density. Using classical statistical mechanics, we have found that it is possible to define the corresponding microscopic observables and that equations identical in form to the hydrodynamical equations relate these quantities. The macroscopic equations may be obtained from the microscopic (or point function) equations by averaging over a microscopically large though macroscopically small space domain determined by the resolution of one's measurements and averaging over a time interval of the order of the relaxation time of one's measuring instruments.

The microscopically correct hydrodynamical equations are the continuity equation:

$$\frac{\partial}{\partial t}\rho(\mathbf{r};t)=-\nabla_{\mathbf{r}}\cdot[\rho(\mathbf{r};t)\mathbf{u}(\mathbf{r};t)], \quad (1.1)$$

the equation of motion (momentum transport equation):

$$\frac{\partial}{\partial t}[\rho\mathbf{u}]+\nabla_{\mathbf{r}}\cdot[\rho\mathbf{u}\mathbf{u}]=\mathbf{X}+\nabla_{\mathbf{r}}\cdot\boldsymbol{\sigma}, \quad (1.2)$$

and the energy transport equation

$$\frac{\partial E}{\partial t}+\nabla_{\mathbf{r}}\cdot[E\mathbf{u}+\mathbf{q}-\mathbf{u}\cdot\boldsymbol{\sigma}]. \quad (1.4)$$

The quantities appearing in the above equations are defined as follows:¶

$$\rho(\mathbf{r};t)=\sum_{k=1}^{N}m_k\langle\delta(\mathbf{R}_k-\mathbf{r});f\rangle \quad (3.1)$$

= mass density at $\mathbf{r}$.

$$\mathbf{u}(\mathbf{r};t)=\frac{1}{\rho(\mathbf{r};t)}\sum_{k=1}^{N}\langle\mathbf{p}_k\delta(\mathbf{R}_k-\mathbf{r});f\rangle \quad (3.2)$$

= mean molecular velocity (fluid velocity) at $\mathbf{r}$.

$$\mathbf{X}(\mathbf{r};t)=-\sum_{k=1}^{N}[\nabla_{\mathbf{r}}\psi_k(\mathbf{r})]\langle\delta(\mathbf{R}_k-\mathbf{r});f\rangle \quad (3.6)$$

= body force per unit volume due to external fields at $\mathbf{r}$.

$$E(\mathbf{r};t)=E_K+E_\psi+E_V \quad (1.3)$$

= internal energy density at $\mathbf{r}$, where

$$E_K(\mathbf{r};t)=\sum_{k=1}^{N}\left\langle\frac{p_k^2}{2m_k}\delta(\mathbf{R}_k-\mathbf{r});f\right\rangle \quad (3.3)$$

= kinetic energy density,

$$E_\psi(\mathbf{r};t)=\sum_{k=1}^{N}\psi_k(\mathbf{r})\langle\delta(\mathbf{R}_k-\mathbf{r});f\rangle \quad (3.5)$$

= potential energy density associated with external fields, and

$$E_V(\mathbf{r};t)=\frac{1}{2}\sum_{j\neq k}\sum\langle V_{jk}\delta(\mathbf{R}_k-\mathbf{r});f\rangle \quad (3.7)$$

¶ The bracket notation $\langle\ ;f\rangle$ means the expectation value of the quantity appearing to the left of the semicolon over an ensemble having a probability distribution function, $f(\mathbf{R}_1,\cdots,\mathbf{R}_N;\mathbf{p}_1,\cdots\mathbf{p}_N;t)$.

=potential energy density due to molecular interaction. (In defining E_V it is assumed that the potential energy of interaction between two molecules is localized half at each molecule.)

These definitions are completely general. The other quantities, however, appearing in the above hydrodynamical equations, σ and $\mathbf{q}$, have been defined only for a single component, single phase system in which the intermolecular force is central, depending on range only. Their definitions follow.

$$\sigma(\mathbf{r};t)=\sigma_K+\sigma_V \tag{5.12}$$

=stress tensor at $\mathbf{r}$, where

$$\sigma_K=-\sum_{k=1}^{N} m\left\langle\left(\frac{\mathbf{p}_k}{m}-\mathbf{u}\right)\left(\frac{\mathbf{p}_k}{m}-\mathbf{u}\right)\delta(\mathbf{R}_k-\mathbf{r});f\right\rangle \tag{5.13}$$

=kinetic contribution to stress tensor. (This is the dominant term for gases, but relatively unimportant for liquids.) And

$$\sigma_V(\mathbf{r};t)=\frac{1}{2}\int_{3\text{ fold}}\frac{\mathbf{RR}}{R}V'(R)\left\{1-\frac{1}{2}\mathbf{R}\cdot\nabla_{\mathbf{r}}+\cdots\right.$$

$$\left.\frac{1}{n!}(-\mathbf{R}\cdot\nabla_{\mathbf{r}})^{n-1}+\cdots\right\}\rho^{(2)}(\mathbf{r},\mathbf{r}+\mathbf{R};t)d\mathbf{R} \tag{5.15}$$

=intermolecular force contribution to stress tensor. (This is the dominant term for liquids.)

$$\mathbf{q}(\mathbf{r};t)=\mathbf{q}_K+\mathbf{q}_V \tag{6.20}$$

=heat current density at $\mathbf{r}$, where

$$\mathbf{q}_K(\mathbf{r};t)=\sum_{k=1}^{N}\left\langle\frac{m}{2}\left|\frac{\mathbf{p}_k}{m}-\mathbf{u}\right|^2\left(\frac{\mathbf{p}_k}{m}-\mathbf{u}\right)\delta(\mathbf{R}_k-\mathbf{r});f\right\rangle \tag{6.21}$$

=heat current due to transport of thermal kinetic energy, and

$$\mathbf{q}_V(\mathbf{r};t)=-\frac{1}{2}\mathbf{u}(\mathbf{r};t)\cdot\int_{3\text{ fold}}\left[V(R)\mathbf{1}-\frac{\mathbf{RR}}{R}V'(R)\right.$$

$$\left.\times\left\{1-\frac{1}{2}\mathbf{R}\cdot\nabla_{\mathbf{r}}+\cdots+\frac{1}{n!}(-\mathbf{R}\cdot\nabla_{\mathbf{r}})^{n-1}+\cdots\right\}\right]$$

$$\times\rho^{(2)}(\mathbf{r};\mathbf{r}+\mathbf{R};t)d\mathbf{R}+\frac{1}{2}\int_{3\text{ fold}}\left[V(R)\mathbf{1}-\frac{\mathbf{RR}}{R}V'(R)\right.$$

$$\left.\times\left\{1-\frac{1}{2}\mathbf{R}\cdot\nabla_{\mathbf{r}}+\cdots+\frac{1}{n!}(-\mathbf{R}\cdot\nabla_{\mathbf{r}})^{n-1}+\cdots\right\}\right]$$

$$\cdot\mathbf{j}_1^{(2)}(\mathbf{r};\mathbf{r}+\mathbf{R};t)d\mathbf{R} \tag{6.23}$$

=contribution to heat current density by molecular interaction.

In the definitions of σ_V and $\mathbf{q}_V$ the following quantities appear.

$$\rho^{(2)}(\mathbf{r},\mathbf{r}';t)=\sum_{j\neq k}\sum\langle\delta(\mathbf{R}_j-\mathbf{r})\delta(\mathbf{R}_k-\mathbf{r}');f\rangle \tag{3.8}$$

=pair density at $\mathbf{r}$ and $\mathbf{r}'$, the probability per (unit volume)^2 that one particle (any particle) will be at $\mathbf{r}$ and another at $\mathbf{r}'$.

$$\mathbf{j}_1^{(2)}(\mathbf{r},\mathbf{r}';t)=\sum_{k\neq i}\sum\left\langle\frac{\mathbf{p}_k}{m_k}\delta(\mathbf{R}_k-\mathbf{r})\delta(\mathbf{R}_i-\mathbf{r}');f\right\rangle \tag{3.10}$$

=projection onto the space of $\mathbf{r}$ of the particle current density at $\mathbf{r}$, $\mathbf{r}'$ in pair space, =particle current density at $\mathbf{r}$ if another particle is at $\mathbf{r}'$ multiplied by the particle density at $\mathbf{r}'$.

The differential operator, $\nabla_{\mathbf{r}}$, occurring in the definitions of σ_V and $\mathbf{q}_V$ operate on $\rho^{(2)}(\mathbf{r},\mathbf{r}+\mathbf{R};t)$ and $\mathbf{j}_1^{(2)}(\mathbf{r},\mathbf{r}+\mathbf{R};t)$ with $\mathbf{R}$ held fixed. Since in the interior of a fluid $\rho^{(2)}$ and $\mathbf{j}_1^{(2)}$ are slow functions of $\mathbf{r}$ (holding $\mathbf{R}$ fixed), changing negligibly for $\mathbf{r}$ varying by a displacement whose length is of the order of the "range" of intermolecular forces, all terms beyond the first may be neglected in the brace appearing in the definitions of σ_V and $\mathbf{q}_V$. This yields the simplified expressions:

$$\mathbf{q}_V(\mathbf{r};t)=\frac{1}{2}\int_{3\text{ fold}}\left[V(R)\mathbf{1}-\frac{\mathbf{RR}}{R}V'(R)\right]$$

$$\cdot[\mathbf{j}_1^{(2)}(\mathbf{r},\mathbf{r}+\mathbf{R};t)-\mathbf{u}(\mathbf{r};t)\rho^{(2)}(\mathbf{r},\mathbf{r}+\mathbf{R};t)]d\mathbf{R} \tag{6.24}$$

$$\sigma_V(\mathbf{r};t)=\frac{1}{2m^2}[\rho(\mathbf{r};t)]^2\int_{3\text{ fold}}\frac{\mathbf{RR}}{R}V'(R)g^{(2)}(\mathbf{r};\mathbf{R};t)d\mathbf{R} \tag{5.17}$$

where the correlation function $g^{(2)}$ is defined by

$$\rho^{(2)}(\mathbf{r};\mathbf{r}+\mathbf{R};t)=\frac{1}{m^2}\rho(\mathbf{r};t)\rho(\mathbf{r}+\mathbf{R};t)g^{(2)}(\mathbf{r};\mathbf{R};t). \tag{5.16}$$

The pressure is defined by

$$P(\mathbf{r};t)=-\tfrac{1}{3}\,\mathrm{Trace}\sigma(\mathbf{r};t). \tag{5.18}$$

In an ensemble which is in equilibrium with a temperature T, the pressure is

$$P_{\text{eq}}=\frac{\rho}{m}kT-\frac{2\pi}{3}\left(\frac{\rho}{m}\right)^2\int R^3V'(R)g^{(2)}(R)dR. \tag{5.21}$$

This is the equation of state, obtainable by other methods as well.

APPENDIX

The part of the stress tensor at the point $\mathbf{r}$ due to intermolecular forces is defined so that

$$\sigma_V(\mathbf{r};t)\cdot d\mathbf{S}=\text{"the force acting across } dS\text{."} \tag{A.1}$$

First we imagine a plane tangent to dS at $\mathbf{r}$. This plane divides the fluid into two parts. That portion into which the vector $d\mathbf{S}$ points we shall refer to as "outside of dS;" the other portion is "inside of dS."

The interaction forces acting on the fluid are all between pairs of molecules. Let us say that the force between a pair of molecules "acts across dS" if the line of centers between these molecules intersects dS between the molecules.‖ This can only happen (for infinitesimal dS) if one molecule of the pair is "inside dS" and the other is "outside." By convention, the "force acting across dS" is the force acting on the molecule inside dS.

If a molecule is located at $\mathbf{r}'$ inside dS, and another at $\mathbf{r}'+\mathbf{R}$ outside of dS, then the force acting on the molecule at $\mathbf{r}'$ is

$$(\mathbf{R}/R)V'(R). \tag{A.2}$$

This force "acts across dS" only if $\mathbf{r}'+\alpha\mathbf{R}$ terminates on dS for some α between 0 and 1.

Keeping $\mathbf{R}$ fixed, the volume of the element at $\mathbf{r}'$, over which $\mathbf{r}'+\alpha\mathbf{R}$ terminates on dS for α between α_0 and $\alpha_0+d\alpha$, is $d\mathbf{S}\cdot\mathbf{R}d\alpha$.

The probability of finding a molecule (any molecule) in this volume and another at $\mathbf{r}'+\mathbf{R}$ with the relative displacement $\mathbf{R}$ ranging over a volume $d\mathbf{R}$ is

$$\rho^{(2)}(\mathbf{r}',\mathbf{r}'+\mathbf{R})(d\mathbf{S}\cdot\mathbf{R}d\alpha)d\mathbf{R} = \rho^{(2)}(\mathbf{r}-\alpha\mathbf{R};\mathbf{r}-\alpha\mathbf{R}+\mathbf{R})(d\mathbf{S}\cdot\mathbf{R}d\alpha)d\mathbf{R}. \tag{A.3}$$

The error in replacing $\mathbf{r}'$ by $\mathbf{r}-\alpha\mathbf{R}$ is an infinitesimal of a higher order, since the difference between $\mathbf{r}'$ and $\mathbf{r}-\alpha\mathbf{R}$ is an infinitesimal (the vector from $\mathbf{r}$ to some other point on dS).

The total force acting across dS is, therefore, the integral of the product of (A.2) and (A.3).

"The force acting across dS"

$$= d\mathbf{S}\cdot\int\left\{\int_0^1 \frac{\mathbf{RR}}{R}V'(R)\rho^{(2)}(\mathbf{r}-\alpha\mathbf{R},\mathbf{r}-\alpha\mathbf{R}+\mathbf{R})d\alpha\right\}d\mathbf{R} \tag{A.4}$$

where $\mathbf{R}$ ranges over those values only for which $\mathbf{R}\cdot d\mathbf{S}$ is positive (i.e., $\mathbf{R}$ from the inside toward the outside).

‖ This definition of the force "acting across dS" is quite arbitrary, and with another definition we would obtain a different expression for the point function stress tensor. But all definitions must have this in common—that the stress between a pair of molecules be concentrated near the line of centers. When averaging over a domain large compared with the range of intermolecular force, these differences are washed out, and the ambiguity remaining in the macroscopic stress tensor is of negligible order.

Making the change of variable, $\gamma=1-\alpha$, the brace in Eq. (A.4) becomes

$$\left\{\right\} = \int_0^1 \frac{\mathbf{RR}}{R}V'(R)\rho^{(2)}(\mathbf{r}+\gamma\mathbf{R}-\mathbf{R};\mathbf{r}+\gamma\mathbf{R})d\gamma = \int_0^1 \frac{\mathbf{RR}}{R}V'(R)\rho^{(2)}(\mathbf{r}+\gamma\mathbf{R};\mathbf{r}+\gamma\mathbf{R}-\mathbf{R})d\gamma,$$

where we have used the symmetry of $\rho^{(2)}$ with respect to its two arguments. Changing the name of the integration variable γ back to α one notes that the brace is an even function of the vector $\mathbf{R}$. Consequently, (A.4) may be written:

"The force acting across dS"

$$= d\mathbf{S}\cdot\frac{1}{2}\int_{3\text{ fold}}\frac{\mathbf{RR}}{R}V'(R)\left[\int_0^1\rho^{(2)}(\mathbf{r}-\alpha\mathbf{R};\mathbf{r}-\alpha\mathbf{R}+\mathbf{R})d\alpha\right]dR \tag{A.5}$$

where the integration over $\mathbf{R}$ now extends over all space. Since dS was arbitrarily chosen through $\mathbf{r}$, we obtain on comparing (A.1) and (A.5)

$$\boldsymbol{\sigma}_V(\mathbf{r};t) = \frac{1}{2}\int_{3\text{ fold}}\frac{\mathbf{RR}}{R}V'(R)\left[\int_0^1\rho^{(2)}(\mathbf{r}-\alpha\mathbf{R},\mathbf{r}-\alpha\mathbf{R}+\mathbf{R};t)d\alpha\right]d\mathbf{R}. \tag{A.6}$$

$\rho^{(2)}$, appearing in (A.6), may be expanded in a Taylor's series in α.

$$\rho^{(2)}(\mathbf{r}-\alpha\mathbf{R};\mathbf{r}-\alpha\mathbf{R}+\mathbf{R}) = \left\{1-\alpha\mathbf{R}\cdot\nabla\mathbf{r}+\frac{\alpha^2}{2}(\mathbf{R}\cdot\nabla\mathbf{r})^2+\cdots + \frac{\alpha^{n-1}}{(n-1)!}(-\mathbf{R}\cdot\nabla\mathbf{r})^{n-1}+\cdots\right\}\rho^{(2)}(\mathbf{r},\mathbf{r}+\mathbf{R}) \tag{A.7}$$

where it is understood that $\mathbf{R}$ is to be held constant when operating with $\nabla\mathbf{r}$.

Substituting (A.7) into (A.6) and integrating over α from 0 to 1, we obtain:

$$\boldsymbol{\sigma}_V(\mathbf{r};t) = \frac{1}{2}\int_{3\text{ fold}}\frac{\mathbf{RR}}{R}V'(R)\left\{1-\frac{1}{2}\mathbf{R}\cdot\nabla\mathbf{r}+\cdots + \frac{1}{n!}(-\mathbf{R}\cdot\nabla\mathbf{r})^{n-1}+\cdots\right\}\rho^{(2)}(\mathbf{r},\mathbf{r}+\mathbf{R};t)d\mathbf{R}. \tag{A.8}$$

This is identical to the expression given in Eq. (5.15).

Light Scattering Investigation of the Structure of Polystyrene

PAUL OUTER,* CLIDE I. CARR,† AND BRUNO H. ZIMM
Department of Chemistry, University of California, Berkeley, California

(Received February 2, 1950)

Using light scattering, the mean square molecular radius and length of a number of samples of polystyrene have been measured as a function of solvent and temperature. Molecular weights, intrinsic viscosities, and "osmotic second virial coefficients" have also been determined on many of the samples. From the data it may be concluded: (1) that polystyrene molecules are extended and stiffened by steric interactions of the phenyl groups; (2) that the molecules are largely unbranched; (3) that the heat of dilution is negative in some solvents, contrary to the usual situation in hydrocarbon systems; (4) that the osmotic second virial coefficient depends strikingly on molecular weight for a given solvent; (5) that there is a good correlation between this coefficient and the mean square radius at a given molecular weight; (6) that the intrinsic viscosity is strictly proportional to a power of the molecular weight over the molecular weight range from 2,000 to 2,000,000, but that deviations occur at lower molecular weights; (7) that the intrinsic viscosity and mean square radius are functions of solvent at high molecular weights but not at very low molecular weights. Theoretical concepts necessitated by these observations are discussed briefly.

INTRODUCTION

THE light scattering technique of studying the properties of high polymer molecules has one great advantage over other known methods; it yields quantitative values of the mean extension of the polymer chains in a theoretically direct and unambiguous fashion. In the present work polystyrene has been studied in some detail by this method and conclusions have been drawn about the stiffness of the chains, the effect of temperature and solvent on the chains, and an upper limit has been set on the amount of branching compatible with the observed results.

EXPERIMENTAL

The turbidimeter used has been described in a previous paper[1] together with the general technique of measurement and the manner of treating the data.

In Table I are summarized the conditions of preparation of the polymers. In each case the monomeric styrene had been washed free of inhibitor with NaOH solution and dried over $CaCl_2$. For polymers *A*, *B*, and *E* it was also distilled at reduced pressure.

TABLE I. Conditions of polymerization.

Sample	Percent solvent	Benzoyl peroxide concentration	Temperature	Time	Percent conversion
A[a]	none	0.10 percent	70°C	3 days	100
B[a]	none	0.10 percent	70°C	3 days	100
C	CCl_4 (50 percent)	0.5 percent	70°C	24 hours	50
D	CCl_4 (90 percent)	0.5 percent	70°C	24 hours	35
E[a,b]	none	0.10 percent	70°C	3 days	100
F[c]	none	none	150°C	7½ hours	95
150[c]	Anisole (50 percent)	none	150°C	3 hours	50
G	CCl_4 (10 percent)	0.5 percent	70°C	14 hours	83
H	CCl_4 (50 percent)	0.5 percent	70°C	24 hours	60
J	CCl_4 (90 percent)	0.5 percent	70°C	24 hours	45
(2-1-49)	none	none	[d]	[d]	100

[a] Polymerized in sealed tube; all other samples in air.
[b] 0.0055 mole percent divinyl benzene included.
[c] Polymerized under reflux, superheated to 150°.
[d] See text.

Polymers *C*, *D*, and 150 were divided by precipitation into three roughly equal parts and one of these crude fractions was used without further treatment other than drying at 65°C. For polymers *A*, *B*, *E*, and *F* the treatment was more elaborate. Each was divided into about ten fractions by precipitation from a butanone and 1-butanol mixture by successive evaporations of portions of the butanone. Such of the resulting fractions as were used for the present study were then "sharpened" by solution in dioxane and partial precipitation with methanol two to four times. Finally the fractions were dried to constant weight at 65°C. The final mass of each fraction was two to three percent of the original polymer.

Polymers *G*, *H*, and *J*, were treated similarly to *A*, *B*, *E*, and *F* except that the total number of fractions was smaller and each fraction was refractionated only once or twice. The fractions were indexed in order of decreasing molecular weight by numbers appended to the letter symbol of the polymer.

The materials labeled (2-1-49) were fractions prepared by R. S. Spencer of the Dow Chemical Company at Midland, Michigan and distributed by Professor H. Mark of the Polytechnic Institute of Brooklyn for the Commission of Macromolecules of the Union Internationale de Chimie, as part of an international exchange of comparison samples. The preparation of these samples is quoted: "The parent polymer was a thermal, mass polymer prepared according to the following schedule: 48 hours at 77°C, 8 hours at 95°C, and 48 hours at 200°C." The report further indicates that a one-step fractionation was carried out in the conventional manner. The individual measurements on these polymers are summarized in Table IV.

Dibenzyl (1–2 diphenyl ethane) is readily available

* Present address: Laboratoire de Recherches Physiques, A. C. E. C., Charleroi, Belgium. The work was done while this author held the appointments of Fellow of the Belgian American Educational Foundation and Research Fellow of the University of California.

† Present address: General Laboratories of the United States Rubber Company, Passaic, New Jersey.

[1] B. H. Zimm, J. Chem. Phys. 16, 1099 (1948).

and resembles a dimer of styrene in composition and structure. A commercial sample was distilled at low pressure and twice recrystallized from ethanol. The melting point, 51–52°C, agreed with the literature.

Solutions of the materials for light scattering and viscosity were prepared by ordinary methods. Filtration through a Bakelite-impregnated asbestos pad[1] was used to remove dust, except in a few cases, where centrifugation at 15,000 times gravity was necessary to remove an exceptionally persistent haze. The solvents were distilled through an all-glass still just before use. Properties of the solvents were the same as previously described.[1]

As previously, the same solutions were measured in succession at several temperatures without refilling the cell in order to get the temperature dependence of the scattering most accurately.

Intrinsic viscosities were determined at 25°C in the usual manner from the times of flow of the solutions in Ostwald-type viscometers. Kinetic energy corrections were minimized by special construction of the viscometers to keep the shear gradients small. An effort was made to use as dilute solutions as consistent with reasonable precision in order to reduce extrapolation errors.

The intrinsic viscosities of the (2-1-49) fractions in toluene solution were obtained by Maclay and Fuoss.[1a]

RESULTS

The details of the measurement and calculation technique have been already described.[1] As previously, the scattering was measured at six or seven angles from 25° to 143° from several solutions of different concentrations. The results are summarized in Table II and some typical data are shown in Fig. 1, where an attempt was made to obtain enough points to justify the linear extrapolation methods employed. See also Tables III and VII. In all cases the incident illumination was vertically polarized (i.e., electric vector perpendicular to the plane of revolution of the photometer). Concentrations are expressed in grams of solute per cm³ of solution at the temperature of measurement.

The reciprocal intensity function, c/I, where c is the concentration and I the intensity of scattering in arbitrary units, was plotted as described[1] against $\sin^2\vartheta/2+kc$, where ϑ is the angle of scattering and k is an arbitrary constant. For example, Fig. 1 is given. The quantities of interest are the intercept of the plot as c and ϑ approach zero, the ratio of the initial slope of c/I against $\sin^2\vartheta/2$ to the intercept with $c=0$, and the ratio of the initial slope of c/I against c to the intercept with $\vartheta=0$. These quantities are given in columns 3, 4, and 5 of Table II.

A quantity of primary interest is the average extension of the polymer chains. This extension may be expressed as R, the root-mean-square radius of the molecule from its center of mass. However, if the chain is unbranched it is becoming customary to express its size in terms of L, the root-mean-square distance between the ends of the chain. For linear chains $L=6^{\frac{1}{2}}R$.

It has been shown[2] that the ratio of the initial slope to the intercept of c/I against $\sin^2\vartheta/2$ is proportional to R^2, the exact equation being:

$$\frac{16\pi^2R_z^2}{3\lambda^2}=\frac{8\pi^2L_z^2}{9\lambda^2}=\frac{\text{(initial slope)}}{\text{(intercept)}}, \qquad (1)$$

where the second expression has literal meaning only for unbranched chains.

If the sample is polydisperse, R_z^2 and L_z^2 are the "Z-averages" of R^2 and L^2. On the other hand, the molecular weight, M, as calculated by Eq. (2), is a weight average quantity. To convert the Z-average to weight average we divide by the estimated ratio of the Z-average and weight average molecular weights. This ratio has been estimated using the solubility theory of Scott.[3] For the several refractionated materials used in this work it was assumed to be 1.05, and 1.20 for the fractions of material (2-1-49). Henceforth the weight average values of R^2 and L^2 will be called simply R^2 and L^2.

Values of L, the square root of L^2 calculated herein, are given in column 8 of Table II.

The intercepts given in column 3 of Table II are related to the molecular weights of the samples. In accord with the previous paper,[1] we define the *reduced intensity* of scattering at angle ϑ with vertically polarized incident light as $\mathbf{I}_{\vartheta v}$. If i_ϑ is the intensity in absolute units at angle ϑ and distance r in the horizontal plane from a unit volume of the liquid, and I_v^0 is the intensity of the vertically polarized incident beam, $\mathbf{I}_{\vartheta v}=i_\vartheta r^2/I_v^0$. The reduced intensity is independent of r and I_v^0, and

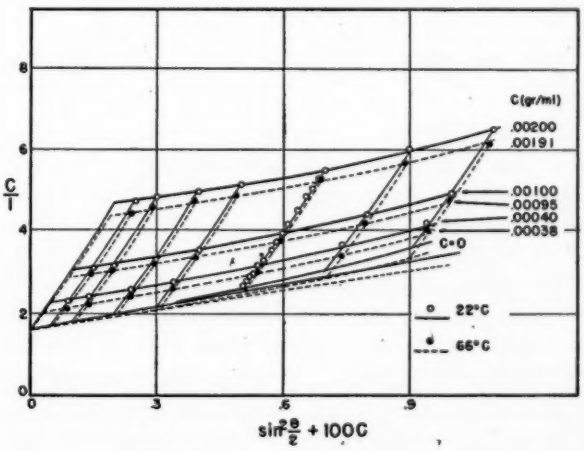

FIG. 1. Reciprocal intensity surface of sample B-2 in dichlorethane at 22°C and 67°C. The 67°C data have been adjusted for the refractive index change so that they may be compared to the 22°C data.

[1a] Private communication from W. N. Maclay and R. M. Fuoss, Sterling Chemistry Laboratory, Yale University, New Haven, Connecticut.

[2] P. Debye, J. Phys. Coll. Chem. **51**, 18 (1947).

[3] R. L. Scott, J. Chem. Phys. **13**, 178 (1945). The results of Wales *et al.* (see reference 21a), from the ultracentrifuge suggest that we may be overestimating the sharpness of our fractions.

TABLE II. Summary of experimental data.

Material	$t°$, C	Intercept, $c/\mathbf{I}_{\vartheta v}$ at $c=0$ and $\vartheta=0$	Slope / intercept, $c=0$	Slope / intercept, $\vartheta=0$	Intrinsic viscosity, cm³/g	z-average length, L_z, A. U.	w-average length, L_w, A. U.	Molecular weight	b, A. U.	$A_2\times10^4$
				Solvent: butanone						
A-1	22	0.826	0.681	300	165	1,100	1,070	1,770,000	5.82	0.86
	67	0.791	0.568	280	—	1,020	995	1,758,000	5.40	0.81
B-2	22	0.896	0.608	260	161	1,041	1,015	1,630,000	5.77	0.81
	67	0.840	0.551	230	150	1,007	980	1,650,000	5.46	0.70
A-2	22	1.11	0.478	220	140	923	900	1,320,000	5.65	0.85
(2-1-49)-2	25	1.49	0.476	210	121	920	840	980,000	6.13	1.05
A-3	22	1.56	0.330	170	117	768	750	940,000	5.58	0.89
A-6	22	2.79	0.18	97	77	560	545	524,000	5.5	0.92
	67	2.68	0.15	92	—	530	515	517,000	5.2	0.89
(2-1-49)-1	25	4.58	0.20	74	60	520	475	318,000	6.1	1.15
A-7	22	6.10	0.09	53	53	410	400	230,000	6.0	1.15
150-2	22	11.9	—	42	32	—	—	123,000	—	1.7
G-1	25	12.5	—	44	32.1	—	—	117,000	—	1.9
(2-1-49)-3	25	13.0	—	36	31.5	—	—	114,000	—	1.6
G-3	25	23.6	—	24	24.3	—	—	62,000	—	1.9
H-1	25	61.0	—	11	13.1	—	—	24,000	—	2.3
C-1	22	87.6	—	7.1	10.9	—	—	16,700	—	2.2
H-3	25	100	—	7.0	10.1	—	—	14,600	—	2.4
J-1	25	457	—	2.2	4.3	—	—	3,200	—	3.5
D-1	22	—	—	—	4.15	—	—	—	—	—
J-3	22	595	—	2.1	3.6	—	—	2,460	—	4.3
				Solvent: butanone (87 percent)-2-propanol (13 percent)						
A-1	22	0.841	0.48	−130	—	925	900	1,740,000	4.9	−0.3
	67	0.793	0.57	0	—	1,020	995	1,752,000	5.4	0.0
B-2	22	0.891	0.46	−70	—	910	885	1,630,000	5.0	−0.2
	67	0.852	0.54	0	—	990	965	1,630,000	5.5	0.0
				Solvent: dichlorethane						
E-2	22	1.47	1.28	900	260	1,450	1,410	1,780,000	7.6	2.54
B-2	22	1.61	1.16	900	278	1,370	1,335	1,570,000	7.6	2.88
	67	1.50	1.05	870	283	1,330	1,295	1,600,000	7.4	2.70
F-1	22	4.65	0.37	405	142	780	760	562,000	7.3	3.60
A-6	22	5.44	0.30	350	138	700	680	480,000	6.9	3.64
150-2	22	—	—	—	45	—	—	—	—	—
H-1	22	112	—	35.3	—	—	—	23,400	—	7.5
C-1	22	169	—	23.2	12.2	—	—	15,500	—	7.5
J-1	25	775	—	4.6	4.50	—	—	3,370	—	6.8
D-1	22	848	—	4.6	4.05	—	—	3,080	—	7

consequently is characteristic of the scattering substance rather than the experimental arrangement. All intensities herein reported are $\mathbf{I}_{\vartheta v}$.

As a result of work by one of the authors (C. I. C.) several standard solutions of known scattering power had been prepared and could be used to determine by direct comparison the absolute values of $\mathbf{I}_{\vartheta v}$ of the solutions here investigated.[4–6] In each case, of course, the scattering of the solvent has been subtracted so that the figures represent the *excess* scattering of the solutions.

A well-known[2] formula relates the weight average molecular weight, M, to the limit of the ratio of the reduced intensity to concentration, as concentration and angle both approach zero:

$$\lim_{c\to0,\ \vartheta\to0}\frac{\mathbf{I}_{\vartheta v}}{c}=\frac{4\pi^2n^2(\partial n/\partial c)^2}{\lambda_0{}^4N_0}M, \qquad (2)$$

where c is concentration, λ_0 wave-length of light in vacuum, N_0 Avogadro's number, and n the refractive index of the solution.

The derivative of refractive index with respect to concentration, $\partial n/\partial c$, has been measured for polystyrene in several solvents[7] at room temperature. To calculate

[4] The details of these determinations are now being prepared for publication. The results were considerably at variance with most of those found in the literature; for example, pure benzene at 25°C was found to give $\mathbf{I}_{90u}=16.3\times10^{-6}$ at a wave-length of 5461A and 48.4×10^{-6} at 4358A, as compared with 34.8×10^{-6} at the latter wave-length (see reference 5) and 11×10^{-6} at 5440A and 15°C (see reference 6). The new values seem to agree much better than the old with Einstein's theoretical equation. The molecular weights in reference 1, being based on the old intensity values for benzene, are therefore in error.

[5] P. Peyrot, Comptes Rendus **203**, 1512 (1936).

[6] J. Cabannes and P. Daure, Comptes Rendus **184**, 520 (1927).

[7] Doty, Zimm, and Mark, J. Chem. Phys. **12**, 144 (1944).

TABLE II.—*Continued.*

Material	t°, C	Intercept, $c/I\partial v$ at $c=0$ and $\vartheta=0$	Slope $\frac{}{\text{intercept}}$, $c=0$	Slope $\frac{}{\text{intercept}}$, $\vartheta=0$	Intrinsic viscosity, cm³/g	z-average length, L, A. U.	w-average length, L, A. U.	Molecular weight	b, A. U.	$A_2\times10^4$
				Solvent: Toluene						
B-2	22	3.22	1.14	1,060	345	1,320	1,290	1,610,000	7.3	3.12
	67	2.80	1.09	800	342	1,310	1,280	1,610,000	7.2	2.48
A-2	22	—	—	—	278	—	—	—	—	—
A-3	22	—	—	—	235	—	—	—	—	—
A-7	22	—	—	—	101	—	—	—	—	—
150-2	22	—	—	—	55	—	—	—	—	—
J-1	25	—	—	—	4.65	—	—	—	—	—
				Solvent: dichlorethane (65 percent)-cyclohexane (35 percent)[a]						
B-2	22	1.50	1.58	1,280	320	1,620	1,580	—[a]	9.0	3.98
	67	1.42	1.47	1,070	300	1,570	1,530	—	8.7	3.32
				Solvent: dichlorethane (35 percent)-cyclohexane (65 percent)[a]						
B-2	22	1.52	1.22	890	280	1,420	1,380	—[a]	7.8	2.76
	67	1.43	1.15	870	290	1,400	1,360	—	7.7	2.70
				Solvent: cyclohexane (94 percent)-dichlorethane (6 percent)[a]						
B-2	22	1.66	0.640	250	130	1,030	1,000	—[a]	5.7	0.78
	67	1.51	0.843	410	225	1,200	1,170	—	6.7	1.27
				Solvent: cyclohexane						
B-2	27.0	—	0.451	−120	—	870	850	—	4.83	−0.37
	31.0	—	0.500	−33	—	920	895	—	5.09	−0.102
	35.0	—	0.548	0	—	960	935	—	5.31	0.0
	39.0	—	0.580	20	—	990	965	—	5.49	0.062
	41.5	—	0.612	83	—	1,020	995	—	5.65	0.258

[a] Mixed solvents of differing refractive indices, therefore molecular weights not calculated. See Ewart, Roe, Debye, and McCartney, J. Phys. Chem. **14**, 687 (1946).

$\partial n/\partial c$ for other solvents and other temperatures the empirical rule of Gladstone and Dale was used. For the present undertaking the rule may be converted into the form:

$$\frac{\partial n}{\partial c}=R_2-\frac{d_1}{d_2}R_1, \qquad (3)$$

$$R_2=\frac{n_2-1}{d_2}, \quad R_1=\frac{n_1-1}{d_1},$$

where 1 and 2 refer to solvent and polymer, respectively, d is the density, and R_1 and R_2 are supposed to be constants independent of the temperature or state of aggregation. For polystyrene all available data, including the refractive index and density of the pure polymer, can be represented quite well with $R_2=0.581$ and $d_2=1.05$ at 20°C and 1.02 at 67°C. Equation (3) has therefore been used with the same value of R_2 to calculate $\partial n/\partial c$ for the higher temperature and other solvents. Values of n_1 and d_1 were taken from standard tables. The results are shown in Table IV. The calculated values were used in all further computations.

For dibenzyl $\partial n/\partial c$ was determined directly by measuring n with a Pulfrich refractometer for the rather concentrated solutions used.

When the scattered light is appreciably depolarized the intensity must be divided by a "Cabannes factor" before the molecular weights are calculated. With vertically polarized incident light the factor is $(3+3\rho_v)/(3-4\rho_v)$, where ρ_v is the depolarization ratio with vertically polarized incident light. If the incident light is unpolarized, the factor becomes $(6+6\rho_u)/(6-7\rho_u)$, with ρ_u the corresponding depolarization factor. The factor ρ_v was less than one percent for all samples except *D*-1 and *J*-1 (two percent), *J*-3 (three percent), and dibenzyl (see Table V). In all cases the depolarization is extrapolated to infinite dilution.

TABLE III. $c/I\partial v$ for fractions of (2-1-49) in butanone at 5460A.

		(2-1-49)-1 concentration, (g/ml) ×100			
ϑ	$\sin^2\vartheta/2$	0.0625	0.250	0.500	
26°	0.05	4.67	5.41	6.30	
36.9°	0.10	4.81	5.52	6.27	
53°	0.20	4.83	5.57	6.48	
66.4°	0.30	5.08	5.57	6.56	
90°	0.50	5.30	5.89	6.90	
113.6°	0.70	5.30	5.86	6.75	
127°	0.80	5.59	6.00	7.04	
		(2-1-49)-2			
		0.0312	0.0624	0.125	0.250
26°	0.05	1.58	1.65	1.86	2.21
36.9°	0.10	1.66	1.76	1.98	2.33
53°	0.20	1.72	1.83	2.06	2.43
66.4°	0.30	1.82	1.90	2.07	2.52
90°	0.50	1.95	2.08	2.24	2.69
113.6°	0.70	2.17	2.24	2.47	2.88
127°	0.80	2.28	2.33	2.55	2.97
		(2-1-49)-3			
		0.0625	0.125	0.250	0.500
90°	0.50	13.1	13.4	13.9	14.7

TABLE IV. Calculated values of refractive index increment, $\partial n/\partial c$, for polystyrene in various solvents, wave-length of 5460A.

Solvent	t°C	n	$\partial n/\partial c$, calc.	$\partial n/\partial c$, exper.
toluene	20	1.496	0.108	0.104[a]
	67	1.472	0.118	—
dichlorethane	20	1.444	0.158	0.161[b]
	67	1.423	0.167	—
cyclohexane	40	1.414	0.179	—
butanone	20	1.378	0.221	0.214[a]
	67	1.359	0.230	—

[a] See reference 7.
[b] Unpublished experiments.

The molecular weights may now be calculated from the intercepts listed in column 3 of Table II and Eq. (2). The results are given in column 9 of the same table. The results on dibenzyl are given separately in Table V.

The ratio of the slope of the plot of c/I against c at $\vartheta=0$ to the intercept is the quantity $2MA_2$, where A_2 is an important constant connected with the intermolecular interactions of the molecules in the solution.[8] When M has been determined, A_2 can be found from the ratios listed in column 5 of Table II. The results are given in column 11.

The intrinsic viscosities in cm³/g (100 times the values in "practical" units) are given in column 6.

In regard to precision, our experience has been that the slopes of most of these plots against angle or concentration are reproducible within ten percent, unless the slope is very small, and the intercepts within five percent.

The averages of the molecular weights obtained in the several solvents are given in Table VI.

DISCUSSION

Effect of Solvent and Temperature on L

The first purpose of this investigation was to study the molecular extension, as measured by L, and its

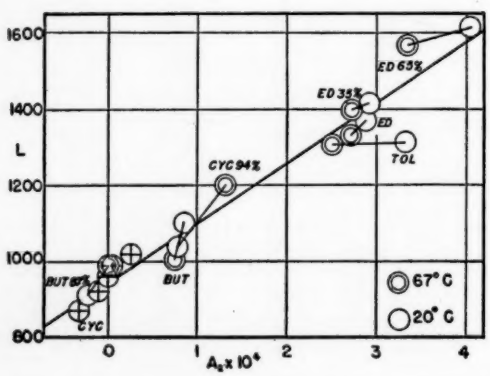

FIG. 2. Root-mean-square length, L, and "second virial coefficient," A_2, of sample B-2 for various solvents and temperatures.

[8] B. Zimm, J. Chem. Phys. 14, 164 (1946).

TABLE V. Dibenzyl (formula weight 182).

	Solvent: dichlorethane	Butanone
$\lim_{c\to 0} \frac{c}{I_{90v}}$	12,700	7,100
dn/dc	0.141	0.205
	0.150	0.105
ρ_v	184	186
Calculated molecular weight		
$A_2\times 10^4$	26	18
$[\eta]$	1.33	1.45
$[\eta]$ (toluene) = 1.33		

correlations with other quantities, especially the interactions between the segments and the molecules of solvents. Some relations of interest can be found in the data of Table II, especially the figures on the sample B-2. Figure 2 also shows some of these data.

In considering these results the following points should be kept in mind. The average extension, L, of a chain will depend on two things: 1. the nature and strength of the potentials opposing rotation around the bonds of the chain skeleton, which may result from steric or other interactions between the groups attached to neighboring chain atoms; 2. the interaction through van der Waals forces of segments of the chain when they happen to approach one another. This latter interaction will be partially counteracted by similar interactions between chain segments and solvent molecules, so that the net effect will depend markedly on the solvent.

For convenience we shall term phenomena of the first type *skeletal* effects, and those of the second type *osmotic*, in recognition of the essential similarity of the latter to the swelling and shrinking of gels.

In connection with the osmotic effect, the "second virial coefficient" of the osmotic pressure, A_2, plays an important part, so that it also must be discussed here.[9] When the osmotic pressure, Π, is expressed as a power series in concentration, c, A_2 is the coefficient of the second power:

$$\Pi = RT\left(\frac{c}{M} + A_2c^2 + A_3c^3 + \cdots\right). \tag{4}$$

A_2 is related to the spatial distribution of the molecules in the solution. It was originally shown by McMillan and Mayer[10] that A_2 is a measure of the deviation of the concentration of solute molecules in the neighborhood of a given molecule from the normal value. When A_2 is large the solute molecules are avoiding one another as a result of their van der Waals "excluded volume," and when it is small or negative they are attracting one another in preference to the solvent. Since the interactions of non-charged chain molecules are the sums of the interactions of their separate segments, large and

[9] P. J. Flory, J. Chem. Phys. 17, 303 (1949), has recently given a discussion that agrees in many respects with our conclusions here.
[10] W. G. McMillan and J. E. Mayer, J. Chem. Phys. 13, 276 (1945).

small values of A_2 should be associated with segment interactions which are on the average repulsive or attractive respectively.

We can tentatively conclude that when A_2 is large the segments, through their excluded volumes, repel one another so that the molecule is swollen, but when A_2 is made smaller the molecule will shrink. When A_2 is zero the *average* interaction of the segments vanishes (repulsive and attractive effects balance) and the molecule will have an extension characteristic of the rigidity of the chain with a minimum of complicating solvent effects. In this way the skeletal effects may be isolated.

The data on sample *B*-2 in Fig. 2 show a remarkably close correlation of the mean extension L and the parameter A_2. In only one case does a point deviate from the straight line by more than twice the expected experimental error. This seems to be true regardless of the temperature or chemical nature of the solvent. It is also noteworthy that the osmotic effect is able to change the mean extension of a molecule by a factor of almost two. The effect could be made even larger if the polymer would stay in solution in appreciable amounts when A_2 is made smaller than -0.5×10^{-4}.

The value of L at which A_2 is zero for sample *B*-2 is 950A. Following this argument, we may conclude that this is the value characteristic of this material when the osmotic effect vanishes and only skeletal effects are present.

Several authors[11,12] have shown how the skeletal effects may be calculated for an unbranched chain in which there are hindering torques about the carbon-carbon bonds in the chain. With L in angstrom units, the formula is

$$L=2.18\left(\frac{1+\langle\cos\phi\rangle_{Av}}{1-\langle\cos\phi\rangle_{Av}}\right)^{\frac{1}{2}}n^{\frac{1}{2}}=bn^{\frac{1}{2}}, \qquad (5)$$

where n is the number of chain bonds and $\langle\cos\phi\rangle_{Av}$ is the average value of the cosine of the angle the plane through the i'th and $(i+1)$'st bonds makes with the plane through the $(i-1)$'st and i'th bonds. Using the data on sample *B*-2, $\langle\cos\phi\rangle_{Av}$ is found to be 0.720. Since $\langle\cos\phi\rangle_{Av}$ is zero if there is free rotation about the bonds, it is evident that the chain is much extended over the free rotation size.

To discover the kind of interactions that might be expected between styrene residues in the chain, we have constructed a wooden scale model of a section of the chain, photographs of which are shown in Fig. 3. From the model it is evident that rotation can only occur freely over an angle of about 100° before a collision results between the phenyl groups and other parts of the chain. The exact number of degrees varies with the over-all configuration, but 100° is a good representative value. It therefore seems plausible to assume that in the real molecule the angle ϕ could vary freely from $-\alpha$ to $+\alpha$, but not beyond this point, where α is a constant of the order of 50°. As Benoit[12] has shown, this assumption yields the formula $\langle\cos\phi\rangle_{Av}=\sin\alpha/\alpha$. If $\langle\cos\phi\rangle_{Av}$ is 0.720, α must then be 78°, in rough agreement with the model.

FIG. 3. Scale models of a section of a polystyrene chain. The same model, curled in different ways, is shown in all three pictures.

Further evidence comes from the temperature coefficient of L. It would be most favorable if L could be obtained accurately at $A_2=0$ at several temperatures, but such an experiment requires changing the solvent as well as the temperature with the result that both theoretical and experimental uncertainties become too great.

An indirect line of attack is the following: From the classical theory of solutions of non-polar materials it is known that the solvents of greatest A_2 are those in which the solution is athermal and in which the colligative constants, such as A_2, change very little with temperature. If this is also true for the osmotic effect on the extension of the molecule, then the observed negative temperature coefficient of L at the maximum value of A_2 should be mainly due to skeletal effects. Actually there is also a small decrease of A_2 with temperature here also, which might account for part of the observed coefficient of L.[13] Hence the observed coefficient at the maximum value of A_2, the solution in the dichlorethane (65 percent)-cyclohexane (35 percent) mixture, represents the maximum possible for skeletal effects. This

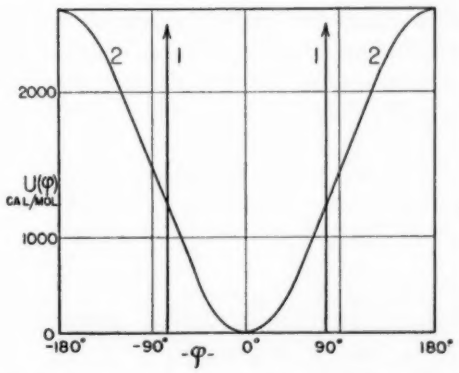

FIG. 4. Possible potentials hindering rotation about the carbon-carbon bonds of the polystyrene chain. Curve (1), extremely hard potential; (2), sinusoidal potential.

[11] W. J. Taylor, J. Chem. Phys. **16**, 257 (1948).

[12] H. Benoit, J. Chim. Phys. **44**, 18 (1947); J. Polymer Sci. **3**, 376 (1948); H. Kuhn, J. Chem. Phys. **15**, 843 (1947).

[13] A_2 is a complicated quantity which is known to depend not only on the value of L but also on the mean effects of the forces between the segments. The observed decrease of A_2 might therefore result from a net decrease in the repulsive interactions of the segments, resulting from a change in the molecular arrangement of the solvent. Such a decrease would be accompanied by a decrease in the osmotic swelling of a single molecule.

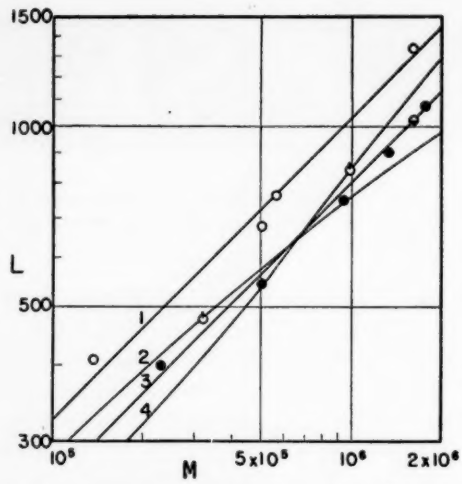

FIG. 5. Root-mean-square length, L, as function of molecular weight, M, on logarithmic scales for polystyrene at 22°C. Circles are experimental points: solid circles, fractions of polymer A in butanone; flagged circles, fractions of (2-1-49) in butanone; half-filled circle, B-2 in butanone; open circles, several materials in dichlorethane. Lines are theoretical relations for: (1), unbranched molecules, in dichlorethane; (2), (3), and (4) are fitted to butanone data; (2), for molecules with one branch on the average for 3000 styrene units; (3), unbranched molecules; (4), mixture of rings and chains with half the molecules rings at a molecular weight of 700,000.

value of dL/dt is approximately minus 0.1 percent per degree.

The temperature coefficient of L may be discussed in terms of the potential energy of rotation about the carbon-carbon skeletal bonds of the chain. Two possible potential functions are shown in Fig. 4. Curve 1, a step-function, represents the case already discussed in which the styrene residue may rotate freely only over a range of 2α. Curve 2 is a sine wave potential which has been used by W. J. Taylor in discussing the properties of the normal paraffins. This is the one, of the several possibilities, that has the smallest temperature coefficient. The temperature coefficients of L may be computed from these curves by the standard methods of statistical mechanics. It is found that dL/dt is zero for curve 1. For curve 2, from Taylor's figures, we may find that the height of the maximum of the potential is 2700 cal./mole and the temperature coefficient is minus 0.18 percent per degree. The experiments, as well as the physical nature of the problem, seem to favor an intermediate form of potential which is steeper than the sine wave but not as abrupt as the step-function, although the precision of the results is not such as to rule out either possibility completely.

Branching and Ring Formation in Polystyrene

The proportionally between L and $n^{\frac{1}{2}}$, Eq. (5), only holds if the chains are unbranched or if they are all closed rings. Theoretically, the change from a linear to a branched or ringlike chain at constant molecular weight, M, decreases L (L is here defined as $6^{\frac{1}{2}}R$ for a branched molecule). In some current work[14] the quantitative formulas have been calculated for the case where random branching is present.

It is assumed for simplicity that the polymerization process distributes the branch units at random among the molecules, and that the fractionation procedure then divides the material into a series of fractions, each of a different but homogeneous molecular weight, but with the branch units still distributed at random, i.e., the ratio of branch units to monomer units is the same for all fractions. Each fraction is then a mixture of many different kinds of branched and unbranched molecules, but the average number of branches per molecule is proportional to the molecular weight of the fractions. When for a series of fractions 2 $\log L$ is plotted against $\log M$, a characteristic curve is obtained, whose position gives the average number of branch units per molecule and hence the average ratio of branch units to monomer units.

Ring formation may be treated similarly. If it is assumed that ring closure will occur with a probability inversely proportional to L^3, the simplest plausible assumption,[14] another characteristic curve results.

In Fig. 5, are shown some of these curves fitted to some of the data from Table II. The most significant data are those obtained with butanone, since here the osmotic effects (as shown by A_2) are small. It can be seen that a reasonable fit is obtained only for the following alternatives: 1, the molecules are all rings, or 2, a rather unlikely mixture of ringed and branched forms giving approximately a straight plot, or 3, there may be branches, but less than one per 3,000 styrene units. The last alternative seems much the most probable.

The plot of the dichlorethane data shows that L is

TABLE VI. A_2, μ, and molecular weight.

Material	Average molec. wt.	Dichlorethane $A_2\times10^4$	Dichlorethane μ	Butanone $A_2\times10^4$	Butanone μ
E-2	1,780,000	2.54	0.478	—	—
A-1	1,755,000	—	—	0.86	0.4914
B-2	1,610,000	2.88	0.475	0.81	0.4919
A-2	1,320,000	—	—	0.85	0.4915
(2-1-49)-2	980,000	—	—	1.05	0.4895
A-3	940,000	—	—	0.89	0.4911
F-1	562,000	3.60	0.468	—	—
A-6	507,000	3.64	0.468	0.92	0.4906
(2-1-49)-1	318,000	—	—	1.15	0.4885
A-7	230,000	—	—	1.15	0.4885
B-9	138,000	5.22	0.454	—	—
150-2	123,000	—	—	1.7	0.483
G-1	117,000	—	—	1.9	0.481
(2-1-49)-3	114,000	—	—	1.6	0.484
G-3	62,000	—	—	1.9	0.481
H-1	23,700	7.5	0.434	2.3	0.477
C-1	16,100	7.5	0.434	2.2	0.478
H-3	14,600	—	—	2.4	0.476
J-1	3,290	6.8	0.440	3.5	0.465
D-1	3,110	7	0.438	—	—
J-3	2,460	—	—	4.3	0.457
dibenzyl	182	26	0.30	18	0.32

[14] W. H. Stockmayer and B. H. Zimm, J. Chem. Phys. **17**, 1301 (1949).

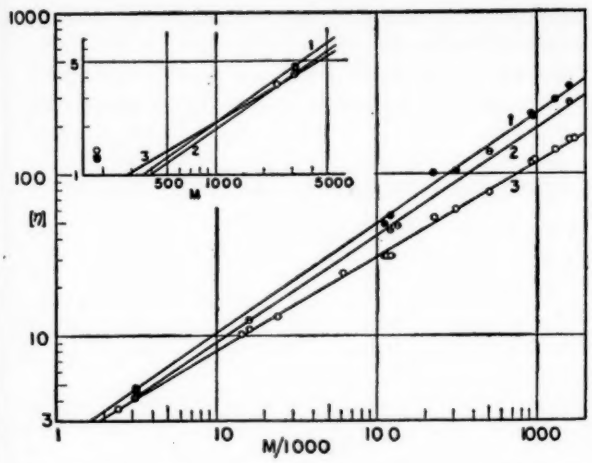

FIG. 6. Intrinsic viscosity, $[\eta]$, against molecular weight, M, on logarithmic scales. Curve (1), Mark-Houwink relation for toluene; (2), the same for dichlorethane; (3), the same for butanone. The inset shows the continuation of these curves to very low molecular weights and the data on dibenzyl.

approximately proportional to $M^{\frac{1}{2}}$ here also. The osmotic effect therefore does not change very rapidly with molecular weight. These data also include sample *F*-1, which was prepared at 150°C, and which falls on the same curve as the others.

We may conclude that polystyrene as ordinarily made with peroxide catalysts is not branched to a significant extent.[15]

This result appears at first sight to contradict the discovery of Bamford and Dewar[16] that chain transfer occurs frequently in the polymerization of styrene. From their figures transfer to the monomer would occur about three times in the life of a kinetic chain in a thermally initiated polymer at 70°C. Ideally, each molecular chain initiated by transfer would then finally become a branch on another chain, so that the molecules would contain several branches on the average. However, if the double bond in the monomer unit to which transfer occurred were shielded from further reaction by the chain growing on it, the degree of branching would

TABLE VII. c/I_{90v} for some fractions of low molecular weight in dichlorethane at 5460A.

Fraction *J*-1		Fraction *H*-1	
c, g/ml	c/I_{90v}	c, g/ml	c/I_{90v}
0.0143	826	0.00383	128
0.0308	878	0.00670	138
0.0400	921	0.01072	154
0.0500	956	0.0179	182
0.0667	1,002	0.0268	219
0.1000	1,143		

[15] The data on sample *E*-2, which contained 55 parts per million of cross linking agent, do not contradict the previous statement. There should be less than one branch per molecule in this sample, so that theory would predict a decrease of b due to branching of less than ten percent, not much larger than the experimental error.

[16] C. H. Bamford and M. J. S. Dewar, Proc. Roy. Soc. (London) **A192, 309, 329 (1948).**

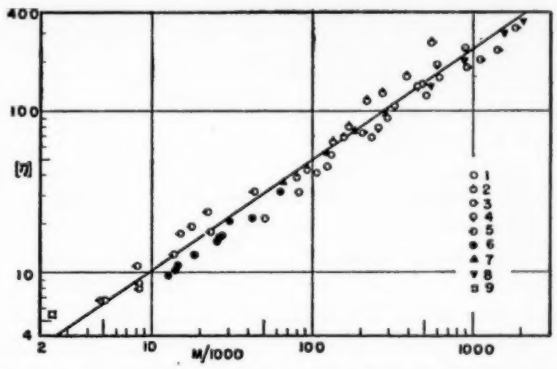

FIG. 7. Comparison of our Mark-Houwink relation for toluene with the results of other workers. (1), Gregg and Mayo (see reference 22), osmotic data on whole polymers; to compare with our fractions $[\eta]$ has been divided by $\Gamma(2.69)=1.53$, as suggested by Bamford and Dewar (see reference 16); (2), Schulz and Husemann (see reference 30); (3), Goldberg, Hohenstein, and Mark (see reference 19); (4), Bueche (see reference 21); (5), Bamford and Dewar, data on whole polymers with $[\eta]$ divided by $\Gamma(2.69)=1.53$, as suggested by these authors (see reference 16); (6), Gregg and Mayo (see reference 22), data from end-group analysis of whole polymers, $[\eta]$ divided by 1.53; (7), Wales *et al.* (see reference 21a), weight average molecular weights from the ultracentrifuge; (8), Alfrey, Bartovics, and Mark (see reference 20), samples prepared at 60°C; (9), Kemp and Peters (see reference 23), sample *B*-4; if these authors' cryoscopic measurements are extrapolated to infinite dilution the point is brought much closer to our curve.

be less than one. In the same way transfer directly to polymer would be discouraged. Such effects, together with the fact that transfer is less important in catalytically initiated polymerizations, may account for our failure to find branching.

The Change of the Virial Coefficient A_2 with Molecular Weight

In Table VI is shown the virial coefficient A_2 for several comparable samples whose only difference is chain length. The important fact appears, contrary to a widely held notion, that A_2 is far from constant as the molecular weight is varied. A change of about threefold from the highest to the lowest molecular weight is evident in the solvent dichlorethane. Some such change has been predicted theoretically,[8,17] but the magnitude of the effect is a surprise.

Data on polystyrene in the literature are fragmentary so that effective comparison is difficult. For materials of high molecular weight our results agree fairly well numerically with those of other authors. The only data that also cover a wide range of molecular weights are those of Flory[17a] with polyisobutylene. He did not find a variation of A_2 like ours, although it is possible that a trend in A_2 might have been masked by an opposite variation of A_3, the third virial coefficient. Such a variation of A_3 is quite apparent in polystyrene; for example, osmotic measurements by Schick[18a] on a sample of molecular weight 540,000 in toluene solution

[17] P. J. Flory, J. Chem. Phys. **13,** 453 (1945).

[17a] P. J. Flory, J. Am. Chem. Soc. **65,** 372 (1943).

TABLE VIII. Mark-Houwink constants for polystyrene.

	Fractions at 25°C $[\eta]=KM^a$; $M=k([\eta]/100)^b=\kappa[\eta]^b$*		
	Butanone	Dichlorethane	Toluene
a	0.58	0.66	0.69
K	0.039	0.021	0.017
b	1.71	1.51	1.45
k	740,000	360,000	293,000
κ	280	340	368

* $[\eta]$ is expressed in cm³/g; $[\eta]/100$ is the intrinsic viscosity in practical units.

yielded A_3 equal to 5×10^{-3}, while our data (Table VII) on sample J-1 of molecular weight 3290 in dichlorethane, a similar solvent, do not allow A_3 to be greater than 1×10^{-3}. In this connection we may note that light scattering generally permits the measurements to be extended to lower concentrations than osmotic pressure with high molecular weight samples, hence allowing A_2 and A_3 to be separated more surely. In fact, our measurements sometimes do not even overlap the lowest concentration at which Flory made osmotic measurements.

Obviously this should be a subject for further study.

Huggins[18] and Flory[17] originally proposed the equation,

$$A_2=\frac{1}{d_2^2V_1}(\tfrac{1}{2}-\mu), \tag{6}$$

where d_2 is the density of the polymer, V_1 the molar volume of the solvent, and μ a parameter whose value should be small compared to $\frac{1}{2}$ in solutions in which the heat of dilution is small, e.g., polystyrene-dichlorethane. Calculated values of μ are given in Table VI. It can be seen that μ is actually small in the direction of agreement with the theory only at the lowest molecular weights, the deviations being greater the greater the molecular weight.

An extension or revision of the solution theory seems to be indicated.

The Effect of Temperature and Solvent on A_2

The implications of the interrelated effects of solvent and temperature on A_2 are too complicated to be discussed fully here. However there are several noteworthy points. As previously observed in the case of toluene,[1] A_2 has a negative temperature coefficient in good solvents. This implies that these systems have negative heats of dilution. On the other hand the temperature coefficient is positive in "bad" solvents where A_2 is small, as would be expected from the current theory of solutions. However the magnitude of the temperature coefficient is much different in systems in which cyclohexane is the main constituent from those in which butanone predominates. It follows that while the free energies of dilution of these latter two types of systems are approximately the same, the heats and entropies of dilution are markedly different.[18a]

Another noteworthy point is that a mixture of cyclohexane and dichlorethane is a better solvent than either alone.

Intrinsic Viscosity and Molecular Weight

A log-log plot of intrinsic viscosity against molecular weight is shown in Figs. 6 and 7. In Fig. 7 we have also included results of some other workers, by means of which we can compare our molecular weights with theirs. (There has been no attempt to include *all* the relevant work on polystyrene in Fig. 7).

Goldberg, Hohenstein, and Mark[19] have determined osmotic molecular weights on fractions of an emulsion polymer prepared at 63°C. Their molecular weights are higher than ours by about fifteen percent on the average.

Alfrey, Bartovics, and Mark[20] have likewise made osmotic measurements on solutions of polystyrene prepared at several temperatures. Their measurements on their samples prepared at 60°C are higher than ours by about fifteen percent.

Bueche[21] has made light scattering measurements on a polymer prepared principally at 100°C. If it is assumed that his intrinsic viscosities in benzene solution are comparable to ours in toluene, his results straddle our curve.

Wales *et al.*[21a] report ultracentrifugal measurements on polystyrene fractions. Their weight average molecular

TABLE IX. Ratio of intrinsic viscosity, $[\eta]$, to cube of mean square length, L, for sample B-2 in several solutions.

Solvent	Temperature	$[\eta]$	$L\times10^8$	$L^3/[\eta]\times10^{17}$
toluene	22	345	1320	0.68
	67	342	1310	0.66
dichlorethane (65 percent)—cyclohexane (35 percent)	22	320	1620	1.33
	67	300	1570	1.30
dichlorethane (35 percent)—cyclohexane (65 percent)	22	280	1420	1.02
	67	290	1400	0.95
dichlorethane	22	278	1370	0.93
	67	283	1330	0.83
butanone	22	161	1041	0.71
	67	150	1007	0.68
cyclohexane (94 percent)—dichlorethane (6 percent)	22	130	1030	0.84
	67	225	1200	0.77

[18] M. L. Huggins, J. Chem. Phys. **9**, 440 (1941).

[18a] Similar results have been found in osmotic measurements: Doty, Brownstein, and Schlener, J. Phys. Coll. Chem. **53**, 213 (1949); Schick, Doty, and Zimm, J. Am. Chem. Soc. **72**, 530 (1950).

[19] Goldberg, Hohenstein, and Mark, J. Polymer Sci. **2**, 503 (1947).

[20] Alfrey, Bartovics, and Mark, J. Am. Chem. Soc. **65**, 2319 (1943).

[21] A. M. Bueche, J. Am. Chem. Soc. **71**, 1452 (1949).

[21a] Wales, Williams, Thompson, and Ewart, J. Phys. Chem. **52**, 983 (1948).

weights and intrinsic viscosities agree very well with our curve.

The osmotic measurements of Schulz and Husemann[30] cross our curve. These authors used an unusual method of treating their osmotic data.

At the lower molecular weights are the results of Bamford and Dewar,[16] based on end-group analysis of unfractionated polymers. They calculate from a theoretical molecular weight distribution the intrinsic viscosity-molecular weight relation for fractions. Their molecular weights tend to be lower than ours. The question of branching in polystyrene, which they raise, has already been discussed.

Gregg and Mayo[22] have made a study very similar to Bamford and Dewar's. Their molecular weights are much higher however. At the higher molecular weights they also made osmotic measurements.

Kemp and Peters[23] made cryoscopic measurements on some polystyrene fractions. Their results on materials comparable to ours straddle our curve.

The agreement of our results with the formula weight of dibenzyl is excellent.

The order of agreement of the various measurements is satisfactory for many purposes, although it is disappointing that it is not better.

Our results may be represented very well, with the exception of dibenzyl, by the Mark-Houwink empirical relation, $[\eta]=KM^a$. The constants K and a are shown in Table VIII. Nowhere does the Staudinger relation, $[\eta]$ proportional to M, have validity.

Debye and Bueche[24] and Kirkwood and Riseman[25] have recently given theories of the intrinsic viscosity. However, since Kirkwood has more recently pointed out[26] that the theories must be modified to take account of Brownian motion, we will refrain from making detailed comparison. However the effects to be expected when the solvent is changed are probably still qualitatively correct, at least. The theories predict that for a given sample of high molecular weight the intrinsic viscosity should vary approximately as L^3, but for a sample of low molecular weight the variation should be more nearly as L^2.

As a test of the theory at high molecular weights, Table IX gives the ratio of $[\eta]$ to L^3 for sample B-2 under different conditions. As predicted, the ratio is mainly constant, although it must be admitted that there is more variation than would be expected from the probable experimental error alone.

At low molecular weights it was impossible to measure L directly because the molecules were too small compared to the wave-length of the light. However, if we assume only that $[\eta]$ is sensitive to L, perhaps varying as L^2, it becomes significant that the curves of Fig. 6 draw together as the molecular weight decreases. For example, the change in intrinsic viscosity of sample B-2 ($M=1{,}610{,}000$) on going from dichlorethane to butanone is a factor of 1.73, while for sample C-1 ($M=16{,}100$) the factor is only 1.1. This can only mean that L becomes less dependent on solvent at lower molecular weights.[27]

The conclusion is that the osmotic effect is important for long chains but not for short ones.[28] As a result the root-mean-square length, L, will not be strictly proportional to the square root of the molecular weight except in a "bad" solvent where the osmotic effect is practically zero. This point skould be kept in mind when attempting to obtain the amount of branching from the relation between L and M. (Fortunately the effect does not seem to be large enough in butanone to change our preceding conclusions about branching.)

For compounds of very low molecular weight, less than 1000, the hydrodynamic theory is not a useful approach to the study of the intrinsic viscosity. In this region the effects of solute molecular weight and of solvent viscosity and heat of dilution become quite different from those found at higher molecular weights. The data on the intrinsic viscosity of dibenzyl are a case in point. Much more extensive studies have been made in this region by other workers.[29]

It has been claimed that the temperature of polymerization has an effect on the relation between molecular weight and intrinsic viscosity.[20,30] The effect has variously been attributed to branching and to isomerization of the chain skeleton. Unfortunately we do not have sufficient data to throw much light on this question. However it is interesting to point out that intrinsic viscosities as well as mean length for samples F-1 and 150-2 are well in accord with those of the other samples, despite the fact that the former were polymerized at 150°C and the latter at 70°C.

Very recently E. D. Kunst of the University of Paris has reported a study of the light scattering of polystyrene and polyisobutylene.[31] There seems to be quite extensive agreement between his work and ours.

[22] R. A. Gregg and F. R. Mayo, J. Am. Chem. Soc. **70**, 2373 (1948).
[23] A. R. Kemp and H. Peters, Ind. Eng. Chem. **34**, 1097 (1942).
[24] P. Debye and A. M. Bueche, J. Chem. Phys. **16**, 573 (1948).
[25] J. G. Kirkwood and J. Riseman, J. Chem. Phys. **16**, 560 (1948).
[26] J. G. Kirkwood, Rec. Trav. Chim. Pays-Bas, **68**, 649 (1949).
[27] Similar effects are noted among the data of Kemp and Peters.[23]
[28] This conclusion has also been obtained by Flory[9] on theoretical grounds.
[29] For example, H. A. Stuart, Zeits. f. Naturforschung **3a**, 196 (1948); E. Kuss and H. A. Stuart, *ibid.* **3a**, 204 (1948).
[30] G. V. Schulz and E. Husemann, Zeits. f. physik. Chemie (B) **39**, 246 (1938); G. V. Schulz, Makromolec. Chem. **3**, 146 (1949). See, however, Gregg and Mayo (reference 22).
[31] E. D. Kunst, Rec. Trav. Chim. Pays-Bas **69**, 125 (1950).

The Kinetics of Phase Transitions in Binary Systems*

HOWARD REISS
Department of Chemistry, Boston University, Boston, Massachusetts
(Received February 10, 1950)

A *kinetic* theory of phase transitions in two-component systems is presented which is applicable to the transitions, vapor to liquid and liquid to liquid. The rate of the transition is characterized by a two-dimensional vector which can be used in conjunction with the equation of continuity to develop a partial differential equation which determines the kinetics of the process.

A new type of energy surface is introduced, and an investigation of its salient features enables one to simplify the solution of the differential equation mentioned above. This purely kinetic treatment makes possible the evaluation of the unknown coefficient found in the older quasi thermodynamic treatment of transition rates in two component systems.

I. INTRODUCTION

THE work of Volmer,[1] Becker and Doring,[2] Zeldovich,[3] and Frenkel[4] has led to a satisfactory kinetic treatment of phase transitions in one-component systems. No purely kinetic treatment exists for transitions occurring in two-component systems, e.g., the condensation of a gaseous mixture or the separation of one liquid phase into two. Up until now transitions in binary systems have been treated using the thermodynamic technique of Volmer.[5] This technique is based upon the theory of fluctuations,[6] and has as its object the calculation of the rate at which fluctuations occur which lead to stable fragments of a new phase. This rate, I^*, can be expressed as

$$I^* = Ce^{-\omega_0/kT}, \tag{1}$$

where ω_0 is the reversible work which must be expended in order to produce an embryo having a size and composition such that it can remain in equilibrium with the mother phase. An embryo thus critically composed is called a nucleus. In (1) k is the Boltzmann constant, T, the absolute temperature, and C is an unknown coefficient.

In spite of the mystery surrounding the nature of C, Eq. (1) is useful because of the singular behavior of the exponential factor. As the mother phase becomes more and more metastable (e.g., supersaturated), this factor suddenly increases from a very small value to an almost infinite value. The point at which this occurs represents a critical limit of metastability at which the rate of transition passes from an infinitesimal value to an enormous value, and beyond which the mother phase can no longer exist. If C is neither extremely small nor excessively large, the degree of supersaturation corresponding to this critical limit can be determined with reference to the behavior of the exponential factor alone.

Indeed, phase transitions either proceed so slowly or so rapidly, depending upon which side of the critical limit is being considered, that, practically, it is impossible to measure anything about them (except in rare instances[7]) save the location of the limit itself. Nevertheless, in order to apply Eq. (1) on an *a priori* basis it is necessary to know something about the magnitude as well as the variability of C. In certain cases the nature of C may be such as to influence the location of the critical limit.

The evaluation of C can only be accomplished by means of a truly kinetic approach. Becker and Doring[2] were the first to succeed in developing such an approach for one-component systems. The success of their development was based primarily upon the fact that the rate controlling steps in the transition were connected with the growth of embryos in the neighborhood of the nuclear size.

In this paper we shall attempt to develop a kinetic theory for phase transitions in binary systems, and to evaluate C, for such systems.

II. THE EQUILIBRIUM DISTRIBUTION OF EMBRYOS

Attention will be restricted to either the condensation of a gaseous mixture or the separation of a liquid into two phases. Even under conditions for which the mother phase is stable, there will be local, transient, inhomogeneities in the mother phase corresponding to the formation of embryos of new phases. A dynamic equilibrium will arise in which the number of embryos having a given size and composition remains constant. The dependence of this number on size and composition can be computed (at least for embryos containing more than about fifty molecules) by generalizing a scheme which has been used by Frenkel[8] and Bijl[9] to characterize the embryo distribution in a one-component system.

* This research has progressed under the sponsorship of the Geophysical Research Directorate, Air Force Cambridge Research Laboratories, Air Materiel Command.

[1] Volmer, *Kinetik der Phasenbildung* (Edwards Brothers, Inc., Ann Arbor, 1945).
[2] Becker and Doring, Ann. d. Physik **24**, 719 (1935).
[3] Zeldovich, J. Exper. Theor. Phys. U.S.S.R. **12**, 525 (1942).
[4] Frenkel, *Kinetic Theory of Liquids* (Oxford University Press, London, 1946).
[5] Volmer, Zeits. f. Physik Chemie **119**, 277 (1926).
[6] J. C. Slater, *Introduction to Chemical Physics* (McGraw-Hill Book Company, Inc., New York, 1939), p. 101.
[7] H. Reiss, J. Chem. Phys. **18**, 1 (1950).
[8] J. Frenkel, J. Phys. **1**, 315 (1939).
[9] Bijl, dissertation, Leiden (1939).

It can be shown[10] that the inaccuracy of this procedure when applied to embryos with less than fifty molecules in no way invalidates its application to larger embryos, and it will further appear that the distribution of large embryos is all that is necessary for the study of the kinetics of the transition.

In the present case not only size, but composition as well, distinguishes an embryo. For this reason, in computing the distribution it is necessary to formulate the problem somewhat differently from Frenkel, but the basic ideas are really the same. The mother phase is thought of as consisting of molecules of the components, A and B, together with embryos of all sizes and compositions. An embryo of a given size and composition is regarded as a definite species of molecule. The total number of molecules (including molecular embryos) present will be denoted by F. A particular molecular embryo will be characterized by the numbers of single molecules, a and b, of species A and B, that it contains. Thus $N(a, b)$ represents the number of embryos having a molecules of A and b molecules of B, which are present at equilibrium. The partial molecular free energy corresponding to embryos of kind (a, b) can be assumed to be

$$a\lambda_a+b\lambda_b+\alpha(a, b)[av_a+bv_b]^{\frac{1}{3}}+kT\log\frac{N(a, b)}{F}, \quad (2)$$

where λ_a and λ_b are the partial molecular free energies of A and B in a solution having the same composition as the embryo, existing at the pressure *outside* of the embryo. The second term represents the contribution due to the embryonic surface. Here (considering spherical embryos only)

$$\alpha(a, b)=4\pi\sigma(a, b)(3/4\pi)^{\frac{1}{3}}, \quad (3)$$

where $\sigma(a, b)$ is the surface tension of an embryo of kind (a, b). Strictly speaking $\sigma(a, b)$ is only defined for an embryo which can persist in equilibrium with the remainder of the mother phase, but if we consider embryos for which a and b are not too different from the critical values of a and b, denoted by x and y, respectively, corresponding to such an embryo we may attach asymptotic meaning to $\sigma(a, b)$. As it has been pointed out, only embryos of this type exert appreciable influence upon the rate of transition. The partial molecular volumes, v_a and v_b, of the material in the embryo are considered to be independent of pressure. Indeed, only if the embryos are considered to be incompressible can the surface contribution be represented as in (2).

The third term represents that part of the partial molecular free energy which arises because the embryo (a, b) is part of a solution dilute with respect to (a, b). In (2) the contribution due to the energy of rotation of the embryo as a whole has been neglected[11] since it is small for embryos of larger size.

With the help of (2) the total free energy of the mother phase, φ, can be written in the form

$$\varphi=a_0\mu_a+b_0\mu_b+\sum_{a, b}N(a, b)\left[a\lambda_a+b\lambda_b+\alpha(av_a+bv_b)^{\frac{1}{3}}+kT\log\frac{N(a, b)}{F}\right], \quad (4)$$

where a_0 and b_0 are the numbers of single molecules of A and B present, and μ_a and μ_b are the partial molecular free energies of these molecules. The requirement at equilibrium is

$$\delta\varphi_{T, P}=0, \quad (5)$$

subject to the conservation conditions

$$\delta a_0+\sum_{a, b}a\delta N(a, b)=0 \quad (6)$$

$$\delta b_0+\sum_{a, b}b\delta N(a, b)=0. \quad (7)$$

The treatment applied by Frenkel to one component systems can be improved by noting the solution of (5), (6), and (7) can be found without further knowledge concerning the natures of μ_a and μ_b, provided only that we make use of the Gibbs-Duhem* equation in order to write (5) in the form

$$\delta\varphi_{T, P}=\mu_a\delta a_0+\mu_b\delta b_0+\sum_{a, b}\left[a\lambda_a+b\lambda_b+\alpha(av_a+bv_b)^{\frac{1}{3}}+kT\log\frac{N(a, b)}{F}\right]\delta N(a, b)=0. \quad (8)$$

The simultaneous solution of (6), (7), and (8) is further expedited by the use of the Lagrange method of undetermined multipliers.[12] The result of applying this method is

$$N(a, b)=F\exp\left\{\frac{-[a\Delta\mu_a+b\Delta\mu_b+\alpha(av_a+bv_b)^{\frac{1}{3}}]}{kT}\right\}. \quad (9)$$

Here

$$\Delta\mu_a=\lambda_a-\mu_a \quad (10)$$

$$\Delta\mu_b=\lambda_b-\mu_b. \quad (11)$$

The numerator of the exponent may be called $\omega(a, b)$. It represents the reversible work which must be ex-

[10] See reference 4, p. 379.

[11] See reference 4, p. 381.

* P. S. Epstein, *Textbook of Thermodynamics* (John Wiley and Sons, Inc., New York, 1937), p. 105.

[12] I. S. Sokolnikoff and E. S. Sokolnikoff, *Higher Mathematics for Engineers and Physicists* (McGraw-Hill Book Company, Inc., New York, 1941), second edition, p. 163.

pended in order to form an embryo of kind (a, b) in the mother phase. The sum $\sum N(a, b)$ will always be small compared to a_0+b_0 so that

$$F \simeq a_0+b_0 \tag{12}$$

with good accuracy.

There are three distinct situations, corresponding to the physical set up in a large number of real systems, in which $\Delta\mu_a$ and $\Delta\mu_b$ can be evaluated explicitly. In the first two of these the mother phase is gaseous while the embryos are either ideal or dilute solutions.

Case 1:

(1) mother phase gaseous
(2) embryo ideal

$$\Delta\mu_a = v_a(p-p_a^0)+kT\log(p_a^0/p_a)x_a \tag{13}$$

$$\Delta\mu_b = v_b(p-p_b^0)+kT\log(p_b^0/p_b)x_b. \tag{14}$$

No third inert gas is considered to be present so that $p=p_a+p_b$, the sum of the partial pressures of A and B, respectively. x_a and x_b are the mole fractions of A and B in the embryo while p_a^0 and p_b^0 are the vapor pressures of pure A and B at the temperature, T.

Case 2:

(1) mother phase gaseous
(2) embryo dilute with respect to A

$$\Delta\mu_a = v_a(p-p^*)+kT\log\frac{p_a^*}{x_a^*}\frac{x_a}{p_a} \tag{15}$$

$$\Delta\mu_b = v_b(p-p_b^0)+kT\log\frac{p_b^0}{p_b}x_b. \tag{16}$$

Equation (16) is identical with (14). In (15) p^* is the total equilibrium vapor pressure over any mixture of A and B at the temperature T. The mole fraction of A in this mixture is x_a^* while its partial vapor pressure is p_a^*.

Case 3:

(1) mother phase liquid, dilute with respect to B
(2) embryo dilute with respect to A

$$\Delta\mu_a = kT\log(y_a^*/x_a^*)(x_a/y_a) \tag{17}$$

$$\Delta\mu_b = kT\log(y_b^*/x_b^*)(x_b/y_b). \tag{18}$$

y_a^* and x_a^* are the mole-fractions of A in the mother phase and embryo phase, respectively, when both

$$\begin{array}{c}(a, b+1)\\ \uparrow\downarrow\\ B\\ +\\ (a-1, b)+A\rightleftarrows(a, b)+A\rightleftarrows(a+1, b)\\ \uparrow\downarrow\\ B\\ +\\ (a, b-1)\end{array}$$

FIG. 1.

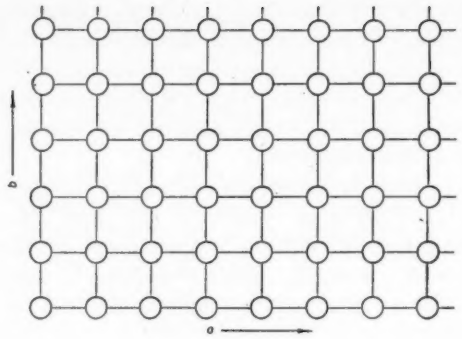

FIG. 2.

phases have compositions corresponding to some equilibrium state at the temperature, T, and the pressure, p, outside of the embryo. The same is true of y_b^* and x_b^*. x_a, y_a, x_b, and y_b have the same meanings as in cases 1 and 2.

In closing it should be mentioned that the distribution (9) remains valid even when the mother phase is metastable, provided that we induce a formal equilibrium, by arbitrarily inhibiting the kinds of embryos which can exist, e.g., disallow the existence of embryos larger than a certain size.

III. BINARY KINETICS

It is necessary to devise a means for organizing the great complexity of single steps leading to the formation or disappearance of a particular embryo. The complications due to the introduction of a new component render it impossible simply to adopt the clever schemes designed for this purpose by Becker and Doring[2] and Zeldovich[3] for one-component systems. Nevertheless, their work can be used as a guide, and certain items of procedure actually can be inserted at points into the present development.

In view of the relatively low probability of a collision between two embryos it can be assumed that embryos grow and diminish by the acquisition or loss of single molecules. An embryo (a, b) can undergo four reactions represented schematically in Fig. 1.

By looking upon (a, b) as specifying a point having the coordinates a and b in a plane all of the reactions (of the kind diagrammed in Fig. 1) proceeding simultaneously, can be represented by a planar lattice as in Fig. 2.

An embryo of type (a, b) is represented by the lattice point whose coordinates are a and b. The lines connecting the lattice points take the place of the arrows in Fig. 1. Since the reaction along any line segment connecting two lattice points is reversible, there will be a *net* rate at which embryos corresponding to one lattice point traverse the connecting line (so to speak) and become embryos corresponding to the other lattice point, this rate being the difference between the rates of the forward and reverse reaction. The net rate at which embryos of kind (a, b) move horizontally and become embryos of kind $(a+1, b)$ will be called $I_a(a, b, t)$

where t stands for time. The net rate at which embryos of kind (a, b) move vertically to become embryos of kind $(a, b+1)$ will be called $I_b(a, b, t)$.

Both I_a and I_b can be evaluated by generalizing a method developed by Frenkel[13] for the treatment of one component systems. Accordingly

$$I_a=f(a, b, t)S(a, b)\beta_a - f(a+1, b, t)S(a+1, b)\gamma^{(a)}(a+1, b) \quad (19)$$

$$I_b=f(a, b, t)S(a, b)\beta_b - f(a, b+1, t)S(a, b+1)\gamma^{(b)}(a, b+1). \quad (20)$$

In these equations $f(a, b, t)$ stands for the number of embryos of kind (a, b) present at the time, t. $S(a, b)$ is the surface area of an embryo of this size, while β_a and β_b represent, respectively, the rates at which molecules of species A and B strike unit area of embryo surface. If the mother phase is gaseous,

$$\beta_a=\frac{p_a}{(2\pi m_a kT)^{\frac{1}{2}}} \quad (21)$$

$$\beta_b=\frac{p_b}{(2\pi m_b kT)^{\frac{1}{2}}}, \quad (22)$$

where m_a and m_b are the respective molecular masses. The evaluation of β_a and β_b when the mother phase is liquid will be discussed in a later paper. $\gamma^{(a)}(a+1, b)$ and $\gamma^{(b)}(a, b+1)$ are the rates at which molecules of species A and B leave unit areas of surface of embryos of kind $(a+1, b)$ and $(a, b+1)$, respectively.

$\gamma^{(a)}$ and $\gamma^{(b)}$ can be determined in terms of the distribution function (9) by arbitrarily inhibiting the system in the manner described at the end of Section II, so that a formal equilibrium arises (even though the mother phase is metastable) in which

$$I_a=I_b=0 \quad (23)$$

by virtue of the principle of detailed balance.† Furthermore, in this equilibrium

$$f(a, b, t)=N(a, b), \quad \text{etc.} \quad (24)$$

The substitution of (19) and (20) into (23), and of (24) into the result yields the relations

$$\gamma^{(a)}(a+1, b)=\frac{N(a, b)S(a, b)\beta_a}{N(a+1, b)S(a+1, b)} \quad (25)$$

$$\gamma^{(b)}(a, b+1)=\frac{N(a, b)S(a, b)\beta_b}{N(a, b+1)S(a, b+1)}. \quad (26)$$

Substituting (25) and (26) into (19) and (20) leads to

[13] See reference 4, p. 393.
† See reference 6, p. 91.

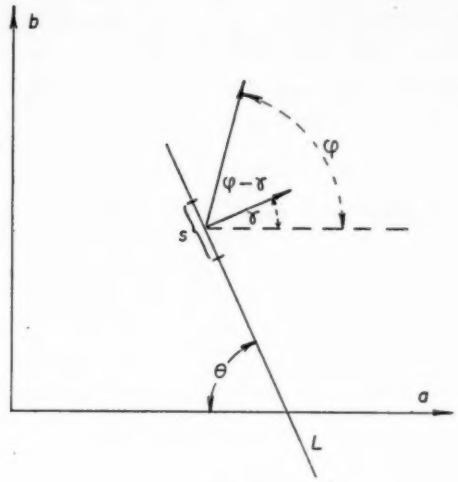

FIG. 3.

the expressions

$$I_a(a, b, t)=N(a, b)S(a, b)\beta_a \times\left[\frac{f(a, b, t)}{N(a, b, t)}-\frac{f(a+1, b, t)}{N(a+1, b, t)}\right] \quad (27)$$

$$I_b(a, b, t)=N(a, b)S(a, b)\beta_b \times\left[\frac{f(a, b, t)}{N(a, b, t)}-\frac{f(a, b+1, t)}{N(a, b+1, t)}\right]. \quad (28)$$

For large embryos the sets of numbers a and b may be regarded as continuous, and (27) and (28) may be rewritten as

$$I_a=-NS\beta_a\left[\frac{\partial}{\partial a}\left(\frac{f}{N}\right)\right]_b \quad (29)$$

$$I_b=-NS\beta_b\left[\frac{\partial}{\partial b}\left(\frac{f}{N}\right)\right]_a. \quad (30)$$

Consider, now, the total flow of embryos across a segment, s, of a line, l, in the a, b-plane which is tilted at an angle, θ, to the negative direction of the a-axis (Fig. 3).

This flow, J, will be given by

$$J=n_a I_a+n_b I_b, \quad (31)$$

where n_a and n_b are the numbers of streams of I_a and I_b which the line segment, s, intersects. In terms of Fig. 2, n_a and n_b are the number of horizontal and vertical lines, respectively, which s intersects. The validity of (31) depends upon s being small enough so that I_a and I_b can be considered constant over its length. If, at the same time s is large enough so that it intersects an appreciable number of streams

$$n_a=s\sin\theta \quad (32)$$

$$n_b=s\cos\theta. \quad (33)$$

Therefore,

$$J=s[I_a \sin\theta+I_b \cos\theta]. \tag{34}$$

The angle that the normal to s makes with the a-axis is $\gamma=(\pi/2)-\theta$. In terms of γ, (34) becomes

$$J=s[I_a \cos\gamma+I_b \sin\gamma]. \tag{35}$$

Next, it is possible to define a vector **I** whose components in the a and b directions are I_a and I_b, respectively. The angle φ at which this vector is tilted with respect to the a-axis is defined by the equations

$$I_a=I\cos\varphi \tag{36}$$

$$I_b=I\sin\varphi. \tag{37}$$

Insertion of (36) and (37) into (35) yields

$$J=sI\cos(\varphi-\gamma)$$

or for the flow across unit length of line

$$\frac{J}{s}=I\cos(\varphi-\gamma). \tag{38}$$

Since $(\varphi-\gamma)$ is the angle between **I** and the normal to s, it is seen that the flow density across any line is merely the component of **I** in the direction of the normal to the line. Therefore, the flow at any point in the a, b-plane can be described in the usual manner by the vector **I**. Of course, this vector loses its significance when restricted to a single lattice point since the flow is really divided at such a point. It only gains significance when the flow across a line segment is considered, and when this segment intersects a *number* of individual streams.

According to the equation of continuity**

$$-\mathrm{div}\mathbf{I}=-\left(\frac{\partial I_a}{\partial a}+\frac{\partial I_b}{\partial b}\right)=\frac{\partial f}{\partial t}, \tag{39}$$

or in terms of (29) and (30)

$$\frac{\partial}{\partial_a}\left[NS\beta_a\frac{\partial}{\partial a}\left(\frac{f}{N}\right)\right]+\frac{\partial}{\partial_b}\left[NS\beta_b\frac{\partial}{\partial b}\left(\frac{f}{N}\right)\right]=\frac{\partial f}{\partial t}. \tag{40}$$

The solution of this partial differential equation subject to suitable boundary conditions should, in principle, enable one, through the use of (29) and (30), to determine the flow at any time, at any point in the a, b-plane. However, Eq. (40) retains its validity only at the beginning of the transition process, since the transition alters the properties of the mother phase and consequently $N(a, b)$ becomes time dependent while β_a and β_b cannot be defined.

A similar difficulty is encountered in the treatment of one-component systems. It is resolved by confining attention to intervals of time short enough so that only an inappreciable fraction of the transition has occurred. In this manner the flow during these intervals can be computed, and the critical limit is assumed to be defined by those conditions under which the initial flow first becomes very great. Of course, when the conditions are such that the initial flow is small the interval of time during which the one-component analogue of (40) is applicable may be quite long. On the other hand when it becomes small one is not interested in using the equation for more than a short time anyway.

Since the number of single molecules so greatly exceeds the number of embryos it may be considered constant during this interval. In this manner a quasi steady state is reached in which

$$\partial f/\partial t=0. \tag{41}$$

The one-dimensional analogue of (40) is therefore reduced to an ordinary differential equation which can easily be solved subject to the boundary conditions

$$f\to N \quad \text{for small embryos,} \tag{42}$$

$$f\to 0 \quad \text{for very large embryos.} \tag{43}$$

Although in the case of (40) itself the restriction to early times is permissible, subject to the attendant condition (41), the result is still a partial differential equation whose solution, subject to the boundary conditions

$$f(a, b)\to N(a, b) \quad \text{for} \quad a+b\to 0 \tag{44}$$

$$f(a, b)\to 0 \quad \text{for} \quad a+b\to\infty, \tag{45}$$

is not simple, so that the procedure employed in the one-component case does not facilitate matters in the two-component case.

Let us consider more carefully what it is that we must compute. The numerator of the exponent in (9), $\omega(a, b)$, the reversible work necessary for the formation of an embryo of kind (a, b) can be plotted as a surface whose elevation depends upon (a, b). In certain regions on this surface an embryo will be able to increase its size with a decrease of $\omega(a, b)$, or, in other words, with a decrease in free energy. Embryos which pass into these regions may, therefore, be regarded as stable fragments of a new phase. Since we are interested in calculating the rate at which such fragments form, it is necessary to compute the rate at which embryos flow over the boundaries of the projections of these regions on the a, b-plane. This rate may be called the *nucleation rate*, I^*, and is a measure of the rate at which the phase transition occurs. If the solution of (40) subject to (41), (44) and (45) was available, the calculation of the nucleation rate would be immediately possible.

In principle the solution could be obtained by the use of numerical methods, and these together with a plot of the ω-surface would enable one to evaluate the nucleation rate. Such a procedure, however, is extremely tedious and is well worth avoiding by recourse to a new type of approximation which can be most conveniently

** See reference 12, p. 429.

explained by reference to certain salient features of the ω-surface.

IV. THE ENERGY SURFACE

In this section the nature of the energy surface $\omega(a, b)$ will be considered under those circumstances, such that the conditions of cases 1, 2, and 3, defined at the end of Section II, are satisfied. Actually, these cases are identical from the functional point of view so that, for convenience, only case 1 will be considered specifically. Assuming case 1

$$\omega(a,b)=aH_a+bH_b+akT\log\frac{a}{a+b}+bkT\log\frac{b}{a+b}+\alpha(a,b)(av_a+bv_b)^{\frac{1}{3}}, \quad (46)$$

where

$$H_a=v_a(p-p_a^0)+kT\log\frac{p_a^0}{p_a} \quad (47)$$

$$H_b=v_b(p-p_b^0)+kT\log\frac{p_b^0}{p_b}. \quad (48)$$

At a given temperature the surface tension, σ, of an embryo which can persist in equilibrium with the mother phase (a nucleus) is determined purely by the chemical potentials μ_a and μ_b of components A and B in the mother phase.[14] Consequently, even if more than one type nucleus were possible the surface tensions of all would be the same. Let x and y be the critical values of a and b corresponding to a nucleus. The values of x and y are determined by the equations

$$(\partial\omega/\partial a)_{T,\,p,\,\sigma,\,b}=(\partial\omega/\partial b)_{T,\,p,\,\sigma,\,a}=0, \quad (49)$$

where the σ held constant has the value corresponding to a nucleus. Inserting (46) into (49) yields the result

$$-kT\log[x/(x+y)]=H_a+\tfrac{2}{3}\alpha v_a(xv_a+yv_b)^{-\frac{1}{3}} \quad (50)$$

$$-kT\log[y/(x+y)]=H_b+\tfrac{2}{3}\alpha v_b(xv_a+yv_b)^{-\frac{1}{3}}, \quad (51)$$

which, upon being solved, gives the required x and y.

Using (46) and the constant value of σ corresponding to the nucleus, it can be shown (for the neighborhood of (x, y)) that

$$\left[\frac{\partial^2\omega}{\partial a\partial b}\right]^2-\left(\frac{\partial^2\omega}{\partial a^2}\right)\left(\frac{\partial^2\omega}{\partial b^2}\right)=\frac{kT}{(a+b)}\frac{2\alpha}{9(av_a+bv_b)^{4/3}}\left[v_a\left(\frac{a}{b}\right)^{\frac{1}{3}}+v_b\left(\frac{b}{a}\right)^{\frac{1}{3}}\right]^2+\left[\frac{2\alpha v_av_b}{9(av_a+bv_b)^{4/3}}\right]^2>0. \quad (52)$$

This means that in this neighborhood $\omega(a, b)$ cannot possess any maxima or minima,[15] so that (x, y) can be neither a maximum nor a minimum. It can be shown that (x, y) is a saddle point, i.e., a point at which the curvature of the surface is negative in one direction and positive in the direction at right angles to this direction. This can be shown in the following manner. Introduce the transformation

$$a=x+r\cos\vartheta, \quad b=y+r\sin\vartheta \quad (53)$$

where ϑ is the angle that the radius vector, r, originating at (x, y), makes with the a-axis. Substituting (53) into (46), and differentiating twice with respect to r, gives for the curvature at $r=0$, i.e., at (x, y),

$$\left(\frac{\partial^2\omega}{\partial r^2}\right)_{r=0}=\frac{kT\cos^2\vartheta}{x}+\frac{kT\sin^2\vartheta}{y}-\frac{kT(1+2\sin\vartheta\cos\vartheta)}{x+y}-\frac{2\alpha[v_a\cos\vartheta+v_b\sin\vartheta]^2}{9[xv_a+yv_b]^{4/3}}. \quad (54)$$

That the directions of steepest descent and steepest ascent are at right angles to each other can be demonstrated by calculating the extremal values of (54) in their dependence upon ϑ. Setting

$$[\partial/(\partial\vartheta)][(\partial^2\omega/\partial r^2)_{r=0}]=0, \quad (55)$$

produces the equation

$$\frac{\left[kT\left(\frac{1}{y}-\frac{1}{x}\right)-\frac{2\alpha(v_b^2-v_a)^2}{9[xv_a+yv_b]^{4/3}}\right]}{\left[\frac{kT}{x+y}+\frac{2\alpha v_av_b}{9[xv_a+yv_b]^{4/3}}\right]}=\frac{1}{\tan\vartheta}-\tan\vartheta. \quad (56)$$

This is a quadratic in $\tan\vartheta$. If $\tan\vartheta_1$ is one solution it is seen that

$$\tan\vartheta_2=-1/(\tan\vartheta_1) \quad (57)$$

is the other solution. Equation (57) is merely another way of expressing the relation,

$$\vartheta_2=\vartheta_1+\pi/2, \quad (58)$$

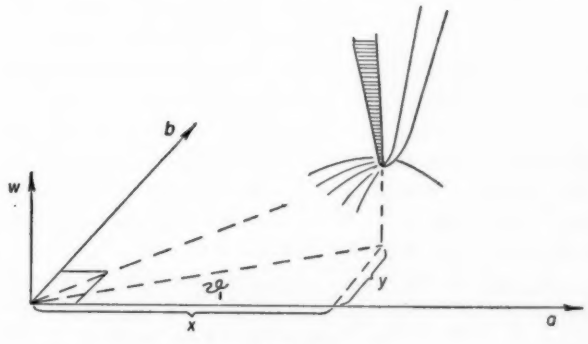

FIG. 4.

[14] MacDougall, *Thermodynamics and Chemistry* (John Wiley and Sons, Inc., New York, 1939), third edition, p. 363.

[15] See reference 12, p. 161.

in view of the fact that the range of ϑ in which we are interested is $0 \leqslant \vartheta \leqslant \pi$. Therefore, there are only two extrema and they refer to mutually perpendicular paths. These extrema must have opposite signs, otherwise (x, y) would be a maximum or a minimum, in violation of (52). It may thus be concluded that (x, y) is a saddle point.

In practice, the second term in both the numerator and denominator of the left member of (56) is very small compared to the first. As an example, let the mother phase be a gaseous mixture wherein component A is water and B is ethyl alcohol. The following conditions hold:

$T = 298°\text{K}$
[16] $p_a^0 = 23.76$ mm
$p_b^0 = 59$ mm
$p_a = 25$ mm
$p_b = 30$ mm
$x = 26500$ molecules
$y = 7200$ molecules
[17] $\sigma(x, y) = 29.63$ dynes/cm

The value used for $\sigma(x, y)$ was the value measured for a bulk liquid having the same composition, in equilibrium with its own vapor. The partial pressures above this bulk will therefore differ from the p_a and p_b specified above. However, when the mother phase is gaseous the error introduced by this choice of σ will be small. Of course, the computation was carried forward upon the assumption that the alcohol-water solution was ideal. Since only an order of magnitude is desired this approximation introduces no difficulty.

Using the data listed above, the ratio of the second to the first term in the numerator of the left member of (56) is found to 0.037, while in the denominator the ratio is 0.050. Actually, the influence of the second terms in determining ϑ_1 and ϑ_2 is even less than is reflected in these ratios. In most cases, they may be ignored in (56).

When this is done, the two roots are found to be

$$\tan\vartheta_1 = y/x \tag{59}$$

$$\tan\vartheta_2 = -x/y. \tag{60}$$

Substituting ϑ_1, defined by (59) into (54) yields

$$\left(\frac{\partial^2\omega}{\partial r^2}\right)_{r=0,\vartheta=\vartheta_1} = -\frac{2\alpha[v_a x + v_b y]^{\frac{3}{2}}(x+y)}{9(x^2+y^2)}, \tag{61}$$

which is negative so that $\omega(a, b)$ has a maximum *along the path* through (x, y) determined by ϑ_1.

It is interesting to note that this path is the line drawn from the origin in the a, b-plane, through (x, y). The saddle is shown in Fig. 4. It must be borne in mind that not only has the previous analysis been based upon the relations described in cases 1, 2, and 3 at the end of Section II, but that also the value of σ employed has been that corresponding to the nucleus at (x, y). This σ has been used as a constant in the neighborhood of (x, y) in order to obtain some idea concerning the nature of the surface in this neighborhood. So long as attention is confined to the neighborhood of (x, y) the equations of the foregoing analysis are essentially correct.

The demonstration of the existence of the saddle in cases 1, 2, and 3 which admittedly can be physically real, and, which, in fact, represent fairly common situations, serves to help us estimate the general picture. There remains the question as to whether the path, from the origin through the saddle, is the lowest energy path for the growth of stable fragments of a new phase. It is very attractive to regard it as such. In the majority of circumstances it undoubtedly will be so, but a conclusive answer rests upon an actual plot of the energy surface using the correct, variable σ. It is quite possible, depending upon the peculiar nature of the substances forming the system, that under certain conditions lower energy paths are available.[18] In such cases the approximation to be described in the next section will not be entirely valid, and the numerical solution of the problem, as described at the end of Section III, will be necessary.

V. THE RATE OF NUCLEATION

In the last section it was demonstrated, under conditions for which $\Delta\mu_a$ and $\Delta\mu_b$ could be evaluated explicitly, that the nucleus point (x, y) was a saddle point. In this region the energy surface, ω, has a pass whose axis is the line drawn from the origin through (x, y), and whose sides rise steeply in the direction perpendicular to this axis. If consideration is restricted to those systems for which the growth path through the pass is the one whose crest is lowest, the nucleation rate I^* can be approximated using the following procedure.

First, introduce the linear transformation corresponding to a rotation of the axes a and b, counterclockwise, through the angle ϑ_1. These new axes may be called the a' and b' axes. Notice that the a' axis is the axis of the pass through (x, y), now called (x', y'). The transformation is specified by

$$a = a'\cos\vartheta_1 - b'\sin\vartheta_1 \tag{62}$$

$$b = a'\sin\vartheta_1 + b'\cos\vartheta_1. \tag{63}$$

The components of $\mathbf{I}$ parallel to the new axes may be denoted by $I_{a'}$ and $I_{b'}$, respectively. If we assume the steady state, then, according to (39)

$$\frac{\partial I_{a'}}{\partial a'} + \frac{\partial I_{b'}}{\partial b'} = 0. \tag{64}$$

Now in the region of the pass, at least, the flow will be so pronounced along the axis of the pass, i.e., in the a' direction that by comparison any lateral flow may be

[16] Int. Crit. Tab., Volume III, pp. 210, 217.
[17] See reference 16, Volume IV, p. 467.
[18] See reference 1, p. 155.

considered to be zero. This amounts to the assertion

$$I_{b'}=0 \tag{65}$$

which when substituted into (64) yields

$$(\partial I_{a'})/(\partial a')=0. \tag{65a}$$

In other words, the flow

$$I_{a'}=I=I(b') \tag{66}$$

is a function of b' only in the vicinity of the pass. This approximation may even hold well in regions far from the pass, especially in the vicinity of the a' axis. However, even if it does not, it will be seen that the rate controlling phenomena occur in the neighborhood of the pass, so that we can proceed to evaluate the nucleation rate, I^*, using (66). This rate will be given by

$$I^*=\int_{-\infty}^{\infty} I(b')db'. \tag{67}$$

A word of explanation is now in order. The free energy surface, ω, differs from the usual potential energy surface utilized in discussing ordinary chemical kinetics. The usual surface plots energy as a function of the relative space positions of the particles involved in the reaction. The surface, ω, besides being a *free* energy surface, plots energy as a function of the composition and size of an embryo as it grows towards the point where it can be a stable fragment of a new phase. Furthermore, in the present calculation we will not eliminate *all* alternative paths, besides the one of lowest energy, from consideration (as is done in ordinary reaction kinetics), but shall actually make allowance for the cross-sectional profile of the pass by carrying out the integration indicated in (67).

Returning to the calculation, since $I=I_{a'}$ it follows that

$$I_b/I_a=\tan\vartheta_1=y/x \tag{68}$$

and that

$$I_a=I(b')\cos\vartheta_1. \tag{69}$$

In terms of the rotated coordinates

$$\frac{\partial(f/N)}{\partial a}=\frac{\partial(f/N)}{\partial a'}\cos\vartheta_1-\frac{\partial(f/N)}{\partial b'}\sin\vartheta_1 \tag{70}$$

$$\frac{\partial(f/N)}{\partial b}=\frac{\partial(f/N)}{\partial a'}\sin\vartheta_1+\frac{\partial(f/N)}{\partial b'}\cos\vartheta_1. \tag{71}$$

Substituting (70) and (71) into (29) and (30), and the result into (68) yields

$$(\beta_a-\beta_b)\sin\vartheta_1\cos\vartheta_1(\partial/\partial a')(f/N) = (\beta_b\cos^2\vartheta_1+\beta_a\sin^2\vartheta_1)(\partial/\partial b')(f/N). \tag{72}$$

By substituting (70) into (29) and the result into (69) there is obtained the relation

$$I(b')=-\beta_a NS\left[\frac{\partial}{\partial a'}\left(\frac{f}{N}\right)-\tan\vartheta_1\frac{\partial}{\partial b'}\left(\frac{f}{N}\right)\right], \tag{73}$$

which can be simplified by replacing $\partial/\partial b'(f/N)$ with the aid of (72) to

$$\frac{I(b')[\beta_b+\beta_a\tan^2\vartheta_1]}{\beta_a\beta_b[1+\tan^2\vartheta_1]}\frac{1}{NS}=\frac{\partial}{\partial a'}\left(\frac{f}{N}\right). \tag{74}$$

Integration can now be carried out partially with respect to a', subject to the boundary conditions (see (44) and (45))

$$(f/N)\to 1, \quad a'\to 0 \tag{75}$$

$$(f/N)\to 0, \quad a'\to\infty \tag{76}$$

leading to the result

$$I(b')=\frac{\beta_a\beta_b[1+\tan^2\vartheta_1]}{[\beta_b+\beta_a\tan^2\vartheta_1]}\cdot\frac{1}{\displaystyle\int_0^{\infty}\frac{da'}{NS}}. \tag{77}$$

The evaluation of the integral can be accomplished in the following manner.[19] The function

$$(1/N)=(1/F)\exp[\omega(a',b')/kT] \tag{78}$$

has such a pronounced maximum in the a' direction, at (x',y') that little error is incurred by removing S from the integrand as the constant $S(x',y')$ and replacing $\omega(a',b')$ by its quadratic approximation in the neighborhood of (x',y'), i.e.,

$$\omega(a',b')\simeq\omega(x',y')+\frac{1}{2}\frac{\partial^2\omega(x',y')}{\partial a'^2}(a'-x')^2 + \frac{\partial^2\omega(x',y')}{\partial b'\partial a'}(a'-x')(b'-y') + \frac{1}{2}\frac{\partial^2\omega(x',y')}{\partial b'^2}(b'-y')^2. \tag{79}$$

The linear terms do not appear in (79) because (x',y') is a saddle point. The cross term can also be ignored at the saddle point.

Now, define

$$\omega_0=\omega(x',y') \tag{80}$$

$$-P=-\frac{1}{2}\frac{\partial^2\omega(x',y')}{\partial a'^2}>0 \tag{81}$$

$$Q=-\frac{1}{2}\frac{\partial^2\omega(x',y')}{\partial b'^2}>0. \tag{82}$$

[19] See reference 4, p. 395.

The inequalities (81) and (82) are satisfied because $2P$ is merely the negative curvature at (x', y') in the direction ϑ_1, while $2Q$ is the positive curvature in the direction ϑ_2. Finally, introduce the translation

$$u=a'-x' \tag{83}$$

$$v=b'-y'. \tag{84}$$

With these ideas and definitions

$$\int_0^\infty \frac{da'}{SN}=\frac{1}{FS(x', y')}\exp\left(\frac{\omega_0+Qv_2}{kT}\right)\times\int_{-\infty}^{\infty}\exp\left(-\frac{Pu^2}{kT}\right)du$$

$$=\frac{1}{FS(x', y')}\left(\frac{\pi kT}{P}\right)^{\frac{1}{2}}\exp\left(\frac{\omega_0+Qv^2}{kT}\right) \tag{85}$$

provided that x' is fairly large. Replacing the integral in (77) by (85) and inserting the result into (67) yields

$$I^*=\frac{\beta_a\beta_b[1+\tan^2\vartheta_1]FS(x', y')}{[\beta_b+\beta_a\tan^2\vartheta_1]}\left(\frac{P}{\pi kT}\right)^{\frac{1}{2}}e^{-\omega_0/kT}\times\int_{-\infty}^{\infty}\exp\left(-\frac{Qv^2}{kT}\right)dv$$

$$=\frac{\beta_a\beta_b[1+\tan^2\vartheta_1]FS(x', y')}{[\beta_b+\beta_a\tan^2\vartheta_1]}\left(\frac{P}{Q}\right)^{\frac{1}{2}}e^{-\omega_0/kT}. \tag{86}$$

If ϑ_1 is extremely small the lower limit of the integral in (86) may not be fixed at $-\infty$ without incurring some error. However, these situations will arise very infrequently (ϑ_1 has to be *extremely* small) and when they do arise the integral can be evaluated using a table of probability functions.[20]

[20] N. A. Lange., *Handbook of Chemistry* (Handbook Publishers, Inc., Sandusky, 1941), fourth edition, Appendix, p. 257.

Comparing (86) with (1) reveals that the coefficient C can now be expressed as

$$C=\frac{\beta_a\beta_b[1+(y^2/x^2)]FS(x', y')}{\beta_b+\beta_a(y^2/x^2)}\left(\frac{P}{Q}\right)^{\frac{1}{2}} \tag{87}$$

where we have written y/x for $\tan\vartheta_1$.

The form of C is quite interesting. Notice that Q is the curvature of the saddle in the direction ϑ_2. When this curvature is high it means that the pass is narrow and has very steep sides. Consequently, it could be expected that the flow through the pass would be decreased, and the nucleation rate reduced. This is just what happens, for Q appears in the denominator of C, and thus lowers I^* when it is large. Similarly when P, the negative curvature in the direction of flow, ϑ_1, is high, a narrower barrier must be negotiated and so the flow should be increased. That this is so appears from the fact that P is in the numerator of C.

If the new phase is dilute with respect to one component, say B, then y/x will be small and to a good approximation

$$C=\beta_a S(x', y')F(P/Q)^{\frac{1}{2}} \tag{88}$$

so that β_b will exert negligible influence upon I^*.

In closing, attention should be directed to the fact that in the evaluation of ω_0 the surface tension $\sigma(x', y')$ corresponding to the nucleus should be used. When the mother phase is gaseous, little error is incurred by using, in place of $\sigma(x', y')$, the surface tension of a similarly composed liquid bulk in equilibrium with its own vapor. On the other hand, in case the mother phase is liquid it is important to use, not the tension corresponding to an equilibrium between two bulk phases one of which has the composition of the nucleus, but the actual tension corresponding to the equilibrium between the nucleus and the mother phase. When the nucleus and the mother phase are oppositely dilute, as above, the correct tension can be determined by subjecting the two phases in bulk equilibrium to the pressure, p, where

$$p=[2\sigma(x', y')]/r \tag{89}$$

and under this condition measuring the surface tension. In (96), r is the radius of the nuclear embryo. Since $\sigma(x', y')$ is unknown and, in fact, is being measured, the reverse procedure of computing r must be employed.

On the Isotopic Chemistry of Carbonates and a Paleotemperature Scale*

J. M. McCrea†
Kent Chemical Laboratory, University of Chicago, Chicago, Illinois
(Received January 30, 1950)

The temperature variation of the fractionation of oxygen in exchange reactions between dissolved carbonate and water and between calcite and water are calculated on theoretical grounds, and checked experimentally. In the course of the experiments it was necessary to investigate several methods of decomposing calcium carbonate to carbon dioxide for mass spectrometer analysis. A method was developed for growing calcium carbonate from solution with the same isotopic composition as the carbonate shells of organisms produced at the same temperature from water of the same isotopic composition, and the results of these experiments at various temperatures are expressed in an equation relating the temperature of formation with the isotopic composition of the calcium carbonate and of the water.

INTRODUCTION

In recent years the slight separation of isotopes in exchange equilibria between chemical species has been studied both theoretically and experimentally. On the theoretical side, this separation or fractionation turns out to be temperature dependent.[1] Experimentally, measurements of the fractionation have usually been made at one temperature only, but the hydrogen-water exchange of protium and tritium has been studied over a considerable temperature range.[2] Because of the intriguing possibilities of studying marine climatology in the geologic past by an investigation of the oxygen isotopic composition of carbonate fossils, the present studies of the temperature variation of the oxygen isotope fractionation in exchanges between water and carbonate ion in solution and between water and calcium carbonate were undertaken.[1] The conditions under which the results obtained may be related to paleotemperature determinations have been discussed elsewhere,[3] but in a number of instances these are strictly parallel to those of the laboratory experiments described here.

THEORETICAL CONSIDERATIONS

The methods of calculating the fractionation factor for an exchange between two chemical species in the gaseous or dissolved state from spectroscopic data have been reviewed, and a large number of numerical results given.[1] As it is of interest in connection with experimental results to follow, the case of the carbonate-water exchange will be considered in some detail. The fractionation factor, α, is the ratio of the two isotopes in one phase divided by the corresponding ratio for the other phase, and in the case of carbonate ion and water,

$$\alpha=\frac{3[CO_3^{18=}]+2[CO^{16}O_2^{18=}]+[CO_2^{16}O^{18=}]}{3[CO_3^{16=}]+2[CO_2^{16}O^{18=}]+[CO^{16}O_2^{18=}]}\Big/\frac{[H_2O^{18}]}{[H_2O^{16}]}.$$

Provided that the equilibrium constants for the exchange reactions between the various carbonate ions are those given by the symmetry numbers, this expression for α reduces to the expression for the equilibrium constant for the reaction

$$H_2O^{18}+\tfrac{1}{3}CO_3^{16=}=H_2O^{16}+\tfrac{1}{3}CO_3^{18=}.$$

This equality of fractionation factor and equilibrium constant appears to be a very good approximation except in the case of hydrogen isotopes, and in view of the lack of knowledge of the vibration frequencies of the mixed type of ion and the great complexity of any method of calculating these frequencies, the equality will be assumed in the present case.

In extending the calculation of fractionation to the crystalline case, effects due to the lattice motion must be considered, as well as the internal motion of polyatomic ions. Several not too satisfactory assumptions are made in order to obtain relations which may be used to calculate numerical results. The degrees of freedom necessary for $CaCO_3$ may be grouped as six of internal vibration in the carbonate, six of lattice vibration, and three of a type of lattice vibration corresponding to rotation of the carbonate ion. As the spectroscopic data from which the calculations will be made show that the carbonate ion in calcite has the same symmetry as in aqueous solution, the isotope shift of a given ion frequency is taken as the same fraction of the frequency for either state. The contribution to the fractionation between states due to any given mode of vibration, wave number ω, may be found by forming

$$\frac{Q\omega^*}{Q\omega}=\exp\frac{hc(\omega-\omega^*)}{2kT}\cdot\frac{1-\exp-hc\omega/kT}{1-\exp-hc\omega^*/kT}$$

for both states, and evaluating

$$(\pi(Q\omega^*/Q\omega)\text{crystal}/\pi(Q\omega^*/Q\omega)\text{ solution})^{1/n}$$

where n is the number of atoms exchanging to produce $CO_3^{*=}$ from $CO_3^{=}$, 1 for carbon and 3 for oxygen.

Using a representation of the lattice motion in terms of Debye and Einstein relations with θ as the Debye

* A portion of a dissertation submitted to the Department of Chemistry, University of Chicago, in partial fulfillment of the requirements for the degree of Doctor of Philosophy (June, 1949).
† Present address: Experimental Station, Ralston, Alberta, Canada.
[1] H. C. Urey, J. Chem. Soc. 592 (1947).
[2] J. Black and H. Taylor, J. Chem. Phys. **11**, 395 (1943).
[3] H. C. Urey, Science, **108**, 489 (1948).

TABLE I. Estimation of fractionation between carbonate ion in calcite lattice and in aqueous solution.

	Mode of motion							
	θ	ϕ_t	ϕ_r	ω_1	ω_2	ω_3	ω_4	All
Conversion ratios								
Oxygen ($CaCO_3^{18}$)	0.976454	0.976454	0.942809	0.942682	0.988800	0.985295	0.943267	
Carbon ($CaC^{13}O_3$)	0.995876	0.995876	1.000000	1.000000	0.968628	0.970000	0.998333	
Wave number, calcite	(180°)	156	284	1086	879	1434	712	
Wave number, $CO_3^=$(aq.)				1063	879	1415	680	
Contribution to O^{18} fractionation, ‰								
at 0°C	1.80		(10.0)	1.12	0.00	0.45	2.68	(7.85)
at 25°C	1.51		(8.3)	1.00	0.00	0.44	2.36	(6.82)
Contribution to C^{13} fractionation, ‰								
at 0°C	0.95		0.00	0.00	0.00	2.98	0.27	4.20
at 25°C	0.01		0.00	0.00	0.00	2.75	0.24	3.80

temperature corresponding to three degrees of freedom and ϕ_t, ϕ_r as characteristic temperatures referring to the remaining degrees of freedom and with

$$D(x)=\frac{3}{x}\int_0^x \frac{x^3dx}{\exp x-1}$$

as the Debye energy function,

$$-\ln Q^*/Q=(F^*-F)/RT$$

$$=-\frac{9}{8}(\theta^*-\theta)/T+3\ln\frac{1-\exp-\theta^*/T}{1-\exp-\theta/T}$$

$$+D(\theta/T)-D(\theta^*/T)$$

$$+\frac{3}{2}(\phi_t^*-\phi_t)/T+3\ln\frac{1-\exp-\phi_t^*/T}{1-\exp-\phi_t/T}$$

$$+\frac{3}{2}(\phi_r^*-\phi_r)/T+3\ln\frac{1-\exp-\phi_r^*/T}{1-\exp-\phi_r/T}.$$

If it is assumed that $\theta^*/\theta=\phi_t^*/\phi_t$, then the relations

$$\theta^*/\theta=(M_{Ca}\cdot M_{CO_3}/M_{Ca}^*\cdot M_{CO_3}^*)^{\frac{1}{2}}$$

and

$$\phi_r^*/\phi_r=(I_{CO_3}/I_{CO_3}^*)^{\frac{1}{2}}$$

cause Q^*/Q for the crystal to approach Q^*/Q for the solution as T approaches infinity, and give the desired vanishing fractionation between the crystal and solution at high temperatures.

The above treatment is quite crude, particularly in regard to the treatment of rotation as an Einstein function of characteristic temperature ϕ_r. In numerical calculation, the rotational contribution to fractionation made in this way turns out to be entirely too great compared with translation and vibration. This may be due to the neglect of the zero-point energy term arising from the "caging" effect of adjacent molecules in the solution. For the oxygen exchange, the rotational contribution is assumed to be the same as the translational. For the carbon exchange, with the moment of inertia of the ion unaltered by the exchange, the rotational contribution must be zero.

Numerical values for the vibration frequencies are available for carbonate, both in aqueous solution and in calcite.[4,5] The temperatures ϕ_t and ϕ_r will be taken to correspond to the Raman frequencies assigned to lattice motions of the translational and rotational type. From heat capacity measurements at low temperatures, θ is known.[6] This information and the results of the calculation of the fractionation between aqueous carbonate and calcite are given in Table I. In this table and later, it is usually convenient to adopt an abbreviating notation for expressing differences in isotopic composition and fractionating effect.[3] Thus if the isotope ratio in one sample is $(1+0.001x)$ times that in a given sample, the two are said to differ in isotopic composition by x‰, and if the fractionation factor for an exchange between two compounds is $(1+0.001a)$, the fractionation between the two compounds is said to be a‰. The fractionation between aqueous carbonate and calcite given in Table I is used to obtain the value for the fractionation factor between calcite and water listed in Table II. The other results listed in Table II were calculated by the usual methods.

Over the temperature range of Tables I and II, the fractionation factors for the exchanges between carbonate and water and between calcite and water are

TABLE II. Certain fractionation factors at various temperatures.

Exchange of O^{16} and O^{18} between	Temperature, °C 0.0	8.0	17.0	25.0
$CO_3^=$(aq.)−O	1.1046_3	1.0998_4	1.0948_3	1.0907_2
H_2O(g)−O	1.0741_3	1.0716_2	1.0689_8	1.0667_7
H_2O(l)−H_2O(g)	1.0103_5	1.0095_9	1.0089_9	1.0083_0
$CO_3^=$(aq.)−H_2O(l)	1.0176_1	1.0162_6	1.0148_6	1.0137_6
Calcite−H_2O(l)	1.0254_8	1.0237_8	1.0210_1	1.0205_4

[4] G. Herzberg, *Molecular Spectra and Molecular Structure II, Infrared and Raman Spectra of Polyatomic Molecules* (D. Van Nostrand Company, Inc., New York, 1945), p. 178.

[5] R. S. Krishnan, Proc. Ind. Acad. Sci. **22A**, 182 (1945).

[6] T. C. Anderson, J. Am. Chem. Soc. **56**, 340 (1934).

TABLE III. Mass distribution in natural carbon dioxide.[a]

Mass	Contributing species	Individual abundance	Relative abundance of given mass[b]
44	$C^{12}O_2^{16}$	0.9842	0.9842
45	$C^{13}O_2^{16}$	1.095×10^{-2}	0.01172
	$C^{12}O^{16}O^{17}$	7.7×10^{-4}	
46	$C^{12}O^{16}O^{18}$	4.025×10^{-3}	0.00403
	$C^{13}O^{16}O^{17}$	8.6×10^{-6}	
	$C^{12}O_2^{17}$	1.5×10^{-7}	
47	$C^{13}O^{16}O^{18}$	4.48×10^{-5}	4.63×10^{-5}
	$C^{12}O^{17}O^{18}$	1.6×10^{-6}	
	$C^{13}O_2^{17}$	1.7×10^{-9}	
48	$C^{12}O_2^{18}$	4.12×10^{-6}	4.13×10^{-6}
	$C^{13}O^{17}O^{18}$	1.8×10^{-8}	
49	$C^{13}O_2^{18}$	4.6×10^{-8}	4.6×10^{-8}
All	All	1.0000	1.0000

[a] Taken to contain 1.10 percent C^{13}, 0.039 percent O^{17} and 0.204 percent O^{18}.

[b] Slight differences between the relative abundances of the masses and the relative intensities of the ion beams may be expected, but the isotope effect in ionization without bond rupture should be much less than that with bond rupture discussed for the case of propane by J. Bigeleisen, J. Chem. Phys. **17**, 334 (1949).

very well expressed by relations linear in the absolute temperature with coefficients of $1/T$ of 12.6 and 15.9, respectively. Differentiating, the temperature coefficients of the fractionation factors for these exchanges are $-12.6/T^2$ and $-15.9/T^2$, or in the ‰ notation, $-1.26\times10^4/T^2$ and $-1.59\times10^4/T^2$.

REMARKS ON NATURAL ABUNDANCES

Aside from one case, the isotopic compositions met with in the following experimental work lie within the range of those found in naturally occurring substances, but this is so merely because the various exchange reactions were studied at the natural abundance level. In the theoretical discussion just given, an assumption regarding the distribution of isotopes among the various carbonate ions was made. As a consequence of this assumption, the fractionation factor α reduced to the equilibrium constant for a reaction, and as a result became independent of actual isotope abundance in the system. Although the problem of measurement would be somewhat simplified if the $O^{18}:O^{16}$ ratio were closer to unity, the same final results would be expected. The methods adopted are such that it would be inconvenient at the present time to work at other than the natural abundance level where large quantities of water are available. As a matter of orientation, it is noted that surveys of isotopic abundances indicate a spread of about 50‰ around average natural abundances of 1.1 percent C^{13}, 0.039 percent O^{17} and 0.204 percent O^{18}.[7–9] In order that the results might be used in connection with the investigation of paleotemperatures, the water used for a large number of the experiments was of marine origin.

[7] G. T. Seaborg and I. Parlman, Rev. Mod. Phys. **20**, 585 (1948).

[8] A. O. Nier and E. A. Gulbranson, J. Am. Chem. Soc. **61**, 697 (1939).

[9] M. Dole and R. L. Slobod, J. Am. Chem. Soc. **62**, 471 (1940).

TABLE IV. Composition of carbon dioxide samples prepared by acid decomposition of carbonates at 25°C.

Preparing acid	Oxygen isotopic composition, ‰ Difference from standard $CaCO_3$ sample A	B	C	Mean difference between preparations A and B	B and C
H_3PO_4 (*ca.* 100 percent)	−3.07	−10.42	−21.15	7.3_6	10.7_8
	−3.27	−10.63	−21.47		
$HClO_4$ (*ca.* 71 percent)	−8.69	−14.33	−25.13	5.8_1	10.5_4
	−9.27	−15.44	−26.74		
HBr aq. (*ca.* 47 percent)	−4.59	−12.27	−24.15	7.5_4	11.9_0
	−4.91	−12.32	−24.23		
H_2SO_4 (*ca.* 98 percent)	−12.19	−18.70	−26.90	5.2_5	8.2_7
	−14.16	−19.51	−27.65		
	−15.19				

MEASUREMENT OF ISOTOPIC DIFFERENCES

The determinations of differences in isotopic compositions were made by a double-collecting Nier-type mass spectrometer tube with gas handling and electronic systems designed for the measurement of small differences.[10,11] The probable error of the difference determination of O^{18} in CO_2 was usually less than 0.05‰ for differences less than 15‰ during stable operation of the instrument as given by the recorder chart, but the reproducibility of a repeated analysis after the gas sample had been completely removed from the gas reservoir on the mass spectrometer and then reintroduced as about 0.15‰, as other effects are introduced in transferring the gas.

PREPARATION OF CARBON DIOXIDE

Considerable difficulty was experienced in obtaining a carbon dioxide from a given calcium carbonate as reproducibly as the mass spectrometer analyzed a given

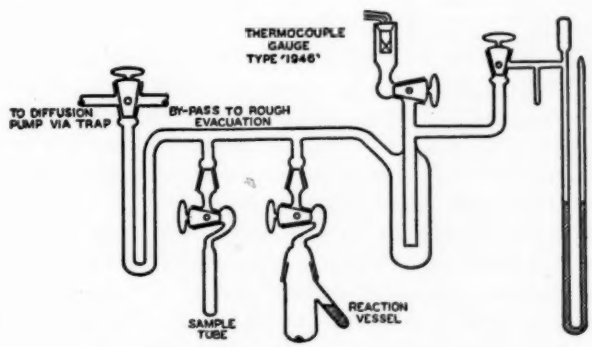

FIG. 1. Gas preparation apparatus.

[10] A. O. Nier, Rev. Sci. Inst. **18**, 398 (1947).

[11] Details of the mass spectrometers will be reported by C. R. McKinney, J. M. McCrea, S. Epstein, H. A. Allen, and H. C. Urey.

TABLE V. Comparison of thermal and acid decomposition.

Sample of $CaCO_3$	Oxygen isotopic composition of CO_2, ‰ Difference from standard: Thermal	Acid (H_3PO_4)	Difference between methods
16/A02-3	−8.7	−2.7	6.0
25/A02-3	−10.3	−3.9	6.4
32/A02-3	−11.5	−4.8	6.7
57/A02-3	−14.0	−8.8	5.2
Average	—	—	6.1

TABLE VI. Precipitated carbonates of the calcium group (25°C)[a].

Precipitating ion	Oxygen isotopic composition ‰ difference from standard: In Florida coast water	In Lake Michigan water
Ca^{++}	-3.1_7	-10.5_3
Sr^{++}	-3.0_5	-10.3_1
Ba^{++}	-3.4_1	-10.6_2

[a] Rapidly precipitated from solution 0.049*M* in Na_2CO_3 and 0.00034*M* in $NaHCO_3$.

gas sample. For a method to be satisfactory, there may be no exchange of oxygen with reagents or vessels. If one-third of the carbonate oxygen is left out of the gas sample, the splitting must occur reproducibly. The gas produced should contain no impurity which could contribute ion beams of the same m/e as carbon dioxide. For this reason ethanol, acetone, and hydrocarbon solvents were kept out of contact with the apparatus, and chloroform and carbon tetrachloride were used as grease solvents. The Apiezon Products' grease "*N*" and wax "*W*" were found satisfactory for use with the gas handling systems. It is difficult to obtain a carbon dioxide which is free of ion beams derived from trace impurities in the mass range 40–55, even after the background of the mass spectrometer is allowed for. The ideal case for a given isotopic composition may be recognized when the relative intensities of the ion beams are those calculated for the theoretical distribution of the isotopes among the possible molecular species. An example of such a distribution is shown in Table III.

THERMAL DECOMPOSITION OF CARBONATE

Since thermal decomposition involves no reagents, several samples of carbon dioxide were prepared by inductively heating a platinum crucible containing calcium carbonate inside a cooled glass chamber. Although essentially quantitative decomposition was found to occur, the isotopic composition of gas obtained from a given carbonate sample showed a large variation. As far as could be seen, this variation was not caused by changes in the decomposition temperature or rate of heating. An effect due to the state of division was noted. The gas obtained by decomposition of fragments of a calcite crystal weighing about 0.1 g each gave differences in isotopic composition from a reference gas in the range −25.5 to −27.3‰, with an average for five samples of −26.5, while powdered samples of the same material gave gas of composition −23.5 to −24.2‰, with an average for six samples of −23.9. In the face of this effect, efforts were made to exchange the oxygen of calcium oxide and carbon dioxide at temperatures around 1000°C, and then to mix up the isotopes by a repeated decomposition and reformation of calcium carbonate. The result of either of these procedures was to effect about 50 percent of the possible exchange in ten minutes, and little more after that. This behavior in isotopic exchange is strikingly parallel to the way in which calcium oxide absorbs carbon dioxide rapidly up to about 50 percent of theoretical, and only very slowly after that. Thus the kinetics of the decomposition of calcium carbonate thermally are such that carbon dioxide can not be obtained with the desired reproducibility of isotopic composition.

ACID DECOMPOSITION OF CARBONATE

Several general conditions must be met by an acid solution which is used to prepare carbon dioxide for mass spectrometer analysis from an alkaline earth carbonate. The salts produced in the decomposition reaction should be soluble in the solution, or a protective coating on the carbonate will slow or stop the reaction. Nitric acid, by decomposition to nitrogen dioxide, yields an intolerable impurity of molecular mass 46, and formic acid must be rejected for similar reasons. In view of the known exchange between water and carbon dioxide, a solution with a low concentration of water is desirable. Of the non-oxy-acids, 47 percent reagent hydrobromic acid seems best suited, while the concentrated oxy-acids perchloric, sulfuric, and phosphoric, when present in excess, dissolve calcium carbonate completely. With an oxy-acid there is the possibility of exchange between the anion and carbon dioxide, and if there is, the acid is unsuited for this purpose. Using portions of three arbitrary calcium carbonates, *A*, *B*, *C*, decomposition using various acids was performed to find out experimentally which were suitable.

The system used for carrying out the decomposition

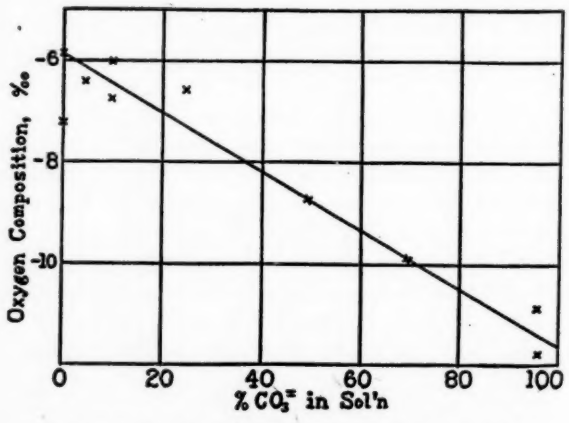

FIG. 2. Isotopic variation of $CaCO_3$ precipitate with solution composition at 25°C.

is shown in Fig. 1. The reaction vessel containing the powdered carbonate (40 to 100 mg) in the main tube and the acid (5 to 10 cc) in the side arm can be evacuated, and then tipped to pour the acid on the carbonate. After the gas is generated (this may take some 30 min. in the case of phosphoric acid), the carbon dioxide is expanded into the rest of the evacuated system, and then condensed into the U-trap with liquid nitrogen cooling. The system is pumped to remove any residue of non-condensible gas. The carbon dioxide is measured in the manometer, and then transferred to a sample tube to be used on the mass spectrometer manifold. By means of the thermocouple gauge, the pressure in the system may be followed, and unless the pressure falls below 10^{-2} mm of Hg on the first condensation and below 10^{-3} on the later ones, the preparation is not considered satisfactory.

The results of the analysis of carbon dioxide samples obtained from the three carbonates mentioned above and four decomposing acids are shown in Table IV. The greater scatter and the reduced differences in the last two columns of the table in the case of sulfuric acid would seem to indicate that an exchange process is taking place. The other acids show a greater reproducibility, and the differences are much the same for all three, although not statistically so. There can be no doubt that different acids give a different product gas from the same carbonate sample. The gas is satisfactorily pure in the required mass range for all four acids. As a matter of interest, some early results using the thermal decomposition method are compared in Table V with those using phosphoric acid decomposition. Again there is a difference in the gas produced from the same carbonate. A difference of about 6‰ has been noticed between the carbon dioxide produced by the action of aqueous hydrochloric acid and that produced by the thermal decomposition method in another case.[9]

Because of its very low vapor pressure, phosphoric acid is rather more readily handled in the vacuum system, and the activity of water in its concentrated solutions is less than that for the other acids mentioned, a state of affairs which is likely to lead to a low exchange rate between the solution and carbon dioxide. To verify that the exchange is small, a tracer 100 percent phosphoric acid was made by dropping water of composition 1.5 percent O^{18} on the appropriate amount of phosphorus pentoxide chilled to liquid nitrogen

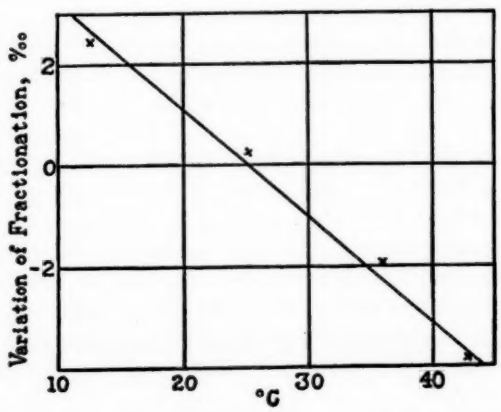

FIG. 3. Temperature variation of oxygen fractionation, $HCO_3^- - H_2O$.

TABLE VII. Isotopic variation of precipitated calcium carbonate with carbonate-bicarbonate composition of solution.

Synthetic concentration[a] $NaHCO_3$	Synthetic concentration[a] Na_2CO_3	Percent $CO_3^=$ in solution	Precipitation Time in thermostat before	Precipitation pH kept above 8.5 during?	Oxygen isotopic analysis, ‰ difference from standard
0.300*M*	0.000*M*	0.0	7 days	No	-5.8_5
			12	Yes	-7.2_6
0.262	0.0125	4.5	7	No	-6.4_1
0.225	0.025	10.0	7	No	-6.0_1
			12	Yes	-6.7_7
0.150	0.050	25.0	5	Yes	-6.5_9
0.075	0.075	50.0	5	Yes	-8.7_2
0.0375	0.0875	69.8	5	No	-9.8_7
			5	Yes	-9.8_8
0.000	0.100	95.6	7	No	-11.7_9
			12	Yes	-10.8_6

[a] Lake Michigan water was used as solvent.

TABLE VIII. Temperature variation of the fractionation of oxygen between bicarbonate and water.

Temperature, °C	Oxygen analysis, ‰ difference from standard	Variation in fractionation, ‰ of 25° value[a]
12±0.5	-2.5_1	$+2.4_0$
25.1	-5.7_0	$+0.2_0$
36.0	-7.8_3	-1.9_4
42.9	-9.6_8	-3.8_0

[a] 25° value as found by least squares.

TABLE IX. Temperature variation of isotopic composition of carbonate dissolved in water.

Temp. °C	Days in thermostat	Oxygen analysis ‰ difference from standard	Percent $CO_3^=$	Hydrolysis correction ‰	Variation ‰ of 25° value
Precipitation of $CO_3^=$ as $CaCO_3$ from a solution in water from South District Waterworks, Chicago, Illinois, August, 1948 0.0485*M* in Na_2CO_3 and 0.00034*M* in $NaHCO_3$					
14	8	-9.5_4	$95._0$	-0.3_2	$+1.5_1$
25.1	8	-10.9_3	$93._2$	-0.4_0	$+0.0_3$
36.2	7	-12.4_6	$91._0$	-0.4_7	-1.5_8
44.4	7	-13.6_8	$89._2$	-0.5_2	-2.8_4
Precipitation of $CO_3^=$ as $CaCO_3$ from a solution in Monterey Bay water collected at Pacific Grove, California, June, 1947 0.0738*M* in Na_2CO_3 and 0.00074*M* in $NaHCO_3$					
16.2	6.5	-3.1_2	$95._4$	-0.2_9	$+0.9_5$
16.2	8.5	-2.7_5			
25.9	6.5	-3.3_5	$94._2$	-0.3_4	$+0.1_7$
25.9	8.5	-3.9_6			
31.8	6.5	-4.4_7	$93._2$	-0.3_7	-0.8_8
31.8	8.5	-4.8_6			
57.0	6.5	-7.8_6	$87._8$	-0.5_0	-4.7_0
57.0	8.5	-8.8_4			

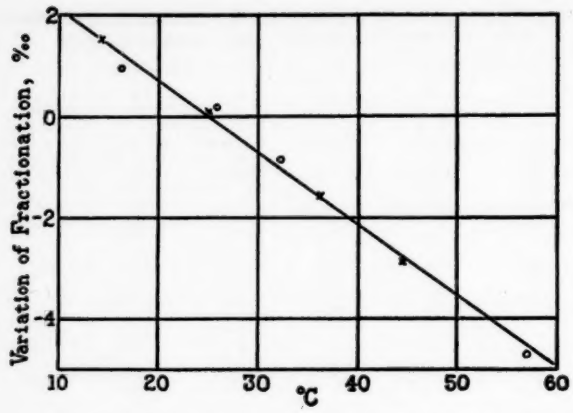

FIG. 4. Temperature variation of oxygen fractionation, $CO_3^{=}-H_2O$ (x–Lake Michigan water series; o–Monterey Bay water series).

temperatures. This acid, with an isotopic composition of 0.70 percent O^{18} or 3400‰ greater than normal oxygen, produced a carbon dioxide only 8.5‰ richer in O^{18} than that produced using normal acid. The amount of isotope mixing is then 0.0025 of the maximum possible, and any exchange effects are negligible in the decomposition of natural carbonates with an unenriched phosphoric acid.

There was no observed evolution of heat in the decomposition, and the composition of the gas is only slightly, perhaps not even significantly, altered by the temperature at the start of the reaction. Using samples of a given powdering of a calcium carbonate shell, gas samples gave check analyses of 1.09 and 1.01‰ in the case of decomposition at 14°C, 1.00 and 0.95‰ at 25°C, and 0.43 and 0.43‰ at 37°C. A variation of concentration of the phosphoric acid between 85 and 100 percent is accompanied by a similar slight variation in the isotopic composition of the gas produced. The acid decompositions in the following investigation were performed at 25°C with a phosphoric acid of specific gravity 1.80 (95 percent H_3PO_4), made by adding phosphorus pentoxide to the usual 85 percent acid. As a result of impurities which char in commercially available grades of phosphorus pentoxide, the resulting solution has a brownish tinge, but it performs the decomposition of the carbonates reproducibly to 0.1‰ as is illustrated by the three sets of duplicate determinations just mentioned.

PRECIPITATION OF CARBONATE AND BICARBONATE

In all but highly alkaline solutions, tracer experiments have shown that carbonate and water exchange by a hydrolysis of carbonate to bicarbonate, carbonic acid and dissolved carbon dioxide. The exchanging steps take place among carbonic acid, water and carbon dioxide and among carbon dioxide, bicarbonate, and hydroxide. At 25°C, the half-time of the reaction is 28 hr. at *p*H 11, and decreases with decreasing *p*H.[12]

[12] G. A. Mills and H. C. Urey, J. Am. Chem. Soc. **62**, 1019 (1940).

If there is no exchange between solid calcium carbonate and water, a brief consideration of the ionization relationships in an aqueous carbonate-bicarbonate system shows that the rapid precipitation of calcium carbonate from such a solution and subsequent examination of carbon dioxide produced from the carbonate gives a means of studying the oxygen isotopic equilibria in the system. Using the rough values of $10^{-6.5}$ and $10^{-10.5}$ for the first and second ionization constants of carbonic acid and 10^{-8} for the solubility product of calcium carbonate, the concentrations of carbonate, bicarbonate, and carbon dioxide are given by $[CO_3^{=}]=10^{-5}$, $[HCO_3^{-}] = 10^{5.5}[H^+]$ and $[H_2CO_3 + CO_2 \text{ aq.}] = 10^{12}[H^+]^2$ when the calcium concentration is $10^{-3}M$. If the *p*H of the solution is maintained greater than nine during precipitation, less than one percent of the carbon of a carbonate-bicarbonate solution of greater han $0.1M$ concentration will escape precipitation. As a result of the marked increase in solubility of calcium carbonate with ionic strength, a somewhat larger excess of calcium is required to effect the same completeness of precipitation in a solution of marine salinity.[13]

Calcium carbonate samples were prepared from aqueous carbonate-bicarbonate solutions by precipitation. When the precipitation was carried out in the temperature range 15 to 60°C, rapidly coagulating precipitates were obtained, while outside that range gelatinous ones were formed. It was found that the isotopic composition of the coagulating precipitates formed under the same concentration and equilibration temperature conditions differed at the most by 0.5‰, while variations of 5‰ were met with in the case of the gelatinous form. The solutions from which the carbonate and bicarbonate were precipitated were made up in natural waters treated to remove alkaline earth ions without changing the oxygen isotopic composition. This was usually done by precipitating these ions as carbonates, as a complete distillation of marine waters from the salt residue is less convenient. The details of concentration and time of thermostatting before precipitation of carbonate and bicarbonate in the form of calcium carbonate on the addition of excess $3M$ calcium chloride solution are given in subsequent tables. The precipitate was separated by filtration, washed, and dried in air or in a vacuum dessicator. As no variation in isotopic composition was observed as a result of variation in the time of filtration, washing, and drying, the coagulated precipitate does not exchange rapidly with air or water.

The method of removing the alkaline earth ions from water by precipitation usually leaves the carbonate-bicarbonate solution made up in the water supersaturated with respect to calcium carbonate, and this may be slowly deposited during the thermostatting period as a thin white encrustation on the walls of the

[13] Sverdrup, Johnson, and Fleming, *The Oceans, Their Physics, Chemistry and General Biology* (Prentice-Hall, Inc., New York, 1946), pp. 192–210.

containing vessel. In one case there was sufficient deposit to compare the isotopic composition of this crust with the precipitate from the calcium chloride addition, and the former was $2.9_0‰$ richer in C^{13} and $5.8_8‰$ richer in O^{18}. At 32°C, this is of the order of the estimate of the fractionation between carbonate ion in solution and calcium carbonate, and offers immediate explanation of the wide variability of the gelatinous precipitates. When first formed, the calcium carbonate has the same isotopic composition as the ion in solution, but if the solid is built up very slowly, there is time for each layer to reach the equilibrium between the solid state and the solution. With coagulating precipitates, the build-up of solid is so fast that the composition of the solution is maintained, with the encrustation it is so slow that the bulk has an isotopic composition which is in equilibrium with the water, and with the gelatinous precipitate it is slow enough to allow partial exchange, giving an erratic isotopic composition. As is shown by the results of Table VI, if calcium, strontium, and barium carbonates are precipitated in coagulating form under the same conditions of temperature and concentration, all yield a carbon dioxide of the same isotopic composition. By far the most likely set of conditions to give these results is that the isotopic composition of the three carbonates is the same, and that there is no difference in the acid decomposition process with a change of metal ion in the carbonate.

Although the results listed in Table VII and graphed in Fig. 2 are not as consistent as might be desired, they show a linear variation of the isotopic composition of the precipitate with the proportion of carbonate in the carbonate and bicarbonate of the aqueous solution, and establish that the isotopic composition of the fast-formed precipitate is the average of the oxygen present in the carbonate and bicarbonate at the time of precipitation. In the calculation of the ionic composition of the solutions from their stoichiometry, it is necessary to use the infinite dilution values of the ionization constants of water and bicarbonate, as activity data are lacking at these concentrations.[14] The least-squares solution of the results gives $5.7_4‰$ as the fractionation between carbonate and bicarbonate at 25°C, and a different series of precipitations gave $6.3_7‰$. The value of $5.9‰$ is used to make hydrolysis corrections to later data on the carbonate-water exchange.

The results on the temperature variation of the bicarbonate-water fractionation shown in Table VIII and Fig. 3 are not extensive enough to justify any but a linear composition-temperature relationship, and the least-squares value of the temperature coefficient is $-0.19_7‰$ per °C. The water used for these solutions was laboratory distilled water, and no particular significance can be attached to the constant term in the equation.

[14] H. S. Harned and B. B. Owen, *The Physical Chemistry of Electrolytic Solutions* (Reinhold Publishing Corporation, New York, 1943), p. 492.

Two series of experiments showing the temperature variation of the carbonate-water fractionation are listed in Table IX. A correction for the varying hydrolysis of carbonate with temperature has been made using the results for the bicarbonate just mentioned and the carbonate-bicarbonate fractionation data. By expressing the results relative to 25°C, both series of experiments may be shown in a single graphical representation as in Fig. 4. A least-squares analysis linear in the temperature gives slopes of $-0.142_0‰$ per °C and $-0.143_1‰$ per °C, and a difference of $7.1_9‰$ in O^{18} content between the samples of water from Monterey Bay and Lake Michigan. Expressing the slopes in terms of ‰ of the 25°C value, -0.143_6 and -0.143_8 are obtained. This agreement is much better than is statistically called for, and the uncertainty of the degree of hydrolysis renders the value $-0.144‰$ per °C less reliable than would be indicated statistically. The calculated value at 31.5°C, the mean temperature of the experiments, is $-0.135‰$ per °C, and the agreement between the two numbers is considered good.

SLOW FORMATION OF CARBONATE SOLIDS

The way in which an encrustation of an alkaline earth carbonate can be slowly laid down on the walls of a vessel containing the appropriate bicarbonate solution as carbon dioxide is gradually removed is much more comparable to the manner of growth of a carbonate shell than is the precipitation process just discussed. As will be found experimentally, the temperature coefficient for this type of deposit, which represents solid-state equilibrium conditions, should be different from that for the ion. A suitable bicarbonate solution may be made by taking a slight excess of the carbonate powder (1.5 g/l of water for calcium, strontium or

TABLE X. Temperature variation of the composition of slowly formed calcium carbonate.

Temperature °C	O^{18} Analysis, ‰ difference from standard — Various preparations					Average
	Formed from a bicarbonate solution in Florida water					
−1.2	4.1_7	3.6_3				3.9_0
+6.9	1.7_3	2.0_1	1.9_2			1.8_9
13.6	1.1_7	1.6_5	0.3_1	0.5_7		0.9_2
19.9	-0.3_7	-0.1_0	-0.5_9	-0.4_6		-0.3_3
25.1	-1.9_5	-1.2_4	-1.5_8			-1.5_9
31.8	-1.6_8	-2.8_2	-2.5_7	-2.6_4		-2.4_3
	Formed from a bicarbonate solution in Cape Cod water					
+3.8	1.5_0	2.1_9				1.8_4
7.3	0.9_9	1.9_1	1.4_3	0.6_0	1.2_6	1.4_2
	1.8_7	1.8_6				
13.6	0.0_8	-0.4_5	-0.1_0	-0.5_6	-0.5_9	-0.3_2
18.0	-1.3_1	-0.8_5	-0.7_6	-1.3_2	-1.2_0	-1.0_9
	-1.1_1					
25.0	-2.9_8	-2.9_4	-3.5_8	-3.3_5	-2.9_1	-3.0_2
	-3.0_3	-2.9_1	-2.7_7	-2.5_3	-2.6_7	
	-2.7_8	-2.2_4	-3.4_6	-3.5_9	-3.5_6	
31.9	-3.9_8	-4.1_0				-4.0_4
45.8	-5.7_0	-5.8_9	-5.7_8			-5.7_9
59.8	-8.1_0	-8.2_1	-7.7_0			-8.0_0
79.8	-11.1_8	-11.1_1	-11.0_8	-10.9_2		-11.0_7

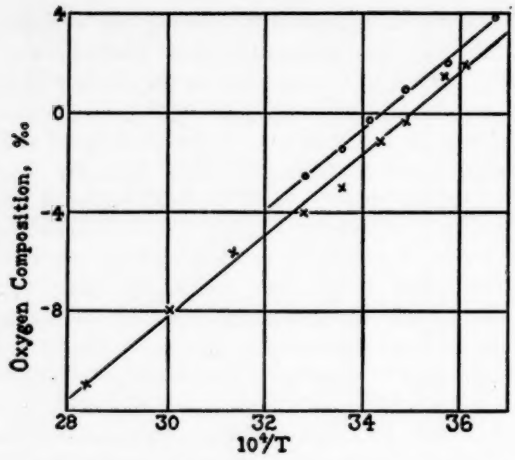

FIG. 5. Variation of isotopic composition of $CaCO_3(s)$ with reciprocal of deposition temperature from H_2O (x–Cape Cod series; o–Florida water series).

barium, 15 g/l for magnesium) and adding the desired water; then, if a partial pressure of an atmosphere of carbon dioxide is maintained over the solution while the latter is well shaken, a large part of the powder will be dissolved, and after filtration, the solution may be stored in bulk for long periods if cool and well-stoppered.

About 200 cc of this solution is placed in a round-bottom flask maintained at constant temperature and the carbon dioxide is gradually removed, either by diffusion alone, or by a finely dispersed stream of nitrogen previously saturated by passage through water of the same isotopic composition as the solution. In from 5 to 24 hr. a white encrustration forms on the walls of the vessel and, in the case of nitrogen sweeping, on the dispersing jet also. If the structure of the deposit is to be determined by x-ray, a powder may be obtained by scraping the walls. Otherwise a flask with a ground joint and acid-holding side arm is used. The deposit on the disperser may be examined microscopically, and if dense enough can provide a gas sample as well.

The x-ray analyses of the samples showed either nearly pure aragonite or an approximately equal mixture of calcite and aragonite. Microscopically, the deposits were confused aggregates of crystalline matter, occasionally showing isolated crystals of good geometry. There was a tendency to form smaller crystals at lower temperatures.

Two waters were used for the bulk of the encrustation experiments, one collected near Palm Beach, Florida, in September, 1948, and the other near East Orleans, Massachusetts, on the Atlantic side of Cape Cod, during a rainy period in December, 1948. The respective salinities of 36.7 and 32.2‰ make it not surprising that there is a difference in the oxygen composition of the calcium carbonate obtained from the two waters at the same temperature. The average difference of the carbonates is 1.1_4‰ and a few subsidiary experiments measuring this difference in composition by allowing carbon dioxide to come to equilibrium directly with excess of the waters gave a larger value of 1.6_0.

As successive calcium carbonate deposits formed from the same stock solution at the same temperature showed a spread of as much as 1‰, considerable attention was focussed on possible variations in the deposition process. No relationship was observed between composition and crystal structure, seeded or spontaneous crystallization, time before crystallization, or the method of removing carbon dioxide from the bicarbonate solution. Only the coarsest estimate of the rate of deposition can be made under these conditions, but it appears that the variation is not correlated to this either. The situation is unsatisfactory, in that a set of four determinations may show a spread of only 0.3 ‰ while another set yields a spread of 1‰ or more, and the variability inherent in the chemical manipulations as performed is somewhat more than four times that arising from the mass spectrometer determinations. The other calcium group carbonates precipitated by this method gave results not significantly different from those for calcium carbonate at 25°C. Ionic strength also gave no significant effect on the composition of the carbonate in solutions up to $3M$ in sodium chloride.

The results showing the variation of the isotopic composition with temperature are listed in Table X. As may be seen in Fig. 5, the variation is well expressed by a relation linear in the reciprocal of the absolute temperature. Least-squares relations for the Florida and Cape Cod waters, respectively, are

$$\Delta O^{18} = 1.57_9 \times 10^4/T - 54.2_7$$

and

$$\Delta O^{18} = 1.64_8 \times 10^4/T - 57.6_4.$$

If the values given by these relations are compared in the middle of the temperature range of the experiments, say at 295°K, the figure 1.1_4‰ is obtained as the difference in isotopic composition of the waters. This may then be subtracted from the Florida results, and a repetition of the least-squares process gives

$$\Delta O^{18} = 1.62_0 \times 10^4/T - 56._{75},$$

as the relation embodying all data and giving the composition of the carbon dioxide produced by phosphoric acid decomposition of calcium carbonate laid down from Cape Cod water in terms of the deposition temperature. The average deviation of an individual result from the relation is 0.38‰. Where both a wall and a disperser sample from the same preparation were available, each was given a weight of two-thirds as compared to unity for a single sample for a given preparation. The value 1.62×10^4 is the coefficient of $1/T$ in the relation for the variation of the fractionation when the fractionation is expressed in ‰ of the fractionation at 286.5°K, the temperature at which $\Delta O^{18} = 0$. The corresponding calculated value is 1.56×10^4, and the agreement is considered to be as good or better than the theoretical soundness of the calculation.

THE CARBONATE PALEOTEMPERATURE SCALE

If a value 0.75‰ heavier in O^{18} than Cape Cod water is tentatively taken for the mean ocean, the temperature-composition relationship for the slowly formed carbonate may be given as

$$t = 16.0 - 5.1_7\Delta O^{18} + 0.09_2(\Delta O^{18})^2,$$

where t is the temperature in °C.[15] This result may be compared with the line drawn on the plot of preliminary data for natural samples of biological origin.[3] When it is taken into account that the reference gas in use at that time was −0.95‰ different from the standard, the line corresponds to a linear equation

$$t = 18 - 5.4_4\ \Delta O^{18}.$$

Both these equations give the same result for the temperature difference between two marine carbonates in terms of O^{18} content to better than one degree in the range 0 to 35°C. Individual temperatures, dependent on local isotopic composition, are uncertain until the latter has been determined, and if it is $(A+0.75)$ ‰ greater than that of Cape Cod water, then

$$t = 16.0 - 5.1_7(\Delta O^{18} - A) + 0.09_2(\Delta O^{18} - A)^2.$$

The average deviation of an individual experimental result from this relation is 2°C in the series of slow precipitations just described.

SUMMARY FOR THE FRACTIONATIONS CONSIDERED

In these experiments, only the temperature variation of the fractionation between the carbonates and water has been measured, while the fractionation has not been measured. The heat of reaction may be calculated readily by expressing the fractionation factor in the form

$$\alpha = K = K_t[1 + 0.001f(T)]$$

as $RT^2\dfrac{d\ln K}{dT}$ becomes $\dfrac{0.001RT^2}{1+0.001f(T)}\cdot\dfrac{df(T)}{dT}$.

Numerical values are given in Table XI. The fractionation between aqueous carbonate and bicarbonate at 25° was found to be 5.9‰.

TABLE XI. Calculated and experimental results at 25°C.

Exchange of O^{18} between	Calculated fractionation factor	Temperature coefficient ‰ per °C Calc.	Exp.	Heat of reaction cal. per gram atom exchange
$CO_3^=$(aq.) − H_2O(l)	1.014	−0.140	−0.144	25.4
Calcite − H_2O(l)	1.021	−0.175	−0.183	32.4
HCO_3^-(aq.) − H_2O(l)	—	—	−0.197	34.8

[15] An investigation of the isotopic composition of the ocean is being carried out by S. Epstein, L. Dean, and H. C. Urey, and the value 0.75‰ is only an estimate based on the Cape Cod and Florida waters and a possible linear relation between salinity and composition.

CONCLUSION

In the experiments just described, the temperature dependence of the fractionation of oxygen in carbonate-water systems has been studied in considerable detail. The results have compared on the whole satisfactorily with theoretical calculations. The isotopic composition of calcium carbonate slowly formed from aqueous solution has been noted to be usually the same as that produced by organisms at the same temperature. As a result a relation giving the growth temperature in terms of isotopic composition has been obtained, and with certain restrictions it may be used to determine paleotemperatures. In the course of the work, further interesting features of the chemistry of oxygen isotopes in reactions involving carbonates have been observed.

The writer is indebted to Dr. L. R. Blinks of the Hopkins Marine Station, Pacific Grove, California, for the Monterey Bay water, and to Dr. H. A. Lowenstam of the Department of Geology, University of Chicago, for the water from Florida. The x-ray determinations were made through the kindness of Mr. D. F. Clifton of the Institute for the Study of Metals, University of Chicago. As a result of a discussion with Dr. J. E. Mayer, the preliminary treatment of the solution-crystal fractionation was much improved. The development of the mass spectrometers for this work was made possible through aid in the form of a grant from the Geological Society of America. The writer is very fortunate in having had available the facilities of the Institute for Nuclear Studies, and thanks the Institute and the University of Chicago for fellowship aid. Deepest appreciation goes to his laboratory companions, Mr. C. R. McKinney and Dr. S. Epstein, for cooperation and helpful suggestions throughout the course of the work. This interesting problem fundamental to the study of paleoclimatology was suggested by Dr. H. C. Urey, whose deep and continued interest in its progress was a determining factor in its successful completion.

APPENDIX

At the time this work was done, it appeared that there was an inconsistency between the reports of loss of C^{14} activity in precipitated barium carbonate and the lack of any appreciable exchange of carbonate oxygen observed, as any mechanism which leads to the exchange of carbon must also lead to oxygen exchange, although the converse is not necessarily true. An article published during the preparation of the manuscript, reporting in rather more detail experiments on the carbon exchange, gives a picture which is quite in accord with the results on oxygen exchange.[16] The nature of the carbonate precipitate in filtration was directly correlated to the C^{14} exchange with carbon dioxide in a moist atmosphere, and it was also noted that barium carbonate and aqueous carbonate did not show any carbon exchange in one week.

The lack of phosphorous exchange between phosphate and phosphite likewise is a necessary but not a sufficient condition for the lack of oxygen exchange in the phosphoric acid decomposition process.[17]

[16] G. Samos, Science **110**, 663 (1949).

[17] Ionin, Lukovnihov, Neimen, and Nesmeyanov, Doklady Akad. Naul. S.S.S.R. **67**, 463 (1949), abstracted in Chem. Abs. **43**, 7815a (1949).

Thermodynamics and the Canonical Distribution

R. EISENSCHITZ
Queen Mary College, University of London, London, England
(Received January 30, 1950)

The hypothesis is made that the thermodynamic energy and the virtual work done in a reversible process are statistical averages of the corresponding mechanical quantities and that the averages comply with the laws of thermodynamics. These assumptions are shown to be sufficient for deriving the canonical distribution so far as the distribution on the energy scale is concerned.

PREMISSES AND DEFINITIONS

IN this note the attempt is made to derive the canonical distribution function from assumptions that are less stringent than those usually made.

It is assumed that the system under consideration is described in terms of a mechanical model which is specified by an energy given as a function of the coordinates and momenta (q, p) and of external coordinates (X). At first the validity of classical mechanics is postulated.

The hypothesis is made that there is a non-negative distribution function such that the thermodynamical energy (U) and the virtual work $(P_X \cdot \delta X)$ are the mean values of the corresponding mechanical quantities. Denoting the distribution function by $f(p, q, X, \tau)$ where $\tau = 1/kT$ and the energy by $H(p, q, X)$ this means that

$$U = (1/Z)\int \cdots \int H f dq dp, \tag{1}$$

$$P_X \cdot \delta X = -(1/Z)\left\{\int \cdots \int (\partial H/\partial X) f dq dp\right\} \cdot \delta X, \tag{2}$$

$$Z = \int \cdots \int f dp dq, \tag{3}$$

where the integrals are extended over the whole phase space. P_X is here the generalized force. Denoting the Helmholtz free energy by F the distribution function is conveniently normalized in such a way that

$$Z = \exp(-\tau F). \tag{4}$$

The general thermodynamic relations have then the form

$$U = -\partial(\log Z)/\partial\tau, \tag{5}$$

$$P_X = \partial(\log Z)/\tau\partial X. \tag{6}$$

Let ϵ be the value of the energy $(\epsilon \geq 0)$, and the phase volume be defined as

$$W(\epsilon, X) = \int \cdots \int_{H(p, q, X) \leqslant \epsilon} dp dq.$$

By solving the equation

$$W(\epsilon, X) = \omega$$

the energy is obtained as a function of the phase volume

$$\epsilon = E(\omega, X).$$

The distribution function f may in principle vary at constant energy; the probability distribution on the energy scale is then obtained by integration, so that the probability for finding the system at the energy ϵ or less is given by

$$(1/Z) \cdot r(\tau, X, \epsilon) = (1/Z) \cdot R(\tau, X, \omega)$$

$$= (1/Z)\int \cdots \int_{H(p, q, X) \leqslant \epsilon} f dp dq \tag{7}$$

and the probability for finding it between ϵ and $\epsilon + d\epsilon$ is equal to

$$(1/Z)(\partial r/\partial\epsilon)d\epsilon = (1/Z)(\partial R/\partial\omega)d\omega.$$

THE THERMODYNAMIC CONDITIONS

The derivation of thermodynamic quantities does not require the complete distribution function but only the distribution in energy. Obviously

$$Z = \int_0^\infty (\partial R/\partial\omega)d\omega = \int_0^\infty (\partial r/\partial\epsilon)d\epsilon \tag{3a}$$

$$U = (1/Z)\int_0^\infty E \cdot (\partial R/\partial\omega)d\omega = (1/Z)\int_0^\infty (\partial r/\partial\epsilon)\epsilon d\epsilon. \tag{1a}$$

In order to show that the distribution in energy determines the generalized force, the integrand of (2) is transformed

$$(\partial H/\partial X) \cdot f = [\partial(Hf)/\partial X] - H \cdot (\partial f/\partial X).$$

The right-hand side is, apart from f or $\partial\rho/\partial X$, constant at constant energy thus admitting integration at constant energy

$$\left[(\partial/\partial X)\int \cdots \int H f dp dq\right] - \int \cdots \int (\partial f/\partial X) H dp dq$$

$$= \left[(\partial/\partial X)\int_0^\infty (\partial R/\partial\omega) E d\omega\right] - \int_0^\infty (\partial^2 R/\partial\omega\partial X) E d\omega$$

This difference is equal to

$$\int_0^\infty (\partial E/\partial X)(\partial R/\partial\omega)d\omega = -\int_0^\infty [(\partial W/\partial X)/(\partial W/\partial\epsilon)](\partial r/\partial\epsilon)d\epsilon.$$

It follows that

$$P_X = -(1/Z)\int_0^\infty (\partial E/\partial X)(\partial R/\partial\omega)d\omega \qquad (2a)$$

is in fact determined by the function $R(\tau, X, \omega)$.

In order to comply with the laws of thermodynamics the distribution functions r or R have to satisfy the Eqs.

$$\int_0^\infty [(\partial r/\partial\epsilon)\epsilon + (\partial^2 r/\partial\epsilon\partial\tau)]d\epsilon = 0 \qquad (8)$$

$$\int_0^\infty [(\partial E/\partial X)(\partial R/\partial\omega) + (1/\tau)\{\partial^2 R/\partial\omega\partial X\}]d\omega = 0 \qquad (9)$$

which are derived from (1a), (3a), (5) and (2a), (3a), (6), (7) respectively.

THE EXPONENTIAL FACTOR

In every material system the thermodynamic functions are proportional to the number of constituents if this number is large enough. The distribution function in energy may therefore be replaced by the distribution function appropriate to a large number of independent constituents provided that the latter are of macroscopic magnitude. (The case of transition points or other thermodynamic singularities is not covered by this assertion or the subsequent arguments.)

In a system consisting of a large number of independent, macroscopic constituents the distribution function on the energy scale is necessarily a normal distribution

$$\partial r/\partial\epsilon = (Z/\Delta(2\pi)^{\frac{1}{2}})\cdot\exp[-(\epsilon-U)^2/2\Delta^2], \qquad (10)$$

where Z, U, $\Delta = (\langle\epsilon^2\rangle - U^2)^{\frac{1}{2}}$ are functions of τ and X. Let N be the number of independent constituents and U_0, Δ_0 be the quantities corresponding to one constituent; then $U = NU_0$, $\Delta = N^{\frac{1}{2}}\Delta_0$.

Expressing the integrand of (8) in terms of (10)

$$(\partial^2 r/\partial\epsilon\partial\tau) + (\epsilon\partial r/\partial\epsilon) = (\partial r/\partial\epsilon)[\{(\epsilon-U)[(\partial U/\partial\tau)+\Delta^2]/\Delta^2\} + \langle\{[(\epsilon-U)/\Delta^2]-1\}(\partial\log\Delta/\partial\tau)\rangle]$$

it is seen that every term on the left-hand side is proportional to N whereas the corresponding terms on the right-hand side have canceled and the remaining terms are proportional to $N^{\frac{1}{2}}$, N^0. Solving this equation in terms of an expansion in powers of $1/N$ it follows that

$$\partial r/\partial\epsilon = \exp(-\epsilon\tau)\cdot[\partial g(\epsilon, X)/\partial\epsilon] + 0(N^{-1}), \qquad (11)$$

where $g(\epsilon, X)$ is an undetermined non-negative function of ϵ and X.

The integrand of (9) can be transformed:

$$\partial^2 R/\partial\omega\partial X = (\partial^2 r/\partial\epsilon\partial X) + (\partial E/\partial X)(\partial^2 r/\partial\epsilon^2).$$

The external coordinates are considered as defined for every constituent (X_0); the external coordinates corresponding to the whole system are equal to their sum.

Expressing $\partial E/\partial X$ as a function of the energy

$$\partial E/\partial X = \chi(\epsilon), \quad \partial E_0/\partial X_0 = \chi_0(\epsilon)$$

it follows that

$$\langle\chi(\epsilon)\rangle = \langle\chi_0(\epsilon)\rangle.$$

Taking account of the fact that a variation of the energy of the system is equal to N times the variation of the energy of a constituent it follows that

$$\langle(\partial\chi/\partial\epsilon)\rangle = \langle(\partial\chi_0/\partial\epsilon)\rangle/N,$$
$$\langle(\partial^2\chi/\partial\epsilon^2)\rangle = \langle(\partial^2\chi_0/\partial\epsilon^2)\rangle/N^2.$$

Expanding χ in the neighborhood of $\epsilon = U$

$$\chi = \alpha + \beta(\epsilon-U) + \gamma(\epsilon-U)^2$$

it follows that

$$\langle\chi\rangle = \alpha+\gamma\Delta^2, \quad \langle(\partial\chi/\partial\epsilon)\rangle = \beta, \quad \tfrac{1}{2}\langle(\partial^2\chi/\partial\epsilon^2)\rangle = \gamma$$

and α, β, γ are seen to be proportional to N^0, N^{-1}, N^{-2} and

$$|\chi(\epsilon)-\chi(U)| \le |\beta\Delta| + |\gamma\Delta^2| = N^{-\frac{1}{2}}\beta_0\Delta_0 + 0(N^{-\frac{1}{2}})$$

and α is equal to $-P_X$.

Expressing the integrand of (9) in terms of (10)

$$(\partial^2 R/\partial\omega\partial X) + [\tau(\partial E/\partial X)(\partial R/\partial\omega)] = (\partial r/\partial\epsilon)[\{(\epsilon-U)[(\partial U/\partial X)-\alpha]/\Delta^2\} + 0(N^{-\frac{1}{2}})]$$

an argument similar to that as applied to the integrand of (8) shows that

$$\partial R/\partial\omega = \exp(-E\tau)\cdot[\partial D(\omega)/\partial\omega] + 0(N^{-\frac{1}{2}}) \qquad (12)$$

and

$$\partial g(\epsilon, X)/\partial\epsilon = \partial D(\omega)/\partial\omega, \quad \partial D/\partial X = 0. \qquad (13)$$

Owing to the small magnitude of Δ, the upper limit of integration in (3a) may be taken as U and it can be shown that this leads to

$$Z = \exp(-\tau U)\cdot J,$$

where the "weight function" J is equal to $D(\omega)$. According to the thermodynamic relation between the entropy (S) and Z it follows that

$$S = k\cdot(\log J) \qquad (14)$$

and is accordingly a function of the phase volume independent of the external coordinates.

Equation (14) yields a partial determination of thermodynamic quantities from the mechanical model without knowledge of the functional relation between J and W. Any adiabatic change of X leaves S constant

so that the adiabatic $X-U$-relation as determined by

$$S(U, X)=\text{const}$$

is the same as the relation between X and ϵ as derived from

$$W(\epsilon, X)=\text{const}$$

which is a consequence derived from the mechanical model.

STATISTICAL QUANTUM MECHANICS

In quantum mechanics there is no non-negative distribution function f but, regarding the distribution in energy, the requirements of quantum mechanics are met by letting ϵ and ω assume discrete values only. The discrete points of the distribution function approach with increasing N a continuous curve given by (10) so that Eqs. (10), (12), (13), (14) remain valid, even at the lowest temperatures. There is accordingly a temperature range with almost certainty for finding the system in the ground state. This range may be varied by variation of the external coordinates and may in principle be shifted to arbitrarily high temperatures. In this range $\omega=1$ and the convention is made that $D(1)=1$.

THE WEIGHT FUNCTION

Let in a system such as previously specified the relation between weight function and phase volume of a constituent be expressed by

$$J_0=D(W_0). \tag{15}$$

If the external coordinates are equal in all constituents

$$J=J_0{}^N, \quad W=W_0{}^N. \tag{16}$$

If by variation of the external coordinates the energy levels of $N-1$ constituents are shifted to sufficiently high values, then

$$J=J_0, \quad W=W_0 \tag{17}$$

and this variation of the external coordinates does not affect the functional relation between J and W. It follows from (15) and (17) that

$$J=D(W) \tag{18}$$

and from (16) and (18) that

$$J=D(W_0{}^N) \tag{19}$$

whereas according to (15) and (16)

$$J=[D(W_0)]^N. \tag{20}$$

Equations (19) and (20) are incompatible unless

$$J=W^a, \tag{21}$$

where a is any positive constant, determining the units of temperature and entropy according to

$$S=ka\cdot(\log W).$$

Usually it is taken that $a=1$. With a suitable choice of a calculated thermodynamical quantities must agree with experiment unless the premisses as laid down at the beginning of this note are wrong. It follows that these premisses are sufficient for determining the distribution function on the energy scale in accordance with the current theory. The possible variation of probability at constant energy is, from this point of view, to be regarded as unknown rather then assumed to be necessarily zero.

Absolute Intensities of Characteristic Infra-Red Absorption Bands of Aliphatic Hydrocarbons

S. A. FRANCIS
Beacon Laboratories of The Texas Company, Beacon, New York

(Received February 17, 1950)

Integrated intensities of the 2900, 1460, and 1370 cm^{-1} infra-red absorption bands have been measured for twelve aliphatic hydrocarbons. The results are interpreted on the basis that the hydrocarbon molecule behaves like a non-interacting mixture of $-CH_3$, $\diagdown CH_2 \diagup$ and $-CH \diagup\diagdown$ structural groups. The unit structural group intensities are 4.41×10^{-7}, 3.81×10^{-7}, and 1.39×10^{-7} cm^2/(molecule second) for the CH_3, CH_2 and CH groups respectively in the 2900 cm^{-1} band; 0.544×10^{-7} and 0.232×10^{-7} for the CH_3 and CH_2 groups in the 1460 cm^{-1} band; and 0.394×10^{-7} for the CH_3 group in the 1370 cm^{-1} band. Values calculated for the CH bond dipole moment divided by the equilibrium CH bond length vary from approximately 0.2×10^{-18} to 0.4×10^{-18} c.g.s. units. Values of approximately -0.75×10^{-10} are obtained for the change in CH bond dipole moment with change in CH bond length.

THE nature of the vibrations which give rise to the infra-red absorption of aliphatic hydrocarbons in the regions 2850–3000 cm^{-1}, 1450–1500 cm^{-1}, and 1350–1420 cm^{-1} are fairly well established on the basis of the vibrational assignments for simple molecules and of the comparative examination of the spectra of a large number of more complex molecules. The group of bands in the region 2850–3000 cm^{-1} are produced by vibrational modes which consist mainly of CH bond stretching motions;[1] those in the regions 1450–1500 cm^{-1} and 1350–1420 cm^{-1} to modes which consist mainly of H−C−H angle deformations.[2] Table I gives the nature of the vibrational motions and the approximate positions of the corresponding infra-red absorption bands in these three spectral regions. Deviations from the spectral positions assigned in Table I of more than 20 cm^{-1} are seldom observed for aliphatic hydrocarbons. Hence, to this order of approximation the spectrum of an aliphatic hydrocarbon in these three regions appears as if it were produced by a non-interacting mixture of CH_3, CH_2, and CH structural units; that is, structural units consisting of primary, secondary, and tertiary carbon atoms, each with three, two, and one attached hydrogen atoms respectively.

That this picture is only approximately correct is indicated by differences in the band shapes of isomers and by the splitting of the 1370 cm^{-1} band when more than one methyl group is attached to the same carbon atom.

The present work was undertaken to determine whether the intensities of the bands in these three spectral regions could be interpreted on the basis of the simple picture of the aliphatic hydrocarbon acting as a mixture of the above three types of structural units. The results indicate that this picture is adequate for predicting the absorption intensities generally within about 10 percent, and with somewhat better accuracy in a number of cases.

[1] J. J. Fox and A. E. Martin, Proc. Roy. Soc. **A175**, 208 (1940).
[2] R. S. Rasmussen, J. Chem. Phys. **16**, 712 (1948).

EXPERIMENTAL PROCEDURE

The absorption data were obtained with an evacuated recording spectrometer[3] using as the dispersing element an echelette replica grating ruled with 3610 lines per inch. The spectral slit widths employed were 1.1 and 0.8 cm^{-1} in the 2850 and 1430 cm^{-1} regions respectively. The data were corrected for stray radiation, which amounted to about 2 percent of the incident radiation.

The samples examined were solutions of National Bureau of Standards Standard Hydrocarbon Samples in carbon tetrachloride. Measurements were made at a number of different concentrations in the range 0.2–0.02 molar for each compound. The transmission through a 0.5-mm cell filled with sample was compared in each case with the transmission through the same cell filled with pure solvent.

Molecular integrated intensities were calculated from the transmission data according to the relation

$$A=\int_{\text{band}} \alpha(\nu)d\nu = 1/NL\int_{\text{band}} \ln(I_0/I)d\nu, \qquad (1)$$

where A = integrated intensity, N = number of molecules per cm^3, L = cell thickness in cm, I_0 = transmission through cell filled with CCl_4, I = transmission through

TABLE I. Characteristic vibrations of aliphatic hydrocarbons.

Type of motion	Number of normal modes per group	Approximate frequency (cm^{-1})
CH_3 Non-symmetric stretching	2	2962
CH_2 Non-symmetric stretching	1	2926
CH Stretching (tertiary carbon)	1	2890
CH_3 Symmetric stretching	1	2872
CH_2 Symmetric stretching	1	2853
CH_2 Deformation	1	1465
CH_3 Non-symmetric deformation	2	1450
CH_3 Symmetric deformation	1	1375

[3] The spectrometer was that described by R. A. Oetjen, J. Opt. Soc. Am. **35**, 743 (1945). The data are now obtained on a Brown strip-chart recorder rather than photographically.

TABLE II. Integrated intensities of 2900, 1460, and 1370 cm^{-1} bands of aliphatic hydrocarbons.

Compound	Experimental intensities $\left(\frac{cm^2}{molecule\ sec.}\right)\times 10^7$			Calculated intensities[a] $\left(\frac{cm^2}{molecule\ sec.}\right)\times 10^7$		
	2900 cm^{-1} band	1460 cm^{-1} band	1370 cm^{-1} band	2900 cm^{-1} band	1460 cm^{-1} band	1370 cm^{-1} band
n-pentane	19.88	1.77	0.50	20.25	1.78	0.79
2,2-dimethylbutane	21.97	2.25	1.34	21.46	2.41	1.58
2,3-dimethylpentane	24.70	2.61	1.46	24.23	2.41	1.58
2,4-dimethylpentane	24.50	2.49	1.62	24.23	2.41	1.58
3,3-dimethylpentane	24.77	2.73	1.38	25.27	2.64	1.58
3-ethylpentane	25.99	2.54	0.85	26.05	2.33	1.18
2,2,3-trimethylbutane	23.38	2.68	2.16	23.45	2.72	1.97
2,2-dimethylhexane	27.66	2.53	1.52	29.07	2.87	1.58
2,3-dimethylhexane	28.77	2.73	1.57	28.04	2.64	1.58
n-octane	32.32	2.48	0.75	31.68	2.48	0.79
2,2,3,3-tetramethylpentane	28.79	3.34	2.60	30.28	3.50	2.36
2,2,4,4-tetramethylpentane	31.67	3.62	2.61	30.28	3.50	2.36

[a] Calculated from Eq. (2) and unit structural group intensities in Table III.

cell filled with sample, and ν = frequency of radiation in cycles/second. The original procedure for obtaining integrated intensities was to plot $\log(I_0/I)$ *vs.* ν and to integrate the curve with a planimeter. The integrals are now obtained with equal accuracy and with a great saving in time directly from the transmission data by means of a logarithmic integrator which was built at this laboratory.[4]

The integrated intensities showed no systematic variation with concentration in the range employed here provided the maximum optical density was below about 0.8. Consequently no extrapolation of the integrated intensity to zero concentration was required, and the final values for the intensities are averages of the individual measurements.

EXPERIMENTAL DATA

The integrated intensity per molecule of the 2900, 1460, and 1370 cm^{-1} bands of twelve aliphatic hydrocarbons are given in Table II and will be discussed in the following section. The estimated uncertainty of the 2900 cm^{-1} band intensities is about 5 percent and of the 1460 and 1370 cm^{-1} band intensities about 10 percent. One of the sources of uncertainty is the fact that the sample transmission remains below that for the same cell filled with pure solvent even at large distances from the center of the absorption band. This general absorption is proportional to concentration. The cause of the absorption is not understood, and hence it is not clear whether it should be included in the intensity measurements. This general absorption is included in the intensities reported here, the procedure being to terminate the integration at a point in the wings of the band where $\ln(I_0/I)$ remains sensibly constant.

COMPARISON WITH THEORY

If the hypothesis is correct that the aliphatic hydrocarbons can be treated as a non-interacting mixture of CH_3, CH_2, and CH structural groups, as far as the 2900, 1460, and 1370 cm^{-1} band intensities are concerned, the integrated intensity A_ν of a band will be given by

$$A_\nu = N_{CH_3}a_\nu + N_{CH_2}b_\nu + N_{CH}c_\nu, \qquad (2)$$

where N_{CH_3}, N_{CH_2}, and N_{CH} are the number of CH_3, CH_2, and CH groups respectively in the molecule and a_ν, b_ν, and c_ν are the respective unit intensities for these three groups. Best values for a_ν, b_ν, and c_ν, determined from the data for all twelve compounds by the least squares method, are given in Table III for the 2900, 1460, and 1370 cm^{-1} bands. Since, according to Table I, CH groups do not absorb in the 1460 cm^{-1} region and CH_2 and CH groups do not absorb in the 1370 cm^{-1} region, c_{1460}, b_{1370} and c_{1370} are assigned the value zero. The intensities for the individual compounds, calculated from the empirically determined values for a_ν, b_ν, and c_ν, are given in the last three columns of Table II for comparison with the measured intensities. The over-all agreement between calculated and measured intensities is expressed by σ_A in the last column of Table III. The values for σ_A are within the estimated experimental error except in the case of the 1370 cm^{-1} bands for a few compounds having only two or three CH_3 groups.

TABLE III. Best values for unit structural group intensities (cm^2/molecule sec.).

Spectral band (cm^{-1})	$a_\nu(\times 10^7)$	$b_\nu(\times 10^7)$	$c_\nu(\times 10^7)$	$\sigma_A(\times 10^7)$[a]
2900	4.412	3.809	1.388	0.85
1460	0.544	0.232	(0)	0.16
1370	0.394	(0)	(0)	0.21

[a] σ_A = standard error of estimate of intensity for a compound

$$= \left[\frac{\sum_{i=1}^{n}(A_{measured} - A_{calculated})^2}{n-r}\right]^{\frac{1}{2}}.$$

n = number of compounds.
r = number of parameters determined or degrees of freedom.

Despite the good over-all agreement between predicted and experimental results in the preceding treatment, there are some indications that the picture of non-interacting structural groups is not completely satisfactory. For example, 2,2,3,3-tetramethylpentane and 2,2,4,4-tetramethylpentane, which contain the same number of each type of structural group, differ by 10 percent in the intensity of the 2900 cm^{-1} band. This indicates that the intensity is affected not only by the number of structural groups but also by their arrangement in the molecule. However, effects of this latter kind seem to be small and, in general, not detectable. There is also an indication that the 1370 cm^{-1} band intensity per CH_3 group increases slightly with increasing number of CH_3 groups in the molecule.

DETERMINATION OF CH BOND PARAMETERS

The preceding analysis provides empirical values for the unit structural group intensities; these unit intensities can be employed in conjunction with the method of

[4] The integrator will be described in a separate paper.

Thorndike, Wells, and Wilson[5] and a normal coordinate treatment of the structural groups to obtain values for the CH bond dipole moment and the change in CH bond moment with change in internuclear distance.

If one assumes that each normal coordinate can be treated as a harmonic oscillator coordinate and that the electric moment of the structural group is a linear function of the normal coordinates, the integrated intensity is related to the change in electric moment by the expression

$$A_i=\frac{\pi(\epsilon+2)^2}{27c_m\epsilon}\left(\left|\frac{\partial\mu_x}{\partial Q_i}\right|^2+\left|\frac{\partial\mu_y}{\partial Q_i}\right|^2+\left|\frac{\partial\mu_z}{\partial Q_i}\right|^2\right). \quad (3)$$

A_i is the integrated intensity per structural group of the fundamental band of the ith normal mode, Q_i the corresponding normal coordinate, c_m the velocity of light in the medium, ϵ the dielectric constant of the solvent[6] and μ_x, μ_y, and μ_z the components of the vector dipole moment. The internal coordinates, R_k, are linearly related to the normal coordinates by the expression

$$R_k=\sum_i L_{ki}Q_i. \quad (4)$$

If the dipole moments of the bonds are additive, then, for the vector dipole moment $\bar{\mu}$, the relation holds that:

$$\partial\bar{\mu}/\partial Q_i=\sum_k(\partial\bar{\mu}/\partial R_k)L_{ki}. \quad (5)$$

The integrated intensity then is

$$A_i=\frac{\pi(\epsilon+2)^2}{27c_m\epsilon}\left\{\left|\sum_k\frac{\partial\mu_x}{\partial R_k}L_{ki}\right|^2+\left|\sum_k\frac{\partial\mu_y}{\partial R_k}L_{ki}\right|^2+\left|\sum_k\frac{\partial\mu_z}{\partial R_k}L_{ki}\right|^2\right\}. \quad (6)$$

TABLE IV. Bond moments and derivatives from unit structural group intensities.

	Vibrational motion	Case I	Case II
$q(\times10^{10})$	CH_3, symmetric	+0.416	+0.352
c.g.s. units	CH_3, non-symmetric	+0.219	+0.168
	CH_2	+0.229	+0.229
$E(\times10^{10})$	CH_3	−0.737 or +0.673	−0.759 or +0.661
c.g.s. units	CH_2	−0.816 or +0.796	−0.816 or +0.796
	CH	±0.690	±0.690

When valence type internal coordinates are employed, the quantities $\partial\bar{\mu}/\partial R_k$ are of two kinds, representing either the change in dipole moment of the structural group with change in a CH bond length or with change in an H−C−H bond angle. Hence, if the CH bonds are identical in the three structural groups considered here, from the structural group geometry and the coefficients L_{ki} it is possible to express the intensities of the normal modes in terms of two quantities q and E which are defined as the CH bond dipole moment divided by the equilibrium CH bond length and the change in CH bond dipole moment with change in internuclear distance respectively. q and E are positive or negative depending upon whether they are directed parallel or antiparallel respectively with a vector directed along the CH bond from carbon to hydrogen.

In order to obtain the coefficients L_{ki}, normal coordinates were calculated for the three structural groups using the frequencies given in Table I and assuming a potential energy function of the form

$$2V=f_r\sum r_i^2+f_\delta R^2\sum\delta_{ik}^2. \quad (7)$$

f_r and f_δ are force constants associated with changes in CH bond lengths and H−C−H bond angles respectively, r_i and δ_{ik} are changes in CH bond lengths and H−C−H bond angles respectively, R is the equilibrium CH bond length and the summations are over all the CH bonds and H−C−H bond angles respectively in the structural unit. The calculated normal coordinates and force constants are given in Appendix I. From these coordinates and Eq. (6) the following expressions are obtained for the intensities in cm²/(molecule second) of the absorption bands.

CH_3 *Group.*—Symmetric modes:
1370 cm⁻¹: $(2.167q^2-0.060qE)\times10^{13}$
2900 cm⁻¹: $(0.919E^2+0.257qE+0.018q^2)\times10^{13}$.

Non-symmetric modes:
1470 cm⁻¹: $(9.610q^2-0.502qE+0.007E^2)\times10^{13}$
2900 cm⁻¹: $(7.949E^2+2.105qE+0.139q^2)\times10^{13}$.

CH_2 *Group.*—Non-symmetric mode:
2900 cm⁻¹: $3.974\times10^{13}E^2$.

Symmetric Modes:
1470 cm⁻¹: $(3.932q^2-0.142qE+0.001E^2)\times10^{13}$
2900 cm⁻¹: $(1.884E^2+0.539qE+0.039q^2)\times10^{13}$.

CH *Group.*—
2900 cm⁻¹: $2.909\times10^{13}E^2$.

From these expressions and the unit structural group intensities in Table III values of q were calculated for the CH_2 group, the CH_3 group in its symmetric deformation mode and the CH_3 group in its doubly degenerate non-symmetric deformation modes, and values of E for the CH, CH_2, and CH_3 groups. The calculated values are given in Table IV under Case I. Only positive values for q have been considered, based upon the relatively greater electronegativity of carbon

[5] Thorndike, Wells, and Wilson, J. Chem. Phys. **15**, 157 (1947).
[6] The dependence of the intensity upon ϵ has been given previously by R. E. Richards and W. R. Burton, Trans. Faraday Soc. **45**, 874 (1949). The effective field in a spherical cavity in a dielectric is $E(\epsilon+2)/3$, where E is the electric intensity. The factor $1/(c_m\epsilon)$ arises from the relation that the mean intensity of a plane wave in a dielectric is $E_0^2c_m\epsilon/8\pi$, where E_0 is the amplitude of the electric intensity.

compared with hydrogen. The value of q for the CH_3 group in its symmetric mode is approximately twice as large as the value obtained for the CH_3 group in its non-symmetric mode. The latter value, 0.22×10^{-10}, agrees very closely with the value, 0.23×10^{-10}, obtained for the CH_2 group. These results indicate that q is dependent upon the type of vibration.

The values of E for the CH_2 and CH_3 groups differ significantly. However, the agreement is better for the negative values than the positive ones, and this may be an indication that E is actually of opposite sign from q. This is interpreted to mean that the CH bond dipole moment decreases with increase in bond length. That this result might be expected is indicated by Mecke's[7] conclusion that the dipole moment and its change with bond length have opposite signs for the HCl bond and for the OH bond in water vapor.

The value -0.74×10^{-10} obtained here for E for the CH_3 group is identical with the negative value obtained by Thorndike[8] from his data on ethane in the gas phase. Thorndike obtained values for q of approximately 0.31×10^{-10} and 0.09×10^{-10} from the non-symmetric and symmetric vibrations of ethane respectively. The former value is in fair agreement with the value 0.22×10^{-10} obtained here, but his value from the symmetric mode is much smaller than that obtained here. It is interesting, however, that the 1370 cm^{-1} band is comparatively weak for n-pentane, and this may indicate a decrease in the intensity of this band with decreasing chain length.

The fact that a smaller value for E was obtained here for the CH group than for the CH_2 and CH_3 groups is not considered significant since this group makes only a small contribution to the measured intensities and hence its unit intensity can be determined with relatively little precision.

The effects of various assumptions concerning the force fields existing in the CH_2 and CH_3 groups upon E and q were studied, and in particular an attempt was made to find a force field which would yield the same value for E for both CH_2 and CH_3. The inclusion in the potential energy of cross terms of the type $f_r'r_jr_k$ or $f_\delta'\delta_{ik}\delta_{i'k'}$ does not affect the intensities, since f_r' and f_δ' appear only on the diagonal in the F matrix for the symmetry coordinates. However, the inclusion of a force constant for the interaction between stretching and bending internal coordinates does affect the intensity relations. Normal coordinates are given in Appendix II for the CH_3 group based upon the potential energy function

$$2V=f_r(r_1^2+r_2^2+r_3^2)+f_\delta R^2(\delta_{12}^2+\delta_{13}^2+\delta_{23}^2)$$
$$+f_{r\delta}R[r_1(\delta_{12}+\delta_{13})+r_2(\delta_{12}+\delta_{23})+r_3(\delta_{13}+\delta_{23}). \quad (8)$$

$f_{r\delta}$ was arbitrarily assigned a value -0.212×10^5 dynes/cm. The values for E and q calculated from these normal coordinates are given in Table IV under Case II. The relationship between the q's obtained from the 1370 and 1470 cm^{-1} band intensities is essentially the same as obtained with $f_{r\delta}=0$. However, the values for E for the CH_2 and CH_3 groups are somewhat closer together although still significantly different. While the assumption of a larger negative value for $f_{r\delta}$ would bring the values of E for CH_2 and CH_3 into closer agreement, the large value required for this interaction term does not seem reasonable.

The present results cannot be satisfactorily interpreted by assigning a single pair of values for E and q for the CH, CH_2, and CH_3 structural groups. The q obtained for the CH_3 symmetric deformation mode is approximately twice as large as that obtained for the CH_3 non-symmetric deformation mode. Similarly the value of E obtained for the CH_2 group differs from that obtained for the CH_3 group. Since it was not possible to obtain the intensities of the individual normal modes in the 2900 cm^{-1} band due to overlapping, it is not possible to determine whether E is also dependent upon the type of vibration. It seems reasonable to conclude that the dipole moment expression for the CH_3 group must contain cross terms of considerable magnitude involving the bond-bending internal coordinates, and the possibility of other types of cross terms is definitely not ruled out.

The author wishes to thank Dr. L. C. Roess for many helpful discussions throughout the course of the work, and Mr. J. E. Scardefield for carrying out many of the measurements.

APPENDIX I

The normal coordinates and force constants calculated for the three structural groups using the frequency assignments in Table I and a force field represented by Eq. (7) are:

CH.—
$Q_1=1.239\times10^{-12}r_1$
$f_r=4.55\times10^5$ dynes/cm.

CH_2.—Non-symmetric mode:
$Q_1=0.865\times10^{-12}(r_1-r_2)$
$f_r=4.55\times10^5$ dynes/cm.

Symmetric modes:
$Q_2=0.886\times10^{-12}(r_1+r_2)-0.023\times10^{-12}R\delta_{12}$
$Q_3=0.088\times10^{-12}(r_1+r_2)+0.867\times10^{-12}R\delta_{12}$
$f_r=4.54\times10^5$ dynes/cm
$f_\delta=0.57\times10^5$ dynes/cm.

CH_3.—Symmetric modes:
$Q_1=0.733\times10^{-12}(r_1+r_2+r_3)-0.014\times10^{-12}R(\delta_{12}+\delta_{13}+\delta_{23})$
$Q_2=0.067\times10^{-12}(r_1+r_2+r_3)+0.675\times10^{-12}R(\delta_{12}+\delta_{13}+\delta_{23})$
$f_r=4.73\times10^5$ dynes/cm
$f_\delta=0.92\times10^5$ dynes/cm.

Non-symmetric modes:
$Q_3=0.861\times10^{-12}(r_2-r_3)+0.016\times10^{-12}R(\delta_{13}-\delta_{12})$
$Q_4=-0.103\times10^{-12}(r_2-r_3)+0.554\times10^{-12}R(\delta_{13}-\delta_{12})$
$Q_5=0.497\times10^{-12}(2r_1-r_2-r_3)+0.009\times10^{-12}R(2\delta_{23}-\delta_{12}-\delta_{13})$
$Q_6=-0.060\times10^{-12}(2r_1-r_2-r_3)+0.320\times10^{-12}R(2\delta_{23}-\delta_{12}-\delta_{13})$
$f_r=4.65\times10^5$ dynes/cm
$f_\delta=0.46\times10^5$ dynes/cm.

[7] R. Mecke, Zeits. f. Physik **107**, 595 (1937).
[8] A. M. Thorndike, J. Chem. Phys. **15**, 868 (1947).

APPENDIX II

The normal coordinates and force constants calculated for the CH_3 group using the frequency assignments in Table I, the potential energy function given by Eq. (8), and assuming a value $f_{r\delta} = -0.212\times10^5$ dynes/cm are:

Symmetric modes:

$$Q_1 = 0.717\times10^{-12}(r_1+r_2+r_3) - 0.107\times10^{-12}R(\delta_{12}+\delta_{13}+\delta_{23})$$
$$Q_2 = 0.165\times10^{-12}(r_1+r_2+r_3) + 0.667\times10^{-12}R(\delta_{12}+\delta_{13}+\delta_{23})$$
$$f_r = 4.465\times10^5 \text{ dynes/cm}$$
$$f_\delta = 1.090\times10^5 \text{ dynes/cm.}$$

Non-symmetric modes:

$$Q_3 = 0.848\times10^{-12}(r_2-r_3) + 0.069\times10^{-12}R(\delta_{13}-\delta_{12})$$
$$Q_4 = -0.185\times10^{-12}(r_2-r_3) + 0.550\times10^{-12}R(\delta_{13}-\delta_{12})$$
$$Q_5 = 0.490\times10^{-12}(2r_1-r_2-r_3) + 0.040\times10^{-12}R(2\delta_{23}-\delta_{12}-\delta_{13})$$
$$Q_6 = -0.107\times10^{-12}(2r_1-r_2-r_3) + 0.318\times10^{-12}R(2\delta_{23}-\delta_{12}-\delta_{13})$$
$$f_r = 4.536\times10^5 \text{ dynes/cm}$$
$$f_\delta = 0.483\times10^5 \text{ dynes/cm.}$$

THE JOURNAL OF CHEMICAL PHYSICS VOLUME 18, NUMBER 6 JUNE, 1950

Chemical Reactions of Energetic Chlorine Atoms Produced by Neutron Capture in Liquid Systems*

J. M. Miller and R. W. Dodson
Chemistry Department, Columbia University, New York City, New York
and
Chemistry Department, Brookhaven National Laboratory, Upton, New York

(Received January 13, 1950)

The fraction of the radioactive energetic chlorine atoms, formed by radiative neutron capture, that react with inactive carbon tetrachloride to give radioactive carbon tetrachloride, or with a solvent to give other radioactive organic halides, was studied as a function of composition in solutions of carbon tetrachloride in silicon tetrachloride, cyclohexane, and benzene. The reactions of similarly formed atoms were also studied for solutions of chlorine in cyclohexane and in benzene.

No significant effect of the temperature of the bombarded solution or of the energy of the neutrons was found.

The results are examined in terms of a theory which predicts the concentration dependence of some of the observed reactions, and alternative descriptions are suggested. It is concluded that the observed reactions occur before the recoil atoms are reduced to thermal equilibrium, and that particular reactions predominate in certain energy ranges.

INTRODUCTION

IN 1934 Szilard and Chamers[1] found that about 60 percent† of the radioactive I^{128} formed in ethyl iodide by radiative neutron capture can be extracted from the organic liquid into a reducing aqueous solution. The similar treatment[2a,2b] of several other organic halides showed that usually 40–60 percent of the halogen activity can be extracted from the irradiated organic liquid. Lu and Sugden[2c] determined the effectiveness of several different extractants for the bromine activity arising from the neutron bombardment of ethylene dibromide and bromobenzene. They found in both these cases that the most effective extracting solutions are those which will chemically remove elementary bromine from the organic liquid. By electrolyzing ethyl iodide after neutron bombardment, Fay and Paneth[2d] were able to collect about 60 percent of the activity on the anode when carrier iodide was present and the anode was of a material that reacts with halogens.

Libby[2b] has found that about 99.5 percent of the unextracted radioactivity formed in the (n,γ) reaction with bromine nuclei in bromobenzene exists as bromobenzene. However the chemical form in which the unextracted activity exists in some other organic halides has been shown by Gluckauf and Fay[2a] to include a considerable fraction of molecules in which the radioactive halogen has replaced a hydrogen. The replacement of a hydrogen atom by an active halogen was conclusively demonstrated by Reid[3] who found that the neutron irradiation of iodine dissolved in pentane resulted in the reaction of 30 percent of the radio iodine with the solvent to form active amyl iodide.

The results cited above evidently lead to the conclusion that a fraction of the molecules containing nuclei that have captured neutrons must break up as a consequence of the neutron capture and leave the active halogen in some form that can be extracted by an ap-

* Research carried out, in part, under the auspices of the AEC.

[1] L. Szilard and T. A. Chalmers, Nature **134**, 462 (1934).

† The fraction of the activity which is not extracted by the particular method employed has sometimes been termed the "retention." The word is occasionally used in this sense in the present paper. It is in general not synonomous with the more definite quantity, yield of a particular species containing radioactive material, with which we are principally concerned.

[2a] E. Gluckauf and J. W. Fay, J. Chem. Soc. **4**, 390 (1936).

[2b] W. F. Libby, Science **93**, 283 (1941).

[2c] Lu and S. Sugden, J. Chem. Soc. **7**, 1273 (1939).

[2d] J. W. Fay and F. H. Paneth, J. Chem. Soc. **4**, 384 (1936).

[3] A. F. Reid, Phys. Rev. **69**, 530 (1946).

propriate aqueous solution. This fraction must at least equal the fraction of the activity that can be extracted, and may be greater.

The energy required for the molecular rupture is supplied by the recoil of the nucleus upon emission of a gamma-ray consequent to the capture of the neutron. If only a single gamma-ray is emitted, the energy of the recoil nucleus will be given by

$$E_R=(537E_\gamma^2)/m.$$

(E_γ is expressed in Mev, m is the mass number of the active nucleus, and the recoil energy is in ev.) Although this may be quite large compared to bond energies, (e.g., about 1.2×10^7 cal./mole for a 6-Mev gamma-ray from Cl^{38}), Suess[4] has pointed out that only a fraction of this energy will appear in the internal degrees of freedom of the molecule. This fraction is given by $M-m/M$, where M is the molecular weight of the compound. In all but the most extreme cases, however, bond rupture should occur. Various questions about energy partition in recoil processes have been discussed by Edwards and Davies.[5]

Since not all of the radioactive atoms can be extracted by an aqueous solution, it might be thought that molecular rupture does not occur in all the molecules that capture neutrons. This non-rupture could be due to a cancellation of gamma-ray momenta if the excited nucleus emits its excess energy in a cascade. However, it can be shown that unless a large number of gammas are emitted in the cascade sufficient cancellation is very improbable. Furthermore, the observation that the yield of extracted activity is altered either by adding[2c,6] other compounds to the liquid being bombarded or by irradiating an organic halide[2a,5,6] vapor instead of a liquid shows that retention of activity, rather than being the result of a purely nuclear phenomenon, must have a basis in chemistry. Indeed, the evidence indicates that essentially all neutron captures will result in molecular rupture. The problem to be considered in this paper centers about the reactions by which the energetic radioactive fragment reenters a molecule.

The "liquid cage" model, suggested by Franck and Rabinowitch[7] to help explain low quantum yields in the photolysis of liquids, was used by Lu and Sugden[2c] for the interpretation of the reactions of the radioactive fragments. Their considerations involved the idea that the fragments of the ruptured molecule are trapped in a liquid cage and can either recombine or react with the solvent molecules in the wall of the cage. (The possible reaction of newly formed excited molecules with the solvent molecules was also suggested.) The recombination will leave the active halogen in the form of the parent compound, while a reaction with solvent molecules can give either new organic halides or halogen compounds that are extractable by an aqueous solution. These ideas were extended by W. F. Libby[8] who used the assumption that the collisions of the recoil atom are non-ionizing "billiard ball" impacts, and introduced as an energy parameter the minimum energy required for a radioactive atom to penetrate the walls of the"liquid cage." The predictions of this model, particularly in connection with the effect of varying the composition of the irradiated solutions, have subsequently been given by Miller, Gryder, and Dodson.[9]

The investigations to be described were directed toward an elucidation of the chemical reactions entered into by the radioactive Cl^{38} atoms formed through neutron capture by stable Cl^{37}, and in particular to furnish experimental results which can be compared with the existing theory[8,9] of these reactions. It must be emphasized that in this research the only reactions examined were those involving the radioactive halogen. The reactions may have given rise to chains, but the products of the possible chain reactions were not found except insofar as they contained the active halogen. This was necessarily true as the sole evidence for the occurrence of a reaction was the presence of active nuclei in the appropriate products.

The nature of the phenomena studied makes it impossible to measure the rate of the reactions in the ordinary chemical kinetic sense. Instead one can only determine the relative yields of radioactive compounds formed in the various reactions of the recoil halogen atom. The yield of a given compound is defined as the fraction of the total radioactivity, of a specified isotope, that is found chemically indistinguishable from that given compound.

The variation of yield with the concentration of the reactants, temperature of the bombarded solution, and energy of the captured neutrons was investigated.

The yield of a given radioactive compound was determined experimentally by adding a carrier portion of the compound of interest to the irradiated solution, separating it, and comparing its chlorine activity with the total chlorine activity.

PROCEDURE

Counting Apparatus

To obviate the conversion of organic chlorides into precipitates such as AgCl, the activity of each sample was determined by counting a liquid solution of the active compound contained in a cylindrical jacket placed around, and coaxial with, an ordinary glass, thin-wall, argon-ethyl alcohol filled Geiger-Müller tube. Reproducible geometry was obtained by employing standard taper joints (male joint on the Geiger-Müller tube and female on the jacket) to support the jacket when in position around the counter. Inevitable differ-

[4] H. Suess, Zeits f. physik. Chemie **B45**, 312 (1940).
[5] R. R. Edwards and T. H. Davies, Nucleonics **2**, 44–56 (1948).
[6] W. F. Libby, J. Am. Chem. Soc. **62**, 1930 (1940).
[7] J. Franck and E. Rabinowitch, Trans. Faraday Soc. **30**, 125 (1934).
[8] W. F. Libby, J. Am. Chem. Soc. **69**, 2523 (1942).
[9] Miller, Gryder, and Dodson, J. Chem. Phys. **18**, 865 (1950).

ences among the jackets were empirically corrected for with respect to the radiation detected. The maximum variation among the jackets was reflected in an effect of 6 percent on the counting rate.

The effect of the density of the liquid counted upon the self-absorbtion of the radiation was evaluated experimentally for the radiation from Cl^{38}. With the jackets and counter just described, a change in density from 1.0 to 1.6 decreased the counting rate by 19 percent.

Materials

The carbon tetrachloride, obtained from Eimer and Amend, was stated to be C. P. (passing A.C.S. specifications), sulfur-free, and had a boiling range of 76 to 76.5 degrees. The fraction retained after two distillations boiled over a range of 0.1 degrees.

The technical grade silicon tetrachloride obtained from Eimer and Amend was distilled twice in an open system and twice in vacuum. The fraction retained boiled over a range of 0.1 degree.

Cyclohexane from the Amend Drug and Chemical Company, Inc., which was stated to be C. P., was extracted three times with concentrated H_2SO_4, washed with distilled water, and dried first with Drierite and then with Na metal. The fraction retained, after a distillation from Na, boiled in a range of 0.2 degree.

The Eastman Kodak cyclohexylchloride used as a carrier was distilled once.

Baker and Adamson's thiophene-free, reagent grade benzene was dried for a week with Na and subsequently distilled over Na with the retained fraction boiling over a 0.2 degree range.

The carrier chlorobenzene, obtained from the Amend Drug and Chemical Company, Inc., was distilled once.

Methods

Carbon Tetrachloride-Silicon Tetrachloride Solutions.—Solutions of carbon tetrachloride in silicon tetrachloride were prepared in vacuum by distilling each component first into a bulb of calibrated volume and from there into a sample tube which was ultimately sealed. Thus the volume of the two components used in each sample was known. A few of the sealed tubes were kept for several weeks during which time there was no evidence of the formation of silicon dioxide.

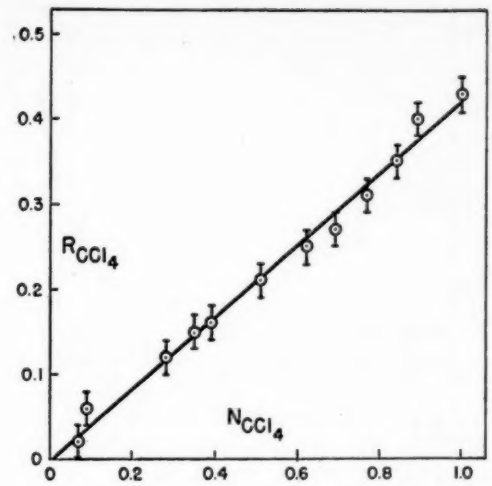

FIG. 1. The yield of radioactive carbon tetrachloride as a function of mole fraction carbon tetrachloride in carbon tetrachloride-silicon tetrachloride solutions.

After the sample had been irradiated for about five minutes with neutrons (paraffin moderated) from the Columbia 37-in. cyclotron, the sample tube was broken open and the contents slowly dropped into an aqueous 6f sodium hydroxide solution. The solution was surrounded by an ice bath in order to minimize loss of carbon tetrachloride by evaporation. The sample tube was also washed with several portions of 6f sodium hydroxide, for it was found in preliminary experiments that up to 70 percent of the activity that can be extracted into the aqueous phase is adsorbed on the wall of the container used for the neutron irradiation. The washings were added to the aforementioned extracting solution, which contained at least 20 ml of base per ml of silicon tetrachloride in the original sample.

After the aqueous and organic phases were separated and made up to known volumes in volumetric flasks, a sample of each was drawn into a jacket and the counting rate determined at least five times during the course of two or three hours.

TABLE I. The yield of radioactive carbon tetrachloride in solutions of carbon tetrachloride—silicon tetrachloride.

Mole fraction carbon tetrachloride	Active carbon tetrachloride
1.00	0.43
0.89	0.40
0.84	0.35
0.77	0.31
0.70	0.27
0.62	0.25
0.51	0.21
0.39	0.16
0.35	0.15
0.28	0.12
0.09	0.06
0.07	0.02

TABLE II. Yields in carbon tetrachloride-cyclohexane solutions.

Mole fraction carbon tetrachloride	Radioactive carbon tetrachloride	Radioactive chloro-cyclohexane	Summation organic yields	Total organic yield (experimental)
1.00	0.43	—	0.43	—
0.99	0.25	0.14	0.39	—
0.97	0.21	0.14	0.35	—
0.91	0.15	0.12	0.27	0.29
0.85	0.10	0.11	0.21	0.23
0.69	0.08	0.10	0.18	—
0.57	0.06	0.10	0.16	0.18
0.43	0.05	0.11	0.16	0.17
0.22	0.03	0.11	0.14	0.15
0.10	0.03	0.11	0.14	—
0.05	0.04	0.11	0.15	—

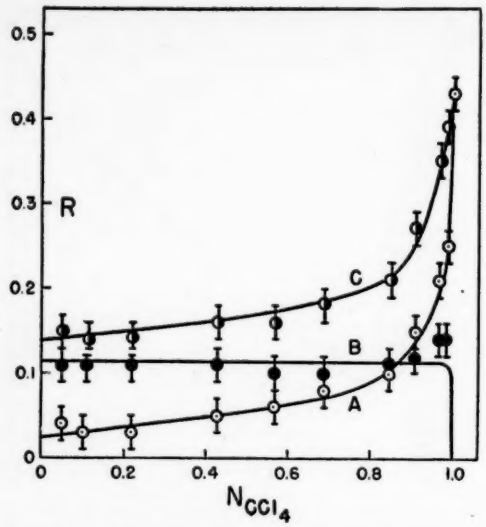

FIG. 2. The yields, R, of (A) radioactive carbon tetrachloride, (B) radioactive cyclohexylchloride, and (C) sum of (A) and (B) as functions of the mole fraction of carbon tetrachloride in carbon tetrachloride-cyclohexane solutions.

Carbon Tetrachloride-Cyclohexane Solutions.—The solutions to be bombarded were prepared by pipetting the desired volume of the components into 250-ml soft glass, glass stoppered bottles. Within five to fifteen minutes after removal from the neutron flux, 25 ml of 6f sodium hydroxide was added to the bottle in which the irradiation occurred and the mixture was vigorously agitated for several minutes. After the phases were separated, carrier chlorocyclohexane was added to the organic phase, which was subsequently fractionally distilled. The separated activities were then diluted and aliquots counted.

Carbon Tetrachloride-Benzene Solutions.—The procedure used with this system was similar to that outlined in the previous section, except chlorobenzene was used as a carrier instead of chlorocyclohexane.

Chlorine-Cyclohexane Solutions.—The solutions were prepared by bubbling dried chlorine gas through the hydrocarbon. The concentrations of solutions prepared in this manner were determined by thiosulfate titration of an aqueous iodide extract.

The solutions were bombarded in 100-ml volumetric flasks with stoppers waxed on so as to prevent appreciable loss of halogen by evaporation.

TABLE III. Counting rate of fractions taken during the distillation of carbon tetrachloride, cyclohexylchloride, and cyclohexane.*

Fraction	Counts per minute
1st 2 ml	403±15
2nd 2 ml	210±10
23rd 2 ml	240±14
28th 2 ml	248±15
2 ml out of last 10 ml left in pot.	238±13

* Starting solution contained 50 ml of carbon tetrachloride, 5 ml of cyclohexane, and 25 ml of carrier cyclohexylchloride.

Since in this case no attempt was made to distinguish between active cyclohexylchloride and any other activity that might be present in the form of a lower boiling organic chloride, the separation involved only extraction with 6f sodium hydroxide.

Chlorine-Benzene Solutions.—The procedure followed with this system was identical to that described in the preceding section.

RESULTS

Carbon Tetrachloride-Silicon Tetrachloride.—The yield of active carbon tetrachloride as a function of the mole fraction of carbon tetrachloride is given in Table I and in Fig. 1. An estimate of the counting and handling errors in this and all other experiments described, unless specifically stated otherwise, indicates a precision of 0.02 units in the measured values of the yields.

It is evident that the yield of radioactive carbon tetrachloride is very nearly proportional to the mole fraction of carbon tetrachloride in the irradiated solution. This is the result anticipated on the basis of the theory previously cited.[9] In sharp contrast is the behavior of systems containing hydrocarbons as diluents (see below).

The possibility of thermal exchange of chlorine between active carbon tetrachloride and inactive silicon tetrachloride was examined in order to ascertain if this process was affecting the results. Radioactive carbon tetrachloride was prepared by extracting an irradiated carbon tetrachloride sample with a sodium hydroxide solution. The remaining active carbon tetrachloride was washed with water, shaken for several minutes with Drierite, decanted, mixed with an equal number of moles of silicon tetrachloride, and allowed to stand for forty minutes. The separation was accomplished in the manner already described. The activity of the silicon tetrachloride fraction was found to be only one percent of what it would be if complete exchange had occurred; hence thermal exchange need not be taken into account in interpreting the results of these experiments.

Carbon Tetrachloride-Cyclohexane.—The yield of radioactive carbon tetrachloride and cyclohexylchloride as a function of N (mole fraction of carbon tetrachloride) is given in Table II and plotted in Fig. 2. The first column of Table II gives N, the second column gives the yield of radioactive carbon tetrachloride, the third gives the yield of radioactive cyclohexylchloride, the fourth gives the total organic yield as calculated by summing columns two and three, and the fifth gives the total organic yield

TABLE IV. Yields at different temperatures in carbon tetrachloride-cyclohexane.*

Temperature	Active carbon tetrachloride	Active chlorocyclohexane
25°C	0.06	0.10
0°C	0.07	0.12

* Mole fraction carbon tetrachloride 0.57.

TABLE V. Yields in carbon tetrachloride-benzene solutions.

Mole fraction carbon tetrachloride	Active carbon tetrachloride	Active chlorobenzene	Organic yield
1.00	0.43	—	0.43
0.99	0.30	0.12	0.42
0.97	0.27	0.16	0.43
0.92	0.23	0.22	0.45
0.90	0.22	0.24	0.46
0.82	0.17	0.21	0.38
0.65	0.12	0.22	0.34
0.53	0.12	0.22	0.34
0.38	0.10	0.20	0.30
0.29	0.08	0.18	0.25
0.23	0.06	0.20	0.26
0.15	0.07	0.20	0.27
0.08	0.06	0.18	0.24

as determined experimentally (fraction of activity retained in organic phase after aqueous extraction). Comparison of columns four and five indicates a satisfactory conservation of activity during the distillation process and lends support to the precision claimed above.

The apparent yield of active carbon tetrachloride does not seem to go to zero as the mole fraction of carbon tetrachloride approaches zero. This probably indicates the formation of some lower boiling organic chloride. Further evidence on this point is found in Table III, which gives the results of an experiment in which a fractionation of the higher and lower boiling products was performed. The data indicate that 97 percent of the active lower boiling component exists as carbon tetrachloride and essentially all of the higher boiling activity is cyclohexylchloride. It is possible, therefore, that about 3 percent of the activity in the carbon tetrachloride fraction was actually in the form of a lower boiling substance.

Since one of the important questions in the interpretation of "hot-atom" reactions is the assignment of the energy interval in which the reactions occur, it seemed desirable to make measurements at different temperatures. The results of such an experiment are given in Table IV. It is seen that a temperature change of 25°C has no effect within experimental error.

Carbon Tetrachloride-Benzene.—The very rapid drop in yield of active carbon tetrachloride caused by the addition of cyclohexane, in contrast to the effect observed upon the addition of silicon tetrachloride, was entirely unexpected in terms of the physical impact theory.[9] In order to find out more about this effect, it seemed desirable to vary the hydrogen-carbon ratio of the diluent, and for this purpose experiments were performed with benzene as a diluent. The results are presented in Table V and Fig. 3, which give the active carbon tetrachloride and chlorobenzene yields as functions of the mole fraction of carbon tetrachloride. The first column of Table V gives the mole fraction of carbon tetrachloride, the second and third columns give the yields of active carbon tetrachloride and chlorobenzene respectively, and the last column gives the total organic yield as determined by summing columns two and three. In spite of the physical and chemical differences of this diluent, the yield curves are seen to be qualitatively similar to those observed with cyclohexane.

The results of a fractionation of the higher and lower boiling fractions of one of the solutions indicate that 90 percent of the active lower boiling fraction is carbon tetrachloride and 88 percent of the active higher boiling fraction is chlorobenzene. These data are presented in Table VI. As in the carbon tetrachloride-cyclohexane system, the apparent yield of active carbon tetrachloride does not go to zero with the mole fraction of carbon tetrachloride. Taken in conjunction with the data in Table VI, this is again evidence for the formation of a small amount of a lower boiling organic chloride.

The effect of temperature upon the yields in carbon tetrachloride-benzene solutions was examined with the results given in Table VII. Again no significant difference is found between the results at room temperature and those at ice temperature.

Chlorine-Hydrocarbon Solutions.—Free chlorine was substituted for carbon tetrachloride in a series of experiments in order to check the assumption that the initial state of combination of the atom capturing a neutron has no effect on its subsequent fate except insofar as the free atom reacts with molecules of the parent type.

The total organic retention (fraction of activity not extractable) after neutron bombardment of chlorine dissolved in cyclohexane is given in Table VIII. Analyses of the chlorine solutions before and after bombardment showed that no significant loss of chlorine occurred during the irradiation.

The retentions are slightly higher than expected from the results with carbon tetrachloride, but it is believed that the differences are not significant.

In contrast to the behavior of chlorine-cyclohexane

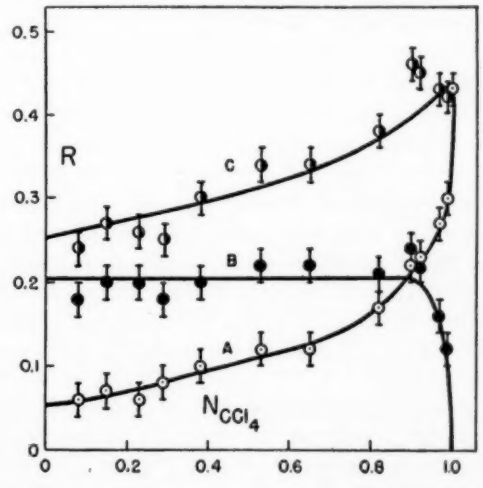

FIG. 3. The yields, *R*, of (A) radioactive carbon tetrachloride, (B) radioactive chlorobenzene, and (C) sum of (A) and (B) as functions of the mole fraction of carbon tetrachloride in carbon tetrachloride-benzene solutions.

TABLE VI. The counting rate of fractions taken during the distillation of carbon tetrachloride, chlorobenzene, and benzene.*

Fraction	Counts per minute
1st 15 ml	23,866±240
2nd 15 ml	18,146±200
3rd 15 ml	17,000±180
7th 10 ml	8,966±100
9th 10 ml	7,500± 95
last 10 ml	13,066±140

* Starting solution contained 50 ml of carbon tetrachloride, 5 ml of benzene, and 50 ml of carrier chlorobenzene.

TABLE VII. Yields at different temperatures in carbon tetrachloride-benzene.*

Temperature	Active carbon tetrachloride	Active chlorobenzene
25°C	0.12	0.23
0°C	0.13	0.26

* Mole fraction carbon tetrachloride 0.53.

TABLE VIII. Total organic retention in chlorine-cyclohexane solutions.

Mole fraction chlorine	Total organic retention
0.003	0.20±0.06
0.022	0.17±0.02

solutions, the total organic retention with chlorine-benzene solutions is markedly dependent on the concentration of chlorine, even in dilute solutions, as indicated by the data in Table IX. At mole fraction 0.001 the retention is not significantly different from that found with carbon tetrachloride-benzene at infinite dilution.

Further Examination of the Higher Boiling Radioactive Compounds Formed in Benzene.—The marked concentration dependence of the total retention in dilute chlorine-benzene solutions suggested the formation of active species other than chlorobenzene. Indeed this might be expected from what is known about the photochemical behavior of chlorine-benzene solutions. Noyes *et al.*[10] have found that the main product of the photolysis, at moderate chlorine concentrations, is a solid material that ranges in composition from $C_6H_6Cl_6$ to C_6Cl_{12}. Chlorobenzene is also found with a relative yield that increases with decreasing chlorine concentration. Hence, these materials were added as carriers after neutron irradiation in an examination of the higher boiling fraction in the chlorine-benzene system and a re-examination of this fraction in the carbon tetrachloride-benzene system.

The mixture of chlorinated benzenes was prepared by illuminating a solution of chlorine in benzene with radiation from a mercury discharge lamp.

Thus, in neutron irradiated solutions of chlorine in benzene and carbon tetrachloride in benzene the activity, after base extraction, was examined in three fractions; a fraction containing carbon tetrachloride and benzene, a fraction containing chlorobenzene, and the fraction remaining with the solid product of the photolysis.

The yields of chlorine activity in the three fractions are given in the first row of Table X.

A comparison of the first and second rows of Table X indicates a significant difference in the nature of the reactions giving higher boiling activities in these two systems.

In agreement with the data of Table VI, it is found that about 90 percent of the higher boiling active compound in the carbon tetrachloride-benzene system is chlorobenzene.

The Effect of Neutron Energy Upon the Retention to CCl_4.—The examination of the effect of the energy of the captured neutron upon the reactions of the recoil atom is made difficult by the decrease in the radiative capture cross section with increase in neutron energy which magnifies the effect of stray slow neutrons. An attempt to circumvent this difficulty was made by removing all paraffin moderator and surrounding the bombarded sample with Cd sheets and B_2O_3. Four determinations of the total retention to CCl_4 under these conditions showed no significant deviation from the retention found with moderated neutrons. Thus no evidence of an energy effect is found in this experiment.

DISCUSSION

As stated previously, the recoil from gamma-emission very probably results in the rupture of every carbon tetrachloride molecule in which neutron capture by chlorine occurs. The nature of the primary fragments from carbon tetrachloride has never been directly studied; however, Wechsler and Davies[11] have tenta-

TABLE IX. Total organic retention in chlorine-benzene solutions.

Mole fraction chlorine	Total organic retention
0.00095	0.16±0.08
0.0010	0.20±0.02
0.0090	0.39±0.02
0.015	0.43±0.02
0.040	0.54±0.02

TABLE X. Yields in chlorine-benzene and carbon tetrachloride-benzene solutions.

Solution	Relative activity in lower boiling fraction	Relative activity in chlorobenzene	Relative activity in solid carrier
Chlorine* in benzene	0.01	0.08	0.35
Carbon tetrachloride** in benzene	0.12	0.22	0.02

* Mole fraction chlorine 0.015.
** Mole fraction carbon tetrachloride 0.65.

[10] Smith, Noyes, and Hart, J. Am. Chem. Soc. **55**, 4444 (1931).

[11] S. Wechsler and T. H. Davies, Brookhaven Conference on the Chemical Effects of Nuclear Transformations, BNL-C-7, Appendix.

tively reported a positive charge on about 20 percent of the active fragments resulting from neutron bombardment of ethyl bromide in the vapor phase. The fraction of the active fragments with charge was different for the two active isotopes of bromine; and these investigators suggest that the charge is due to internal conversion of soft gamma-rays from the excited bromine nuclei. It is not known whether the gamma-rays from the excited Cl^{38} nuclei are internally converted. If internal conversion does not occur it is reasonable to assume that the active fragment is a chlorine atom rather than a positive or negative ion. This assumption is plausible since the motion of a 400-ev chlorine nucleus is quite slow compared to orbital electron motions. Thus the perturbation due to the nuclear recoil will be adiabatic and the probability of electronic transitions will be small. However, even if internal conversion does occur, the fact that the first ionization potential of atomic chlorine is thirteen volts[12] whereas the appearance potential of unipositive carbon tetrachloride is eleven volts[13] would insure the rapid neutralization of positive chlorine ions. We will therefore assume that in the systems studied, active chlorine atoms are formed at a high energy (*ca.* 400 ev) and in the process of cooling, or after having cooled, these atoms enter into chemical reactions which lead to their incorporation into the various molecular species observed.

If it is accepted that every neutron capture results in molecular rupture, the point of departure for any considerations on the reactions which form stable molecules must depend upon whether these reactions occur with active species in thermal equilibrium with their surroundings, or whether the energy distribution of the reacting active atoms is governed by the cooling process. If the latter case is correct, it is of further interest to know the energy range in which the reactions occur. The lack of temperature dependence exhibited in Tables IV and VII, and also found by Lu and Sugden[2c] in other systems, can be taken as support for the latter case.‡[14] It is of course possible, in the case of several competing reactions, that the lack of temperature dependence arises from an essential equality of the activation energy for these competing reactions, but this is not very probable. It is further worthy of mention that reactions occur with these hot atoms which do not occur thermally or photochemically. An example of this is an experiment of Rollefson and Libby,[15] who illuminated active chlorine dissolved in inactive carbon tetrachloride. It was found that after enough light had been absorbed to dissociate every chlorine molecule four times, there was no activity found as carbon tetrachloride. This is in contrast to the experiments just described in which 43 percent of the active chlorine atoms exchange with the carbon tetrachloride in the absence of other molecular species. Evidently, therefore, the exchange reaction between atomic chlorine and carbon tetrachloride occurs with chlorine atoms having an energy spectrum governed by the slowing down process, and in an energy range substantially above thermal.

With these assumptions the yield of radioactive carbon tetrachloride can be formally expressed as follows:

$$R=\int_0^\infty pN(E)W(E)dE, \qquad (1)$$

where p is the probability that a collision of an active chlorine atom is a collision with a carbon tetrachloride molecule, $N(E)dE$ is the number of active chlorine atoms making collisions per unit time in an energy interval dE at E (this is taken as a steady state quantity normalized to one hot atom formed per unit time), and $W(E)$ is the probability that the exchange reaction occurs in a collision with a carbon tetrachloride molecule at energy E. We may assume that below some critical energy, $W(E)$ will vanish. This critical energy can be considered as the activation energy for the reaction, although it is not necessarily identical with the activation energy determined in the conventional manner. It seems unlikely that collisions at very high energy will lead to stable chemical binding, in other words, we expect $W(E)$ to become small in the upper part of the energy interval.

The only existing theory that enables one to express $N(E)$ and $W(E)$ as explicit functions of the energy is one based on proposals by W. F. Libby.[8] The model employed in this approach (which will hereinafter be designated as the "physical impact theory") for reactions in the high energy range, involves non-ionizing billiard-ball collisions as the mechanism for energy loss of the "hot atoms" and introduces a second critical energy parameter, the minimum energy required for an atom to escape a liquid cage. This model was employed by Miller, Gryder, and Dodson[9] to evaluate $N(E)$ and $W(E)$ in Eq. (1) and thereby calculate R. The calculation was mainly concerned with the influence of other molecular species on the yields of given compounds into which the recoil atom may be incorporated. This influence manifests itself in the terms $N(E)$ and p. Some results immediately derivable from this treatment are given in Fig. 4. The curves show the yield of active carbon tetrachloride calculated for different assumed conditions, plotted against the probability that the impact partner in a collision is a chlorine atom in a carbon tetrachloride molecule. Curve A refers to the system carbon tetrachloride-silicon tetrachloride. In the calculation of curve A it is assumed that the carbon and

[12] W. Latimer, *Oxidation Potentials* (Prentice-Hall, Inc., New York, 1948), p. 14.

[13] R. F. Baker and J. T. Tate, Phys. Rev. **53**, 683 (1938).

‡ It should be noted that a pronounced difference in the yields of dibromipropanes formed in the neutron irradiation of isopropyl bromide at 25°C and at −196°C has been reported (see reference 15). Whether this is principally a temperature effect or a phase effect has not yet been established.

[14] L. Friedman and W. F. Libby, Conference on the Chemical Effects of Nuclear Transformations, BNL-C-7, and J. Chem. Phys. **17**, 647 (1949).

[15] G. K. Rollefson and W. F. Libby, J. Chem. Phys. **5**, 569 (1937).

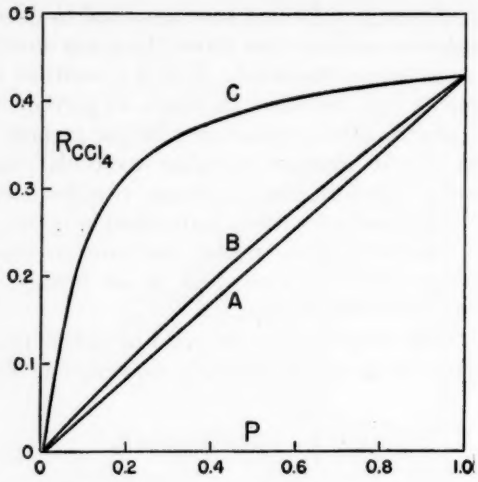

FIG. 4. The yield, R_{CCl_4}, of radioactive carbon tetrachloride predicted by the physical impact theory as a function of the probability that collision of a radioactive chlorine atom is a collision with a carbon tetrachloride chlorine atom in solutions of (A) carbon tetrachloride-silicon tetrachloride (ignoring collisions with carbon or silicon atoms), (B) carbon tetrachloride-hydrocarbon (ignoring collisions with hydrogen atoms and carbon-tetrachloride carbon atoms), (C) carbon tetrachloride-hydrocarbon (ignoring collisions with the carbon atoms).

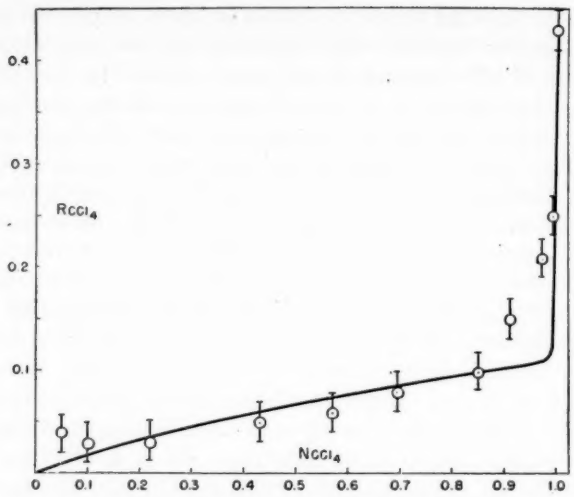

FIG. 5. A comparison of the yield of radioactive carbon tetrachloride as predicted by the physical impact theory (after allowing for the reactions with cyclohexane) with the experimentally determined yield (after correcting for the lower boiling activity that is not carbon tetrachloride) in the carbon tetrachloride-cyclohexane system.

silicon atoms are completely shielded and do not participate significantly in collisions, and thus that every impact partner is a bound chlorine atom. Curves *B* and *C* refer to the carbon tetrachloride-hydrocarbon systems with different assumptions as to the effective impact partners. Curve *B* takes into account only collisions with bound chlorine atoms and with carbon atoms. (A quite similar curve is obtained if hydrogen atoms are also included.) Curve *C* takes into account only collisions with bound chlorine and with hydrogen atoms, i.e., it is assumed that carbon atoms in the hydrocarbon are completely shielded by hydrogen.

The curves in Fig. 5 are not immediately comparable with the experimental curves in Figs. 1–3, since in the latter the abscissas are the mole fraction of carbon tetrachloride instead of the probability that a collision partner is of a specified type. The appropriate transformation from mole fraction to probability is

$$P_i = \frac{N_i \sigma_i}{\sum_j N_j \sigma_j},$$

where the subscript i designates a given atomic species present in a given molecular species, and j runs over all atomic species present in each type of molecule. N represents mole fraction and σ the collision cross section for a given atomic species (distinguished by subscript) in the given molecule. The cross sections introduced here refer to impacts which occur at high energy so that it is not proper to equate them to the cross sections calculated from interatomic distances or from van der Waals radii. However, since p is determined by the ratios of cross sections it is probably a fair approximation to employ bond radii in this calculation. The physical impact theory does not provide a means of estimating the absolute value of the yield since the parameters which enter (essentially given by the yield found when pure parent compound is irradiated) can at present be determined only by experiments of the type reported here. The significant comparison is that of the form of the yield curves.

If the impact cross section of chlorine is assumed to be the same in silicon tetrachloride and in carbon tetrachloride, the experimental curve in Fig. 1 is directly comparable to curve *A* in Fig. 4 (since their abscissas become identical); and there is seen to be good agreement between experiment and theory.

Unfortunately, however, no plausible combination of cross-section magnitudes has been found which will bring the carbon tetrachloride yield curves for cyclohexane or benzene solutions (Figs. 2 and 3) into agreement with either curve *B* or curve *C* of Fig. 4. It is evident that curve *C* (the case of hydrogen atoms shielding the carbon atoms) is made untenable. That this is so is not surprising since the maximum angular deviation in the path of a chlorine atom elastically scattered by a hydrogen atom is only 1/38 radian; hence the shielding of the carbon atoms by hydrogen atoms must be quite small.¶ But it is also apparent that the theoretical curve *B* lacks an important feature of the two experimental curves, *viz.* the very rapid decrease in yield of active carbon tetrachloride upon the addition of small amounts of hydrocarbon.‖

¶ This was kindly pointed out to us by Professor W. F. Libby.

‖ Lu and Sugden (reference 2c) observed a similar effect when aniline is added to organic halides and ascribed it to a Menschutkin type reaction between a newly formed radioactive molecule of the parent species and an aniline molecule in the cage wall. However, the very similar result observed in the present work with hydrocarbon diluents indicates that the effect may not be correlated with any familiar reaction which occurs at thermal energies.

Since the addition of small amounts of hydrocarbon should not produce a drastic decrease in p (Eq. (1)), nor should it have a large effect upon $W(E)$ (this point will be amplified below), it is indicated that the addition of small quantities of hydrocarbon causes a rapid decrease of $N(E)$ in the energy region where $W(E)$ makes an important contribution. The physical impact theory[9] predicts just the contrary effect upon $N(E)$, and furthermore does not account for the replacement of a hydrogen atom by an active halogen in any appreciable yield; hence it is appropriate to inquire whether there is any connection between these two discrepancies. A clue to the rapid drop in yield of active carbon tetrachloride may well lie in the equally rapid rise of the yield of active hydrocarbon chloride taken in conjunction with the essential lack of dependence of the hydrocarbon chloride yield on the composition of the solution below $N=0.90$. The constancy of the hydrocarbon chloride yield suggests that the chlorine atoms which react with the hydrocarbon diluent to give hydrocarbon chloride are atoms that are not capable of reacting efficiently with carbon tetrachloride to give stable compounds; otherwise competition should result in composition dependence. Further, at no time in their immediately previous history has reaction with carbon tetrachloride been very probable. This leads to the hypothesis that the fomation of radioactive hydrocarbon chloride is the first reaction that the active chlorine atom can participate in with appreciable probability while in the process of losing energy by collision. On this picture one is led to assume that every active chlorine atom reacts with hydrocarbon to give an excited intermediate complex which then decomposes to yield either active hydrocarbon chloride (or possibly active hydrogen chloride), or the original active chlorine atom which can then participate in other reactions. For if this were not true, the fraction of these atoms that so react with the hydrocarbon would be a function of the composition of the solution and hence the hydrocarbon halide yield would not be composition independent. The fact that this assumption must apply when the solution contains only about one part in ten to twenty of hydrocarbon should, in principle, yield the information necessary for a calculation of the width of the energy interval in which the reaction can occur, because each active chlorine atom must make a sufficient number of collisions in this energy interval to encounter a hydrocarbon molecule at least once. However, in view of the very approximate nature of the assumptions involved, we have not felt it profitable to make the calculation.

Thus the initial rapid decrease in yield of active carbon tetrachloride is qualitatively explained because small quantities of the hydrocarbon insure reaction with the active chlorine atoms before they have lost enough energy to exchange effectively with carbon tetrachloride; and hence some of the active chlorine atoms are made unavailable for the exchange reaction with carbon tetrachloride. This would suggest that after an allowance is made for the active chlorine atoms which react with the hydrocarbon, the intrinsic composition dependence of the yield of carbon tetrachloride, as predicted by the physical impact theory, might exhibit itself more clearly. This eventuality is manifest in Figs. 5 and 6 which show the measured carbon tetrachloride yields and predicted curves for the dependence of yield on mole fraction for the cyclohexane and benzene systems respectively. These curves were calculated by assuming that:

(1) Every radioactive recoil atom forms an excited intermediate complex with the hydrocarbon diluent (except for very small concentrations of benzene in carbon tetrachloride, when the probability of this is less than unity and is evaluated from the data).

(2) This complex can decompose by any of at least four reaction paths, each path characterized by a definite probability which is independent of the composition of the system. Products of these paths are, respectively, chlorine substituted hydrocarbon, the lower boiling active component found with carbon tetrachloride, free active chlorine atoms (which can subsequently exchange with carbon tetrachloride by the impact mechanism), an extractable compound of chlorine which does not exchange with carbon tetrachloride (possibly hydrogen chloride).

The values of p appropriate to given values of N were calculated from bond radii.[16] The probability of decomposition into cyclohexylchloride, or chlorobenzene, was obtained from the composition-independent value of yield of this substance. That for decomposition into lower boiling active compounds was estimated from the fractional distillation data. The probability of the process which gives extractable but non-exchanging species was not independently measured, but was arbitrarily chosen for best fit. (These values were 0.63 for the

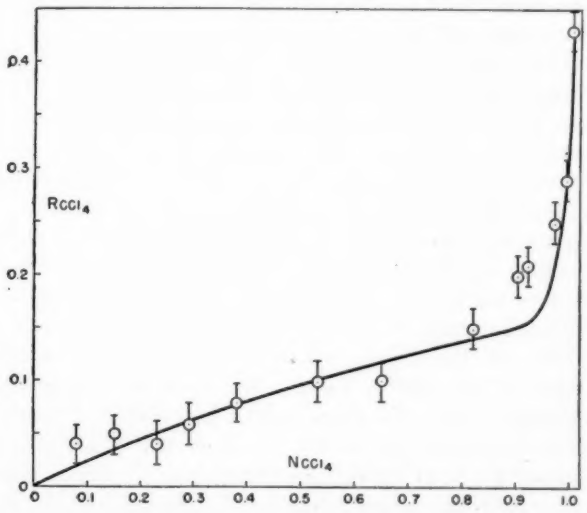

FIG. 6. A comparison of the yield of radioactive carbon tetrachloride as predicted by the physical impact theory (after allowing for the reactions with benzene) with the experimentally determined yield (after correcting for the lower boiling activity that is not carbon tetrachloride) in the carbon tetrachloride-benzene system.

[16] L. Pauling, *The Nature of the Chemical Bond* (Cornell University Press, Ithaca, 1942), p. 53.

cyclohexane system and 0.40 for the benzene system.) It is seen that the calculated curves can be well fitted to the measured points, except in the neighborhood of the sharp knee. This region will require further careful study.

Thus we see that when the special features of the reactions between the recoil atoms and hydrocarbon diluents are isolated, the substantial effects remaining are consonant with the physical impact theory. It is evident, however, that much further investigation will be necessary before its areas of applicability and its limitations can be established.

In view of the fact that it is necessary to account for reactions (e.g., hydrogen substitution) not provided for by the physical impact theory, and of the fact that the occurrence of these reactions casts doubt on a basic assumption (elastic atom-atom collisions) of this theory, it seems advisable to inquire whether the results which have been treated by it could be interpreted in terms of other ideas. Indeed, one can relinquish entirely the idea of elastic atom-atom collisions, and consider the intrinsic concentration dependence of the carbon tetrachloride retention exhibited in Figs. 5 and 6 to be the consequence of competing chemical reactions which occur in an energy range below that in which the radioactive hydrocarbon chloride is formed, but enough above thermal energy so that the usual temperature dependence of reactions will not appear.

A group of such competing reactions could be, for example,

$$\text{(A)}\quad Cl^* + CCl_4 \rightarrow CCl_3Cl^* + Cl$$
$$\text{(B)}\quad Cl^* + CCl_4 \rightarrow ClCl^* + CCl_3$$
$$\text{(C)}\quad Cl^* + RH \rightarrow HCl^* + R.$$

The experimental curves can be fitted by assigning relative cross sections for these reactions. (These cross sections are not necessarily those which would be inferred from the temperature independent term of the conventional absolute reaction rate expressions for each reaction of this set.) The relative cross sections will differ from those assumed for the above calculation of p from N. They no longer refer only to the probability of impact, but also include the probability that a specified reaction occurs. They are thus analogous to cross sections for nuclear processes. If it is assumed that all the active chlorine atoms react either with the hydrocarbon in the higher energy range to form active hydrocarbon chloride (or the other species previously mentioned) or in the manner given in reactions A–C, the relative cross sections of the reactions A:B:C are in the ratio of 1:1.3:11 for carbon tetrachloride-benzene, and 1:1.3:14.4 for carbon tetrachloride-cyclohexane. If, on the other hand, not all of the active chlorine atoms react before attaining thermal equilibrium, a more detailed analysis can be carried out which involves the impact cross sections of the reacting species, the probability of a reaction in a collision of the appropriate kind, and the average number of collisions made by a radioactive chlorine atom in the reactive energy range. Such a calculation cannot yield unique values of these parameters with the data at hand and will not be presented here.

The latter interpretation can also be applied to the observed carbon tetrachloride yield in the carbon tetrachloride-silicon tetrachloride system. The similarity of carbon tetrachloride and silicon tetrachloride would tend to make their relative effectiveness in these kinds of competing reactions depend only upon their relative concentration, and further would tend to make the respective energy ranges in which they could react with chlorine atoms very nearly alike. The proportionality between yield and mole fraction would thus be qualitatively accounted for.

With respect to the systems containing dissolved chlorine the following may be added to the remarks which appear in the presentation of the results. Since the chlorine atoms which survive reaction with hydrocarbon must ultimately find themselves in water extractable form after cooling to thermal energy, competition between reactions analogous to A, B, and C does not affect the over-all retention. Further, since an experimental method for differentiating among the various forms of extractable activity has not yet been devised, it is not at present possible to give numerical specification to the reaction cross sections of the competing processes in which the atoms that have escaped hydrocarbon chloride formation may be involved. The observation that the presence of chlorine dissolved in benzene has an effect upon the fate of the hot atoms that is consistent with photo-chemical results serves to emphasize the fact that ordinary, as well as extraordinary, reactions must be considered in a discussion of "hot atom" chemistry.

In the foregoing discussion it was stated that the addition of small quantities of hydrocarbon would have little, if any, effect upon p or $W(E)$ of Eq. (1). In this connection, two possible ways in which $W(E)$ could be affected by the addition of hydrocarbon without change in the basic assumptions of the physical impact model should be considered. The first of these is suggested by the interpretation Lu and Sugden[2e] gave for the rapid decrease in retention consequent to the addition of aniline; i.e., a newly formed radioactive carbon tetrachloride molecule, before dissipating its excess energy to the walls of the liquid cage, may react with a hydrocarbon molecule in the wall of the cage to give either stable active carbon tetrachloride, active hydrogen chloride, or active hydrocarbon chloride. The resultant abrupt reduction in $W(E)$ would explain the rapid decrease in the carbon tetrachloride yield and would, indeed, predict the rapid increase in hydrocarbon chloride yield. However, it would also predict that the hydrocarbon chloride yield would be composition dependent, since the yield of its precursor depends on the composition. This is clearly in disagreement with the experimental results. The second manner in which $W(E)$ might be rapidly decreased by the addition of small amounts of hydrocarbon arises from the result of the

physical impact theory that the yield of radioactive carbon tetrachloride is proportional to the minimum energy required to escape a liquid cage.[8,9] Thus if the addition of a small quantity of hydrocarbon caused a large decrease in this parameter, the yield would be abruptly lowered. However, this does not lead to any reasonable picture of the way in which hydrocarbon chloride is formed in constant yield.

CONCLUSIONS

The chemical reactions of radioactive recoil chlorine atoms formed by neutron capture observed in this investigation are reactions which lead to the formation of chemically stable compounds containing the radioactive chlorine. The results indicate that these reactions occur predominantly with chlorine atoms which have lost most of their original kinetic energy but have not yet been reduced to the thermal range. This conclusion is drawn from comparison of the yields of radioactive carbon tetrachloride and of hydrocarbon chloride. For, the energy of the chlorine atom which forms the latter product must not be very large, else the result would not simply be the replacement of a hydrogen by a chlorine, but rather the carbon skeleton would be splintered and there would be a large variety of active organic products. On the other hand, the exchange reaction with carbon tetrachloride, which can in principle occur at the high initial energy but not with appreciable probability at thermal, appears to occur at a lower energy than the substitution reaction with hydrocarbon.

The consistency between the data and calculations based on the physical impact theory indicates that this theory may be useful in predicting the behavior of other systems. However, in order to achieve this consistency it was necessary to supplement the theory by considerations not contained in it. It is therefore evident that this approach does not in itself suffice to describe the chemical reactions of recoil atoms.

A more accurate description of these processes is probably to be formulated in terms of a more familiar chemical approach to the various reactions which are observed. Such an approach must allow for the fact that the reactions occur at energies governed by the slowing down process. This energy distribution will have a profound effect upon the competition among the various possible reactions.

THE JOURNAL OF CHEMICAL PHYSICS VOLUME 18, NUMBER 6 JUNE, 1950

The Study of Restricted Rotation by Gas Diffraction

J. KARLE AND H. HAUPTMAN
U. S. Naval Research Laboratory, Washington, D. C.
(Received December 27, 1949)

A probability function has been derived which characterizes the variation of an interatomic distance affected by the restricted internal rotation of a molecule. The probability function takes into account the general vibration of the molecular frame in addition to the internal libration. The theory and practice are developed for determining the values of the parameters in the probability function directly from experiment. In addition the contribution from this probability distribution to the intensity of electron scattering is derived.

THE study of the scattering patterns of molecules which undergo restricted internal rotation affords a method for investigating this motion. Previous theoretical studies have been made of the intensity patterns for molecules undergoing internal torsions.[1,2] In these investigations the torsional oscillation was treated as a separate entity and the additional effect of the over-all vibration of the molecular frame was neglected. Recent developments in the technique for obtaining quantitative diffraction data and their theoretical interpretation[3] permit a detailed study of internal motion in molecules. It is therefore desirable to develop a restricted rotation theory which includes the effects not only of the torsional oscillation but also the general vibration of the molecular frame.

The general theory of the effect of small vibrational motion on scattering by gas molecules has been developed by R. W. James[4] which shows that, to a very good approximation, the contribution of the general vibration of the molecule to the probability function describing an interatomic distance is of Gaussian form. In this paper a theory of the effect of internal rotation on scattering by gases is developed in which the probability function describing the variation in interatomic distance (for distances that vary with the torsional oscillation) is given in terms of two independent contributions. One is the contribution of the restricted rotation based upon the quadratic form of the potential barrier at small angles, and the other is a Gaussian contribution as suggested by the theory of James.[4]

[1] P. Debye, J. Chem. Phys. **9**, 55 (1941).
[2] J. Karle, J. Chem. Phys. **15**, 202 (1947).
[3] I. L. Karle and J. Karle, J. Chem. Phys. **17**, 1052 (1949).
[4] R. W. James, Physik. Zeits. **33**, 737 (1932).

THE PROBABILITY FUNCTION

The potential function hindering internal rotation is assumed to have the form for small angles, ϕ,

$$V=K\phi^2, \tag{1}$$

where K is some constant.[5] It follows that the probability function for small internal vibrations, $P'(\phi)$, which neglects the effect of the general vibration of the frame, is given by[2,6]

$$P'(\phi)d\phi=(2b/\pi^{\frac{1}{2}})\exp(-b^2\phi^2)d\phi \tag{2}$$

where b^2 is defined according to quantum theory by,

$$b^2=\alpha\tanh(h\nu/kT). \tag{3}$$

The quantity h is Planck's constant, k is the Boltzmann constant, T is the absolute temperature, $\alpha=8k\pi^2I/h^2$, $\nu^2=K/2I\pi^2$ and I is the reduced moment of inertia equal to $I_1I_2/(I_1+I_2)$, where I_1 and I_2 are the moments of inertia of the rotating groups at the ends of the molecule about the molecular axis. When $h\nu$ is small compared to kT, (3) becomes

$$b^2=K/kT. \tag{4}$$

Expression (1) may be transformed to a function of r, the distance separating a pair of atoms which changes in the course of a torsional oscillation. The interatomic distance r for the *trans*-position at equilibrium is related to the angle of rotation, ϕ, by

$$r=(c_1+c_2\cos\phi)^{\frac{1}{2}}, \tag{5}$$

where $c_1=(l_2^2+l_1^2)/2$ and $c_2=(l_2^2-l_1^2)/2$ and where l_2 is the maximum possible value of r in the course of a complete rotation (*trans*-position) and l_1 is the smallest possible value of r (*cis*-position). From (5) we obtain for small oscillations,

$$P'(\phi)d\phi\equiv P''(r)dr=2(\beta/\pi)^{\frac{1}{2}}\times\exp[-\beta(l_2^2-r^2)]\frac{rdr}{(l_2^2-r^2)^{\frac{1}{2}}} \tag{6}$$

defined over the range $l_1\leq r\leq l_2$, where

$$\beta=2b^2/c_2. \tag{7}$$

The effect of the general vibration of the molecular frame may be introduced by recognizing that this motion causes l_2 in (6) to vary. As suggested by the theory developed by James,[3] the form of this contribution to the probability function should be Gaussian,

$$\Pi(R)dR=(h/\pi)^{\frac{1}{2}}\exp[-h(l_2-R)^2]dR, \tag{8}$$

where $\Pi(R)dR$ is the probability of finding the maximum possible spacing of an atom pair between R and $R+dR$. If l_2 is replaced by R in (6), we may write the general probability function in terms of the product of that for the internal oscillation (6) and that for the general vibration of the frame (8),

$$P(r)dr=\frac{2(\beta h)^{\frac{1}{2}}}{\pi}rdr\int_r^{(r^2+d^2)^{\frac{1}{2}}}\exp[-h(l_2-R)^2]\times\exp[-\beta(R^2-r^2)]\frac{dR}{(R^2-r^2)^{\frac{1}{2}}} \tag{9}$$

where d is the diameter of the circle of rotation given by $l_1^2=l_2^2-d^2$. The lower limit in (9) is r since R can be no smaller than r. The quantity R is the maximum value which r can assume. The upper limit is obtained by recognizing that the maximum spacing between R and r occurs when the pair of rotating atoms passes through their minimum separation satisfying the relation, $R^2-r^2=d^2$. The quantity d varies somewhat as the molecule vibrates. This may be neglected since d is sufficiently large to permit its replacement by infinity.

Expression (9) may be transformed using the relation, $z^2=R^2-r^2$, to give

$$P(r)=\frac{2(\beta h)^{\frac{1}{2}}}{\pi}r\exp\left[\beta\left(r^2-\frac{hl_2}{h+\beta}\right)\right]\times\int_0^d\frac{\exp\left[-(h+\beta)\left((z^2+r^2)^{\frac{1}{2}}-\frac{hl_2}{h+\beta}\right)^2\right]}{(z^2+r^2)^{\frac{1}{2}}}dz. \tag{10}$$

By keeping the first term in the binomial expansion of $(z^2+r^2)^{\frac{1}{2}}$ in the denominator, the first three terms in the exponent of (10) and replacing d by infinity, we obtain,

$$P(r)=\frac{2(\beta h)^{\frac{1}{2}}}{\pi}\exp[-h(r-l_2)^2]\times\int_0^\infty\exp\left(-\frac{hl_2}{4r^3}z^4-\left(h+\beta-\frac{hl_2}{r}\right)z^2\right)dz \tag{11}$$

defined for $0\leq r\leq\infty$. This is a useful form for $P(r)dr$, the probability of finding the spacing of a pair of atoms between r and $r+dr$ owing to both the internal libration and the remaining modes of vibration of the frame. The approximation inserted into the denominator of (10) causes $P(r)$ to be too large by less than two percent in the vicinity of $r=l_2$ for values of the parameters commonly met in practice. The effect of the approximation in the exponent is negligible.

The application of the probability function, $P(r)dr$, to scattering by gas molecules is twofold. For assumed values of its parameters, $P(r)$ may be used to compute the intensity of scattering from pairs of atoms whose

[5] If a particular shape is assumed for the potential function, e.g. $V=V_0(1-\cos\sigma\phi)/2$, where V_0 is the height of the potential barrier and σ is a symmetry number, K may be evaluated. In this case $K=V_0\sigma^2/4$ for small vibrations. However, these simple sine-like shapes and combinations thereof are probably rather rough approximations in most cases.

[6] This treatment is rigorous for symmetric top molecules. For molecules which are almost symmetric tops, the theory is applicable to a good approximation.

interatomic distances are affected by the internal rotation, or its parameters may be evaluated from the Fourier sine transform of the experimental molecular scattering data. The procedure for obtaining the values of the parameters in $P(r)$ directly from experiment will be considered first.

PROBABILITY DISTRIBUTION FROM EXPERIMENT

It was shown by Debye[1] that the Fourier transform of molecular scattering data gives the probability distribution functions for the interatomic vibrations. The procedure for handling the electron diffraction data has been given.[3] In this method the function which is computed is

$$T(r)=\int_0^{s_0} sI(s)\exp(-as^2)\sin sr\,ds \qquad (12)$$

where s is a function of the scattering angle θ and the wave-length λ ($s=(4\pi\sin\theta/2)/\lambda$), $I(s)$ is the molecular scattering from which the variable scattering factors have been effectively removed and a is chosen so that the upper limit of the experimental range, s_0, may be replaced by ∞ without altering significantly the value of $T(r)$. The desired function, however, is

$$D(r)=\int_0^{\infty} sI(s)\sin sr\,ds, \qquad (13)$$

which is the same as (12) with $s_0=\infty$ except for the factor, e^{-as^2}. It has been shown[1] that

$$D(r)=\frac{\pi}{2}\sum_{i=1}^{\frac{1}{2}n(n-1)} c_i\frac{P_i(r)}{r}, \qquad (14)$$

where the summation is over all interatomic distances in a molecule composed of n atoms, c_i is a constant related to the ith interatomic distance, ideally the product of

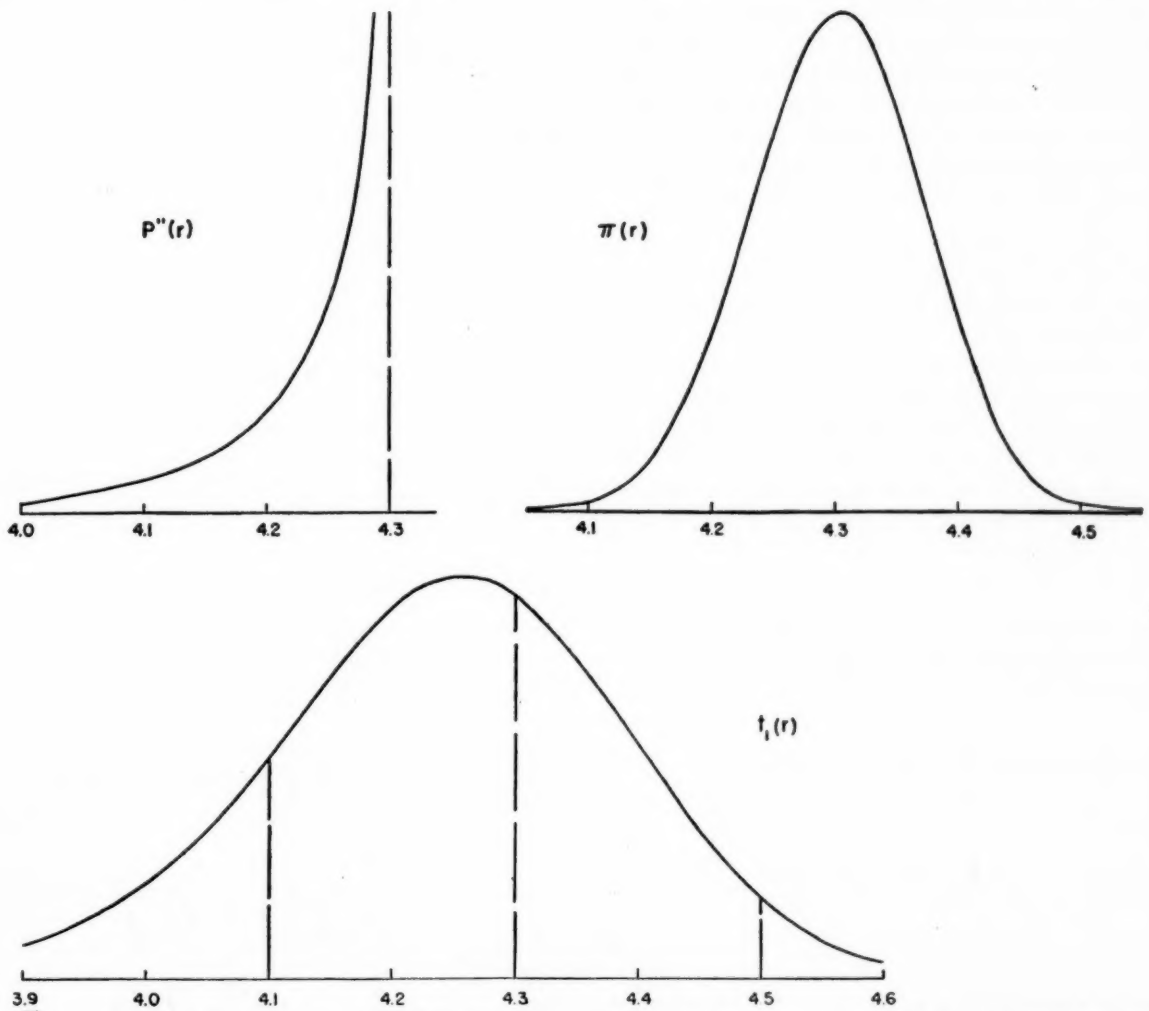

FIG. 1. The curve $P''(r)$ is the probability distribution for internal rotation in the absence of the vibration of the molecular frame (formula (6), where $l_2=4.30$ and $\beta=1$). The curve $\Pi(r)$ is the Gaussian probability for the over-all vibration of the frame (formula (8), where $l_2=4.30$ and $h=100$). The curve $t_1(r)$ is the joint probability distribution taking into account both types of motion and in addition the spreading caused by the damping function in (12) (formula (26), where $l_2=4.30$, $\beta=1$, $h=100$ and $a=0.0057$). The curve $t_1(r)$ is not only asymmetric about the equilibrium distance l_2, but its maximum is also shifted to the left of l_2.

the atomic numbers of the ith pair of atoms, and $P_i(r)$ is the probability function associated with the ith interatomic distance. The quantity $D(r)$ may be obtained from $T(r)$ by means of the following relation,[3]

$$T(r)=\frac{1}{(4\pi a)^{\frac{1}{2}}}\int_{-\infty}^{\infty}D(\rho)\exp(-(\rho-r)^2/4a)d\rho \quad (15)$$

where $D(\rho)$ is seen to be odd from (13). If the probability distribution for an interatomic distance in (14) affected by internal rotation is termed $P(r)$ and its contribution to $T(r)$ is called $t(r)$ we have from (15),

$$t(r)=\frac{c}{4}(\pi/a)^{\frac{1}{2}}\int_{-\infty}^{\infty}\frac{P(\rho)}{\rho}\exp(-(\rho-r)^2/4a)d\rho \quad (16)$$

where $P(\rho)$ is defined for negative ρ by means of $P(-\rho)=-P(\rho)$. The possibility of studying the contribution of individual terms in (14) to the function $T(r)$ computed from experimental data depends upon the fact that these contributions either do not superimpose or that if they do superimpose, they may be separated. In general $D(r)$ plotted against r appears as a series of Gaussian or modified Gaussian peaks whereas $T(r)$ is of the same functional form but appears as a broadened out version of $D(r)$. The broadening depends upon the size of a in (12).

Our present problem concerns the evaluation of the parameters in (11) from experiment. It is therefore necessary to express $t(r)$ in terms of the parameters in $P(r)$ by the use of (16).

Two alternative approximations are introduced into (11) for convenience in integrating. The coefficient of z^4 in the exponent of (11) is first replaced by $h/4r^2$ and then replaced by $hl_2^2/4r^4$ to give by means of (16) the functions $t_1(r)$ and $t_2(r)$ respectively. These two functions differ negligibly, as may be expected, since the main contribution of (11) is in the vicinity of $r=l_2$. The details of obtaining $t_1(r)$ from (16) will now be considered.

The coefficient of z^4 in (11) is considered now to be $h/4r^2$ and by performing the transformation $hz^4/4r^2=x^4$, we get from (16)

$$t_1(r)=c(\beta h^{\frac{1}{2}}/2\pi a l_2)^{\frac{1}{2}}\int_0^{\infty}\exp[-x^4+2h^{\frac{1}{2}}l_2x^2]\times\int_{-\infty}^{\infty}\exp[-h(\rho-l_2)^2-2(h+\beta)\rho x^2/h^{\frac{1}{2}}-(\rho-r)^2/4a]d\rho dx. \quad (17)$$

Since the contributions to (16) and (17) for negative ρ are negligible, we do not use the definition $P(-\rho)=-P(\rho)$ but use $P(\rho)$ as now defined for all ρ. The factor $(4\rho^2/h)^{\frac{1}{2}}$ has been replaced by $\rho(4/hl_2^2)^{\frac{1}{2}}$ with negligible error. If we complete the square in (17) and define

$$A=[(4ah+1)/4a]^{\frac{1}{2}}, \quad (18)$$

$$B=(h+\beta)x^2/Ah^{\frac{1}{2}}-(r/4a+hl_2)/A, \quad (19)$$

$$E_1=4a(h+\beta)^2/h(4ah+1), \quad (20)$$

and

$$F=2(h+\beta)(r+4ahl_2)/h^{\frac{1}{2}}(4ah+1), \quad (21)$$

the integral with respect to ρ may be evaluated, and (17) becomes

$$t_1(r)=\frac{c}{A}(\beta h^{\frac{1}{2}}/2al_2)^{\frac{1}{2}}\exp[-(h(r-l_2)^2)/(4ah+1)]\times\int_0^{\infty}\exp[-(1-E_1)x^4+(2h^{\frac{1}{2}}l_2-F)x^2]dx. \quad (22)$$

If the transformation $(1-E_1)x^2=w^4$ is introduced into (22), the integral with respect to x becomes

$$(1-E_1)^{-\frac{1}{4}}\exp(q_1^2)\int_0^{\infty}\exp[-(q_1-w^2)^2]dw, \quad (23)$$

where

$$1-E_1=[h(4ah+1)-4a(h+\beta)^2]/h(4ah+1) \quad (24)$$

and

$$q_1=\frac{2h^{\frac{1}{2}}l_2-F}{2(1-E_1)^{\frac{1}{2}}}=\frac{l_2h(1-4a\beta)-r(h+\beta)}{(4ah+1)^{\frac{1}{2}}[h(4ah+1)-4a(h+\beta)^2]^{\frac{1}{2}}}. \quad (25)$$

The integral (23) may be evaluated[7] and (22) finally becomes,

$$t_1(r)=\frac{\pi c}{4A}(\beta h^{\frac{1}{2}}/2al_2)^{\frac{1}{2}}(1-E_1)^{-\frac{1}{4}}\times\exp\left[-\frac{h(r-l_2)^2}{4ah+1}\right]|q_1|^{\frac{1}{2}}\exp(q_1^2/2)\cdot\begin{cases}I_{-1/4}\left(\frac{q_1^2}{2}\right)+I_{1/4}\left(\frac{q_1^2}{2}\right), & q_1\geq 0\\ \text{or}\\ I_{-1/4}\left(\frac{q_1^2}{2}\right)-I_{1/4}\left(\frac{q_1^2}{2}\right)\equiv\frac{\sqrt{2}}{\pi}K_{1/4}\left(\frac{q_1^2}{2}\right), & q_1<0\end{cases} \quad (26)$$

[7] D. R. Hartree and S. Johnston, Manchester Memoirs **83**, 183 (1938–39).

where the I and K are Bessel functions defined by Watson.[8]

If the coefficient of z^4 in (11) is approximated with $hl_2^2/4r^4$ and an analysis is performed similar to that in relations (17) to (26), we obtain for $t_2(r)$ an expression whose form is similar to $t_1(r)$.

For values of the parameters h and β expected in practice (h about 50→100, $\beta<3$) the functions t_1 and t_2 show a negligible difference. The function t_1 is simpler to use in practice. The good agreement between t_1 and t_2 justifies the two approximations to the coefficient of z^4 in (11) on which $t_1(r)$ and $t_2(r)$ are based.

The function $t_1(r)$ is computed from the interaction of the function $P''(\rho)$ given by (6) and $\Pi(R)$ given by (8). The shapes of $P''(\rho)$ and $\Pi(R)$ are shown in Fig. 1. The function $t_1(r)$ computed with $l_2=4.30$, $\beta=1$, $h=100$, and $a=0.0057$ is also shown in Fig. 1 and its shape is an obvious consequence of the shapes of $P''(\rho)$ and $\Pi(R)$. The experimental investigation of 1–2 dichloroethane[9] produced a radial distribution curve computed from (12) whose shape was similar to $t_1(r)$ in Fig. 1 in the vicinity of the Cl—Cl distance.

The electron diffraction method can determine the value of β and therefore K by means of (7) and (3) or (4). The potential energy for small angles is then obtained from (1). On the other hand, the spectroscopist can evaluate certain of the extrema occurring along the potential curve. With regard to the investigation of the potential barrier hindering rotation it is seen that spectroscopy and electron diffraction complement one another.

INTENSITY FUNCTION

The contribution to the intensity of molecular scattering from a pair of atoms whose interatomic distance is affected by internal rotation may be obtained from,

$$I(s)=\int_0^\infty P(r)\frac{\sin sr}{sr}dr. \tag{27}$$

It will be seen that the replacement of the lower limit of integration by $-\infty$ is helpful in evaluating (27). This is legitimate if the coefficient of z^4 in (11) is assumed to be $hl_2^2/4r^4$ previously used to obtain the function t_2, an approximation of negligible error as indicated in the previous section. We make this approximation and perform the transformation $hl_2^2z^4/4r^4=x^4$ on (11), giving on insertion into (27),

$$I(s)=\frac{2}{\pi s}(2\beta h^{\frac{1}{2}}/l_2)^{\frac{1}{2}}\int_0^\infty e^{-x^4}\int_{-\infty}^\infty \exp\Big[-h(r-l_2)^2 - \frac{2(h+\beta)x^2}{l_2h^{\frac{1}{2}}}r^2+2h^{\frac{1}{2}}x^2r\Big]\sin sr\,dr\,dx. \tag{28}$$

[8] G. N. Watson, *Theory of Bessel Functions* (The Macmillan Company, New York, 1945).

[9] J. Ainsworth and J. Karle, Am. Soc. X-Ray and Electron Diffraction Meeting, Philadelphia (1949).

We define

$$L^2=h+2(h+\beta)x^2/l_2h^{\frac{1}{2}}, \tag{29}$$

$$M=-\frac{h^{\frac{1}{2}}l_2+x^2}{(1+2(h+\beta)x^2/h^{\frac{1}{2}}l_2)^{\frac{1}{2}}}, \tag{30}$$

and

$$N=-M^2+hl_2^2=2l_2\beta x^2/h^{\frac{1}{2}}-(1+2\beta/h)^2x^4. \tag{31}$$

If the term $2\beta/h$ is neglected in the coefficient of x^4 in (31), thus decreasing the value of the integral by less than four percent (an error which will be partially corrected later), the integration with respect to r in (28) may be performed, giving

$$I(s)=\frac{2}{s}(2\beta h^{\frac{1}{2}}/\pi l_2)^{\frac{1}{2}}\int_0^\infty \exp[-2l_2\beta x^2/h^{\frac{1}{2}}-s^2/4L^2] \times(\sin(-sM/L)/L)dx. \tag{32}$$

The following expansions, derived by means of the binomial expansion from (29) and (30), are introduced into (32) with negligible error:

$$\frac{1}{4L^2}=\frac{1}{4h}-\frac{(h+\beta)}{2h^{5/2}l_2}x^2+\frac{(h+\beta)^2}{h^4l_2^2}x^4, \tag{33}$$

and

$$\frac{M}{L}=-l_2+\frac{(h+2\beta)}{h^{\frac{1}{2}}}x^2-\frac{2(h+\beta)(h+2\beta)}{h^3l_2}x^4. \tag{34}$$

In addition, L in the denominator of the integrand of (32) is replaced by $h^{\frac{1}{2}}$, making $I(s)$ too large by less than 2 percent, thereby compensating partially for the approximation introduced in deriving (32). For convenience $\sin(-sM/L)$ is replaced by $e^{-is M/L}$ in (32) and then the imaginary part of this new integral is evaluated. If we define

$$\gamma=\frac{2l_2\beta}{h^{\frac{1}{2}}}-\frac{(h+\beta)s^2}{2l_2h^{5/2}}+\frac{is(h+2\beta)}{h^{\frac{1}{2}}}, \tag{35}$$

and

$$\delta=\frac{(h+\beta)^2s^2}{h^4l_2^2}-\frac{i2s(h+\beta)(h+2\beta)}{h^3l_2}, \tag{36}$$

(32) becomes

$$I(s)=(\text{i.p.})\frac{2}{s}(2\beta/\pi l_2h^{\frac{1}{2}})^{\frac{1}{2}}\exp\Big[-\frac{s^2}{4h}+isl_2\Big] \times\int_0^\infty \exp[-\delta x^4-\gamma x^2]dx \tag{37}$$

where (i.p.) refers to the imaginary part. This integral may be evaluated for complex γ and δ by means of its

Maclaurin expansion,

$$4\int_0^\infty \exp[-z^4-2pz^2]dz = \sum_{n=0}^{\infty}(-1)^n\Gamma\left(\frac{2n+1}{4}\right)\frac{(2p)^n}{n!}, \quad (38)$$

where $p=\gamma/2\delta^{\frac{1}{2}}$, giving the generalization of (26) for complex argument,

$$I(s)=(\text{i.p.})(\pi\beta/2l_2h^{\frac{1}{2}})^{\frac{1}{2}}\cdot\frac{1}{s} \times\exp\left[-\frac{s^2}{4h}+isl_2\right]\delta^{-\frac{1}{4}}(\mp p)^{\frac{1}{2}}\exp(p^2/2) \cdot\begin{cases} I_{-1/4}\left(\frac{p^2}{2}\right)+I_{1/4}\left(\frac{p^2}{2}\right), & -\frac{\pi}{2}<arg-p\leq\frac{\pi}{2} \\ \text{or} & \\ I_{-1/4}\left(\frac{p^2}{2}\right)-I_{1/4}\left(\frac{p^2}{2}\right) \equiv\frac{\sqrt{2}}{\pi}K_{1/4}\left(\frac{p^2}{2}\right), & -\frac{\pi}{2}<arg p\leq\frac{\pi}{2} \end{cases}. \quad (39)$$

In practice the magnitude of p is large and the real part of $p^2/2$ is large and negative. This permits an asymptotic evaluation of (39) making use of the relation,

$$(\mp p)^{\frac{1}{2}}\exp(p^2/2)\left[I_{-1/4}\left(\frac{p^2}{2}\right)\pm I_{1/4}\left(\frac{p^2}{2}\right)\right] \sim(2/\pi p)^{\frac{1}{2}}\left(1-\frac{3}{16p^2}+\cdots\right). \quad (40)$$

If the term $3/16p^2$ in (40), which is of the order of one percent, is neglected and the result then substituted into (39) we obtain

$$I(s)=(\text{i.p.})(2\beta/\gamma l_2h^{\frac{1}{2}})^{\frac{1}{2}}\cdot\frac{1}{s}\exp\left[-\frac{s^2}{4h}+isl_2\right]. \quad (41)$$

Expression (41) may be obtained directly from (37) by setting $\delta=0$. From (35), we have

$$\gamma=\frac{2l_2\beta}{h^{\frac{1}{2}}}(1-\mu s^2+ivs), \quad (42)$$

where

$$\mu=(h+\beta)/4l_2^2\beta h^2 \quad (43)$$

and

$$v=(h+2\beta)/2l_2\beta h. \quad (44)$$

On substituting (42) into (41) we obtain the final result for a pair of atoms whose equilibrium position is the *trans*-position,

$$I(s)=\frac{e^{-s^2/4h}}{[(1-\mu s^2)^2+(vs)^2]^{\frac{1}{4}}}\cdot\frac{\sin(sl_2-\theta/2)}{sl_2} \quad (45)$$

where

$$\tan\theta=\frac{vs}{1-\mu s^2}. \quad (46)$$

The magnitude of θ increases with s and amounts to about one radian at $s=20$. As $h\to\infty$, (45) reduces to expression (20) of reference 2 which neglects the contribution from the general vibration of the molecular frame. As $\beta\to\infty$, the phase shifting term $\theta/2$ in (45) may be set equal to zero and the fourth root of the polynomial in s may be set equal to unity with negligible error. This leads to the expression

$$e^{-s^2/4h}\sin sl_2/sl_2$$

which is the contribution of a Gaussian probability function to the intensity of scattering.

Force Constants for the Fluoromethanes

E. L. PACE
Morley Chemical Laboratory, Western Reserve University, Cleveland, Ohio
(Received February 14, 1950)

A calculation, involving vibrational potential functions of a general quadratic type restricted to small displacements, has been used to evaluate force constants, singly or in linear combination, for the fluoromethanes, and simultaneously, to confirm new assignments of the fundamentals of CF_3H and CF_2H_2 arising from a detailed experimental study of their Raman spectra. The results indicate considerably greater bond strengths than expected from a mere extrapolation of the properties of analogous halogen derivatives. Particularly significant is the order of interaction terms involving the C−F stretching and the F−C−F bending motions of the molecules.

I. INTRODUCTION

IN many physical properties, the fluoromethanes resemble methane more closely than the analogous chlorine or bromine compounds. This fact is of theoretical interest because this discontinuity in properties of analogous halogenated compounds should be reflected in the molecular structure, and particularly, in the forces operating around a C−F bond. Information concerning the order of these forces can be derived from force constant calculations based on fundamental frequency assignments made from infra-red and Raman absorption spectra.

The subject of the force constants of fluorocarbons has been considered in detail previously in only two instances. In one, an approximate form of a potential energy function restricted to the interaction terms involving bond bending with bond stretching motions was used in the development of the secular equations for the normal vibrations of CF_4 and C_2F_6.[1] Stepanov[2] computed a set of force constants for the fluoromethanes as part of a general study of the halogenated methanes. The results of this work should be discounted from the standpoint that, in allowing large variations in the size of identical force constants transferred between molecules, the evaluation of a unique set of force constants or confirmation of the correct frequency assignment was not possible. Recent experimental work in the infrared fine structure[3] of CF_2H_2 and polarization measurements[4] of lines in the Raman spectra of CF_2H_2 and CF_3H show quite definitely that the frequency assignments which were confirmed by the force constant calculation were incorrect in several of the frequencies.

The present treatment repeats, in a sense, the work of Stepanov. The investigation, which was started without prior knowledge of Stepanov's results, had brought out inconsistencies in the frequency assignments of CF_2H_2 by Wagner[5] and CF_3H by Glockler,[6] which were only resolved with the help of more complete infra-red and Raman spectra.

TABLE I. Interaction force constants.

Change of coordinate	r	η	R	β	α
r	f_{r1}	$f_{r\eta 1}, f_{r\eta 2}$	f_{rR1}	$f_{r\beta 2}$	$f_{r\alpha 1}, f_{r\alpha 2}$
η		$f_{\eta 1}, f_{\eta 2}$	$f_{R\eta 2}$	$f_{\beta\eta 2}$	$f_{\alpha\eta 1}, f_{\alpha\eta 2}$
R			f_{R1}	$f_{R\beta 1}, f_{R\beta 2}$	$f_{R\alpha 1}, f_{R\alpha 2}$
β				$f_{\beta 1}, f_{\beta 2}$	$f_{\beta\alpha 1}, f_{\beta\alpha 2}$
α					$f_{\alpha 1}, f_{\alpha 1'}, f_{\alpha 2}$

[1] E. L. Pace, J. Chem. Phys. **16**, 74 (1948).
[2] Stepanov, Acta Physicochimica **20**, 174 (1945).
[3] Hugh B. Stewart and Harald H. Nielsen, Phys. Rev. **75**, 640 (1949).
[4] Rank, Shull, and Pace, J. Chem. Phys. **18**, 885 (1950).

II. THE SECULAR EQUATIONS

The potential energy functions of the fluoromethanes have been assumed of the general quadratic type restricted to small displacements. The force constants in these involve the change or interaction of the five internal coordinates (1) r, the change in the C−H bond distance (2) η, the change in the H−C−H bond angle (3) R, the change in the C−F bond distance (4) β, the change in the F−C−F bond angle, and (5) α, the change in the H−C−F bond angle. Besides the five principal force constants involving directly the change in the coordinates, there are some twenty-five different interaction force constants as summarized in Table I. The interaction force constants are divided into two general classifications. The primary interaction constants involve either two stretch coordinates or an angle bend coordinate with another angle bend or a stretch coordinate with a bond in common. The secondary interaction constants include the cases of a stretch and angle bend coordinate or two angle bend coordinates without a common bond in the molecule. In the table of

TABLE II. Secular matrices for CH_4.

Symmetry type	F matrix	G matrix
A_1	$[f_r]$	$[\mu_H]$
E	$[f_\eta]$	$[3\mu_H r^2]$
F_2	$\begin{bmatrix} f_r & 0 \\ & f_\eta \end{bmatrix}$	$\begin{bmatrix} \mu_H+4/3\mu_C & -(8/3)r\mu_C \\ & r^2(2\mu_H+16/3\mu_C) \end{bmatrix}$

[5] J. Wagner, Zeits. f. physik. Chemie **B45**, 69 (1939).
[6] G. Glockler and W. F. Edgell, J. Chem. Phys. **9**, 224 (1941).

TABLE III. Secular matrices for CH_3F.

Symmetry type	F matrix	G matrix
A_1	$\begin{bmatrix} f_r & 0 & 0 \\ & f_R & (1/2)(6^{\frac{1}{2}})(f_{R\eta 2}-f_{R\alpha 1}) \\ & & (1/2)(f_\alpha+2f_{\alpha 1'}+f_\eta-4f_{\alpha\eta 1}) \end{bmatrix}$	$\begin{bmatrix} \mu_H+1/3\mu_C & -(1/3)(3^{\frac{1}{2}})\mu_C & -(4/3)\tau\mu_C \\ & \mu_F+\mu_C & (4/3)(3^{\frac{1}{2}})\tau\mu_C \\ & & \tau^2(2\mu_H+16/3\mu_C) \end{bmatrix}$
E	$\begin{bmatrix} f_r & 0 & 0 \\ & f_\alpha-f_{\alpha 1'} & -(f_{\alpha\eta 1}-f_{\alpha\eta 2}) \\ & & f_\eta \end{bmatrix}$	$\begin{bmatrix} \mu_H+4/3\mu_C & -(1/3)(2^{\frac{1}{2}})(3\epsilon+\tau)(\mu_C) & (4/3)(2^{\frac{1}{2}})\tau\mu_C \\ & \tau^2\mu_H+(3/2)\epsilon^2\mu_F+(1/6)(3\epsilon+\tau)^2\mu_C & (1/2)(\tau^2)\mu_H-(2/3)(\tau)(3\epsilon+\tau)\mu_C \\ & & \tau^2(5/2\mu_H+8/3\mu_C) \end{bmatrix}$

TABLE IV. Secular matrices for CF_2H_2.

Symmetry type		
	F matrix	
A_1	$\begin{bmatrix} f_r & 0 & 0 \\ & f_R-f_{R1} & (1/3)(6^{\frac{1}{2}})(f_{R\alpha 1}+f_{R\alpha 2}-f_{R\beta 1}-f_{R\eta 2}) \\ & & (1/3)(f_\alpha+f_{\alpha 1}+f_{\alpha 1'}+f_{\alpha 2}+f_\beta+f_\eta+2f_{\beta\eta 2}-4f_{\beta\alpha 1}-4f_{\alpha\eta 1}) \end{bmatrix}$	$\begin{bmatrix} 0 \\ f_{R\beta 1}-f_{R\eta 2} \\ -(1/6)(6^{\frac{1}{2}})(f_\beta-2f_{\beta\alpha 1}-f_\eta+2f_{\alpha\eta 1}) \\ (1/2)(f_\beta-2f_{\beta\eta 2}+f_\eta) \end{bmatrix}$
	G matrix	
	$\begin{bmatrix} \mu_H+2/3\mu_C & -2/3\mu_C & -(2/3)(3^{\frac{1}{2}})(\epsilon-\tau)\mu_C \\ & \mu_F+2/3\mu_C & (2/3)(3^{\frac{1}{2}})(\epsilon-\tau)\mu_C \\ & & (3/2)\tau^2\mu_H+(3/2)\epsilon^2\mu_F+(2)(\epsilon-\tau)^2\mu_C \end{bmatrix}$	$\begin{bmatrix} (2/3)(2^{\frac{1}{2}})(\epsilon+\tau)\mu_C \\ -(2/3)(2^{\frac{1}{2}})(\epsilon+\tau)\mu_C \\ (1/2)(6^{\frac{1}{2}})[\tau^2\mu_H-\epsilon^2\mu_F-(4/3)(\epsilon^2-\tau^2)\mu_C] \\ \tau^2\mu_H+\epsilon^2\mu_F+(4/3)(\epsilon+\tau)^2\mu_C \end{bmatrix}$
	F matrix	G matrix
A_2	$[f_\alpha-f_{\alpha 1}-f_{\alpha 1'}-f_{\alpha 2}]$	$[3/2\tau^2\mu_H+3/2\epsilon^2\mu_F]$
B_1	$\begin{bmatrix} f_r & 0 \\ & f_\alpha+f_{\alpha 1}-f_{\alpha 1'}-f_{\alpha 2} \end{bmatrix}$	$\begin{bmatrix} \mu_H+4/3\mu_C & -(2)(\epsilon+\tau/3)\mu_C \\ & (1/2)\tau^2\mu_H+(3/2)\epsilon^2\mu_F+(3)(\epsilon+\tau/3)^2\mu_C \end{bmatrix}$
B_2	$\begin{bmatrix} f_R-f_{R1} & (2^{\frac{1}{2}})(f_{R\alpha 1}-f_{R\alpha 2}) \\ & f_\alpha-f_{\alpha 1}+f_{\alpha 1'}-f_{\alpha 2} \end{bmatrix}$	$\begin{bmatrix} \mu_F+4/3\mu_C & -(2)(\tau+\epsilon/3)\mu_C \\ & (3/2)\tau^2\mu_H+(1/2)\epsilon^2\mu_F+(3)(\tau+\epsilon/3)^2\mu_C \end{bmatrix}$

TABLE V. Secular matrices for CF_3H.

Symmetry type	F matrix	G matrix
A_1	$\begin{bmatrix} f_r & 0 & 0 \\ & f_R+2f_{R1} & (1/2)(2^{\frac{1}{2}})(2f_{R\beta 1}+f_{R\beta 2}-f_{R\alpha 1}-2f_{R\alpha 2}) \\ & & (1/2)(f_\alpha+2f_{\alpha 1}+f_\beta+2f_{\beta 1}-4f_{\beta\alpha 1}-2f_{\beta\alpha 2}) \end{bmatrix}$	$\begin{bmatrix} \mu_H+\mu_C & -(1/3)(3^{\frac{1}{2}})\mu_C & (4/3)(3^{\frac{1}{2}})\epsilon\mu_C \\ & \mu_F+1/3\mu_C & -(4/3)(\epsilon\mu_C) \\ & & \epsilon^2(2\mu_F+16/3\mu_C) \end{bmatrix}$
E	$\begin{bmatrix} f_R-f_{R1} & f_{R\alpha 1}-f_{R\alpha 2} & -(f_{R\beta 1}-f_{R\beta 2}) \\ & f_\alpha-f_{\alpha 1} & -(f_{\beta\alpha 1}-f_{\beta\alpha 2}) \\ & & f_\beta-f_{\beta 1} \end{bmatrix}$	$\begin{bmatrix} \mu_F+4/3\mu_C & -(1/3)(2^{\frac{1}{2}})(3\tau+\epsilon)\mu_C & (4/3)(2^{\frac{1}{2}})\epsilon\mu_C \\ & (3/2)\tau^2\mu_H+\epsilon^2\mu_F+(1/6)(3\tau+\epsilon)^2\mu_C & (1/2)\epsilon^2\mu_F-(2/3)(\epsilon)(3\tau+\epsilon)\mu_C \\ & & \epsilon^2(5/2\mu_F+8/3\mu_C) \end{bmatrix}$

TABLE VI. Secular matrices for CF_4.

Symmetry type	F matrix	G matrix
A_1	$[f_R+3f_{R1}]$	$[\mu_F]$
E	$[f_\beta-2f_{\beta 1}+f_{\beta 2}]$	$[3\epsilon^2\mu_F]$
F_2	$\begin{bmatrix} f_R-f_{R1} & -(2^{\frac{1}{2}})(f_{R\beta 1}-f_{R\beta 2}) \\ & f_\beta-f_{\beta 2} \end{bmatrix}$	$\begin{bmatrix} \mu_F+4/3\mu_C & -(8/3)\epsilon\mu_C \\ & \epsilon^2(2\mu_F+16/3\mu_C) \end{bmatrix}$

interaction constants, the primary type is designated by the subscript 1 and the secondary by the subscript 2. Two primary interactions of a different character are exhibited by the α-coordinate depending on whether the adjacent angles have a common C—H or a common C—F bond. The relevant force constants have been designated $f_{\alpha 1}$, and $f_{\alpha 1'}$, respectively.

The method of Wilson[7] is employed in the derivation of the secular equations for the normal vibrations of the molecules. The **F** and **G** matrices for the various molecules are presented in Tables II through Table VI. In these, the μ's refer to the reciprocal masses, and τ and

[7] E. B. Wilson, Jr., J. Chem. Phys. **9**, 76 (1941).

ϵ to the reciprocal C—H and C—F equilibrium bond distances. The numerical coefficients for the terms are evaluated assuming tetrahedral angles between all bonds. Because the matrices are symmetric with respect to the main diagonal, only the elements on one side of the diagonal are shown.

The elements in the columns and rows containing the force constant f_r, except for f_r, and any interaction terms involving r and η, have been equated to zero.

The values of the molecular parameters for the numerical evaluation of the elements are:

(1) C—H bond distance	1.093A
(2) C—F bond distance	1.35A in CF_2H_2, CF_3H, CF_4 1.42A in CH_3F
(3) C	12.010 atomic weight units
(4) H	1.0080 atomic weight units
(5) F	19.00 atomic weight units

III. METHOD OF SOLUTION

Two methods of approximation involving the r and η coordinates are used. The first assumes that these coordinates are essentially uncoupled in their motion in order to simplify the determination of values of f_r and f_η from the A_1 factor, and E factor of CH_4. Experimental evidence, such as the grouping of C—H stretch and H—C—H bend frequencies in spectra, supports this first-order approximation. The second is the use of the method of approximate factorization of the high frequencies described by Wilson.[7] This operation reduces the order of the **F** and **G** matrices by one with only a small effect on the force constants or lower frequencies.

In order to utilize both the maximum transference of identical force constants between molecules, and the most reliable assignments, the F_2 frequencies of CF_4, the E frequencies of CF_3H and the B_2 frequencies of CF_2H_2 form the foundation on which the results of the calculations rest. In the secular equations for the seven vibrations included in the three classes above, the force constant combination, f_R-f_{R1}, appears three times, and $f_{R\alpha1}-f_{R\alpha2}$ and $f_{R\beta1}-f_{R\beta2}$ twice each. If the consideration is extended to include the A_1 and E frequencies of CF_4, unique values can be derived for the single force constants f_R and f_{R1}, as well as for the linear combinations $f_\beta-2f_{\beta1}+f_{\beta2}$, $f_\beta-f_{\beta1}$, $f_\beta-f_{\beta2}$, $f_{\beta\alpha1}-f_{\beta\alpha2}$, $f_{R\alpha1}-f_{R\alpha2}$, and $f_{R\beta1}-f_{R\beta2}$. Inclusion of the results from the CH_3F and CH_4 frequencies enable the evaluation of all the linear combinations involving the f_α's. In the choice of the possible sets of force constants, the reasonable assumption is made that the secondary interaction constants are smaller than the primary interaction or principal force constants. The order of the uncertainty in the values for the force constants should be of the order of that inherent in the approximations, i.e., two or three percent.

The great concentration of secondary force constants in the A_1 type frequencies of CF_2H_2 and CF_3H renders quite unlikely their unambiguous evaluation even after factorization of the high frequencies. Consequently, no attempt has been made in that direction. However, to demonstrate that the order of the force constants determined by previous considerations was essentially correct, the secondary interaction constants in the combinations of force constants occurring in the A_1 factor of CF_3H were set equal to zero. One of the seven frequencies in the two groups was used to evaluate f_β. The remaining force constant, $f_{R\eta2}$, necessary for the evaluation of the A_1 frequencies of CF_2H_2 was obtained through the use of the combination, $f_{R\alpha1}-f_{R\eta2}$, evaluated from the frequency assignment of CH_3F.

The assignments of the fundamental frequencies which were used in the calculations are summarized in Table VIII. The designation of the frequencies corresponds to that used by Herzberg[8] for halogenated methane derivatives in general.

The existence of sufficient reliable data for CH_3F, CH_4, and CF_4[9–11] which have been critically reviewed by a number of investigators leaves little reason to doubt the assignments of their fundamental frequencies.

The frequency assignments which were assumed for CF_3H and CF_2H_2 were based mainly on recent Raman spectra.[4] The appearance of several new lines and the determination of the polarization of previously observed

TABLE VII. Force constants for the fluoromethanes.[a]

	Fluoromethanes	Chloromethanes[c]	Bromomethanes[c]
f_r	5.042	5.04	5.04
f_η	0.530	0.523	0.523
f_R	6.246	3.383	2.840
f_{R1}	0.967	0.332	0.186
f_α	0.952	0.687	0.589
$f_{\alpha1}$	0.179	0.009	−0.005
$f_{\alpha1'}$	−0.004	−0.034	−0.026
$f_{\alpha2}$	−0.114	−0.065	−0.060
$f_{\alpha\eta1}$	0.017	0.000	0.000
$f_\beta-f_{\beta1}$	1.665	1.044	0.927
$f_\beta-f_{\beta2}$	2.032	1.173	1.022
$f_{R\alpha1}-f_{R\alpha2}$	0.659	0.504	0.457
$f_{R\beta1}-f_{R\beta2}$	0.644	0.587	0.532
$f_{\beta\alpha1}-f_{\beta\alpha2}$	0.304	0.000	0.000
$f_{R\alpha1}-f_{R\eta2}$	0.804	0.340	0.305
f_β	2.143[b]	1.136	1.061
$f_{\beta1}$	0.478[b]	0.092	0.134
$f_{\beta2}$	0.111[b]	−0.037	0.039
$f_{R\eta2}$	−0.145[b]	0.000	0.000

[a] Units of force constants: 10^5 dyne per cm for two stretch coordinates; 10^{-5} dyne for a stretch and bend coordinate; 10^{-11} dyne per cm for two angle bend coordinates.
[b] Evaluated after neglecting secondary interaction constants in the A_1 factor of CF_3H.
[c] See reference 12.

[8] G. Herzberg, *Infrared and Raman Spectra of Polyatomic Molecules* (D. Van Nostrand Company, Inc., New York, 1949), pp. 306–320.
[9] See reference 8, p. 307.
[10] Ta-You Wu, *Vibrational Spectra and Structure of Polyatomic Molecules* (J. W. Edwards, Ann Arbor, Michigan, 1946), second edition, pp. 223–242.
[11] Kenneth P. Yates and Harald H. Nielsen, Phys. Rev. **71**, 349 (1947).

TABLE VIII. Comparison of observed and calculated frequencies.

Molecule	Irreducible representation	Frequency designation	Type coordinate	ν calc. (cm^{-1})	ν obs. (cm^{-1})
CH_4	A_1	ν_1	r	2914	2914
	E	ν_2	η	1499	1499
	F_2	ν_3	r	3074	3020
		ν_4	η	1339	1306
CH_3F	A_1	ν_1	r	2959	2862.9
		ν_2	$\eta(\alpha)$	1498	1467.9
		ν_3	R	1057	1049.5
	E	ν_4	r	3080	3009
		ν_5	η	1470	1469.7
		ν_6	α	1197	1200.0
CF_2H_2	A_1	ν_1	r	2993	2963.4
		ν_2	$\eta(\alpha, \beta)$	1504	1508
		ν_3	R	1130	1078.6
		ν_4	$\beta(\eta)$	552	532.4
	A_2	ν_5	α	1204	1261.7
	B_1	ν_6	r	3084	3029.8
		ν_7	α	1217	1176.1
	B_2	ν_8	α	1435	1435
		ν_9	R	1090	1089.7
CF_3H	A_1	ν_1	r	3047	3062
		ν_2	R	1116	1117
		ν_3	$\beta(\alpha)$	695	697
	E	ν_4	α	1376	1376
		ν_5	R	1153	1152
		ν_6	β	508	508
CF_4	A_1	ν_1	R	904	904
	E	ν_2	β	437	437
	F_2	ν_3	R	1265	1265
		ν_4	β	630	630

lines helped establish values for ν_2 and ν_5 of CF_3H and ν_5 and ν_8 of CF_2H_2 which could be reconciled with a consistent set of force constants for the molecules.

IV. RESULTS AND DISCUSSION

The force constants, evaluated in the preceding manner, are contained in Table VII. Three groups are represented; single force constants, linear combinations of force constants and a set obtained by neglecting the secondary interaction constants present in the combinations in the secular equation for the A_1 frequencies of CF_3H.

It is interesting to compare the analogous force constants for the halogenated methanes even though the comparison may suffer from the use of different potential functions. Therefore, the results of Decius[12] for the chloro-substituted and bromo-substituted methanes are included in Table VII. As the physical properties of the compounds, themselves, tend to show, the strength of the bonds in fluorocarbons is considerably greater than mere extrapolation of analogous halogen derivatives would indicate. Particularly significant is the order of the interactions involving the C—F stretching and the F—C—F bending motions in the molecules.

A comparison of the observed and calculated frequencies is presented in Table VIII. The agreement is, in general, within the order of the approximations made in the treatment of the problem.

It is in the cases of CF_3H and CF_2H_2 that the calculations have served one of their purposes. Here, preliminary calculations brought inconsistencies to light which gave direction to a more thorough study of the study of the spectra of the compounds. Consequently, it is believed that the assignments confirmed by the calculations are essentially correct.

V. ACKNOWLEDGMENT

The progress in the preceding work was very largely dependent on the new spectral data which were obtained concurrently with the development of the calculations. Therefore, the author is greatly indebted to Dr. D. H. Rank of the Spectroscopy Laboratory of The Pennsylvania State College for obtaining detailed Raman spectra of CF_3H and CF_2H_2 and for his cooperation in making the fundamental frequency assignment used in the calculations. Dr. W. H. Pearlson and Mr. D. G. Weiblen of the Minnesota Mining and Manufacturing Company provided help in the case of CF_3H in the form of samples and information concerning its infra-red spectrum.

[12] J. C. Decius, J. Chem. Phys. **16**, 214 (1948).

Vibrational Spectra of Some Fluoromethanes*

D. H. RANK AND E. R. SHULL
Spectroscopy Laboratory, Pennsylvania State College, State College, Pennsylvania

AND

E. L. PACE
Morley Chemical Laboratory, Western Reserve University, Cleveland, Ohio

(Received February 14, 1950)

Depolarization measurements have been made on the Raman spectrum of fluoroform and difluoromethane. Several new lines were observed, all of which had previously been found in infra-red absorption. Several weak lines reported previously could not be found and presumably must be ascribed to impurities in the material used by earlier investigators. The analyses given for the vibration spectra now seem to be in plausible agreement with all the known spectroscopic data on these molecules.

NUMEROUS investigators have made attempts to analyze the vibration spectra of the fluoromethanes. All of these attempts at analysis have been made in the absence of complete spectroscopic data since polarization measurements on the Raman spectra were not available. We have attempted to rectify this situation by obtaining depolarizations for the Raman lines of fluoroform and difluoromethane in the liquid state.

The Raman spectrum of liquid fluoroform has been measured and discussed by Glockler and Leader[1] and Glockler and Edgell.[2] Bernstein and Herzberg[3] have investigated the absorption bands of fluoroform in the near infra-red and have given a vibrational analysis based on their work and the unpublished work of W. C. Price which was obtained in the middle infra-red region of the spectrum.

The Raman spectrum of difluoromethane was obtained by Glockler and Leader[4] and analyzed by Wagner.[5] More recently Stewart and Nielsen[6] have made an extensive infra-red investigation of this molecule.

EXPERIMENTAL

The apparatus used in this investigation was the same as that described previously[7] with modifications described in a more recent paper.[8] In addition, very strong exposures were made with the F/2.0 camera using praseodymium filters[9] in an attempt to find the 936 cm^{-1} frequency of fluoroform reported by Glockler and Leader.[1] In spite of favorable experimental conditions for the observation of this frequency we were unable to find any trace of this line and thus must conclude that the source of this line had been an impurity in the fluoroform used by the previous investigators. Likewise in the spectrum of difluoromethane the frequencies 746 cm^{-1} and 1294 cm^{-1} were not observed, although weaker lines whose infra-red analogues had previously been measured by Stewart and Nielsen[6] made their appearance. Polarization observations were made using the method of polarized incident light[10] which has been in use in this laboratory for the past several years.

DISCUSSION OF SPECTRA

(A) Fluoroform

We have tabulated the conclusions drawn by previous investigators and given our own assignments in Table I. We have also included for comparison purposes the assignment for chloroform given by Herzberg.[11] With regard to the chloroform assignment there is little doubt since the deuterium isotope displacements were observed many years ago by Wood and one of us.[12] More recently the chlorine isotope effect has also been measured in this spectrum.[13] In addition, precise depolarization measurements have been made on these lines.[10,14]

The assignments given by Bernstein and Herzberg[3] ignore the very strong polarized Raman line at 1117 cm^{-1} which almost certainly must be $\nu_2^{CF}(a_1)$. In addition, the polarizations of the 508 cm^{-1} and 697 cm^{-1} lines and the chloroform analogy strongly support the original assignment of Bernstein and Herzberg and contradict their reversal of this assignment in a note added in proof in their paper. The situation now exists that there is a one to one correspondence between the infra-red and Raman spectrum with the single exception that the most highly symmetrical frequency does not appear in the infra-red spectrum. It is certain that this

* This research was carried out on Contract N6onr-269, Task V of the ONR.

[1] G. Glockler and G. R. Leader, J. Chem. Phys. **8**, 699 (1940).
[2] G. Glockler and W. F. Edgell, J. Chem. Phys. **9**, 224 (1941).
[3] H. J. Bernstein and G. Herzberg, J. Chem. Phys. **16**, 30 (1948).
[4] G. Glockler and G. R. Leader, J. Chem. Phys. **7**, 382 (1939).
[5] J. Wagner, Zeits. f. physik. Chemie B45, 69 (1939).
[6] H. B. Stewart and H. H. Nielsen, Phys. Rev. **75**, 640 (1949).
[7] Szasz, Sheppard, and Rank, J. Chem. Phys. **16**, 704 (1948).
[8] Rank, Shull, and Axford, J. Chem. Phys. **18**, 392 (1950).
[9] Rank, Sheppard, and Szasz, J. Chem. Phys. **17**, 84 (1949).
[10] A. E. Douglas and D. H. Rank, J. Opt. Soc. Am. **38**, 281 (1948).
[11] G. Herzberg, *Infrared and Raman Spectra* (D. Van Nostrand Company, Inc., New York, 1945), p. 316.
[12] R. W. Wood and D. H. Rank, Phys. Rev. **42**, 63 (1935).
[13] D. H. Rank and J. A. VanHorn, J. Opt. Soc. Am. **36**, 454 (1946).
[14] D. H. Rank, J. Opt. Soc. Am. **37**, 798 (1947).

TABLE I. Vibrational analysis of the fluoroform spectrum (R—Raman active; I—Infra-red active; B—Blend; P.Pol.—partially polarized. $\Delta\nu$ given in cm^{-1}).

Glockler and Edgell[a] (Liq.)		Fluoroform Bernstein and Herzberg[b] (Gas)		This work (Liq.)			Chloroform Herzberg[c]		Reference[d,e]
$\Delta\nu$	Assign.	Infra-red	Assign.	$\Delta\nu$	Pol.	Assign.	Assign.	$\Delta\nu$	ρ
508.1(5)	ν_{45}	509.4	$\nu_6(e)$	508(v.s.)R	Dep.	$\nu_6^{CF_3}(e)$	$\nu_6^{CCl_3}(e)$	262.0(v.s.)	0.86
696.7(6)	ν_6	703.2(m)	$\nu_3(a_1)$	697(s)R	P.Pol.	$\nu_3^{CF_3}(a_1)$	$\nu_3^{CCl_3}(a_1)$	365.9(s)	0.13
936.8(0)	ν_3								
1116.5(8)	ν_1			1117(v.s.)R	P.Pol.	$\nu_2^{CF}(a_1)$	$\nu_2^{CCl}(a_1)$	668.3(s)	0.026
		1152.4(v.s.)	$\nu_5^{CH}(e)$	1160(w) B R	Dep.	$\nu_5^{CF}(e)$	$\nu_5^{CCl}(e)$	761.2(s)	0.93
		1209(m)	$\nu_2^{CF}(a_1)$	1209 I		$\nu_6+\nu_3$			
1376.2(3)	ν_{89}	1351.5(s)	$\nu_4^{CF}(e)$	1376(s) R	Dep.	$\nu_4^{CF}(e)$	$\nu_4(e)$	1215.6(m)	0.83
3062.0(10)	ν_7	3035.6(s)	$\nu_1^{CH}(a_1)$	3062(s) R	Pol.	$\nu_1^{CH}(a_1)$	$\nu_1^{CH}(a_1)$	3018.9(s)	0.24

[a] See reference 2.
[b] See reference 3.
[c] See reference 11.
[d] See reference 10.
[e] See reference 14.

TABLE II. Vibrational analysis of the spectrum of difluoromethane (I—Infra-red; P.Pol.—partially polarized; S.Pol.—strongly polarized; Dep.—depolarized. $\Delta\nu$ given in cm^{-1}).

Vibrational spectrum of difluoromethane							Vibrational spectrum of dichloromethane[c]		
Wagner[a]		Stewart and Nielsen[b]		This work					
$\Delta\nu$[d]	Assign.	ν	Assign.	$\Delta\nu$	Pol.	Assign.	$\Delta\nu$	Pol.	Assign.
532(5)	ν_4	528.6	$\nu_4(a_1)$	532(m)	P.Pol.	$\nu_4(a_1)$	283(s)	Pol.	$\nu_4^{CCl_2}(a_1)$
746(00)	$\nu_3-\nu_4$								
1054(s)	$2\nu_4$			1054(m)	Dep.	$2\nu_4$			
1079(10)	ν_3			1078(v.s.)	S.Pol.	$\nu_3(a_1)$	700(v.s.)	Pol.	$\nu_3^{CCl}(a_1)$
		1089	$\nu_9(b_2)$	1089 I		$\nu_9(b_2)$	736(s)	Dep.(?)	$\nu_9^{CCl}(b_2)$
		1176	$\nu_7(b_1)$	1170(v.w.)	Dep.	$\nu_7(b_1)$	898(v.w.)	Dep.(?)	$\nu_7(b_1)$ (rocking)
		1116	$\nu_3(a_1)$						
1262(9)	ν_9	1262	$\nu_2(a_1)$	1262(s)	S.Dep.	$\nu_5(a_2)$	1148(w)	Dep.	$\nu_5(a_2)$? (torsion)
1294(0)	ν_5								
		1435	$\nu_8(b_2)$	1435(w)	Dep.	$\nu_8(b_2)$	1255(v.w.)		$\nu_8(b_2)$ (rocking)
1509(3)	ν_8, ν_2	1509	$\nu_5(a_2)$	1508(m)	P.Pol.	$\nu_2(a_1)$	1417(m)	Dep.	$\nu_2^{CH_2}(a_1)$
2837(4)	Not assigned			2837(m)	P.Pol.	$2\nu_8$			
2963(10)	ν_1	2949	$\nu_1(a_1)$	2963(s)	S.Pol.	$\nu_1(a_1)$	2985(s)	Pol.	$\nu_1^{CH}(a_1)$
3030	ν_6	3015.2	$\nu_6(b_1)$	3030(s)	P.Pol.	$\nu_6(b_1)$	3045(s)	Dep.	$\nu_6^{CH}(b_1)$

[a] See reference 5.
[b] See reference 6.
[c] See reference 11.

frequency, 1117 cm^{-1} would be very weak if it is allowed at all in the infra-red. Inspection of A.P.I. spectrogram No. 741† of fluoroform shows that the weak 1117 cm^{-1} band would be completely masked by the very strong 1152 cm^{-1} band. Further inspection of this same spectrogram shows that the intensity of the 1209 cm^{-1} band is relatively small and with a view of the total spectroscopic situation, this band must be regarded as a combination band.

(B) Difluoromethane

We have tabulated the assignments of previous investigators as well as our own assignments in Table II. We have included the vibrational assignments for dichloromethane[11] for comparison purposes. It is to be noted that the notation used by Herzberg interchanges ν_8 and ν_9 when compared to that used by Stewart and Nielsen.[6]

Theoretically all nine vibrational frequencies should be Raman active. There can be no doubt concerning the assignments of $\nu_4(a_1)$, $\nu_3(a_1)$ and $\nu_1(a_1)$ when one considers the frequency, polarization and intensity of the Raman lines alone. It seems reasonable to assign the line at 1508 cm^{-1} to $\nu_2(a_1)$ since it shows definite evidence of being polarized and in addition, this mode has previously been assigned to the highest frequency line of the 1200 to 1400 cm^{-1} group of frequencies in the dichloromethane spectrum. The assignment of $\nu_6(b_1)$ follows unequivocally from polarization and frequency. It can be seen that the b_1 type group is taken care of completely by assignment of 1176 cm^{-1} to $\nu_7(b_1)$ by Stewart and Nielsen[6] from rotational structure considerations.

Thus, there are only three fundamental frequencies left which remain to be definitely assigned, namely two of species B_2 and one of species A_2, all of which should be

† Presumably this spectrogram is part of the "unpublished work of W. C. Price" referred to by Bernstein and Herzberg (see reference 3). Unfortunately the 509 cm^{-1} band is not included on the spectrogram.

depolarized in the Raman spectrum. There are exactly enough remaining lines in the Raman spectrum having the correct polarizations to make the necessary assignments. Stewart and Nielsen[6] have shown unequivocally that two parallel bands appear in the infra-red at 1089 cm^{-1} and 1435 cm^{-1} which belong to the symmetry type B_2. One of these (1435 cm^{-1}) we have observed as a depolarized line in the Raman spectrum. In addition, there is evidence that 1089 cm^{-1} is present in the Raman spectrum although unresolved from the strong polarized 1078 cm^{-1} line. (Photographs of the "weak component," i.e., parallel polarized exciting light, show a definite broadening of the 1078 cm^{-1} line just as though an unresolved weak depolarized line was present.) In this case we shall assign $\nu_9(b_2)$ and $\nu_8(b_2)$ to 1089 cm^{-1} and 1435 cm^{-1} in agreement with Stewart and Nielsen. We shall assign the 1262 cm^{-1} depolarized line as $\nu_5(a_2)$ and ascribe the remaining Raman line 1054 cm^{-1} frequency to the harmonic of $\nu_4(a_1)$. The intensity of this line seems to be rather large for a harmonic, but it is well known that in the Raman spectrum of methane a harmonic appears which is stronger than its fundamental. A theoretical treatment of the force constants of the fluoromethanes will appear in a subsequent paper by Dr. Pace.

We are greatly indebted to Dr. W. H. Pearlson of the Minnesota Mining and Manufacturing Company for supplying us with the fluoroform sample and to Dr. W. S. Murray of Kinetic Chemicals, Inc., Jackson Laboratory, Wilmington, Delaware, for the difluoromethane sample.

THE JOURNAL OF CHEMICAL PHYSICS VOLUME 18, NUMBER 6 JUNE, 1950

Stability of Color Centers in Alkali Halides

RUTH CASLER, PETER PRINGSHEIM, AND PHILIP YUSTER
Argonne National Laboratory, Chicago, Illinois

(Received February 2, 1950)

Color centers have been formed in alkali halide crystals by exposing them to x-rays, electron bombardment, and pile irradiation, and their stability with respect to temperature and light bleaching has been investigated. In general such crystals contain centers of non-uniform stability. The lower the temperature at which the color centers have been produced, the more unstable they are on the average. In the absorption spectra taken at low temperature of crystals irradiated at low temperature new bands appear on the short wave-length side of the *F*-band which are never observed in crystals irradiated at room temperature and which, on warming the crystal to room temperature, vanish together with a part of the *F*-centers. It is suggested that the instability of some of the color centers formed at low temperature is connected with the presence of these new absorption bands.

AT an early date Przibram and his co-workers stated that color centers produced photo-chemically in alkali halide crystals do not have a uniform stability and that, for instance, the centers in strongly colored crystals seem to be relatively more stable than those in crystals which have received only a weak irradiation.[1] Although occasionally mentioned since then, the subject of stability is little treated in the extensive literature dealing with color centers.

Unfortunately, the problem is complicated by the fact that the behavior of a given salt, such as NaCl or LiF, depends greatly on the origin of the material, its purity, preceding heat treatment, strains, etc. All crystals used in the experiments described in the following were obtained from the Harshaw Chemical Company and underwent no other treatment than exposure in the Argonne pile, irradiation with soft or hard x-rays or with γ-rays, or bombardment with 1-Mev electrons at various temperatures. In samples cleaved from the same single crystal, color centers which are produced under different conditions vary greatly with respect to their stability, and even the centers produced in a given crystal by a particular treatment have by no means all the same stability.

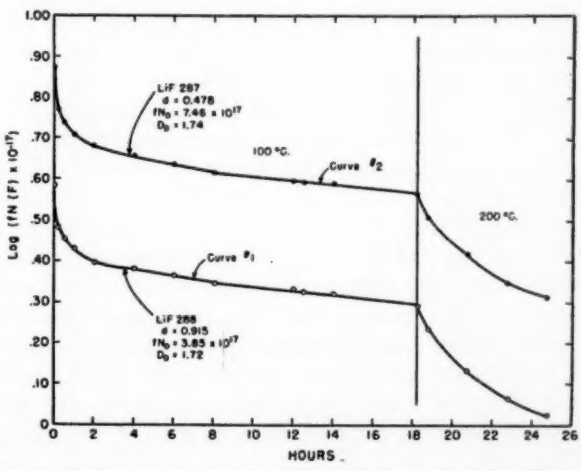

FIG. 1. Temperature bleaching of two LiF samples with different *F*-center concentrations, $N(F)$.

[1] For instance, Wien. Ber. 135, 202 (1926).

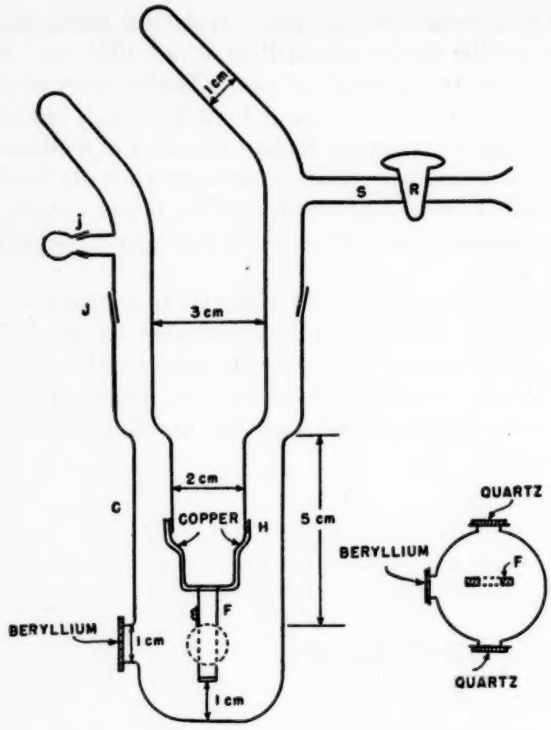

FIG. 2. Tube for irradiating and observing crystals at low temperatures.

During the period immediately following an irradiation by which color centers have been formed in a crystal, the intensity of their coloration in general decreases even if the crystals are kept in the dark at room temperature. Later these losses become much smaller, and, for instance in the case of LiF, the peak of the absorption band at 2480A does not drop by more than a few percent in several months. As soon as the temperature is appreciably raised, the optical density at the peak of the F-band $[D(F)]$ again begins to decrease. This is shown in Fig. 1 for two samples of LiF which had been exposed to a very penetrating radiation, so that the distribution of F-centers is quite uniform throughout the volume. Under these conditions the value of $D(F)$ is proportional to the concentration of F-centers per cc. The numerical value of $N(F)$ can be derived from data which, with the exception of the oscillator strength f, are all known. In the curves of Fig. 1, the drop of $N(F)$ is very steep at first and the curve becomes much flatter later.

Curves 1 and 2 in Fig. 1 represent the decay at 100°C of two LiF crystals with nearly the same $D(F)$, while their $N(F)$ values are in the ratio 1:2, one crystal being twice as thick as the other. Although at $t=0$ the $N(F)$ of Curve 1 is even lower than the $N(F)$ of Curve 2 at $t=18$ hours, the initial slope of Curve 1 is as steep as that of Curve 2 and by no means as flat as the final slope of the latter after 18 hours at 100°C.* Thus every interpretation of the color center decay based on the hypothesis that the course of the decay curves is primarily determined by the density of the various centers is inadequate. It is certain that at a high concentration of F-centers and positive holes and a correspondingly low concentration of negative ion vacancies the recombination of an electron which has been released from an F-center with a positive hole is high and the recapture by a negative ion vacancy is small, while at low F-center concentration the opposite is true. But, if this were the main reason for the decreasing slope of the curves representing the optical density as a function of time, Curve 1 in Fig. 1 would not start with a slope much steeper than the slope of Curve 2 after 18 hours at 100°C.

Although an unequal binding energy of electrons in F-centers with absorption bands identical in peak wavelength and half-width is highly improbable, the existence of F-centers of different stabilities in a crystal is not only shown by the decay curves, but it has been proved experimentally that the relative numbers of centers of different stabilities greatly depend on the conditions under which they are formed. The absorption spectra of crystals of LiF, NaCl, KCl, and KBr which had been exposed at various temperatures to the same doses of soft x-rays (50 kv, 45 ma, beryllium windows, 10 cm from the target) were measured after having been cooled down to liquid N_2 temperature immediately at the end of the exposure so that for every compound all measurements were performed at equal half-widths of the bands. The tube used in these experiments is represented in Fig. 2; it differs from similar tubes, for instance the one described by Flechsig,[2] in that the copper frame, F, serving as crystal holder can be rotated with respect to the windows by means of the ground joint, J. Two windows made of quartz allow the observation of the crystal in transmitted light. Through the third window which is covered with a beryllium foil, the crystal, rotated by 90° from the former position, can be exposed to x-rays or electron bombardment. The crystal holder is soldered to the copper bottom of a Housekeeper seal which forms the lower part of the container for the cooling bath. The leads for a thermocouple in contact with the crystal holder can be introduced through the small ground joint, j. The upper part of the tube, which, when assembled and evacuated, forms a Dewar vessel, is curved in such a way that the cooling liquid does not overflow when the crystal is irradiated in a horizontal position. The larger absorption chamber provided for the Beckman spectrophotometer has been adapted so that the cooling tube can be inserted into it together with a holder for a blank.

Table I lists, under "a," the optical densities at the F-band peaks of four alkali halides which, under the

* After prolonged annealing at high temperatures the shape of the F-band of LiF altered appreciably. However, all points on Fig. 1 were obtained in the annealing range in which such changes play no part.

[2] W. Flechsig, Zeits. f. Physik **36**, 605 (1926).

TABLE I. Optical density, $D(F)$, of crystals irradiated with x-rays at various temperatures and measured at −185°C. (a) Measured immediately after irradiation; (b) measured after having stood at +25°C for one hour.

Temp. of irradiation	−185°C a	−185°C b	−75°C a	−75°C b	+25°C a	+25°C b
KBr	1.28	0.12	1.96	1.27	0.47	0.44
KCl	1.20	0.40	3.0	1.5	0.87	0.85
NaCl	0.31	0.21	1.48	1.3	1.07	1.06
LiF	0.51	0.25	1.13	0.95	1.89	1.89

conditions mentioned above, were obtained after exposures at −185, −75, and +25°C. The table lists, under "b," the optical densities of the same crystals after having been allowed to warm up to room temperature for one hour and then cooled again to −185°. According to a recent paper published by Harten[3] the data contained in Table I are somewhat fortuitous insofar as the relative values of the $D(F)s$ at various temperatures differ depending on the duration of the exposure to x-rays. At higher temperatures the initial rise of $D(F)$ with time is steeper but it soon reaches an equilibrium value. The initial rise is slower at low temperatures, but the value attained after a long-lasting exposure may be appreciably higher than can be reached at higher temperatures. Thus, after a very short irradiation with x-rays, $D(F)$ would probably increase for all crystals* with increasing temperature during the exposure. Only LiF shows such a behavior in Table I, while, according to the data in this table, an optimum temperature seems to exist for the formation of F-centers in the other crystals. Although this may be correct only after exposure to sufficiently large doses, it leads to the conclusion that two effects counteracting each other must participate in the process: a potential barrier opposing the formation of F-centers at low temperature, and another potential barrier opposing their destruction and causing an increasing instability with increasing temperature.

In the formation of F-centers, electrons must pass through the conduction band. It seems natural to assume that the conduction band is more or less disturbed in the neighborhood of every singularity in the lattice, such as a negative ion vacancy, and that this perturbation is equivalent to a potential barrier which the electron must overcome before it can combine with the negative vacancy. On the other hand, it has been assumed that the first u.v. absorption band of alkali halide crystals does not correspond to the transfer of an electron into the conduction band but into an excited state. If this is true, the passage of a high speed electron in the vicinity should also produce such excited states, and only if the thermal energy suffices, will such electrons be raised into the conduction band and eventually form F-centers. There is no doubt, of course, that once an electron is trapped in an F-center, it must be supplied with considerable energy in order to be released from the center. However, it may even be possible that such an electron, after having reached the conduction band, must still overcome a potential barrier for recombining with a positive hole.

The high degree of instability of the centers formed at low temperature, especially in the case of KBr and somewhat less of KCl as demonstrated by a comparison of the columns "a" and "b" in Table I, is very striking. The former loses 90 percent and the latter 66 percent of its F-centers when heated to room temperature after exposure at −185°C (Fig. 3). Even when heated from −185° to −75° the peak of the KCl-band drops by 31 percent. The drop is much smaller when crystals exposed at −75° are warmed up to room temperature. Compared with centers formed at low temperatures, those which are produced at room temperature are relatively stable as long as the temperature is not raised to a higher level. Figure 4 shows the behavior of four KBr crystals, two of which were irradiated at −75° and the others at +30°. The $D(F)$ of the latter is, after a relatively small drop during the first hour, almost constant, while the other curves slope continuously downward even after 120 hours.

The binding energy of electrons in F-centers of additively colored alkali halides has been derived by Smakula from the electronic conductivity of such crystals as a function of the temperature.[4] He found these energies somewhat less than one-half of the excitation energy of the F-centers. According to Smakula, the binding energy is 0.94, 1.0, and 0.84 ev for NaCl, KCl, and KBr, respectively. A difference in

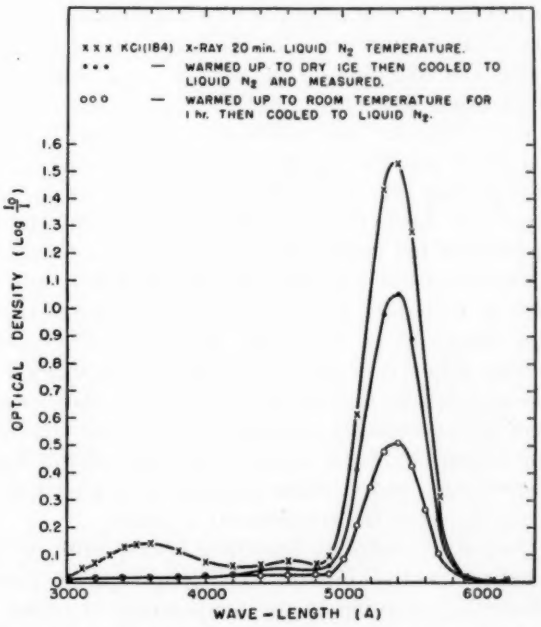
x x x KCl(184) X-RAY 20 min. LIQUID N2 TEMPERATURE.
• • • — WARMED UP TO DRY ICE THEN COOLED TO LIQUID N2 AND MEASURED.
o o o — WARMED UP TO ROOM TEMPERATURE FOR 1 hr. THEN COOLED TO LIQUID N2.
OPTICAL DENSITY (Log I0/I)
WAVE-LENGTH (A)
3000
4000
5000
6000

FIG. 3. Absorption bands of KCl after irradiation at liquid N_2 temperature and after warming up to dry ice and to room temperature.

[3] H. U. Harten, Zeits. f. Physik **126**, 619 (1949).
* In Harten's paper this is proved only for KCl.

[4] A. Smakula, Göttinger Nachrichten **1**, 55 (1934).

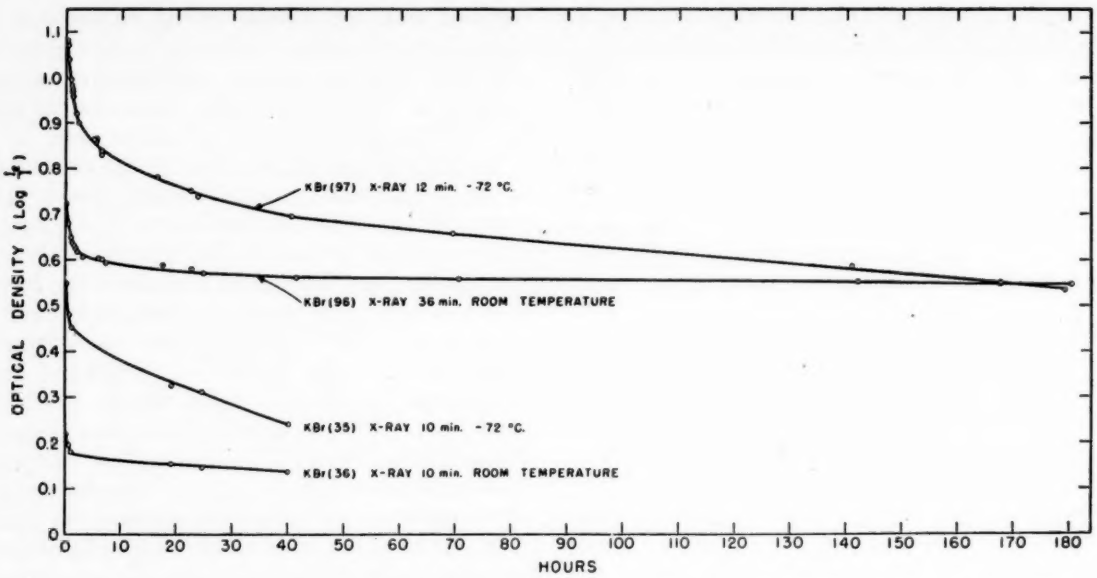
OPTICAL DENSITY (Log $\frac{I_0}{I}$)
KBr(97) X-RAY 12 min. -72 °C.
KBr(98) X-RAY 36 min. ROOM TEMPERATURE
KBr(35) X-RAY 10 min. -72 °C.
KBr(36) X-RAY 10 min. ROOM TEMPERATURE
HOURS

FIG. 4. Spontaneous bleaching at room temperature of KBr crystals x-rayed at dry ice and at room temperature.

binding energy in F-centers produced photo-chemically, but with absorption bands identical in peak wave-length and half-width, can hardly be expected.

It does not seem very probable that, with such high binding energies, the F-bands of KBr and KCl could decay so easily at such low temperatures. With an ionization energy $E=1$ ev the mean lifetime τ of an F-center at 200°K would be of the order of magnitude of 10^4 years, as derived from the equation $1/\tau=s\cdot e^{-E/kT}$ with $s=10^{13}$. For smaller values of s, τ would be even larger, while with $E=0.6$ ev one obtains at 200°K, $\tau=160$ sec., of the right order of magnitude. It is not even certain, however, that the main loss of F-centers during the warming-up period does not occur at a temperature well below 200°K. Thus one must either admit a thermal ionization energy of the F-centers very much smaller than that given by Smakula, or one must assume that the spontaneous bleaching of F-centers at low temperatures is not due to electrons being raised from the ground state of these centers into the conduction band and then recombining with positive holes or V-centers, but to a more direct recombination with some sort of V-centers. As will be discussed in another paper, it is certain that more than one kind of V-center can be formed in a crystal and that some of them are exceedingly unstable so that their characteristic absorption band is observed only at the lowest temperatures and vanishes together with a part of the F-centers, when the temperature is raised.

Even with regard to bleaching by exposure to light absorbed in the F-band (F-light), crystals behave differently according to the temperature at which the color centers were formed. Table II shows the behavior of six KCl crystals which were exposed to x-rays at various temperatures and subsequently bleached by exposure to the radiation from an AH4 Hg-arc lamp through a filter opaque to all wave-lengths below the green Hg line. Thus the bleaching was mostly due to the green and yellow Hg-lines absorbed in the F-band but the spectrum of the lamp contains sufficient intensity in the orange and red to suppress, at least partially, the formation of F'-, R-, and M-bands. The third line of the table lists the initial light absorption at the F-band peak in the various crystals and proves that the differences in bleaching efficiency are in no instance caused by a difference in light absorption. At −185°C the crystal which had been exposed to x-rays at −185° was bleached much more than those in which the F-centers had been formed at higher temperatures. The same holds for a comparison of the bleaching rate at −75°C of the crystals exposed to x-rays at −75° and +25°C, respectively.

If crystals have received so large x-ray doses that they are opaque to F-light and their $D(F)$ can be determined only by extrapolation, crystals that were exposed at −185°C can still be completely bleached by irradiating them with F-light, while this becomes practically impossible for crystals x-rayed at room temperature. Thus the $D(F)$ of a KCl crystal which, after exposure to x-rays at −185° and subsequent warming to room temperature, had a $D(F)=7$ dropped under the action of bleaching light in three hours to 0.5 and in six hours to 0.015, while another KCl sample exposed at room temperature to x-rays and showing an initial

TABLE II. KCl crystals exposed to x-rays and bleached by F-light at various temperatures.

Temperature of							
	x-ray exposure	−185	−75	+25	−75	+25	+25
	bleaching	−185	−185	−185	−75	−75	+25
Initial absorption		99%	99%	97.5%	99%	91%	92%
Drop of $D(F)$ in 20 min.		14%	7%	6%	48%	35%	63%

$D(F)=3.7$ was bleached in five hours to $D(F)=1.8$, and even after 67 hours it still exhibited a $D(F)=0.75$.

On the other hand, the rate of bleaching by F-light is practically independent of the density of F-centers in the crystal. The two sets of curves in Fig. 5 represent the optical densities in the F-band of two samples of LiF with initial F-center concentrations $fN_0(F)=5.18\times10^{17}$ and 2.36×10^{17} per cc and of thicknesses $d=0.389$ mm and 0.968 mm, respectively, so that their initial optical densities were very nearly the same. The crystals were bleached by exposure to the light of a germicidal lamp with 90 percent of the energy in the Hg line 2537A. The various curves were obtained after successive bleaching periods of ten minutes each, except the second curve which corresponds to a bleaching period of only five minutes. The very slight difference in the rate of bleaching appearing in the two sets of curves may be fortuitous; but if it is real, then against expectation the rate is even a little greater in the crystal of the smaller F-center concentration.

When crystals containing F-centers are bleached by irradiation with F-light, electrons are raised in the primary process from the ground state of F-centers to their first excited state; from here they need only small additional energies provided by thermal fluctuations for reaching the conduction band. The low bleaching yield at the lowest bleaching temperatures is, in the main, a natural consequence of these conditions. Already at -78°C, however, every absorbed photon transfers an electron into the conduction band according to Pick.[5] The difference in bleaching yield for centers of identical absorption bands at the same temperature cannot be due to the nature of the F-centers themselves; it can only be due to the receiving end of the process, namely, to the probability of electrons in the conduction band recombining with positive holes which have been stabilized as V-centers. In other words, there are various types of V-centers, characterized by different absorption bands. Only the most unstable of these, with peak at about 3600A, is shown on Fig. 3. At least two other V-bands of higher stability are located in the spectral range between 3000 and 2100A. The various V-centers are characterized by different energies of formation: the positive holes must overcome certain potential barriers before they are stabilized as V-centers, for instance by being "captured" by a positive ion vacancy;[6] and therefore the relative numbers of different types of V-centers depend on the temperature of exposure to x-rays. The capturing cross-sections of the various V-centers for electrons in the conduction band, or rather the potential barriers which the electrons have to overcome in order to recombine with a positive hole, are also different for the different V-centers. If this recombination probability is very low at a given temperature, the recapture of the electron by a negative vacancy becomes relatively large and the F-centers appear to be more stable. These questions together with somewhat similar ideas recently proposed by Alexander and Schneider[7] will be discussed more at length in a subsequent paper. It may be mentioned here, however, that the stability of F-centers depends also on the nature of the radiation by which they were produced. It is smallest after exposure to 1-Mev electrons from a Van de Graaff machine, higher after exposure to soft x-rays from a 50 kv x-ray tube with beryllium window, and highest after exposure to the harder x-rays from the same source filtered through 2 mm of aluminum. Also, here the difference in stability corresponds to the prevailing formation of one or another type of V-band. Furthermore Przibram's result, quoted in the introduction, was confirmed for KCl and KBr; F-centers produced during very short periods (one minute) of exposure to soft x-rays are appreciably less stable than those produced by longer lasting exposure to x-rays of the same intensity. However, under these conditions the V-bands were much too weak and too unstable to be measured.

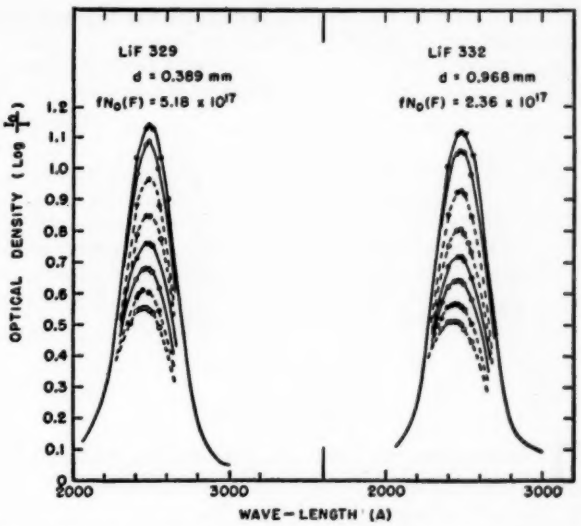

FIG. 5. Bleaching by F-light of two LiF crystals of equal optical densities and different F-center concentrations.

[5] H. Pick, Ann. d. Physik **31**, 365 (1938).
[6] F. Seitz, Rev. Mod. Phys. **18**, 384 (1946).
[7] J. Alexander and E. E. Schneider, Nature **164**, 653 (1949).

The Raman Spectrum of Vinylidene Fluoride*

WALTER F. EDGELL** AND WILLIS E. BYRD
Department of Chemistry, The State University of Iowa, Iowa City, Iowa
(Received January 12, 1950)

The Raman spectrum of vinylidene fluoride has been obtained in the liquid state at −100 to −125°C. The observed frequencies were assigned to the fundamental modes of vibration (and several combinations of these) with the aid of the infra-red data in the literature supplemented by some measurements in our laboratory. A normal coordinate treatment of the vibrations has been carried out using a *simple* valency force field plus one additional term depending upon the square of the change in the F−F distance. It is shown that the repulsion between the F atoms and between each F atom and the π-electrons of the double bond are of major importance.

INTRODUCTION

THE nature of the molecular structure and intramolecular forces in fluorine-containing molecules is of much interest. Vinylidene fluoride was chosen for study because it contains a CF_2 group relatively "isolated" from the rest of the molecule and because isotopic modifications could be prepared with relative ease. Thus it should be possible to obtain eventually, for example, a relatively complete and accurate description of the potential function. This paper is concerned with the Raman spectrum of liquid vinylidene fluoride on which a preliminary report has already appeared.[1]

PREPARATION

The vinylidene fluoride was prepared by pyrolysis of commercial CF_2ClCH_3. The starting material was withdrawn from its cylinder and slowly passed through a platinum tube maintained at about 580 to 600°C. The cracked gases were passed through a cooling tube, a safety bottle and then through an alkali scrubbing tower to remove the acid. From here the gas passed over anhydrous $CaCl_2$ and then over soda lime. Then it was precooled in a trap immersed in dry-ice and acetone and condensed in a liquid air-cooled trap, whose exit tube was protected from the moisture and CO_2 of the air with soda lime and $CaCl_2$. With the above procedure cracking was incipient at about 540°C; at temperatures much above 625°C carbonization took place and some liquid products were formed.

The vinylidene fluoride was purified by distilling from a trap in dry-ice acetone slush to a trap in liquid air, followed by distillation through a Podbelniak column. The material distilled at constant temperature, and a center cut was taken for the spectrographic work.

To test the identity of the compound its molecular weight was determined in a simple gas density balance using a tank of O_2 (from which the water and CO_2 had been removed) as a standard. The average of four runs was 64.58 as compared to a formula value of 64.04; no corrections for the deviation of the gases from the ideal gas law were made.

EXPERIMENTAL

The Raman effect was studied in the liquid state at −100 to −125°C using a Lane-Wells spectrograph. This is a fast spectrograph having a camera of aperture ratio $F/3.5$ somewhat similar to the Schmidt type. The standard Lane-Wells excitation unit was used with the current through the mercury arcs varying from about 11 to 28 amperes in different runs. Very little general background appears on the films with this equipment at the lower currents when care is taken to obtain an optically clear sample. For most of the runs the general background was reduced with Rhodamine-on-cellophane filters.[2] Excitation by 4046A was eliminated with a Wratten 2*A* filter.

The filter jacket of the excitation unit was replaced by a Dewar with plane windows, which contained the Raman tube. The sample was maintained in the liquid state at the desired temperature by a stream of cold, dry air that had passed through coils in dry-ice acetone slush and liquid air.

The Raman spectrum was recorded on Eastman Tri-X Panchromatic films. A slit width of 50 microns was used and the exposures varied from $\frac{1}{4}$ to 10 hours. The frequencies were calculated from the Hartmann dispersion formula using argon as the reference spectrum. The precision of the frequency shifts was at least as good as ± 2 cm^{-1}. Qualitative polarization data for the stronger lines were obtained with Polaroid cylinders.

The results obtained are listed in Table I. All the lines reported have been observed on more than one film. However, the line at 714 cm^{-1} was observed only on the films of greatest exposure and then only very faintly. It is quite possible that it may be due to an impurity present in small amounts. Besides the lines listed, weak lines were found shifted 857 and 1667 cm^{-1} from 4358A. These are believed to be the fundamentals at 915 and 1728 cm^{-1} excited by 4348A. This interpretation is supported by polarization indications and the

* Presented before the Symposium on Fluorine Chemistry of the 116th Meeting of the American Chemical Society.
** Present address: Chemistry Department, Purdue University, Lafayette, Indiana.
[1] Walter F. Edgell and W. Byrd, J. Chem. Phys. **17**, 740 (1949).
[2] John Haskin, Ph.D. Thesis, State University of Iowa, 1948.

fact that these fundamentals give rise to the strongest Raman lines.

DISCUSSION

The microwave spectrum of vinylidene fluoride has been studied by Roberts and Edgell.[3] Their results show that this planar molecule is almost an oblate symmetric top with effective moments of inertia in the ground state of 156.946×10^{-40}, 80.450×10^{-40} and 76.257×10^{-40} g cm^2. The figure axis is the axis of least moment of inertia.

The infra-red spectrum has been studied by Torkington and Thompson.[4] A survey of the infra-red spectrum with low dispersion was made in this laboratory[5] with results essentially in agreement with those earlier reported. However, we do not observe the band centering at about 675 cm^{-1} shown in earlier work[4] as about four times as intense as 612 cm^{-1}. Instead a band somewhat weaker than 612 cm^{-1} is found at about 638 cm^{-1} with a shoulder at about 649 cm^{-1} together with a much weaker band centering at about 679 cm^{-1}. A comparison of the Raman and infra-red results shows the typical liquid-vapor shifts so characteristic of the C—H motions in molecules containing both F and H atoms.

The molecule belongs to the point group C_{2v} for which the selection rules are well known.[6] Reduction of the representation formed by the vibrational coordinates yields: $\Gamma=5A_1+A_2+4B_1+2B_2$. With the above moments of inertia the A_1, B_1 and B_2 fundamentals give rise to type A, B and C bonds[7] respectively in the infra-red. All fundamentals are Raman active. The five A_1 fundamentals may be approximately described as C—F, C—H and C=C stretching vibrations and CH_2 and CF_2 deformation vibrations. The A_2 frequency is torsional and will consist primarily in the motion of the CH_2 group. For the B_1 vibrations the motions are the antisymmetrical C—H and C—F stretching modes and the rocking of the CH_2 and CF_2 groups. The two B_2 modes will consist of the in-phase and out-of-phase wagging of the CF_2 and CH_2 groups. Here again the CH_2 group should have the greater amplitude in both modes.

A comparison of the data with the requirements of the selection rules makes it possible to assign the Raman lines at 3101, 1728 and 915 to the C—H, C=C and C—F stretching vibrations of class A_1 and the lines at 810 and 949 cm^{-1} to the B_2 wagging and the B_1 CH_2 rocking modes respectively. These correspond to the strong infra-red bands at 3055, 1734, 924, 803 and 954 cm^{-1}, all of which have the correct band types. The antisymmetrical C—F and C—H stretching frequencies are the lines at 1280 and 3171 cm^{-1}, respectively, which correspond to infra-red bands of proper type at 1300 and 3140 cm^{-1} respectively. The former frequency shows its characteristic weakness in the Raman spectrum and strength in the infra-red. There is little doubt that the frequency found in the Raman and infra-red spectrum at 549 cm^{-1} is the CF_2 deformation vibration. Its order of magnitude is as expected; its band type is clearly A; and it appears polarized in the Raman effect.

There remains the Raman lines at 449, 603 and 1359 cm^{-1} of at least moderate intensity, which correspond to no strong infra-red bands (449 is beyond the region of reported observation). Yet unassigned are the frequencies of the A_1 CH_2 deformation mode, the B_2 wagging mode, the B_1 CF_2 rocking mode, and the A_2 torsional mode. The first should appear at about 1400 cm^{-1}, the last between 600 and 800 cm^{-1}, and the other two somewhat lower than the torsional region. It is not unreasonable to expect that the electron density is shifted toward the CF_2 end of the molecule with a subsequent reduction in the dipole moment of the C—H bond. Consequently, those vibrations which consist largely of bending motions of the C—H bonds would appear in the infra-red with less intensity than similar vibrations in "normal" molecules where this shift is not present or so pronounced. On such a basis one would expect to find weaker bands resulting from the CH_2 rocking mode, the CH_2 deformation mode and the wagging mode in which the H atoms move out of the plane of the molecule in a direction opposite to that of the motion of the F atoms, the amplitude of the F atoms being much less than that of the H atoms. That this is the case is suggested by the observations.

On this premise the strong, depolarized Raman line at 603 cm^{-1} is assigned to the second B_2 wagging

TABLE I. The Raman spectrum of vinylidene fluoride.*

	Line	Intensity	ρ	Assignment
1.	439 cm^{-1}	M	D	B_1: CF_2 rock.
2.	549	M	P?	A_1: CF_2 def.
3.	603	S	D	B_2: CF_2 wag.
4.	714	VW		A_2: torsion?
5.	810	M	D	B_2: CH_2 wag.
6.	915	VS	P	A_1: C—F stretch.
7.	949	W	D	B_1: CH_2 rock.
8.	1212	VW		2×603
9.	1280	W		B_1: C—F stretch.
10.	1359	M	P?	A_1: CH_2 def.
11.	1389	VW		439+949
12.	1433	VW		2×714?; 2×439+549
13.	1472	VW		549+915
14.	1619	VW		2×810
15.	1718	W	P	A_1: C^{13}=C stretch.
16.	1728	VS	P	A_1: C=C stretch.
17.	1790	VW		439+1359
18.	1893	VW		2×949
19.	3101	W	P	A_1: C—H stretch.
20.	3171	W	D	B_1: C—H stretch.

* ρ = depolarization factor; S = strong; M = medium; W = weak; V = very.

[3] A. Roberts and Walter F. Edgell, J. Chem. Phys. **17**, 742 (1949) and unpublished results.

[4] P. Torkington and H. W. Thompson, Trans. Faraday Soc. **41**, 236 (1945).

[5] Much of this work was done by Dr. George Evans to whom thanks are due.

[6] G. Herzberg, *Infrared and Raman Spectra of Polyatomic Molecules* (D. Van Nostrand Company, Inc., New York, 1945), pp. 106, 252.

[7] Reference 6, pp. 468–489.

TABLE II. Force constants.

Constant	Value	Constant	Value
k_c	8.92×10^5 dynes/cm	$k_\gamma r_F^2$	0.90×10^{-11} dyne-cm/rad.
k_F	3.8	$k_\delta r_H^2$	0.60
k	1.17	$k_\phi r_F^2$	0.66
$k_\alpha r_F^2$	0.335×10^{-11} dyne-cm/radian	$k_\psi r_H^2$	0.16
$k_\beta r_H^2$	0.333		

TABLE III. Comparison of calculated and observed frequencies.

Vibration	Observed*	Calculated
A_1: C=C stretch.	1734 cm^{-1}	1734 cm^{-1}
CH_2 def.	1370	1367
C−F stretch.	924	924
CF_2 def.	549	548
B_1: C−F stretch.	1300	1322
CH_2 rock.	954	951
CF_2 rock.	439(R)	439
B_2: CH_2 wag.	803	817
CF_2 wag.	612	593

* The observed values are from the infra-red of the gas with the exception of 439 cm^{-1}.

vibration. It corresponds to the weak infra-red band at about 612 cm^{-1}, which has the contour of a type C band as required by the symmetry. The Raman line found at 449 cm^{-1} is then assigned to the remaining B_1 rocking vibration. For the CH_2 deformation the remaining Raman line of moderate intensity, 1359 cm^{-1}, is taken. Just what infra-red band corresponds to this motion is not entirely clear, and will be dependent upon the magnitude of the liquid-vapor frequency shift. The band at 1370 cm^{-1} is tentatively chosen since it is closer to the Raman value.

No Raman line of appreciable intensity remains for the torsional vibration. Only the weak line at 714 cm^{-1} appears in the region anticipated and it is tentatively assigned to this mode. No infra-red absorption occurs at this frequency (up to 500 mm in a 10 cm cell) as required by the selection rules.

With the above set of fundamentals it is possible to account for the remaining weak Raman lines and for the infra-red observations to date.[4,5] The complete Raman assignment is summarized in Table I. A more critical test of the assignment would be furnished by infra-red measurements at higher dispersion where band contours for the overtone and combination frequencies would be available.

NORMAL COORDINATE TREATMENT

One of the main purposes of this work was to provide the basis for a normal coordinate treatment of the frequencies of vibration. The method of Wilson[8] was used in setting up the G matrices, which are found in an appendix together with the basic symmetry coordinates.

Previous work by Pace[9] has indicated that compounds containing several F atoms require a number of large cross terms when the potential function is of the valency force field type. An insufficient number of frequencies are available to evaluate independently all the constants required and satisfy the need for valid checks. To avoid these difficulties insofar as possible and to attempt to provide some insight into the origin of the interactions, the following simplified potential function was used:

$$2V=k_H(r_1^2+r_2^2)+k_F(r_3^2+r_4^2)+k_cR_c^2+k_\alpha r_F^2\alpha^2+k_\beta r_H^2\beta^2+k_\phi r_F^2\phi^2+k_\psi r_H^2\psi^2+k_\gamma r_F^2(\gamma_1^2+\gamma_2^2)+k_\delta r_H^2(\delta_1^2+\delta_2^2)+kR_F^2, \quad (1)$$

where r_1 and r_2 are the changes in the C−H distances, r_3 and r_4 in the C−F distances, R_c in the C=C distance, α, β, γ and δ in the FCF, HCH, FCC and HCC angles and ϕ and ψ in the "wagging" angles of the CF_2 and CH_2 groups. The equilibrium C−F and C−H distances are represented by r_F and r_H. R_F is the change in the distance between the F atoms. If the C−H stretching vibrations are "split" from the A_1 and B_1 secular equations and torsion (A_2) is not considered, one is left with nine vibrations and eight valency force field constants. Yet it is certain that at least three cross terms are important, the interaction of r_3 with r_4, α and γ. The last term in the potential function is an attempt to approximate these terms with one constant.

One is now left with nine constants and nine frequencies and therefore no check on the force field. To test its general validity force constants from a simple treatment of ethylene[10] were used for k_c, k_β, and k_δ and the values of k_F, k, k_α and k_γ chosen to give the best agreement with the experimental results for the A_1 and B_1 frequencies, C−H vibrations being excluded. These four constants served to reproduce the seven frequencies with an average deviation of 1.2 percent and a maximum deviation of 2.3 percent. In view of the simplifications involved, it must be considered that this function serves as an adequate approximation for vinylidene fluoride.

To improve the agreement, small changes were made in all constants; k_ϕ and k_ψ were also evaluated from the two wagging frequencies. The resulting values for the force constants are listed in Table II while the comparison between the calculated and observed values are found in Table III.

An examination of Table II reveals first that k is nearly one-third as large as k_F; and this represents forces over and above those acting perpendicular to the C−F bond (i.e. k_α, which presumably arises from the directed character of the bond). Such forces must play an important role in these molecules. They probably approximate the combined effects of repulsions between the F atoms and between each F atom and the π-electrons of the double bond. Second, the high values

[8] E. Bright Wilson, Jr., J. Chem. Phys. **9**, 76 (1941).
[9] E. L. Pace, J. Chem. Phys. **16**, 74 (1948).
[10] Reference 6, p. 184.

of k_ϕ and k_γ relative to k_ψ and k_δ may be interpreted as arising from repulsion between the F atoms and the π-electrons of the double bond. Third, it is tempting to interpret the nearly equal values of $k_\alpha r_F^2$ and $k_\beta r_H^2$ as arising from the directed character of the bonds, but it is probable that this is coincidence.

ACKNOWLEDGMENT

One of us (W.F.E.) wishes to thank the Research Corporation for a grant which made this work possible. Thanks are also due to Dr. George Evans for his work on the infra-red spectrum.

Note added in proof.—While this paper was in press Smith, Nielsen, and Claassen [J. Chem. Phys. **18**, 326 (1950)] have published a paper on the infra-red and Raman spectra of gaseous vinylidine fluoride. Their numerical values for the fundamental frequencies are in good agreement with the gaseous values obtained from the infra-red survey made in our laboratory and found in Table III. The frequency shifts with phase change have been noted above. Their assignment of the fundamentals agrees with that reported here with two exceptions, the torsional mode and the CH_2 deformation frequency. It does not seem possible to decide with certainty between the several possibilities at this time. A study of the spectra of isotopic species should be helpful in this matter.

APPENDIX

The symmetry coordinates used to set up the secular equation are:

A_1: $R_1=(r_1+r_2)\sqrt{2}$; $R_2=(r_3+r_4)\sqrt{2}$; $R_3=R_c$; $R_4=(2\alpha-\gamma_1-\gamma_2)/(6)^{\frac{1}{2}}$; $R_5=(2\beta-\delta_1-\delta_2)/(6)^{\frac{1}{2}}$

A_2: $R_{12}=\theta$

B_1: $R_6=(r_1-r_2)/\sqrt{2}$; $R_7=(r_3-r_4)/\sqrt{2}$; $R_8=(\gamma_1-\gamma_2)/\sqrt{2}$; $R_9=(\delta_1-\delta_2)/\sqrt{2}$

B_2: $R_{10}=\phi$, $R_{11}=\psi$

The potential energy matrix F is obtained from Eq. (1) and the inverse of the above transformation; R_F is eliminated by use of the relation

$$R_F=(r_3+r_4)(1-\cos\alpha)r_F/r_c+\alpha r_F^2\sin\alpha/r_c.$$

The corresponding G matrices are given below.

A_1:

$$\begin{matrix}\mu_H+2\mu_c\cos^2\delta & 0 & \sqrt{2}\mu_c\cos\delta & \sqrt{3}\mu_c\sigma\sin2\gamma & \sqrt{3}\mu_c\tau\sin2\delta\\ & \mu_F+2\mu_c\cos^2\gamma & \sqrt{2}\mu_c\cos\gamma & (6)^{\frac{1}{2}}\mu_c\sigma\sin\gamma & 0\\ & & 2\mu_c & 3\sigma^2(\mu_F+2\mu_c\sin^2\gamma) & (6)^{\frac{1}{2}}\mu_c\tau\sin\delta\\ & & & & 3\tau^2(\mu_H+2\mu_c\sin^2\delta)\end{matrix}$$

B_1:

$$\begin{matrix}\mu_H+2\mu_c\sin^2\delta & 0 & 2\mu_c\eta\sin\delta & 2\mu_c f\sin\delta\\ & \mu_F+2\mu_c\sin^2\gamma & 2\mu_c d\sin\gamma & 2\mu_c\eta\sin\gamma\\ & & \mu_F\sigma^2+2\mu_c(d^2+\eta^2) & 2\mu_c\eta(d+f)\\ & & & \mu_H\tau^2+2\mu_c(f^2+\eta^2)\end{matrix}$$

B_2:

$$\begin{matrix}1/2\mu_F\sigma^2\sec^2\gamma+\mu_c(\eta^2+g^2) & -\mu_c\eta(g+h)\\ & 1/2\mu_H\tau^2\sec^2\delta+\mu_c(\eta^2+h^2)\end{matrix}$$

A_2:

$$1/2(\mu_H\tau^2\operatorname{cosec}^2\delta+\mu_F\sigma^2\operatorname{cosec}^2\gamma)$$

where $\mu_x=1/m_x$; $\sigma=1/r_F$; $\tau=1/r_H$; $\eta=1/r_c$

$d=\sigma\cos\gamma-\eta$; $f=\tau\cos\delta-\eta$; $g=\eta-\sigma\sec\gamma$; $h=\eta-\tau\sec\delta$.

Notice

THE Journal of Chemical Physics is a research journal intended to provide a medium for the publication of research results in the field of chemical physics. The Journal is published by the American Institute of Physics. The only income of the Journal is from subscriptions, from the page charge levied on institutions supporting the research which is published in the Journal, provided they wish to honor the charge, and minor income from the sale of back numbers, etc. The amount of material which can be accepted in the Journal is, in the long run, limited by the subscription income.

Recent increases in the cost of printing and a very considerable increase in the number of manuscripts submitted to the editor's office have resulted in this limitation becoming very real. Individuals who are interested in the health and growth of the Journal will aid this by subscribing to the Journal or by bringing the opportunity to subscribe to the attention of others who may be interested in the Journal.

Letters to the Editor

THIS section will accept reports of new work, provided these are terse and contain few figures, and especially few half-tone cuts. The Editorial Board will not hold itself responsible for opinions expressed by the correspondents. Contributions to this section should not exceed 600 words in length and must reach the office of the Managing Editor not later than the first of the month preceding that of the issue in which the letter is to appear. No proof will be sent to the authors. The usual publication charge ($8.00 per page) will not be made and no reprints will be furnished free.

The Poisoning of Cathodoluminescence in Silver-Activated Cubic Zinc Sulfide

SIMON LARACH
Radio Corporation of America, RCA Laboratories Division, Princeton, New Jersey
April 12, 1950

THE efficiency of inorganic luminescent materials (luminophors) is a function of many variables, among which are composition and structure. The addition of small amounts of particular impurities in the synthesis of certain luminophors is accompanied by a marked increase in the emission intensity, as for example, the ZnS:Ag system. It is also well known[1] that certain other impurities ("poisons") have a detrimental effect on the luminescence process. Few quantitative data exist on the effect of poisons on phosphors excited by cathode rays. It was the purpose of these experiments to obtain quantitative information concerning these effects, using pure materials, carefully controlled methods of synthesis, and measurement under cathode-ray excitation. This involved co-crystallizing small amounts of iron, nickel, and cobalt ions with cubic-ZnS:Ag luminophors, and observing the efficiency under cathode-ray excitation as a function of proportion of poison added.

Spectroscopically pure zinc sulfide,* with particles averaging approximately 250A, was mixed with a solution of silver nitrate to give 0.00015 g Ag per g ZnS. To this, a solution of sodium chloride was added to give 0.02 g NaCl per g ZnS. After thorough mixing, the mixture was divided, and to the separate parts were added varying amounts of iron, nickel, and cobalt as sulfates. Crystallizations† were carried out by heating for eight minutes at 850°C in a stream of purified nitrogen. The cathodoluminescence efficiencies were obtained with a special demountable cathode-ray tube operating at six kilovolts and a current density of one microampere per cm².

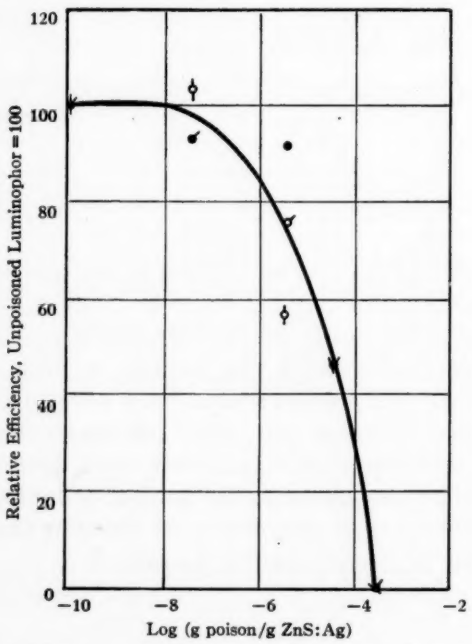

FIG. 1. Relative cathodoluminescence efficiency of cubic-ZnS:Ag as a function of proportion of poison, where ϕ represents cobalt, ● iron, and ♂ nickel.

Within the range of experimental error, the poison-producing results for all three poisons are approximately the same, and can be represented by the curve shown in Fig. 1. It is seen that the poisoning effect is apparent, even in the microgram proportion of poison added, for all three elements tested.

It has been noted[2] that the more potent poisons of luminescence are paramagnetic ions. It is difficult, however, to correlate quantitatively the poison-producing properties of iron, nickel, and cobalt with their magnetic properties. The addition of poisons may serve to increase the probability of non-visible radiative and/or radiationless transitions. It cannot be stated with certainty whether this is due to a lowered efficiency of the energy transfer process from the point of excitation to the activator center, or to an emission shift to the infra-red, or to other mechanisms.[3–5]

The author wishes to acknowledge the assistance of Dr. R. E. Shrader in the measurements of efficiency, as well as the advice of H. W. Leverenz.

* Obtained as ZnS, 33-Z-19, from the RCA Victor Company, Lancaster, Pennsylvania.

† Initial experiments indicated copper contamination when crystallizations were done in silica crucibles. For this reason, all crystallizations reported herein were performed in crucibles of thin platinum foil.

[1] See for example, H. W. Leverenz, *An Introduction to Luminescence of Solids* (John Wiley and Sons, Inc., New York, 1950), p. 333.
[2] Reference 1, p. 335.
[3] Klasens, Ramsden, and Quantie, J. Opt. Soc. Am. **38**, 60 (1948).
[4] F. Urbach and D. Pearlman, J. Opt. Soc. Am. **39**, 690 (1949).
[5] C. G. A. Hill and H. A. Klasens, J. Electrochem. Soc. **96**, 275 (1949).

The Lambda-Temperature in Multimolecular Helium Films

S. V. R. MASTRANGELO
Cryogenic Laboratory, The Pennsylvania State College, State College, Pennsylvania
April 3, 1950

LONG and Meyer[1] and Schaeffer *et al.*[2] point out that helium adsorbed in the first layer (on Fe_2O_3 and charcoal respectively) has a much higher density than that which is predicted by atomic spacing in the liquid. This conclusion was reached by comparison of the v_m obtained from the B.E.T.[3] equation using first krypton at 90.2°K and then helium at liquid helium temperatures. The question which naturally arose concerned the validity of the B.E.T. equation at these low temperatures. Band[4] has shown that the B.E.T. equation could be generalized using the methods developed by Hill.[5] The assumption was made that the first layer is immobilized as in solid helium and that further adsorption takes place on this layer. This resulted in an equation which reduced to the ordinary B.E.T. equation except that v_m could assume values greater than the value given by the liquid density. That the helium adsorbed on the first layer (actually, the first few layers) is immobile and behaves like the solid under high pressure and that the upper layers, as well, appear to be acted on by some surface pressure is born out by the data of Frederikse.[6] These data show a lambda-point only above four layers.[7] The lambda-point for 5–6 layers is at about 1.85°K and moves to higher temperatures as the number of layers increases so that it finally approaches that of the liquid. Moreover, the area under the specific heat curves in the neighborhood of the lambda-increases as the lambda-point temperature increases. When these data are compared with the data of Keesom and

Clusius[8] showing the effect of pressure on the heat capacity of the liquid near the λ-point, it is seen that the λ-point shift of the adsorbed helium is in such a direction as to indicate large pressure effects for the first layers, this pressure decreasing with increasing adsorption. What is more, the lambda-point for 5–6 layers occurs at about 1.85°K which corresponds to a pressure of about 25 atmos. for bulk helium. This is approximately the point at which the λ-line intersects the solid curve in a P,T diagram. Corresponding to this, there is no λ-point for the 3–4 layer coverage according to Frederikse's data, indicating that the film has become "solid." Further observation shows that the heat capacities of the adsorbed films are higher than the liquid below the λ-point and lower than the liquid above the lambda-point. This is the case as well for bulk helium under pressure with the direction and magnitude of the effect in agreement with the λ-point shift pointed out above. These shifts in the λ-point can be used for calculating the pressure in the upper layers from the peak in the heat capacity curves. This will be useful information in developing any statistical model of the helium film and for using this model in the calculation of heats of adsorption, etc. It may be well to point out that a first-order transition corresponding to fusion in bulk helium would be expected somewhat above 4°K at low coverages where the pressure corresponds to several hundred atmospheres.

[1] Long and Meyer, Phys. Rev. **68**, 440 (1949).
[2] Schaeffer, Smith, and Wendell, J. Am. Chem. Soc. **71**, 863 (1949).
[3] Brunauer, Emmett, and Teller, J. Am. Chem. Soc. **60**, 309 (1938).
[4] W. Band, Phys. Rev. **68**, 441 (1949).
[5] T. Hill, J. Chem. Phys. **14**, 263 (1946); **14**, 268 (1946); **15**, 757 (1949).
[6] H. P. R. Frederikse, Physica **XV**, No. 10, 860 (1949).
[7] The number of layers in Frederikse's paper is calculated on the basis of He-He spacing in the liquid rather than v_m calculated from the B.E.T. equation. If the v_m calculated from the B.E.T. equation be used what is here called 4 layers is actually about one layer. It is difficult to correct the other layers for this effect. However, no quantitative conclusions can be reached in any case since the contribution to the heat capacity of each layer should be graphed against temperature to detect the lambda-point in each layer whereas Frederikse graphs the total heat capacity against temperature. Such a procedure would give larger areas under the curves for the lambda-region but does not change the position of the peaks much as shown by a rough treatment of Frederikse's data.
[8] W. H. Keesom and K. Clusius, Proc. Roy. Soc. Amst. **34**, 605 (1931).

Internal Rotation V. The Energy Difference between the Rotational Isomers of 1,2-Dibromoethane

H. J. Bernstein
National Research Council, Ottawa, Canada
April 17, 1950

THE isomerization energy for the rotational isomers of 1,2-dibromoethane has been obtained by the spectroscopic method by Mizushima *et al.*[1] and found to be 1450 cal./mole.

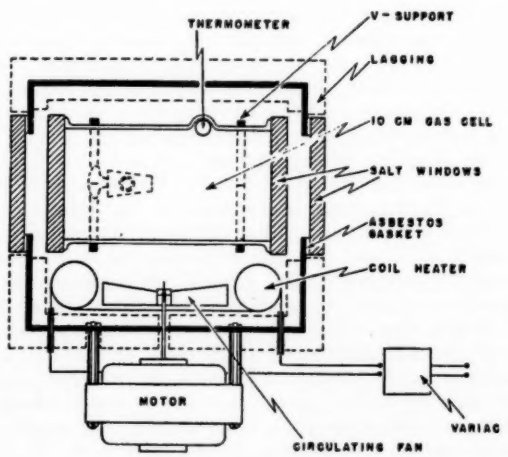

FIG. 1. Apparatus.

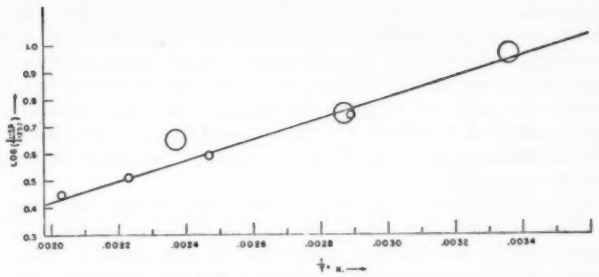

FIG. 2. Plot of log ratio of intensities against $1/T$. The large circles are for a pressure of 10 mm of Hg in a 10-cm cell. The small circles are for a pressure ≈60 mm of Hg in a 10-cm cell.

They obtained this energy (1400 cal./mole) also by measurement of the electric moment as a function of temperature. Gwinn and Pitzer,[2] also, have investigated this molecule by measurement of the electric moment as a function of temperature and find a value of 1.5 cal./mole for the energy difference.

With a specially constructed cell, the plan of which is shown in Fig. 1, the infra-red spectra of gaseous $C_2H_4Br_2$ have been obtained from 25° to 250°C. The thermometer extends into the gas cell through a ground glass joint so that its bulb is in about the middle of the cell, but well out of the path of the beam from the Globar. The cell as shown in Fig. 1 is covered with a close fitting lid when in use. A Perkin-Elmer (Model 12C) infra-red spectrometer was used in conjunction with a Brown recorder to obtain the spectra.

The ratio of the intensity (area under the density curve) of the band at 1192 cm^{-1} to that of the band at 1252 cm^{-1} gives the ratio of the number of *trans*-molecules (C_{2h}) to the number of gauche molecules (C_2).[3] The plot of $\ln\frac{(\text{intensity of 1252 cm}^{-1})}{(\text{intensity of 1192 cm}^{-1})}$ against $1/T$ gives $\Delta H/R$ for the temperature range investigated.[3] Figure 2 shows this straight line plot, the slope of which gives $\Delta H = 1770 \pm 150$ cal/mole.

Other molecules with rotational isomers being investigated here by the spectroscopic method include $CH_2Cl-CHCl_2$, $CHCCl_2-CHCl_2$ and isopentane.

[1] Mizushima, Morino, Watanabe, Simanote, and Yamagouchi, J. Chem. Phys. **17**, 591 (1949).
[2] W. D. Gwinn and K. S. Pitzer, J. Chem. Phys. **16**, 303 (1948).
[3] H. J. Bernstein, J. Chem. Phys. **17**, 258 (1949).

On Discrimination in Mass Spectrometer Ion Sources

G. Careri* and G. Nencini
Centro di Fisica Nucleare del Consiglio Nazionale delle Ricerche, Istituto di Fisica dell'Università, Rome, Italy
April 19, 1950

DISCRIMINATION in mass spectrometer ion sources has been studied by Coggeshall,[1] and the following theoretical curve for peak heights *vs.* ion accelerating voltage has been given:

$$I = pA\left\{4.46 - \frac{1}{2}\frac{1}{(V_1+V_2)^{\frac{1}{2}}}\frac{z}{d}\right\},$$

where I is the ion current intensity, p the true abundance in the gas sample, z the distance among the slits in the source, d the half-width of the second slit and A a constant. The accelerating voltages V_1 and V_2 are respectively the voltage carrying the ions out of the electron path, and the proper accelerating voltage of ions; in practice V_1 is some hundredth part of V_2.

A 60° Nier-type[2] mass spectrometer for light elements which we have built in this laboratory for routine work has been arranged in order to test experimentally Coggeshall's theory, and to find out whether other parameters also occur which influence

the ion current intensities at different accelerating voltages. Our results, which are reported more extensively elsewhere,[3] point to a stronger discrimination than indicated by the theory, and, furthermore, to a sharp dependence on V_1, the first low accelerating voltage in spite of Coggeshall's assumption. Discrimination curves, obtained at several V_1 constant values, show that a lower discrimination is had with the same V_1 values for which the ion current is stronger.

Wide variations of electrons accelerating voltage and trap voltage (between 22.5 and 135 volts, and 22.5 and 90 volts respectively) do not influence discrimination. Gas pressure variation in the ion source can also produce a different discrimination, but a quantitative measurement of this effect is contrasted by the difficulty of reproducing the same pressure conditions; we can say that discrimination becomes larger at increasing pressure. Gases used were N_2 and H_2; a doubtful mass influence is discussed in reference 3.

As a conclusion we can say that the theory is lacking, and that an experimental discrimination curve may be used only if gas pressure conditions are as far as possible reproduced in the ion source. As we have also tested, the way to obtain true and well-reproducible measurements is to operate by magnetic scanning.

* Present temporary address: Institute for Nuclear Studies, University of Chicago, Chicago, Illinois.
[1] N. D. Coggeshall, J. Chem. Phys. **12**, 19 (1944).
[2] A. O. Nier, Rev. Sci. Inst. **18**, 398 (1947). During these measurements the ion source was reduced to Coggeshall's simplified model.
[3] G. Careri and G. Nencini, Nuovo Cimento **7**, 64 (1950).

On the Elimination of Extraneous Scattering in Raman Spectra

H. Dean Mallory*
Department of Chemistry, State University of Iowa, Iowa City, Iowa
April 3, 1950

In view of the increased theoretical and practical importance of fluorocarbons, it is desirable to obtain their Raman spectra as completely as possible. It was in regard to low boiling fluorocarbons that the procedure referred to in this letter was developed.[1] As a class, these compounds are especially troublesome in that nearly all of them exhibit weak Raman scattering. One can expect their Raman spectra to be only about $\frac{1}{10}$ the intensity of those of the corresponding hydrocarbons.

The conventional approach to the problem of background reduction has been through the use of light filters; in work with fluorocarbons, however, dependence on filters alone leaves much to be desired. Runs made in this research were in the liquid phase without filters except those used for special effects such as polarization or suppression of the lower exciting lines. Results obtained point to the possibility that nearly all of the background commonly observed with lengthy exposures is due to light sent into the spectrograph through simple reflection of normal arc continuum by physical contaminants in the Raman sample; Rayleigh scattering of arc continuum is rarely the limiting factor. These contaminants include dust, small particles of drying agent and especially particles of near colloid size of undetermined composition which are commonly present in many chemically pure compounds. The degree of physical purity here achieved has been such that (1) liquefied samples could be greatly superheated before boiling occurred, (2) microscopic examination showed no particles present, and (3) observation of the liquid along the long axis of the Raman tube showed no trace of haze, the liquid appeared optically void under the most severe lighting conditions obtainable. One of the compounds investigated was octafluoropropane.[2] It is believed that 22 of its 27 theoretical fundamentals were observed; Herzberg[3] lists only 13 lines for propane.

In the region between Hg 4358A and the position normally occupied by the highest CH vibration, 27 distinct Raman lines were observed for octafluoropropane, 5 of which probably arose from Hg 4339 and 4348A. In this same region 36 lines were seen for methylfluoroform, 21 of which seemed due to exciting lines lower than Hg 4358A, still others arose from combinations or overtones. With properly prepared samples these lines could be clearly seen virtually free from background.

The Raman tubes were cleaned in the usual way but were then flushed with a non-soap detergent solution and steam. This was done in such a manner that once steam stopped flowing, steam condensing inside the system did not draw in dust laden air. Water was removed from the system as vapor by vacuum pumps and the system thereafter kept under vacuum.

The samples were dried in the gas phase by barium oxide drying agent.[4] Phosphorus pentoxide could not be used since samples were invariably contaminated by contact with it and gave high background spectrograms.

The Raman samples were freed of colloidal impurities by *slow* vacuum evaporation through fritted glass barriers at a temperature 40 degrees or more below their atmospheric boiling points. This step and that of steam flushing were both tedious and time consuming, however, it was possible by such procedure to secure background free spectrograms without the use of filters even though exposure times were used which caused photographic halos to form around the stronger Raman lines. With optically void samples, background reducing filters can be used to greater advantage than commonly supposed and permit exposures of extreme length.

* Present Address: U. S. Naval Ordnance Laboratory, White Oak, Silver Spring, Maryland.
[1] Based on a portion of a thesis presented by H. Dean Mallory in partial fulfillment of the requirement for the degree of Doctor of Philosophy in the Graduate School of the State University of Iowa (February, 1950).
[2] Edgell, Mallory, and Weiblen, "The raman and infra-red spectra of octafluoropropane" (to be published).
[3] G. Herzberg, *Infrared and Raman Spectra of Polyatomic Molecules*, (D. Van Nostrand Company, Inc., New York, 1945).
[4] Barium and Chemicals, Inc., Willoughby, Ohio.

The Infra-Red Spectra of Hydrogen and Deuterium Peroxides in Condensed Phases*

Robert Cooper Taylor**
Metcalf Chemical Laboratories, Brown University, Providence, Rhode Island
April 24, 1950

The investigations of the vibrational spectrum of hydrogen peroxide, particularly in the region of fundamentals, have not been numerous and a high percentage of the reliable data are for the liquid phase. On the basis of the available information, there seem to be two main points of interest. First, the frequency corresponding to the torsional motion of the OH groups around the 0—0 axis has not been conclusively identified, and secondly, no completely satisfactory assignment has yet been proposed for an infra-red band observed in the neighborhood of 2800 cm^{-1}. The assignment of frequencies is somewhat complicated by the fact that extensive hydrogen bonding occurs in the liquid causing greatly broadened lines and marked temperature shifting of bands involved in hydrogen motions.

Recently, Giguère[1] has reported the results of an investigation of the infra-red spectrum of the vapor of hydrogen peroxide and also of the liquid at room temperatures. In the liquid, a rather broad region of absorption with a maximum at about 550 cm^{-1} was noted.† This band was tentatively assigned to the torsional mode and the band observed at 2780 cm^{-1} in the liquid was then suggested to be a triple combination frequency involving ν_3, the 0—0 stretching mode, ν_2, the symmetrical bending mode, and the newly found torsional mode at 550 cm^{-1}.

The present work was begun following an investigation of the Raman spectrum of hydrogen and deuterium peroxides.[2] Inasmuch as it has now been interrupted, it appears desirable to report the data obtained in a preliminary fashion in view of the general interest in this compound.

Hydrogen peroxide containing 10 percent by weight of water was obtained from the Buffalo Electrochemical Company. It was further purified and concentrated by vacuum distillation. Deuterium peroxide was prepared by the method of Feher,[3] the amount of hydrogen present in the final sample being estimated at 8 to 10 percent of the deuterium content based on a comparison of band intensities. The spectra were obtained with a Perkin-Elmer Model 12B which had been modified into a double beam instrument recording directly the percent transmission; a fluorite, rock salt or potassium bromide prism was used depending on the region. The cell used has been described by Wagner and Hornig,[4] the sample being contained in a small silver chloride holder which provided a fixed film thickness of about 15 microns. At the temperatures employed, decomposition during the course of two or three hours was small.

The bands observed for supercooled liquid hydrogen peroxide (99.2 percent) and liquid deuterium peroxide (82.5 percent) at −30°C and for crystalline hydrogen peroxide at −30° and −78° are listed in Table I. The low frequency band noted by Giguère

TABLE I. Infra-red frequencies of hydrogen and deuterium peroxides.

H_2O_2		D_2O_2			
Liq., −30°	Cryst., −30°	Cryst., −78°	Liq., −30°	Sym-metry	Assign-ment
		472 *vw*			
635 *m, br*		660 *s*	538 *m, br*		ν_4(?)
		792 *w*			
878 *vw*		878 *vw*	878 *vw*	*a*	ν_3
1353 *ms*	1365 *s*	1378 *s*	1004 *s*	*b*	ν_6
			(1386 *w*)		
	1418 *w*	1430 *w*		*a*	ν_2
2796 *mw, br*	2743 *m*	2733 *m*	2087 *mw*		$\nu_2+\nu_6$(?)
3360* *vs*	3275* *vs*	3218 *vs*	2482 *vs*	*b*	ν_5
			(3368 *mw*)	*b*	
4715 *vw*	4640 *vw*	4595 *vw*		*A*	$\nu_5+\nu_6$

* Obtained by difference from the combination band, $\nu_5+\nu_6$.

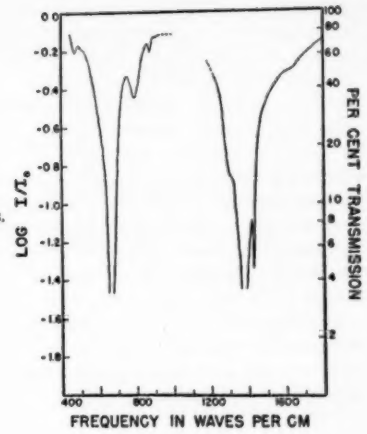

FIG. 1a. Low frequency bands.

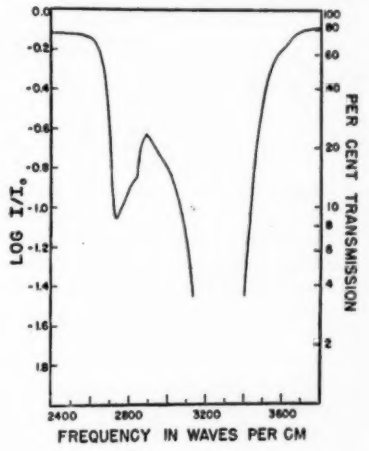

FIG. 1b. The OH region.

was observed in the liquid at −30° as a broad band of moderate intensity with a maximum at 635 cm^{-1}. In the deuterium sample under similar conditions, the maximum appeared at 538 cm^{-1}. The observed ratio of hydrogen to deuterium frequency is thus 1.18, whereas the Teller-Redlich product rule, using the known frequencies[2] of the other vibrations of the same species, predicts a ratio of approximately 1.35 for ν_4, the torsional motion of the OH groups. The spectrum of crystalline hydrogen peroxide at −78° exhibited considerably more detail than the liquid and is shown in Figs. 1a and 1b. Both the intensity and sharpness of the low frequency band increased markedly compared to the liquid and two new bands of low intensity appeared separated from the main maximum by 132 cm^{-1} and 188 cm^{-1} on the high and low frequency sides respectively. The 132 cm^{-1} frequency agrees well with the difference of 135 cm^{-1} found between the main Raman OH band in the crystal and a subsidiary band on its high frequency side[2] and probably can be assigned to a lattice vibration. The spectrum of crystalline deuterium peroxide was not obtained and further experimental work will be necessary to establish conclusively the nature of the band at 660 cm^{-1} in the crystal spectrum.

The unsymmetrical bending mode, ν_6, was also much sharper and more intense in the crystal at −78°; the sharp and rather weak band on its high frequency side appears at the position expected for ν_2, the symmetrical bending mode, which is also allowed in the infra-red but which until now has only been observed in the Raman spectrum. The shoulder on the low frequency side appears due to the first overtone of the 660 cm^{-1} band.

The band around 2800 cm^{-1}, on the basis of the above data, cannot be given the assignment proposed by Giguère. The shape and position of the band at 2733 cm^{-1} in the crystal at −78° suggest that it is due to the unresolved overtones of the two bending modes, ν_2 and ν_6. However, both fundamentals shift to higher frequencies as the crystal temperature decreases, whereas the 2733 cm^{-1} band shifts slightly to lower. Further work over a wider range of temperatures seems necessary for a more satisfactory answer.

It is hoped that work can be resumed on this problem shortly and a more complete account presented in the fairly near future. The author would like to express his appreciation to Dr. Giguère for making his manuscript available in advance of publication.

* This work was supported by the ONR under Contract N6Ori-88, Task Order No. 1.

** Present Address: Department of Chemistry, University of Michigan, Ann Arbor, Michigan.

† Dr. Giguère, in a private communication, reports this band now at 610 cm^{-1} at room temperature.

[1] P. A. Giguère, J. Chem. Phys. **18**, 88 (1950).
[2] R. C. Taylor, Thesis, Brown University, Providence, R. I. (1947).
[3] F. Feher, Ber. d. d. chem. Ges. **72**, 1789 (1939).
[4] E. L. Wagner and D. F. Hornig, J. Chem. Phys. **18**, 296 (1950).

Remarks on Mizushima's Method for the Determination of Surface Area of Powders

YING FU
Department of Chemistry, University of Michigan, Ann Arbor, Michigan
April 14, 1950

RECENTLY Mizushima[1] proposed a method for the determination of surface area of powders using adsorption and adhesion tension data. His method is based on the following

equations:

$$kT\int_1^n \ln\frac{p_s}{p(\nu)}d\nu = a(\sigma_s-\sigma_{sl}), \quad (1)$$

$$a=\frac{kT\int_1^n \ln(p_s/p(\nu))d\nu}{\sigma_{lv}\cos\theta}, \quad (2)$$

where p_s is the saturation pressure of the liquid, $p(\nu)$ is the vapor pressure at which ν molecules of the vapor are adsorbed by a solid of area a, σ_s, σ_{sl}, and σ_{lv} are respectively the interfacial tensions of the solid-vacuum, solid-liquid, and liquid-vapor interfaces and θ is the contact angle. It is believed the theory is fundamentally unsound and the alleged experimental support non-existent.

Equation (1) was obtained by equating the change of free energy, ΔG, of the adsorbate to the change of the available surface energy of the adsorbent. Since these two effects are entirely different, it is not correct to equate the one to the other to obtain Eq. (1). This can be easily demonstrated when the equations for these energy changes are compared. For a single adsorbate at constant temperature,

$$\Delta G=\int \mu d\nu,$$

where μ is the chemical potential; for the adsorbent,

$$\sum_{\substack{\text{all surface}\\ \text{phases}}} \int a d\sigma = -\int \nu d\mu$$

by the familiar Gibbs' equation. Obviously ΔG cannot be identified with $a(\sigma_s-\sigma_{sl})$ as Mizushima has contended.

The transformation of Eq. (1) into (2) by means of du Pré's equation, $\sigma_{vl}\cos\theta=\sigma_s-\sigma_{sl}$, involves another common misconception. The du Pré equation is strictly an equilibrium relation. If a liquid spontaneously spreads on a solid surface, equilibrium evidently does not exist, and the du Pré equation is no longer valid. In such cases it is not permissible to assume that the contact angle is zero, because spontaneous spreading indicates there is *no* contact angle which is quite different from a zero angle. The system toluene-glass used by Mizushima is precisely such a system to which the du Pré equation cannot be applied, because toluene will spontaneously spread on glass. Even granting that it is permissible to apply the du Pré equation to such systems, Mizushima's fourth equation

$$\sigma_{lv}\cos\theta = 46.5 \text{ ergs/cm}^2$$

is still untenable, because $\sigma_{lv}\cos\theta$ can never be greater than the surface tension of toluene, which is 27.9 at 25°C. Mizushima attributed the above relation to Bartell and Merrill[2] without realizing that these authors have never used $\sigma_{lv}\cos\theta$ to evaluate the adhesion tension of systems like toluene-glass.

In the application of adhesion tension ($A\equiv\sigma_s-\sigma_{sl}$) it should be noted that A depends not only on the nature of the liquid and the solid, but also on the structure of the solid surface. For instance, against the same liquid the (111) plane of NaCl would undoubtedly give different adhesion tension value than the (100) plane. Even with amorphous substances such as charcoal different samples will often give different A values against the same liquid.[3] It is, therefore, erroneous to assume that when equal areas of two solids of the same chemical composition are compared, they will invariably show identical energy effects. In order to test his theory, Mizushima compared the ΔG value calculated from the adsorption data of Carver[4] with the adhesion tension value of Bartell and Merrill and obtained excellent agreement. Carver's data, however, were obtained with Pyrex glass while the adhesion tension value cited (46.5 ergs/cm²) was for fused quartz. There is no reason to expect that two such different solids would show the same surface characteristics. Hence these data are not comparable. It is also to be noted that in the adsorption of vapors by plane surfaces at saturation pressure, the change in surface energy is not $a(\sigma_{sl}-\sigma_s)$ but $a(\sigma_{sl}+\sigma_{lv}-\sigma_s)$, because a liquid surface has been created. This factor has not been considered by the author. Furthermore, it is a well-known fact that cleaning agents often roughen glass surfaces to such an extent that the effective surface area may be many times greater than the macroscopic geometric value.[5] Since Carver has subjected his glass to quite drastic treatment, it is very probable that the true area is much greater than the value given in his paper. Hence, Mizushima's ΔG value (44 ergs/cm²) may be easily in error by many hundred percent.

From the above discussion the only conclusion which seems justified is that the close agreement of the two energy values obtained by Mizushima only serves to reveal the incorrectness of his theory.

[1] Mizushima, J. Chem. Phys. **17**, 1357 (1949).
[2] Bartell and Merrill, J. Phys. Chem. **36**, 1178 (1932).
[3] Bartell and Smith, Ind. Eng. Chem. **21**, 1102 (1929).
[4] Carver, J. Am. Chem. Soc. **45**, 63 (1923).
[5] Frazer, Patrick, and Smith, J. Phys. Chem. **31**, 897 (1927).

The Stability of Gaseous Nitryl Chloride

RICHARD A. OGG, JR.* AND M. KENT WILSON
Mallinckrodt Chemical Laboratory, Harvard University, Cambridge, Massachusetts

May 1, 1950

TO date there had been no study of thermodynamic properties of nitryl chloride, $ClNO_2$. However, it appears to be a matter of common belief that nitryl chloride cannot be formed in significant amounts from Cl_2 and N_2O_4, and that it does decompose into these substances.[1] The inferences regarding equilibrium are obvious, and would enable estimation of a rough limit for the standard free energy of formation of $ClNO_2$. In studies aimed at structure analysis we have observed the infra-red absorption spectrum of gaseous $ClNO_2$, prepared both by ozonization[1] of ClNO and by the reaction of chlorosulfonic acid with anhydrous nitric acid.[2] (The latter affords a greatly superior preparative method.) The spectrometer and cells were the same as described previously.[3] In the spectral region between 2 and 16μ there are four strong characteristic bands, at approximately 1700, 1340, 1275, and 795 cm^{-1} respectively. These allow ready detection and quantitative estimation of nitryl chloride in gaseous mixtures.

Immediately after preparation, mixtures of gaseous Cl_2 and N_2O_4 (both at partial pressures of the order of 100 mm Hg) displayed only the bands of N_2O_4 and NO_2. On standing at room temperature there was noted the gradual appearance of the above $ClNO_2$ spectrum accompanied by those characteristic respectively of N_2O_5[3] and ClNO. (The latter has two moderately strong bands at approximately 1790 and 920 cm^{-1}.) Concentrations of the various components became practically constant after some ten hours at room temperature. That these final concentrations correspond closely to chemical equilibrium was shown by variation of the initial concentration of Cl_2 and N_2O_4.

It is apparent that equilibrium in the reaction

$$Cl_2+N_2O_4 \rightleftharpoons 2ClNO_2$$

is rather slowly attained, but that it corresponds to a much greater stability of $ClNO_2$ than had previously been supposed. Variation of temperature over a considerable range indicated that the formation of $ClNO_2$ by the above reaction is an *exothermic* process. The reaction

$$N_2O_5+ClNO \rightarrow N_2O_4+ClNO_2$$

had previously been studied, using a different method, by Mr. Ralph Weston at Stanford University (these studies will be reported elsewhere), and found to be extremely rapid. It is apparent that this equilibrium is also established in the present system, with comparable concentrations of ClNO and $ClNO_2$.

It was further found that the spectrum of $ClNO_2$ appeared in mixtures of O_2 and ClNO, the rate increasing rapidly with addition of N_2O_4. The equilibrium

$$2ClNO+O_2 \rightleftharpoons 2ClNO_2$$

may at high N_2O_4 concentrations be established much more rapidly than the first equilibrium discussed above.

Quantitative study of the three new equilibria reported here provides an excellent approach to the thermodynamic properties of $ClNO_2$. For practical reasons the third reaction above is the most suited to accurate measurement, but the studies on all three prove to be self-consistent, employing known thermodynamic properties of the other substances involved. As a result of these studies, a provisional value for the energy of dissociation of $ClNO_2$ into Cl and NO_2 of some 32 kilocalories per mole has been found. This figure raises grave doubts regarding the kinetic studies of Schumacher and Sprenger.[1] These authors reported a quasi-unimolecular decomposition of nitryl chloride, this dissociation being considered the rate determining step. However, their measured activation energy was only some 21 kilocalories per mole. It is apparent that the decomposition is vastly more complex than postulated by these authors, and that their studies have no value in discussing theories of quasi-unimolecular reactions.

* Currently on leave from Stanford University, California.
[1] D. M. Yost and H. Russell, Jr., *Systematic Inorganic Chemistry* (Prentice-Hall, Inc., New York, 1946).
[2] German Patent 509,405 to Karl Dachlauer.
[3] Ogg., Richardson, and Wilson, J. Chem. Phys. **18**, 573 (1950).

Carrier-Free Radioisotopes from Cyclotron Targets. VIII. Preparation and Isolation of $Cu^{64,67}$ from Zinc*

HERMAN R. HAYMOND, ROY D. MAXWELL,† WARREN M. GARRISON, AND JOSEPH G. HAMILTON
Crocker Laboratory, Radiation Laboratory, and Divisions of Medical Physics, Experimental Medicine, and Radiology, University of California, Berkeley and San Francisco, California
April 24, 1950

THE radio-copper was produced by bombardment of zinc with 19-Mev deuterons in the 60-in. cyclotron at Crocker Laboratory. At this energy, the longer-lived radioisotopes[1] of copper, $Cu^{64,67}$, are produced in a thick target by the nuclear reactions, $Zn^{64}(d, 2p)Cu^{64}$, $Zn^{66}(d, \alpha)Cu^{64}$, $Zn^{67}(d, 2p)Cu^{67}$. Radioisotopes of gallium are produced concurrently by the reactions, $Zn(d, xn)Ga$. The carrier-free radio-copper was separated from the target element and from the radioisotopes of gallium by a solvent extraction method based on the selective solubility of copper dithizonate in carbon tetrachloride. This procedure,[2] originally developed for the colorimetric determination of microgram quantities of copper, quantitatively extracted $Cu^{64,67}$ from solutions containing less than approximately 10^{-8} g of copper, the minimum detectable by colorimetry under the experimental conditions used.

A block of spectrographically pure[3,4] zinc was soldered to a water-cooled aluminum target and bombarded for a total of 20 μa-hr. at an average beam intensity of 10 μa. Approximately 1.0 g of the bombarded surface was removed by milling and dissolved in a minimum volume of 12N HCl. The solution was diluted to 5.5N and the gallium activities were extracted with ether after the addition of 10 mg of $GaCl_3$ carrier. The aqueous phase was evaporated almost to dryness, adjusted to pH 1.0–1.2 with NaOH to a volume of 50 ml and extracted three times with equal volumes of CCl_4 containing 0.001 percent dithizone. Under these conditions, the carrier-free $Cu^{64,67}$ was quantitatively separated from the target element and from traces of gallium which may not have been completely removed in the previous extraction. The CCl_4 phases were combined, washed twice with 0.1N HCl and evaporated to dryness in a porcelain dish. To remove excess dithizone and to destroy the copper dithizone complex, the dish was heated at 500°C for ½ hr. The carrier-free $Cu^{64,67}$ was dissolved in an amount of 0.1N HCl which on neutralization gave an isotonic saline solution of the desired volume for subsequent biological investigation.

The radio-copper was identified by half-life determination, absorption measurement, and by chemical separation with carriers. The decay curve was followed for 500 hr. and showed the 12.8-hr. period[5] of Cu^{64} and a longer-lived activity which after 100 hr. leveled off into a 72-hr. period. This activity, presumably Cu^{67},[6] was followed for four half-lives and accounted for approximately 3.0 percent of the total beta-activity corrected to the time of bombardment. Absorption measurements 10 hr. after bombardment showed the 0.6-Mev beta-particle and 1.2-Mev gamma-ray reported[5,7] for Cu^{64}. A tracer amount of activity added to a 1N HCl solution of Ni, Cu, and Ga in carrier amounts was quantitatively recovered in the CuS fraction following precipitation with H_2S.

We wish to thank Mr. T. Putnam, Mr. B. Rossi, and the 60-in. cyclotron crew at Crocker Laboratory for bombardments and Professor G. T. Seaborg for helpful suggestions.

* This document is based on work performed under Contract No. W-7405-eng-48A for the AEC.
† Lieutenant Colonel, U. S. Army, now stationed at Walter Reed Hospital, Washington, D. C.
[1] G. T. Seaborg and I. Perlman, Rev. Mod. Phys. **20**, 585 (1948).
[2] E. B. Sandell, *Colorimetric Determination of Traces of Metals* (Interscience Publishers, Inc., New York, 1944).
[3] The zinc was obtained from Johnson Mathey and Company. Copper was not detected by spectrographic analysis.
[4] The reagents and solutions used in the isolation of Cu^{64} were tested for copper impurity using the method described in reference 2. The water was triple-distilled from glass.
[5] S. N. Van Voorhis, Phys. Rev. **50**, 895 (1936).
[6] R. H. Goeckermann and I. Perlman, Phys. Rev. **73**, 1127 (1948).
[7] H. Bradt *et al.*, Helv. Phys. Acta. **19**, 219 (1946).

Errata: The Statistical Mechanical Theory of Transport Processes. III. The Coefficients of Shear and Bulk Viscosity of Liquids

[J. Chem. Phys. **17**, 988 (1949)]

JOHN G. KIRKWOOD, FRANK P. BUFF, AND MELVIN S. GREEN
The Gates and Crellin Laboratories of Chemistry, California Institute of Technology, Pasadena 4, California

EQUATION (6) should read

$$\left[\frac{\langle \mathbf{PP}\rangle_{Av}}{m}-m\mathbf{uu}\right]\rho^{(1)}=\rho^{(1)}kT\mathbf{1}-\frac{\rho^{(1)}kT}{\zeta}\left[\dot{\boldsymbol{\varepsilon}}-\mathbf{1}\frac{\nabla\cdot\mathbf{u}}{3}\right],$$

where $\mathbf{1}$ is the unit tensor. The first term $\rho^{(1)}kT/3\zeta$ in the second of Eqs. (10) defining bulk viscosity should be omitted. Likewise, the first term $NmkT/3v\zeta$ of Eq. (45) should be omitted. In the first line of Eq. (16), $\nabla\mathbf{P}_1$ should be changed to $\nabla\mathbf{R}_1$. In the last line of Eq. (36), $I(z)$ should read $I_\alpha(z)$. In the first line of reference 2, the date should be changed from 1945 to 1943.

The change in Eq. (6) removes kinetic energy transport terms from the bulk viscosity, which in any event, are negligible in liquids, for which the theory is designed. The intermolecular force contribution to bulk viscosity remains unaffected by the change.

The change in Eq. (6) is necessitated by the definition of temperature in the non-equilibrium case

$$\langle \Pi^2\rangle_{Av}=3mkT$$

and the retention of ${}^{(1)}\mathbf{F}\dagger$, as yet undetermined by our theory, in Eq. (15), which should read

$$\langle \mathbf{III}\rangle_{Av}-mkT\mathbf{1}=\frac{m}{2\zeta}\Big[\langle \mathbf{III}\rangle_{Av}\cdot\nabla\mathbf{u}+\langle \mathbf{\Pi}\cdot\nabla\mathbf{u}\mathbf{\Pi}\rangle_{Av}+\mathbf{u}\cdot\nabla\langle \mathbf{III}\rangle_{Av}+\frac{\partial\langle \mathbf{III}\rangle_{Av}}{\partial t}-\langle {}^{(1)}\mathbf{F}\dagger\mathbf{\Pi}\rangle_{Av}-\langle \mathbf{\Pi}\,{}^{(1)}\mathbf{F}\dagger\rangle_{Av}\Big]$$

$$\rho^{(1)}\langle {}^{(1)}\mathbf{F}\dagger\mathbf{\Pi}\rangle_{Av}=N\int {}^{(1)}\mathbf{F}\dagger\mathbf{\Pi}f^{(1)}d\mathbf{p}.$$

By taking the trace of both sides of the corrected form of Eq. (15), we obtain

$$\frac{\partial T}{\partial t}+\mathbf{u}\cdot\nabla T+\frac{2}{3}T\nabla\cdot\mathbf{u}-\frac{2}{3mk}\mathrm{Tr}\langle {}^{(1)}\mathbf{F}\dagger\mathbf{\Pi}\rangle_{Av}=0$$

and are led to the corrected form of Eq. (6).

Thus, as in the kinetic theory of gases, there is no momentum transport contribution to the bulk viscosity in view of the non-equilibrium definition of temperature. The intermolecular force term is therefore not only dominant but the only contribution to bulk viscosity.

Bond Hybridization in the Non-Tetrahedral Carbon Atom. The Heats of Combustion of Spiropentane and Methylcyclobutane

GEORGE L. HUMPHREY* AND RALPH SPITZER†
Department of Chemistry, Oregon State College, Corvallis, Oregon
April 20, 1950

THE method of bond hybridization in non-tetrahedral carbon atoms presented by Kilpatrick and Spitzer[1] has been applied to spiropentane and methylcyclobutane and the values obtained for the bond strengths used to calculate the molal heats of combustion of the gases at 25°C. A comparison of the calculated heats of combustion with those obtained from combustion measurements indicates that the method may be fairly reliable in predicting heats of combustion (formation) of cyclic hydrocarbons.

The calorimeter used for the combustion measurements was of the ordinary (isothermal) type converted from the adiabatic system of Gilbert *et al.*[2] The energy equivalent was determined by combustion of benzoic acid, NBS standard sample 39*f*, having the certified value 26,428.4±2.6 int. joules per gram mass for the isothermal heat of combustion under standard conditions.[3] The factor, 4.1833 int. joules per cal., was used in converting to calories. The average value of the energy equivalent of the system found from the calibration experiments was 2805.85 cal./deg. with an average deviation of 0.01 percent and a maximum deviation of 0.02 percent.

The materials for combustion were of the highest purity supplied by the U. S. Bureau of Mines, Bartlesville, Oklahoma, and the NACA. For combustion, the liquids were sealed in glass ampoules and benzoic acid was used as kindler when the usual procedure of adding oil produced no satisfactory combustions. The great difficulty in obtaining good combustions of the highly volatile liquids resulted in only three apparently satisfactory (i.e., no evidence of spattering or carbon deposits in the bomb after combustion) determinations for spiropentane and five for methylcyclobutane before the samples were depleted. From these combustions, there was obtained for the heat of combustion in kcal. per mole of liquid at 25°C and 1 atmos. pressure, $-\Delta H_R = 778.7_2$ for spiropentane, and 801.1_4 for methylcyclobutane, the deviation between extremes being 0.04 percent. For comparison with the theory, these values were converted to the molal heats of combustion of the gases by employing Trouton's rule to calculate the heats of vaporization.

The results of the present work, together with data for some other strained cyclic hydrocarbons, are presented in Table I. For obtaining the calculated values, the method and the data for bond strengths given in reference 1 were employed in conjunction with assumed normal[4] C−C and C−H bond energies of 59 and 87 kcal. The orbitals of the central carbon atom in the spiropentane molecule were assumed to remain tetrahedral and their strengths

TABLE I. Comparison of experimental and calculated values of $-\Delta H_R$(gas) at 25°C, for some strained cyclic hydrocarbons.

Compound	Structural representation	$-\Delta H_R$(gas) experimental kcal./mole	$-\Delta H_R$(gas) calculated kcal./mole
Cyclopropane		504[a]	503.9
Cyclobutane		648[a]	647.6
Cyclopentane		793.6[b]	793.6[d]
Spiropentane		785.3[c]	785.6
Methylcyclobutane		807.8[c]	806.3

[a] G. E. K. Branch and M. Calvin, *Theory of Organic Chemistry* (Prentice-Hall, Inc., New York, 1941). Recently the value 499.9 has been given for cyclopropane by Knowlton and Rossini, J. Research Nat. Bur. Stand. **43**, 113 (1949).
[b] Spitzer and Huffman, J. Am. Chem. Soc. **69**, 211 (1947).
[c] This work.
[d] Only 1 kcal. for torsional strain has been added to the calculated value because of relief of strain by non-planar configurations of the ring. See Kilpatrick, Pitzer, and Spitzer, J. Am. Chem. Soc. **69**, 2483 (1947).

in the directions of the other four carbon atoms (<C−C−C=60°) calculated to be 1.862. The calculated values in Table I contain a torsional strain energy of 2 kcal. per opposed CH_2 group,[5] and the methyl group of methylcyclobutane was regarded as a hydrogen atom in making this correction.

Because of the difficulties accompanying determinations of heats of combustions of highly volatile liquids by use of the bomb calorimeter, there is a possibility that the $-\Delta H_R$ values given above for spiropentane and methylcyclobutane are more uncertain than we have indicated, and they should, therefore, be regarded as preliminary. However, because of the good agreement of the observed and calculated values for $-\Delta H_R$(gas), we feel that our results should be presented at this time.

We are grateful to Professor E. C. Gilbert for many helpful suggestions, and to the General Research Council of Oregon State College for funds which made possible the alteration of the calorimeter. The generosity of the late Dr. Hugh M. Huffman of the Bartlesville Laboratory, and Addison M. Rothrock, NACA, in supplying samples is especially appreciated.

* Present address: Pacific Experiment Station, U. S. Bureau of Mines, Berkeley, California.
† Present address: Harvard University, Cambridge, Massachusetts.
[1] J. E. Kilpatrick and R. Spitzer, J. Chem. Phys. **14**, 463 (1946).
[2] Hughes, Corruccini, and Gilbert, J. Am. Chem. Soc. **61**, 2639 (1939); Davies and Gilbert, *ibid.* **63**, 2730 (1941); for a detailed description of the present calorimeter, combustions, and calculations, see George L. Humphrey, Ph.D. thesis, Oregon State College (1949).
[3] R. S. Jessup, J. Research Nat. Bur. Stand. **29**, 247 (1942).
[4] L. Pauling, *The Nature of the Chemical Bond* (Cornell University Press, Ithaca, New York, 1942).
[5] K. S. Pitzer, Science **101**, 672 (1945).

JUN 23 1950

THE JOURNAL OF CHEMICAL PHYSICS

VOLUME 18 NUMBER 6

JUNE, 1950

Published by the

AMERICAN INSTITUTE OF PHYSICS

Lancaster, Pa. and New York, N. Y.